Stochastic modelling of river morphodynamics

Stochastisch modelleren van riviermorfodynamica

Stochastic modelling
of river morphodynamics

PROEFSCHRIFT

ter verkrijging van de graad van doctor
aan de Technische Universiteit Delft,
op gezag van de Rector Magnificus prof. dr. ir. J.T. Fokkema,
voorzitter van het College voor Promoties,
in het openbaar te verdedigen op donderdag 22 december 2005 om 15.30 uur

door

Bastia Gerarda VAN VUREN
civiel ingenieur
geboren te 's-Hertogenbosch

Dit manuscript is goedgekeurd door de promotoren:
  Prof. dr. ir. H.J. de Vriend
  Prof. drs. ir. J.K. Vrijling

Samenstelling promotiecommissie:
  Rector Magnificus   voorzitter
  Prof. dr. ir. H.J. de Vriend   Technische Universiteit Delft, promotor
  Prof. drs. ir. J.K. Vrijling   Technische Universiteit Delft, promotor
  Prof. dr. ir. H.H.G. Savenije Technische Universiteit Delft
  Prof. dr. R.M. Cooke   Technische Universiteit Delft
  Prof. dr. P.E. Johnson   Pennsylvania State University
  Prof. dr. D.E. Reeve   University of Plymouth
  Dr. ir. M. Kok   Technische Universiteit Delft, HKV_{LIJN IN WATER}

voor Nicole

Summary

Modern river management has to reconcile a number of functions, such as protection against floods and provision of safe and efficient navigation, floodplain agriculture, ecology and recreation. Understanding fluvial processes is important to make this possible, to design effective river engineering works, for operational forecasting and for the maintenance of the river system.

In this thesis the focus is in particular on river morphodynamics. Morphological changes can cause flood safety problems, navigation problems, problems with the water distribution over different river branches and stability or functioning problems with hydraulic structures. They may also influence the groundwater level, which may on its turn affect other functions, such as ecology and agriculture.

In the last century a variety of tools has been developed to help understand and predict river morphodynamic processes. Numerical morphodynamic models have become a commonly used tool in river engineering practice. River systems are of a dynamic and stochastic nature and the underlying processes are not completely understood. An imperfect description of physical processes, along with the inability to accurately quantify the model inputs and parameters, leads to uncertainty in morphodynamic predictions. In addition, a natural river system is subject to uncertainties that are inherent to spatial and temporal processes in nature.

For this reason, identifying the uncertainty sources and assessing their contribution to the overall uncertainty in morphodynamic predictions is necessary in order to come to grips with system behaviour. This calls for a stochastic method that enables us to indicate ranges of possible morphodynamic states, their probability of occurrence and the estimation of undesired morphological effects. Stochastic modelling of river morphology and its potential in present-day river management practice is the topic of this thesis. The principal aims of this thesis are:

1. finding out how to analyse the stochasticity of morphodynamics in non-tidal lowland rivers;
2. identifying sources of uncertainty that can be distinguished and quantifying the relative importance of each uncertainty source to the stochastic morphodynamic river behaviour;
3. investigating the potential of a stochastic model approach to support river engineers and managers in their every-day practice.

Monte Carlo Simulation (MCS) with crude sampling appears to be a robust and suitable method to quantify uncertainties involved in morphodynamic predictions. This method is used throughout this thesis. The principle of MCS is to run a deterministic model repeatedly, each time with a different set of statistically equivalent model inputs.

In this thesis, three different morphodynamic models of the Rhine in the Netherlands are applied in an MCS-mode, viz. (1) a simple hypothetical one-dimensional (1-D) model having dimensions similar to those of the Waal (one of the Rhine branches in the Netherlands), (2) a more realistic, but also more complex multi-branches 1-D Rhine model, and (3) a quasi three-dimensional (3-D) model of the Waal.

The hypothetical 1-D model concerns a highly idealised situation in which the river is schematised as a prismatic channel with an initially plane sloping bed. The hypothetical model is appropriate to make a first investigation of the morphological response, for instance induced by isolated geometrical variations or human interventions. It provides rapid insight into the physical system behaviour and the uncertainties involved. The major drawback of the hypothetical model is that because of its simplification, it is of little use to operation and maintenance practice of real-life rivers. The reason for still using the hypothetical model, is that the potential of a stochastic approach can best be investigated by first examining simple cases in which the morphological processes are fully transparent.

The more complex 1-D Rhine model incorporates more real-life complexity, such as hydraulic structures, variations in geometry and flow resistance, multiple branches and bifurcation points. This results in a complex pattern of morphological behaviour and, correspondingly, a complex propagation of input uncertainties through the system. It shows that in some reaches the uncertainty in the bed response is more pronounced than in others, mainly due to strong spatial changes in geometry, such as bifurcation points, width variation in floodplains and the presence of hydraulic and man-made structures.

The quasi-3D Waal model incorporates multi-dimensional phenomena, such as curvature-induced profile evolution. It turns out that the response statistics of individual points in the cross-sectional profile along the river do not only exhibit fluctuations along the river, but also a strong transversal variation. This transversal variation in the response statistics is not only induced by the presence of bends, but must also be attributed to variations in floodplain width, strong confinements of floodplains by embankments and large open water areas and deep ponds in the floodplains. Confinement of floodplains by embankments in the Waal seems to affect statistics the most.

In river engineering practice, 1-D and quasi-3D morphodynamic models, like the models mentioned above, are commonly used. The applicability of either a 1-D or a more advanced quasi-3D model approach depends on the type of problem and the degree of detail that is required, both in terms of resolution and in terms of physical processes. For strategic planning of the entire river basin, a 1-D model approach is appropriate to provide a first insight into the large-scale

river system response, for instance induced by engineering works. In a later stage, a more advanced type of model might be more appropriate at locations of special interest. To some extent, problems related to cross-sectional profile evolution, can be studied with a 1-D model approach in combination with analytically based post-processing to account for the 2D-transverse slope effect. A correction for the bed deformation in river bends alone may not be sufficient, since the morphological activity induced by strong cross-flows, at locations where floodplains are confined by embankments, seems to be more important for the stochasticity of the river bed. For more detailed types of problems a quasi-3D model is therefore recommended.

The computational effort per individual simulation differs considerably between 1-D and multi-dimensional models. Running complex morphodynamic models in an MCS-setting is rather time-consuming. As this thesis focuses on a first assessment of stochastic methods in river morphology, the less time-consuming 1-D model approach is mostly taken, be it with incidental comparisons with multi-dimensional models. Generic knowledge on the use and the potential of stochastic methods in river morphology has been produced that also holds for multi-dimensional model approaches.

Uncertainties introduced by the model schematisation, numerical solution technique and the specification of future scenarios are left out of consideration in the further analysis. The focus is rather on uncertainty associated with quantifying model inputs and model parameters.
A first ranking of uncertainty sources that are of importance to morphology was obtained with a global sensitivity analysis. Apparently, the morphological response is most sensitive to the parameters of the sediment transport formula, viz. the exponent of the bed shear stress and the critical Shield parameter. Moreover, sensitivity to the river discharge, the grain size of the bed material and the hydraulic roughness of the main channel, is clearly noticed. The impact of these sources is further investigated through MCS.
The interpretation of the MCS-results and the estimation of the relative contribution of different uncertainty sources are not straightforward. Morphodynamic systems exhibit a non-linear behaviour combined with a time and space dependent signature, with model inputs that are mutually correlated and with a time-lagging effect. The size of the confidence interval varies differently for each uncertainty source as a function of time and space and the contributions of all sources do not add up linearly to the overall uncertainty.
Generally speaking, the tuning parameters in the calibration process of the 1-D Rhine model, viz. (1) the hydraulic roughness of the main channel, (2) the critical Shields parameter, and (3) the exponent of the bed shear stress in the transport formula, turn out to be the most important uncertainty sources for the morphological response. The contribution of the uncertainty in the grain size of the bed material to the uncertain morphological response is negligible. The importance of the discharge to morphology exhibits a seasonal variation. This is most significant at locations with non-uniformities in geometry, whereas at locations in a uniform reach, it is less pronounced.

Finally, the potential of a stochastic approach is exposed by means of three applications, in order to clarify how this 'computation-intensive' approach can contribute to river management practice.

The first application showed that the stochastic approach is useful to assist the engineer in optimising the design of engineering works. For the purpose of illustration, various river improvement measures in the Rhine are evaluated. It appears that some locations are more susceptible to proposed engineering measures than others. This holds for the mean response, as well as for the variability and also for the seasonal variation. Knowledge on the spatial and temporal variation of morphological response statistics, can be of importance to the allocation of future river improvement measures.

In morphologically dynamic river systems, morphology may affect flood levels. Most present-day flood level predictions are, however, done with a fixed-bed hydraulic model, in which the geometrical schematisation is a representation of the 'actual' state of the river. We have therefore investigated to what extent morphology affects flood levels and to what extent it is justified to compute flood levels with a fixed-bed hydrodynamic model. The effects of seasonal morphological variations turn out to be negligible. Other morphological phenomena, viz. the long-term spatial variation over years and the morphological variability near the bifurcation point, appear to have a larger effect on the flood levels (order of magnitude 0.1 m). Absolutely speaking, this is still rather small, but it is not small as compared with the centimetre-accuracy claimed for the design water levels for the assessment of the flood defences in the Netherlands, or in the light of plans to spend millions of Euros to river improvement measures that reduce the design water level by a few centimetres. An 'a priori' judgement of safety against flooding on the basis of fixed-bed forecasting in morphologically dynamic river systems seems to be quite misleading, taking the role of morphological changes in flood forecasting into consideration.

The third application showed that the stochastic approach is suitable to statistically assess the river's navigability and evaluate different dredging strategies by their maintenance costs. Apparently, navigability and maintenance dredging are strongly influenced by the stochastic nature of the river behaviour. Conversely, navigation traffic and dredging regimes appear to affect the river morphology statistics. Insight into the statistics of maintenance dredging requirements can help the river manager in drawing up performance-contracts with dredging companies.

In summary, this thesis shows how to analyse the stochastic nature of non-tidal lowland river morphology. It provides insight into the uncertainty sources that contribute most to the stochastic morphodynamic river behaviour. Furthermore, three applications illustrate the potential of a stochastic model approach in river management practice. The conclusion can be drawn that the use of this 'computation-intensive' approach adds value to river engineering and management practice.

Samenvatting

In het moderne rivierbeheer moet rekening worden gehouden met een groot aantal functies van de rivier, zoals de bescherming tegen hoogwater, een veilige en efficiënte scheepvaart, en de agrarische, ecologische en recreatieve functies. Het begrijpen van rivierkundige processen is van belang voor het ontwerp van rivierwaterbouwkundige ingrepen en het beheer en onderhoud van het riviersysteem.

In deze dissertatie richten we ons met name op de riviermorfodynamica. Morfologische veranderingen kunnen immers leiden tot hoogwaterproblemen en overstromingen, scheepvaartproblemen, problemen met betrekking tot de afvoerverdeling op splitsingspunten en stabiliteitsproblemen van waterbouwkundige constructies door erosie. Fluctuaties in de grondwaterstand veroorzaakt door morfologische veranderingen kunnen de ecologie en de landbouw beïnvloeden.

In de afgelopen jaren is aandacht besteed aan de ontwikkeling van een groot aantal modelsystemen en hulpmiddelen om het fysische inzicht in riviermorfologische processen te vergroten. Dit heeft geresulteerd in een reeks numerieke morfodynamische modellen, die in de huidige beheerspraktijk regelmatig worden toegepast. De rivier is echter van nature een dynamisch en onzeker systeem, waarvan de onderliggende fysische processen niet volledig worden doorgrond. Het gebrek aan kennis over de werking van het fysische systeem, en problemen met het instellen van modelparameters, leiden tot onzekerheden in morfologische voorspellingen. Bovendien zijn verschillende tijd- en ruimteafhankelijke processen in de rivier inherent onzeker.

Het is van belang dat onzekerheidsbronnen worden geïdentificeerd en dat de bijdrage van de onzekerheidsbronnen aan de totale onzekerheid in morfodynamische voorspellingen wordt gekwantificeerd. Dit vraagt om een stochastische modelaanpak die ons in staat stelt de bandbreedte van mogelijke morfologische veranderingen, de waarschijnlijkheid daarvan en de kans op ongewenste ontwikkelingen vast te stellen. Dit proefschrift staat in het teken van stochastisch modelleren van de riviermorfodynamica en de mogelijkheden hiervan in de huidige beheerspraktijk. In deze dissertatie onderzoeken we

1. hoe het morfologische gedrag van een laagland rivier die niet door getij wordt beïnvloed op stochastische wijze kan worden gekwantificeerd;

2. welke onzekerheidsbronnen kunnen worden onderscheiden en wat de relatieve bijdrage van elke onzekerheidsbron is aan het stochastische gedrag van de rivier;

3.   wat de mogelijkheden zijn van de toepassing van een stochastische modelbenadering in
          de huidige beheerspraktijk.

Monte Carlo Simulatie (MCS) blijkt een geschikte en robuuste methode om onzekerheden in
riviermorfologische voorspellingen te kwantificeren. Om deze reden is deze methode binnen dit
onderzoek toegepast. MCS bestaat uit een groot aantal runs met een deterministisch model, elk
met een statistisch equivalente invoer. Dit leidt tot een groot aantal modeluitkomsten die elk
een even grote kans van voorkomen hebben. Een statistische analyse van alle modeluitkomsten
geeft inzicht in de onzekerheden van de rivierkundige voorspellingen.

In dit onderzoek zijn drie morfodynamische modellen van de Rijn in Nederland aangewend in
een MCS-modus: (1) een geïdealiseerd model met de dimensies van de Waal, één van de Rijn-
takken in Nederland, (2) een realistischer, maar ook complexer 1-D model van de Nederlandse
Rijntakken met de Bovenrijn, de Waal, de Pannerdensche Kanaal, de IJssel, de Nederrijn en de
Lek, en (3) een quasi-3D model van de Waal.

In het geïdealiseerde model is de rivier geschematiseerd als een prismatisch kanaal met een
vlakke bodem onder een klein verhang. Het model is geschikt voor een eerste inzicht in de
morfologische reactie als gevolg van een lokale verstoring of rivierkundige maatregel. Doordat
het model echter zo sterk is vereenvoudigd, is het minder goed toepasbaar voor detail vraag-
stukken in de beheerspraktijk. Een groot voordeel van dit model is dat de mogelijkheden van
de stochastische modelbenadering snel en eenvoudig kunnen worden onderzocht in een sterk
vereenvoudigde situatie. Het morfologische gedrag in een geïdealiseerde situatie wordt immers
goed begrepen en is volledig transparant.

Het 1-D Rijntakkenmodel is een realistischer afspiegeling van de werkelijkheid. De modelsche-
matisatie bevat waterbouwkundige constructies, hydraulische obstakels, variaties in geometrie,
meerdere takken en splitsingspunten. Dit resulteert in complex morfologisch gedrag, en boven-
dien een complexe interactie van onzekerheden in het systeem. Op riviertrajecten met een sterke
variatie in riviergeometrie, zoals ter plaatse van splitsingspunten, breedtevariaties in uiterwaar-
den en waterbouwkundige constructies, is de onzekerheid in de bodemontwikkeling groter dan
op andere trajecten.

In het quasi-3D Waal model worden morfologische verschijnselen ook in dwarsrichting beschre-
ven. Het quasi-3D Waal model laat zien dat de statistische karakteristieken van de bodemont-
wikkelingen niet alleen in langrichting variëren, maar dat er ook sprake is van een sterke variatie
in dwarsrichting. Deze variatie in dwarsrichting is niet alleen het gevolg van het bodemdwars-
verhang in rivierbochten, ook variaties in uiterwaardbreedte, insnoeringen van uiterwaarden
door winterdijken en de locatie van waterplassen en zandwinputten, spelen een rol. De insnoe-
ring van uiterwaarden door winterdijken blijkt de grootste invloed op het morfologische gedrag
in dwarsrichting te hebben.

In de huidige beheerspraktijk worden de hierboven beschreven 1-D en quasi-3D modellen regel-

matig toegepast. De voorkeur van het ene model boven het andere hangt af van het type probleem dat wordt onderzocht en de mate van detailniveau dat daarbij vereist is. Dit beïnvloedt de keuze van de modelresolutie en de mate waarin fysische processen worden beschouwd. Voor een strategische planning van het gehele rivierbassin is een 1-D benadering geschikt. Deze benadering geeft bijvoorbeeld een eerste indicatie van de grootschalige reactie op een set van rivierkundige maatregelen. In een latere fase worden vaak geavanceerdere modellen ingezet om de effecten van deze maatregelen in zowel langs- als dwarsrichting beter te doorgronden. Middels een nabewerking van de 1-D voorspellingen is het mogelijk tot op zekere hoogte voor het door bochten geïnduceerde 2D-dwarsverhang te corrigeren. Echter, deze correctie alleen is niet voldoende, aangezien de morfologische activiteit sterker lijkt beïnvloed door sterke dwarsstromen ter plaatse van sterke insnoeringen van de uiterwaarden door winterdijken. Voor dit type probleem wordt daarom het gebruik van quasi-3D modellen aanbevolen.

De rekentijd per individuele simulatie verschilt aanzienlijk tussen 1-D and multi-dimensionale modellen. MCS in combinatie met complexe morfodynamische modellen kan zeer rekenintensief zijn. Aangezien dit onderzoek gericht is op een inventarisatie van het gebruik van stochastische modellen in riviermorfologie, is in het vervolg met name gebruik gemaakt van minder rekenintensieve 1-D modellen. Opgedane kennis en inzicht over het gebruik en de mogelijkheden van een stochastische modelbenadering is ook toepasbaar op multi-dimensionale modellen.

Onzekerheden in de modelschematisatie, de numerieke oplossingsmethode en toekomstige ontwikkelingen, zoals klimaatveranderingen, zijn buiten beschouwing gelaten bij het inventariseren van onzekerheidsbronnen. De inventarisatie richt zich met name op onzekerheden die zijn geïntroduceerd door het vaststellen van modelinvoer en modelparameters.

Een eerste volgorde van relevante onzekerheidsbronnen is verkregen middels een gevoeligheidsanalyse. Morfologische voorspellingen blijken het meest gevoelig voor parameters in de sedimenttransportformule, namelijk de exponent van de bodemschuifspanning en de kritische Shieldsparameter. Daarnaast zijn de rivierafvoer, de korrelgrootteverdeling en de hydraulische ruwheid van de hoofdgeul van belang. De invloed van deze onzekerheidsbronnen zijn verder onderzocht in een MCS.

De interpretatie van de MCS-resultaten en het bepalen van de relatieve bijdrage van elke onzekerheidsbron is niet eenvoudig. Morfodynamische systemen vertonen een sterk niet-lineair gedrag. Daarnaast maken de tijd- en ruimteafhankelijke processen, de correlatie en afhankelijkheden tussen modelinvoer onderling en het naijlen van morfologie bij hydraulische condities, een goede interpretatie lastig. Het betrouwbaarheidsinterval van morfologische voorspellingen varieert verschillend voor elke onzekerheidsbron in ruimte en tijd. De totale onzekerheid in de morfologische ontwikkeling is niet simpelweg gelijk aan het lineair optellen van de onzekerheden geïntroduceerd door elke onzekerheidsbron afzonderlijk. De relatieve bijdrage van elke onzekerheidsbron afzonderlijk is daarom moeilijk vast te stellen en varieert als functie van ruimte en tijd.

In het algemeen kan worden gesteld dat de onzekerheid in calibratieparameters van het Rijntak-
kenmodel, namelijk de hydraulische ruwheid van de hoofdgeul, de kritische Shieldsparameter
en de exponent van de bodemschuifspanning in de sedimenttransportformule, het meest bijdra-
gen aan de totale onzekerheid in morfologische voorspellingen. De bijdrage van onzekerheid in
korrelgrootteverdeling lijkt verwaarloosbaar klein. Het relatieve belang van de onzekerheid in
rivierafvoer is seizoensafhankelijk. Dit blijkt met name het geval ter plaatse van locaties met
sterke niet-uniformiteiten in de riviergeometrie.

Tot slot zijn de mogelijkheden van de stochastische modelbenadering in de beheerspraktijk on-
derzocht aan de hand van drie toepassingen.
De eerste toepassing laat zien dat een stochastische benadering geschikt is om het ontwerp van
rivierkundige ingrepen te optimaliseren. Ter illustratie zijn verschillende rivierkundige maat-
regelen op de Rijn geëvalueerd. Sommige locaties blijken gevoeliger voor rivierkundige maat-
regelen dan andere. Dit is merkbaar in de gemiddelde veranderingen, de variabiliteit en de
seizoensafhankelijkheid. Kennis over en inzicht in de onzekerheid in morfologische reacties is
van belang voor een goede afweging tussen verschillende ontwerpalternatieven.
In de huidige praktijk wordt voor hoogwaterstandsvoorspellingen veelal gebruik gemaakt van
hydraulische modellen met een vaste bodemligging. In morfologisch actieve rivieren kan de mor-
fologie hoogwaterstanden echter beïnvloeden. Dit is onderzocht in de tweede toepassing. Het
effect van seizoensvariatie in de bodemligging op hoogwaterstanden blijkt uiterst gering. De
middellange termijn variaties in de bodemligging en de morfologische activiteit rond splitsings-
punten hebben een groter effect op hoogwaterstanden (orde van 0.1 m). Absoluut gezien is dit
effect klein, maar deze bijdrage aanzienlijk in vergelijking tot de centimeter-nauwkeurigheid die
bij het toetsen van waterkeringen in Nederland wordt geclaimd. Gezien de invloed van morfolo-
gie op hoogwaterstanden, moet bij hoogwaterstandsvoorspellingen rekening worden gehouden
met de morfodynamica van de rivier.
De derde toepassing toont de bruikbaarheid van de stochastische modelbenadering aan bij de
beoordeling van de bevaarbaarheid van de rivier en het vereiste onderhoudsbaggerwerk. Beide
worden in belangrijke mate beïnvloed door het stochastische gedrag van de rivier. Inzicht in
de onzekerheid van onderhoudsbaggerwerk kan de rivierbeheerder helpen met het sluiten van
prestatiecontracten met baggermaatschappijen.

Kort samengevat laat dit onderzoek zien hoe het stochastische gedrag van een laagland rivier
die niet door getij wordt beïnvloed kan worden gekwantificeerd. Het geeft inzicht in de onze-
kerheidsbronnen die het meest bijdragen aan de totale onzekerheid in morfologisch gedrag. De
toepasbaarheid en de mogelijkheden van een stochastische modelbenadering ter ondersteuning
van de rivierbeheerder in het ontwerp, beheer en onderhoud van de rivier, is geïllustreerd aan de
hand van drie voorbeelden. Het gebruik van een stochastische modelbenadering in de huidige
beheerspraktijk is veelbelovend.

Contents

Chapter 1

Introduction

1.1 Why study river morphology?

Modern river management has to reconcile a number of functions, such as protection against floods and provision of safe and efficient navigation, floodplain agriculture, ecology and recreation. In recent years, major river floods, like in the Jamuna River in Bangladesh, the Yangtze in China, the Oder and the Vistula in Poland and the Elbe in Germany, have raised people's awareness towards flooding. In Western Europe, severe droughts in the summer of 2003 led to problems for navigation and water supply. In other parts of the world in ephemeral rivers, such as Choshui (Taiwan) and Johila (India), droughts occur on periodic basis in the dry season. Sustainable development of river ecosystems is now an important political issue worldwide. A wide range of measures to control the flow and sediment transport through the river and to accommodate its often conflicting functions is required, especially for multi-function rivers in densely populated areas.

Over the last two hundred years the river Rhine in the Netherlands has faced a series of changes, such as regulation and canalization, construction of levees, confinement of the floodplains and industrialization of its riparian zones. The Rhine became the most important shipping connection between the port of Rotterdam and Germany. Half of the cargo transport to Germany goes via this waterway connection. Due to rapid population growth and economic development in the low-lying polders behind the major levees of the Rhine, flood control and navigability became most important issues in the management of the Rhine branches in the Netherlands.

Understanding fluvial processes, in particular of lowland rivers in densely populated areas, like the river Rhine in the Netherlands, is important. To assist river engineers and managers, predictions at various scale levels are required, viz.

- in planning and design - in order to assess the effectiveness and the impact of river engineering works, to satisfy planning and design specifications;
- in operational forecasting - e.g. information required about the rise of flood levels in order to decide whether detention basins have to be deployed or whether there is a need

> for emergency measures such as evacuation or forced inundation;

- in maintenance - in order to keep the river in shape for flood conveyance and its other functions, such as navigation.

In alluvial rivers the transport of sediment and the resulting changes in river bed topography are important processes. The sediment transport capacity depends on the flow conditions and the sediment characteristics. In general, the water motion tends to pick up sediment and deposit it elsewhere. If the water motion is disturbed, spatial gradients in the sediment flux cause morphological changes. These processes are studied in the discipline of river morphodynamics.

For several reasons the availability of predictive capability concerning river morphodynamics is important. Morphological changes can create high-water problems and flooding (safety), low-water problems (navigation), problems with the water distribution over the different river branches and erosion problems, which may undermine and destabilize the foundations of hydraulic structures.

In the last century a variety of tools has been developed to provide physical insight into the morphodynamic processes. This resulted in a range of mathematical process-based models that are commonly used in present river engineering and management practice. These models describe waves, currents, sediment transport and bed level changes in rivers via a set of mathematical equations based on physical conservation laws. Since in most practical cases these equations cannot be solved analytically, numerical solvers are used. Numerical process-based morphodynamic models have become more powerful with the increase in computer capacity and the development of numerical methods. Various kind of numerical modelling software packages are available, such as the 1-D model system SOBEK and the 2-D and 3-D model system Delft3D of WL|Delft Hydraulics and the MIKE model series of the Danish Hydraulic Institute.

1.2   The need for stochastic modelling of river morphology

Most present-day morphodynamic predictions are based on a deterministic model approach. This means that the morphodynamic response of a river is analysed in a deterministic manner, using carefully chosen model inputs along with calibrated morphodynamic models. Well-calibrated deterministic models have a high capacity to reproduce the morphological change in the past (Southgate, 1999) and are used to forecast the morphological behaviour in the nearby future.

Extrapolation into the future, however, entails uncertainties in predictions. This is strengthened by the fact that many model inputs are stochastic. In fact, the river system behaviour is inherently uncertain. Furthermore, model uncertainties are involved, reflecting the inability to represent the complex physical processes or phenomena through the use of a set of deterministic

differential equations and an empirically derived sediment transport model. Lack of knowledge about the physical system and understanding of its processes make it even more difficult.

In some studies uncertainty is addressed by a qualitative evaluation (sensitivity analysis) and by adopting conservative assumptions and applying safety factors (Van der Klis, 2003). The main disadvantage of this approach is the lack of insight into the likelihood of the predictions. Moreover, conservative design and large safety factors involve societal costs of which the effectiveness is not always clear.

A deterministic model approach appears to be in principle an effective tool to provide a quick and first indication of the physical system behaviour. The choice of parameter settings highly depends on the focus of the river engineer. If one is interested in the 'expected' morphodynamic response, the model parameters and inputs will be set in such a way that the model output will approximate the expected response. This appears to be rather difficult, especially in the case of non-linear models, where the expected value of a prediction based on randomly varying inputs is not equal to the prediction based on the expected value of each input quantity (Gardner & O'Neill, 1983). Whether the computed response reflects the statistical mean or the expected response is uncertain, since the exact model parameters and inputs needed to obtain the statistical mean are unknown. Nor is the stochastic variability around this statistical mean known. So, the usual deterministic approach tells us nothing about the likelihood of the prediction. The ensemble dimension, which contains the possible states that may occur and in particular their probability of occurrence, is not considered. Ignoring uncertainties may lead to an incomplete understanding of the potential morphodynamic behaviour of the river system in the future.

For this reason, identifying the uncertainty sources and assessing their contribution to the overall uncertainty in morphodynamic predictions is necessary in order to come to grips with system behaviour. This calls for a stochastic method that enables indicating ranges of possible morphodynamic states, their probability of occurrence and the estimation of undesired morphological effects. The procedure of uncertainty analysis contain the following steps, viz.(1) inventory of uncertainty sources involved, (2) statistical description of the uncertainty sources, (3) estimation of the (relative) contribution of the uncertainty sources to the uncertainty in the model results, (4) interpretation of the uncertainties in the model results, (5) check with observations. Finally, the results of an uncertainty analysis should be translated into information for design, operational forecasting and maintenance.

A number of stochastic methods exists to cope with uncertainties in system behaviour, such as First Order Reliability Method (FORM), Monte Carlo Simulation (MCS), Stochastic Differential Equations, Numerical Integration, etc. The applicability of these stochastic methods to study the stochastic nature of river morphology depends on how well these methods deal with the strong non-linearity and complexity of river morphodynamics (Van der Klis, 2003).

1.3   Problems with the existing stochastic methods in river engineering

Although most present-day morphodynamic studies are based on a deterministic approach, a limited number of studies incorporated an assessment of uncertainty. Here a short literature review is given to illustrate the present state of knowledge. We discern two main categories of literature, viz. literature in which uncertainty analysis has been applied to (1) analytical models, and (2) numerical morphodynamic models. Some studies focus on a particular component of the morphodynamical processes, the sediment transport module or the flow module, for instance.

An overview of the applications in literature in other research field adjacent to river engineering, viz. Meteorology, Climatology, Hydrology, Ecology, Public Health, and Hydraulic Engineering, is given in Section 3.4.2.

Analytical models

Analytical models are often used as a tool to contribute to the understanding of the essence of the river behaviour, leaving out as much complexity as possible. Analytical models are simpler than numerical model systems, but are less generally applicable.
Scour around a bridge pier is statistically analysed in Chang et al. (1994) and Johnson & Ayyub (1996) by means of Monte Carlo Simulation (MCS). The authors made use of an empirical pier scour model that gives the relation between the maximum pit depth and a number of stochastic input variables. The contribution of a number of (correlated) stochastic variables, viz. the flow depth, the pier width, the Froude number and the sediment gradation, to the maximum scour around a bridge pier is studied in Chang et al. (1994). The imposed correlation structure between the stochastic input variables appears to be important for the assessment of the maximum bridge pier scour. Yeh & Tung (1993) analyse the uncertainty in the maximum pit depth after a certain migration distance using an analytical model of the migration of a pit through the river in combination with the First Order Reliability Method (FORM) and MCS with Latin Hypercube sampling.

Numerical models with the focus on a particular component

Some studies focus on a particular component of the morphodynamical processes, such as the sediment transport module or the flow module.
Yeh & Deng (1993) studied uncertainty involved in two different types of sediment transport formulae, namely the bed load Einstein formula and Yang's formula. Johnson (1996a) discusses the uncertainty involved in the estimation of the excess shear stress that is used to determine the sediment transport capacity and the bedforms that occur under various flow-conditions. Johnson (1996a) made use of MCS.

Gates & Al-Zahrani (1996a) presented the application of the Saint-Venant flow model in a stochastic setting. They focused on the uncertainty in unsteady open-channel flow that is associated with quantifying model parameters. The influence of a set of parameters that are mutually correlated and vary in space and in time, on the flow variables (velocity and depth), is addressed through MCS. It was not the purpose to address uncertainty due to inadequate model formulation. To illustrate the practical applicability of the method, a hypothetical engineering problem was defined for a 10-km reach of the Colombia River (USA), in Gates & Al-Zahrani (1996b). The backwater effect of a barrage design, under flood conditions, is considered.

Duits et al. (2000) discussed the uncertainty involved in flood level predictions in the river Rhine in the Netherlands. To that end, a 1-D and 2-D hydrodynamic model are run in a Monte Carlo-setting. The impact of various uncertainty sources is considered, namely the impact of the hydraulic roughness coefficients, the imposed channel geometry, the bed slope, the stage-discharge relationships and the discharge distribution at bifurcations. It is concluded that not all uncertainty sources are of equal importance to the flood level predictions and that correlation between the uncertainty sources cannot be neglected.

Examining uncertainties involved in particular components of the numerical morphodynamic model system, instead of considering the morphodynamic system as a whole, gives no information on which uncertainty sources are relevant to river morphology.

Numerical morphodynamic models

The principal constituents of a morphodynamic model are a flow module, a sediment transport module and a bottom change module, that are operated in a sequential or cyclic (iterative) mode. Chang et al. (1993), Maurer et al. (1997) and Van der Klis (2003) apply uncertainty analysis to numerical morphodynamic models.

The impact of pipe and bank protection works on morphology and sediment-routing in a section of the Santa Cruz River, adjacent to Green Valley, Arizona, USA, has been stochastically assessed through MCS applied to a numerical model, in Chang et al. (1993). The impact of uncertainty in hydraulic roughness, in grain size, in bed porosity and in the contraction and expansion coefficient is considered. These uncertain model inputs are uncorrelated random variables with uniform distributions, and contribute differently to the uncertainty in model results. The influence of inaccuracy of different input parameters on the deposition of suspended sediment upstream of a river dam is studied in Maurer et al. (1997). A simple 1-D model for unsteady flow is coupled with a sediment transport equation for suspended load to calculate deposition of suspended material. A rectangular channel with a length of 10 km and a steep bed slope of 1/1000 is assumed. A barrage was contemplated for the downstream end of the reach. FORM and MCS are applied to analyse the uncertainty for the deposition of suspended sediment. The probability of the deposition of suspended sediment to exceed a certain

threshold level is estimated, considering four inaccurate input parameters, namely the Manning's hydraulic roughness coefficient, the critical shear stress, the settling velocity and the longitudinal dispersion coefficient. The deposition is most sensitive to the Manning's hydraulic roughness coefficient and the critical shear stress. The settling velocity and the longitudinal dispersion coefficient hardly influence the deposition upstream of the river dam. Maurer et al. (1997) concluded that the FORM is a practicable alternative to MCS.

Van der Klis (2003) investigated the impact of isolated river works, such as main-channel constriction, floodplain lowering and floodplain widening, on the uncertainty in the morphological response in straight prismatic rivers similar to the river Rhine in the Netherlands. A 1-D numerical morphodynamic model has been used. A description of the uncertain model inputs and their order of magnitude in combination with a rough sensitivity analysis gives a first distinction between important and less important inputs. Uncertainty in the river discharge is shown to be the most important with respect to river morphology and is investigated in further detail. Van der Klis (2003) examined the applicability of the FORM and MCS in morphological studies. She showed, however, that FORM is not suitable to estimate the uncertainty in river morphodynamics. The combination of non-linearity and large uncertainties leads to unreliable results.

Practical application of stochastic methods

In the foregoing we have shown examples in literature utilizing stochastic methods while approximating a river by highly simplified schematisations as compared with reality. The complex physical processes and phenomena are described through the use of simplified mathematical expressions, such as empirical formulae or one-dimensional morphodynamic models of a straight prismatic channel. The main advantage is that the opportunities offered by a stochastic approach can be understood best by first examining simplified cases of which the morphological processes are fully transparent. In a later stage, one can gradually increase the complexity of the river schematisations. The experience gained with simplified cases enables the interpretation of uncertainty estimates of more complex situations.

In reality, a river is by no means a prismatic channel with a plane sloping bed. In practice, a river will contain many variations, such as man-made structures, bifurcation points, flood-free areas and variation in geometry, in composition of bed material and in vegetation cover. These variations may influence the water motion, thus producing spatial gradients in the sediment flux and hence morphological changes. In this way, variations in river geometry may act as generators of bottom waves. These bottom waves migrate downstream, (partly) decay, interfere with bottom waves initiated elsewhere in the river and may results in an uncertain morphodynamic response. Ignoring the complexity of the river may therefore lead to an incomplete understanding of the river system behaviour and the uncertainties involved.

This calls for uncertainty analysis using models that describe reality in a less simplified way. One could think of complex one- or two-dimensional models, the suitability of which depends on the character of the river and the user's demands with respect to the application. Numerical simulations with complex morphodynamic models are usually rather time-consuming. The computational effort may increase extremely when running these models in a stochastic mode, using Monte Carlo Simulation or Numerical Integration. Therefore, it is worthwhile to put effort into determining the relative contribution of each source of uncertainty to the overall uncertainty in the model output.

In a number of the aforementioned studies, the translation of results of the uncertainty analysis into information that the user needs is not considered or underexposed. Some of them use stochastic methods to better estimate the impact of river engineering works. But a stochastic method can also be used to assist the river manager in his operation and maintenance practice. The navigability of the river, for instance, can be statistically assessed by estimating the probability of fulfilling navigation requirements as a function of draught. Insight into the statistics of maintenance dredging requirements can help the river manager in drawing up performance-contracts with dredging companies.

The need for and the use of stochastic modelling in present-day river management practice should be subject of further research. The advantages of stochastic methods need to be clearly exposed, in order to contribute to a better insight into the opportunities offered to river engineers and managers to use this 'computation-intensive' approach in river management, including design of measures, operational forecasting and maintenance of the river system.

1.4 Objectives and research questions

The focus of the research presented in this thesis is the application of a stochastic model approach to quantitatively estimate uncertainties in morphodynamic predictions of complex non-tidal lowland rivers at various scale levels. This includes the use of stochastic modelling to support river engineers and managers in their every-day practice.

The general objectives of this thesis are:

1. to study the stochastic nature of non-tidal lowland river morphology and to identify the uncertainty sources that contribute most to the stochastic morphodynamic river behaviour.
2. to produce general knowledge on the application of stochastic methods in river morphology.
3. to investigate the potential of a stochastic approach in river management practice, namely at design, operation and maintenance level.

The scope of this thesis is restricted to the morphological behaviour of non-tidal perennial lowland rivers with fixed banks and sub-critical flow. For the purpose of illustration, the Rhine in the Netherlands is used as a study case throughout this dissertation, but conclusions will be generalized where possible.

The availability of (1) an impressive database that contains 100-years of daily discharge records, annual bed soundings from 1926 onwards, and data on grain size of the bed material, water levels, water depths, dredging activities and navigation draughts, and (2) various numerical morphodynamic models of the river, make the Rhine an appropriate study case. Moreover, the Rhine in the Netherlands is a multi-functional river in a densely populated area, which offers the opportunity to expose the potential of stochastic methods in present-day river management practice.

To meet the objectives, we focus on the following research questions:

- How to carry out stochastic analysis in river morphodynamics? What kind of tools, information and data should be available?
- To what extent can present numerical morphodynamic models, ranging from 1-D to more sophisticated quasi-3D models, be used in a stochastic setting to study the stochastic nature of river morphology?
- Which types of uncertainty can be distinguished in river morphological modelling and which contribute most to the stochastic morphodynamic river behaviour?
- What is the potential of a stochastic approach in river management practice? How can a stochastic approach support river engineers and managers in their every-day practice?

1.5   Terminology

The thesis combines two research fields, namely the field of river morphodynamics and stochastic modelling. To prevent confusion in either research field, we explain some of the terminology as it is applied in this thesis.

Static and dynamic state

Statics is the science that deals with forces that balance each other to keep an object in a state of rest. In river morphology, we refer to a static state if a river system evolves towards an equilibrium state under constant flow conditions. As long as forces change, a static state will never be reached. Dynamics is associated with variations: things change while mutually interacting. A dynamic approach shows how a river system evolves over time, for instance, under varying flow conditions.

Deterministic and stochastic approach

A deterministic approach claims to approximate reality as if everything is exactly known. Yet, the inability to represent the complex physical morphodynamic processes or phenomena through the use of a deterministic model, and the inability to accurately quantify model inputs and parameters, make the assessment of uncertainty involved in deterministic modelling necessary. A stochastic approach is used as a synonym for an uncertainty analysis and a probabilistic approach in this thesis.

Variability and uncertainty

It is not easy to give a definition of uncertainty, other than 'lack of certainty' or 'lack of sufficient knowledge'. According to Oxford's dictionary, for instance, uncertainty stands for 'not sure', 'likely to change', 'not definite or decided' and 'not confident'. Van Gelder (2000) gives numerous synonyms for uncertainty, viz. unsureness, unpredictability, randomness, hazardness, indeterminacy, ambiguity, irregularity, variability and so forth.

Throughout this thesis, we use variability and uncertainty for the same concept. The definitions of variability and uncertainty depend in principle on whether we refer to a hindcast or a forecast mode. So in fact, the words have a slightly different meaning. Stochasticity would be a common denominator for variability and uncertainty.

Confidence interval and uncertainty range

In this thesis, uncertainty in morphology is often expressed in a confidence interval. The 95th and 5th percentile values span, for instance, the 90%-confidence interval, meaning that morphological state have a probability of 90% of falling within this range. The term confidence interval and uncertainty range are used as synonyms.

1.6   Research outline

The objective and the research questions result in the outline of the thesis. The research outline is visualised in Figure 1.1. It consists of three parts:

- Part one: Theoretical background and Methodology
- Part two: Application of Monte Carlo Simulation to morphodynamic models
- Part three: Potential of Monte Carlo Simulation in river management practice

Part one - Theoretical background and Methodology

This part addresses the background of the thesis and the research methodology. The basic theory of river morphology is discussed in Chapter 2. Chapter 3 describes the theoretical background of uncertainty analysis and various stochastic methods. The focus of Chapter 4 is on the research methodology. Tools, such as the stochastic method and the morphodynamic models, used throughout this thesis are discussed.

Part two - Application of Monte Carlo Simulation to morphodynamic models

In Part two, three different numerical morphodynamic models are run in a stochastic setting. Monte Carlo Simulation appear to be a robust and suitable method to quantify uncertainty involved in morphological modelling. We start with a simple 1-D model of the Waal, one of the Rhine branches in the Netherlands, in Chapter 5. This simple model concerns a prismatic channel with an initially plane sloping bed. The main disadvantage of such a model is that it concerns a rather idealised situation. Therefore, the hypothetical model is of little use to operation and maintenance practice of real-life rivers. The step to a more complex model of the Rhine, incorporating the real-life complexity of the river, is made in Chapter 6. Yet, this is still a 1-D model. Using a quasi-3D model of the Waal in a stochastic mode (Chapter 7), must clarify the importance of multi-dimensional phenomena that are not considered in the 1-D approach.

Part three - Potential of Monte Carlo Simulation in river management practice

Part three exposes the potential of stochastic methods in present-day river management practice. In Chapter 8, we show how a stochastic approach can be useful to assist the engineer in optimising the design of engineering works. For the purpose of illustration, various alternatives for river improvement measures in the Rhine are evaluated. The impact of uncertainty in morphological evolution of a river system on the protection against flooding is topic of Chapter 9. We elaborate on the method to predict the navigability and maintenance dredging in the Rhine, when considering uncertainty morphodynamic river behaviour, in Chapter 10.

Finally, conclusions and recommendations are summarised in Chapter 11.

	Chapter 1 Introduction	
Part 1: **Theoretical background and Methodology**	Chapter 2 River morphology	
	Chapter 3 Uncertainties in river morphology	
	Chapter 4 Methodology	
Part 2: **Application of Monte Carlo Simulation to morphodynamic models**	Chapter 5 Hypothetical 1-D model of dimensions similar to those of the Waal	
	Chapter 6 1-D Rhine model	
	Chapter 7 Quasi 3-D Waal model	
Part 3: **Potential of Monte Carlo Simulation in river management practice**	Chapter 8 Morphological impact of river engineering works	
	Chapter 9 Protection against flooding	
	Chapter 10 Navigation and maintenance dredging	
	Chapter 11 Conclusions and recommendations	

Figure 1.1: Thesis outline

Part one: Theoretical background and Methodology

Chapter 2

River morphology

2.1 Introduction

River morphodynamics is known as the dynamic interaction between water and loose-sediment motion, on the one hand, and the bed topography, on the other. Natural changes and human interference may interrupt river processes, which lead to an immediate hydrodynamic response and a delayed morphological response (changes in topography of bed and banks). Morphodynamic river systems are highly non-linear, subject to a continuous input of energy that is internally dissipated, and they exhibit many types of forced and free behaviour.

This chapter starts with an overview of basic theory of river morphology (Section 2.2). In present-day practice, insight into the physical processes in dynamic river systems is obtained with a variety of tools, including models - physical scale models, empirical relations, analytical and numerical models - and field observations and measurements, as is briefly outlined in Section 2.3. In this thesis, we primarily focus on numerical models in order to describe or predict behaviour of alluvial river systems of subcritical flow and carrying non-cohesive bed material. Section 2.4 discusses the use of numerical process-based models in design, operation and maintenance practice, each of which requires information on specific aspects of the morphodynamic behaviour.

2.2 River dynamics

2.2.1 Aspects of river behaviour

A river is considered as a morphodynamic system, as it includes a dynamic feed back between water motion, sediment transport and bed level changes (Figure 2.1). A variety of forcing factors such as natural changes in environmental conditions and human interventions, affect the individual river processes. As the individual elements are mutually coupled, this influence extends to the behaviour of the system as a whole.

De Vriend (1999) states that river behaviour is the result of a randomly forced multi-scale non-linear process and takes place at a wide variety of spatial and temporal scales, from individual grain motion through to the evolution of the entire system. Yet, the river behaviour depends not only on the forcing, the type of river is also important. The morphological behaviour depends on characteristics such as geometry, bed slope and sediment characteristics.

The river has a sediment transport capacity that depends on flow conditions and sediment characteristics, such as density, grain size distribution, shape and uniformity. In general, the water motion tends to pick up sediment and deposit it elsewhere. If the water motion varies in space, spatial gradients in the sediment flux cause morphological changes. These morphological responses influence the water motion and the sediment transport, which in their turn, affect the sediment balance and the bed topography. The river tries to adapt to the situation and re-establish a new dynamic equilibrium state, which is not necessarily static. If the river is in equilibrium at a certain spatial and temporal scale level, there is no divergence in the transport field at that level. A static equilibrium state is in fact a hypothetical state which will hardly ever occur in nature (De Vriend, 1999).
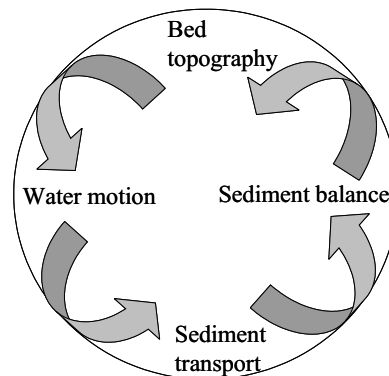
Figure 2.1: Morphodynamic river approach

Combinations of natural and human factors affect the riverbed response. A river system is driven to a large extent by the weather conditions in the basin. Human interventions, like dredging, canalisation, navigation, dam building and floodplain encroachment are important as well. Important natural factors, such as rainfall, river discharge and sediment supply can be affected by human activities. For example, dam and weir management have their impacts on the river discharge. Also climatic change seems to be partly due to 'human' activities. They act upon the river hydrodynamics and can eventually lead to bed level response. Different forcings take place simultaneously with different intensities and different response times, but all affecting the bed level. This makes it rather complex and difficult to relate a particular change in morphology to a specific human activity or change in environmental conditions.

2.2.2 Free and forced morphological behaviour

The morphodynamic river system usually exhibits two types of behaviour: free and forced. Both play an important role in spatial and temporal morphodynamic patterns. The system responses are often non-local and non-instantaneous.

Free behaviour

Free behaviour, sometimes called self-organised behaviour, depends globally on the external forcing. However, the spatial and temporal variations cannot be related in a one-to-one manner to corresponding variations in the forcing factors. This type of behaviour is inherent to the system itself. The external forcing generally provides the energy to make these phenomena occur, but it does not impose their specific variations. Free behaviour is associated with the occurrence of free instabilities in water-sediment-bed interaction: infinitely small perturbations in the bed may tend to grow into a persistent finite-amplitude bed pattern, sometimes fixed in location, sometimes migrating through the river. Free behaviour can be found at various spatial scales (De Vriend, 1999):

- The smallest-scale modes of free morphological behaviour in rivers are bed ripples and dunes. They develop under moderate flow and transport conditions. During floods, the water discharge increases and, consequently, the bedforms increase as well, be it with a certain time lag. Via their influence on the bed roughness, ripples and dunes influence flow and sediment transport at larger scales. This small-scale morphodynamic feedback system may therefore have large-scale effects.

- Another mode of free morphological behaviour is the formation of alternate bars in shallow rivers: a pattern of elongated shoals, occurring alternately near the left and the right bank of the river. Alternate bars are migrating features, which can be metres high and hundreds of metres long. River meandering is influenced by the occurrence of alternate bars, but it is not critically dependent on it (Seminara & Tubino, 1989). Meandering-induced bed topography (with a point bar at the inner bend and a pool in the outer bend) tends to suppress the alternate bars. The point bar and pool configuration in a bend is an example of forced behaviour, in this case imposed by the curvature of the channel. The distinction between forced and self-organised behaviour is sometimes difficult to make.

- At a larger scale, meandering and braiding are examples of free morphological behaviour.

Forced behaviour

In a forced system, the morphological response is directly related to the external forcing. The complexity of this response can be related to the complexity of the forcing conditions. Examples

of forced responses are the 'breathing' of a river bed due to discharge variations through the year and responses associated with human interventions, such as engineering works (De Vriend, 1999). The different external forcing factors are not all of equal relevance to the morphological response.

2.2.3   Multi-scale character of a river system

In each morphodynamic system, a series of scale levels can be distinguished. Assuming that, to some extent, these scale levels can be considered separately, De Vriend (1999) introduces a qualitative scale cascade that is generally applicable to various types of morphodynamic systems (Figure 2.2). At each step of the scale cascade, morphodynamic processes have to be considered in mutual interaction. The figure suggests that spatial and temporal scales of morphological features be mutually related. The following scales can be considered in a morphodynamic river system:

- micro-scale - small-scale bedforms (e.g. ripples and dunes) and vertical segregation of sediment fractions, like bed armouring;
- meso-scale - alternate bars and cross-sectional profile evolution, such as pointbar/pool combinations in bends;
- macro-scale - meandering, braiding, longitudinal profile evolution of river reaches in response to training works or sand mining;
- mega-scale - channel pattern formation at the scale of the river basin.
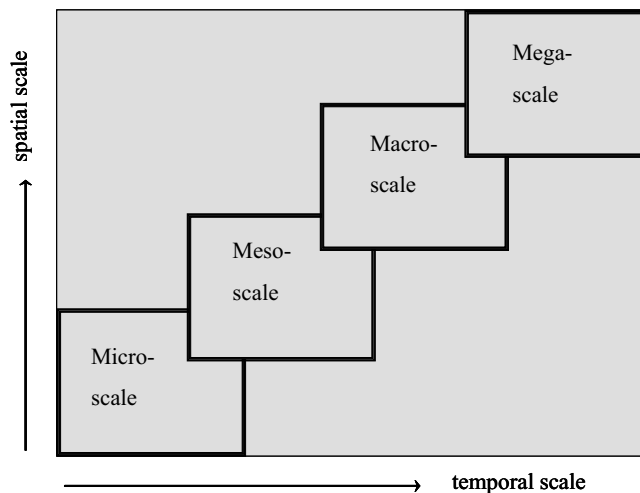
Figure 2.2: Scale cascade (De Vriend, 1999)

The micro- and meso-scale levels represent morphodynamic processes at local scale, whereas processes at reach scale are considered at macro-scale level. At mega-scale level, we refer to processes at river basin scale. The scale-cascade is a qualitative classification of scales and is used to distinguish between morphological features in the Dutch Rhine system in Section 4.3.

2.2.4 Non-linearity and irreversibility of river morphology

Linearity or non-linearity is an important discriminator between dynamic systems. The principle of superposition holds in the linear case. This implies that modes of behaviour do not influence each other and can be considered separately. Non-linear systems are much more complicated. Modes of behaviour mutually interact and can no longer be treated separately. Irregularity and non-basic (chaotic) patterns can be properties of non-linear systems. A river is considered as a non-linear dynamic system. The relationship between the hydrodynamic response and the bed level response is highly non-linear.

For example, the propagation of a hump on the river bed (neglecting the diffusion of the bottom wave) exhibits non-linear behaviour. The propagation speed of the hump is not constant, but increases (non-linearly) with the bed level. The crest of the hump propagates faster than the foot. This means that the hump undergoes deformations: the upstream slope becomes milder, the downstream slope becomes steeper. After some time, the crest will overtake the foot and the hump starts overtopping. In the case of loose sediment, this means that a slip face (or, in mathematical terms, a shock front) forms. The shock front propagates at a speed somewhere between that of the foot and the crest, whence the total length of the hump increases. If the shock front stage is reached, the process becomes irreversible. The observed behaviour of dunes on the river bed during a flood event also exhibits irreversibility.

Irreversibility is an important property of a morphodynamic system, since it means that the morphology depends on the chronology of events. In addition to the frequency, the time sequence of events is relevant (Southgate & Capobianco, 1997).

2.2.5 Morphological time-scales

The scale cascade of De Vriend (1999) assumes that river changes take place at distinctly different scale levels. The speed at which the morphological processes take place can be characterised by a so-called morphological time-scale. De Vries (1975) defined a formula for the morphological time-scale with respect to large-scale aggradation and degradation. Based on this formula a rough estimate can be given of the speed at which the large-scale river morphology reacts to the changes in the river regime. The formula is used to compare the responses of different rivers to identical interferences. The morphological response has both a wave character (propagation of disturbances) and a diffusion character (smoothing and spreading of disturbances). Over short distances the wave character is dominant, while over larger distances the diffusion character is dominant. The morphological time-scale is defined as the time needed for the river bed to be lowered or aggraded by 50% of its ultimate erosion or aggradation due to an abrupt water level change at the downstream end (De Vries, 1975).

The morphological time-scale T_w based on the wave character of the morphology is given by:

$$T_w = \frac{L}{c} \tag{2.1}$$

in which L represents the length section [m] and c is the characteristic propagation speed of morphological features [m/s] that can be estimated with (De Vries, 1965):

$$c = \frac{b}{1 - \epsilon_p} \frac{s}{h} \tag{2.2}$$

in which b represents the degree of non-linearity of the flow velocity factor u in the transport formula $s = f(u)$ [-], s is the volumetric sediment transport rate per unit width [m^2/s], h is the water depth [m] and ϵ_p represents the porosity coefficient [-]. The degree of non-linearity b of $s = f(u)$ at point $(u_0, f(u_0))$ is given by:

$$b = \frac{u_0}{f(u_0)} \left. \frac{df(u)}{du} \right|_{u=u_0} \tag{2.3}$$

In case the transport formula is expressed as a general function of the averaged flow velocity to the power n:

$$s = f(u) = mu^n \tag{2.4}$$

b is approximated by n, viz.:

$$b = \frac{u_0}{f(u)} \left. \frac{df(u_0)}{du} \right|_{u=u_0} = \frac{u_0}{f(u_0)} \cdot m \cdot n \cdot u_0^{n-1} = \frac{u_0}{f(u_0)} \cdot n \cdot \frac{f(u_0)}{u_0} = n \tag{2.5}$$

The morphological time-scale T_d based on the diffusion character of the morphology can be determined as follow:

$$T_d = \frac{L^2}{K} \tag{2.6}$$

in which L is the length section [m] and K the effective diffusion coefficient [m^2/s]. This coefficient can be calculated from (De Vries, 1973):

$$K = \frac{b \cdot s}{3 \cdot i_b} \tag{2.7}$$

in which i_b represents the bed slope [-].

2.3   Field observations, measurements and modelling

In river morphological studies different categories of methods are used: theoretical analysis, field observations and measurements, physical scale modelling, empirical relationships and mathematical modelling are used. In the past, most research was primarily based on field observations

and measurements and physical scale modelling. With the increase of computer facilities, a shift to the use of mathematical models is noticed. The categories are, however, complementary and there is generally little point in preferring one category before the other. All categories of methods have their own strong points and limitations and the combined use provides better insight into the river behaviour.

Generally, preliminary studies are performed for the design of hydraulic structures or other human interventions. These studies include the estimation of the hydraulic effects and the morphological responses. In the early design stage (initiative, feasibility study) basic techniques (e.g. extrapolation from the past, empirical relationships, engineering judgement tools, equilibrium assessments) are used to get a quick indication of what might happen in the river. Detailed mathematical and scale models contribute to the more detailed description of the expected hydraulic and morphological consequences that is needed in the later design stages (functional design, technical design). Whenever the engineering measures have been realised, monitoring the system behaviour based on measurements and global observations, in addition to the use of mathematical models, is required to provide useful information during the operation and maintenance stage.

2.3.1 Field observations and measurements

Field observations and measurements form the basis of the various design and monitoring stages as indicated in the previous section, viz. (1) for basic techniques in the early design stage, such as extrapolation techniques and empirical relations, (2) for model calibration and validation in the later design stages (the amount of data that is available to calibrate and validate the model have its impact on predictive power of the model), and (3) for monitoring the system in operation and maintenance stage.

The quality of field observations and measurements is affected by several factors including:

- Measuring technology - Each instrument and method introduces its own errors and uncertainties. Modernisation of measuring equipment can cause inconsistency to appear in a data series. Inconsistency is a change in the amount of systematic error associated with the recorded data. It can arise from the use of different instruments and methods of observations.
- Measuring frequency - In the Dutch Rhine, for instance, bed soundings have been performed in the alluvial part of the river at cross-sections with a mutual distance of 100 or 125 m, on a yearly basis in the dry season. In fact the data are annual instantaneous recordings: snapshots. The soundings take place in months April through November, after the high water season. This implies that the time interval between successive soundings at a particular location may vary between 0.33 and 1.67 year. It implies that the sampling has a seasonal bias.

- Completeness of registration (gaps in data)
- Post-processing

Another important factor is the homogeneity of the dataset (Dahmen & Hall, 1989). Homogeneity means 'of uniform nature, similar in kind' or 'of the same quality or general property'. Non-homogeneity is a change in the statistical properties of the time-series. Homogeneity is affected by structural and incidental changes in the system. Due to obstrusive alteration in the environment of the 'measured' system, non-homogeneity can be introduced into the data series. Causes of non-homogeneity can be either natural or man-made. For instance, the homogeneity of the bathymetric database of the Dutch Rhine is amongst others affected by large-scale regulation works and dredging activities performed in the 19th and 20th century. Inaccurate and incomplete registration of the latter makes it difficult to homogenise the dataset. A dataset is stationary, if the population statistics are unaffected by the choice of time origin and are free from a significant trend in time. In fact a system could be homogeneous, whereas nonstationary.

With the assessment of the stochasticity of morphology, field observations and measurements have an extra function in this thesis. Adequate treatment of uncertainty starts with a good definition of the statistics of the uncertainty source requiring a large amount of data. Moreover, bathymetric data is required for the validation of the estimated stochasticity of morphodynamics considering various uncertainty sources. Regarding the latter, we have to realise that each bathymetric record reflects a single realisation of the dynamic behaviour of the river system. A particular sequence of conditions, for instance discharge, bed geometry, composition of bed material, etc., made the river evolve into the observed bathymetric state.

2.3.2   Modelling

Models approximate selected aspects of reality for the purpose of understanding the river system behaviour. They can be divided into *data-oriented* and *process-oriented* models.
In *data-oriented* models, measured data are used to derive rules of thumb, empirical relationships and simplified theory to obtain a first indication of the aspects to be described.
Process-oriented models can be divided further into *physical-scale* models and *mathematical* models.

Physical-scale models are applied in situations that are still hard to model otherwise and to study physical processes that are not completely understood. They give a better understanding of physical phenomena. This model type is rather labour-intensive, but can cope with more complicated processes. Scale and model effects make the application of these models rather non-trivial (Jansen et al., 1979).

The category of *mathematical* models contains various axes of classification.
One axis of classification is the process-based models, which are opposite to the behaviour-

oriented models (such as data-based models and empirical relationships). Mathematical process-based models describes waves, currents, sediment transport and bed level changes via a set of mathematical equations based on physical conservation laws, including a number of adjustable model parameters (Jansen et al., 1979).

Another axis of classification refers to analytical and numerical solution methods. Since in most practical cases the model equations cannot be solved analytically, numerical and approximative analytical solutions are sought. Analytical models are often used as a tool to contribute to the understanding of the essence of the river behaviour, leaving out as much complexity as possible. Numerical river models have become more and more powerful with the increase in computer capacity and the development of numerical methods. Hence they are suitable to deal with complex situations.

A third axis of classification refers to the state of description. This concerns the description of the river system at a certain time and spatial domain. The multi-scale character of a river system is discussed in Section 2.2.3.

The axis of classification that refers to how stochastics are included, is related to deterministic and stochastic modelling approaches. A brief introduction on these approaches is given in Section 1.2, we elaborate on this in Section 4.4.

This thesis focuses primarily on numerical process-based models used in a stochastic setting. Stochastic model approaches can be applied more easily to numerical models to analyse the stochasticity of the morphological response.

2.4   Numerical process-based models and engineering problems at different scales

Initial attempts to apply numerical process-based morphodynamic models can be found in the 1950s. In the 1970s, the branch of research was intensified and broadened. Since then, numerical modelling was mostly limited to 1-D models. More recently, numerous two- and 3-D models have been developed to simulate sediment transport processes and morphological changes (Wang & Weiming, 2004).

Numerical process-based models are usually based on mutually coupled deterministic descriptions of small-scale water motion and sediment transport processes. These descriptions have the form of physical conservation laws, viz. the conservation of water mass, the dynamic equation for the water motion (conservation of momentum), the conservation of sediment mass and the dynamic equation of sediment motion (frequently an empirical formula for sediment transport), including a number of adjustable model parameters (Jansen et al., 1979). While defining these continuity and momentum equations, assumptions with respect to steadiness and uniformity have to be made.

Numerical process-based morphodynamic models range from simple 1-D to multi-dimensional models. Each has its own area of applicability, due to the applied assumptions and model formulations. The applicability depends on the type of problem (the degree of detail required), as well as on the amount of data that is available to calibrate and validate the model. For the strategic planning of an entire river basin, a less detailed type of model might be used than for the study of scour around bridge piers, for example.

Increased detail, both in terms of resolution and in terms of physical processes taken into account, requires more computational effort, a larger amount of data and perhaps more unknown coefficients to be calibrated (Vreugdenhil, 2002). On the other hand, increase in detail requires less assumptions regarding physical phenomena. For instance, the flow-conveying floodplains and storage areas in floodplains should be explicitly defined in a 1-D morphodynamic model, whereas it is dynamically computed in a multi-dimensional model. Furthermore, a parametrisation for secondary flow is required in a 2-D model, whereas this is incorporated in a 3-D model.

Based on the problem definition, decisions have to be made about the number of dimensions in the model. In principle, river morphology concerns a 3-D problem. However, fully 3-D models are hardly available for river morphology and most problems do not need to be tackled by means of a 'complete' 3-D description (De Vries, 1993). A degree of schematisation is possible in many cases. Frequently, 1-D and 2-D models are used for morphological computations. A 1-D approach is possible if the width-averaged values of the dependent variables give sufficient information for the problem to be solved. A 1-D model can be used, for instance, to estimate the continuation of the large-scale tilting of the river Waal that was observed in the last century. 1-D models are being used in assessing large-scale processes in large reaches of a river. Problems related to the cross-sectional profile evolution, such as transverse bed slopes and pointbar/pool combinations in river bends, shallow parts at crossings between two opposite river bends and the local morphodynamic conditions at bifurcations require a 2-D model with a parametrisation for secondary flow or a 3-D model. For instance, a 2-D depth-averaged model can be used to establish the kind of bed protection in river bends for navigation purposes. Regions of rapidly varying flow conditions in combination with a complex morphodynamic situation, for instance the local scour development in time around groyne fields, revetments and bridge piers, require a 3-D model approach. The choice of using either a 1-D or a multi-dimensional approach is often a matter of computer capacity, budget and time available.

Chapter 3

Uncertainties in river morphology

3.1 Introduction

In the previous chapter we noted that numerical morphodynamic models have become a commonly used tool in engineering practice, providing insight into the physical system behaviour. The river environment is however of a dynamic and stochastic nature and the underlying processes are not completely understood. This lack of understanding leads to the question whether these processes and the ensuing phenomena can be described by models based on a set of deterministic differential equations and empirically derived sediment transport formulae. Apart from this, model-uncertainty results from the inability to accurately quantify the model parameters. In addition, a natural system, such as a river, is subject to uncertainties that are inherent to spatial and temporal processes in nature. For example, the composition of the bed material is not exactly known and the future discharge is inherently uncertain.

This chapter focuses on uncertainty and the applicability of stochastic methods in physical systems in general and in river systems in particular. Section 3.2 starts with general concepts of uncertainty. We proceed with uncertainty of relevance to river morphology in Section 3.3. A literature review on the present state of knowledge on stochastic modelling in the field of river morphology is given in Section 1.3. The state of knowledge in other research fields adjacent to river engineering, viz. Meteorology, Climatology, Hydrology, Ecology, Public Health, Hydraulic Engineering, is presented in Section 3.4. Background information on a number of stochastic methods is given in the same section. Numerical Integration, Monte Carlo Simulation (MCS), First Order Reliability Method (FORM), Response Surface Replacement Method, and Stochastic Differential Equations are described in detail.

3.2 Uncertainties

3.2.1 A classification of uncertainties

Different types of uncertainties are distinguished as, (Van Gelder, 2000):

- Inherent uncertainty
    - in time
    - in space
- Epistemological uncertainty
    - statistical uncertainty (parameter and distribution type uncertainty)
    - model uncertainty

Natural systems, such as river systems, include *inherent (intrinsic) uncertainties*, both in space and in time. This type of uncertainty represents variations in nature. Inherent uncertainty in time means that the realisation of the stochastic process in the future remains uncertain. Inherent uncertainty in space refers to the variation in space of a process. For instance the composition of bed material is inherently uncertain in time and in space, viz. the composition of the sediment supplied at the upstream boundary is a time-dependent process; lateral sorting of sediment in river bends and downstream fining are space-dependent processes. Neither unlimited data, nor unlimited research can eliminate inherent uncertainty.

Another type of uncertainty is *epistemological uncertainty*. This results from a lack of knowledge about the physical system and/or a lack of data. This type of uncertainty is subdivided into statistical uncertainty and model uncertainty.

Statistical uncertainty is introduced with the description of uncertain factors by amongst others probability distribution functions. These functions and their parameters are usually chosen based on data, a priori information and preferences of the modeller. Statistical uncertainty is generally subdivided into parameter uncertainty and distribution type uncertainty. The more data available, the smaller the statistical uncertainty is. Note that also inherent uncertainties in time and space are often specified using probability distribution functions and their parameters.

Model uncertainty refers to model incompleteness or imperfection. Generally, the model formulation is an approximation of reality, hence introduces uncertainties. Also, the parameters of the mathematical model are not exactly known. Uncertainties introduced by extrapolation of scale model tests to prototype scale and parameter inaccuracies originating from the data used for calibration are examples of model uncertainties.

Theoretical research, data collection and expert judgement are all aimed at increasing knowledge and thus reducing the epistemological uncertainty. Expert opinions (Cooke, 1991) can be used to determine the probability distributions of variables that are difficult to measure.

An uncertainty can be classified as either inherent or epistemological, but the class to which it belongs depends on the model definition. For example, when predicting the water levels under flood conditions with a numerical flow model, the hydraulic condition at the upstream boundary (e.g. the discharge) needs to be specified. This river discharge can be considered as inherently uncertain, whereas the uncertainty in the computed flood levels is a combination of inherent

and epistemological uncertainties. Even on the basis of an infinitely long data record, one could not predict exactly the river discharge that will occur on the 22nd of February next year, for instance. In a rainfall-runoff model (which determines the river discharge from precipitation at basin scale) the river discharge at the same location would include a combination of inherent and epistemological uncertainties, whereas precipitation is characterised as an inherent uncertainty.

A distinction can be made between uncertainties that are constant through the model run (within the time-horizon of the computation and within the spatial model domain - for instance parameters of the sediment transport formula) and 'stochastic' uncertainties that change in time and in space (for instance river discharge) (Van der Klis, 2003).

3.2.2 Sensitivity vs uncertainty analysis

Sensitivity analysis

Prior to an uncertainty analysis, a first selection between important and less important uncertainty sources can be obtained with a sensitivity analysis. Insight into the model sensitivity is achieved by systematically and deterministically varying the model input values one by one and estimating their impact on the model results. The probability of occurrence of a particular model input value is not taken into account.

The most common form of sensitivity analysis is Marginal Sensitivity Analysis (MSA). This method estimates the model output response due to a deterministic perturbation (i.e. no random selection involved) of each separate model input parameter around a selected pivot value. Meanwhile, the other variables are held constant at their pivot value. The combination of pivot values of the inputs, when put into the model, yields the reference model result. The sensitivity of each output quantity to each input quantity is expressed by the variation of each of the output quantities around its reference value, given the variation in the input quantity considered. A dimensionless form, the elasticity, can be obtained by multiplying the sensitivity with the ratio of pivot input value and the reference result.

A sensitivity analysis can also be performed from a global point of view. Local sensitivity concerns the model output variability due to variation in the model input at a selected (pivot) point in parameter space. For a model whose sensitivity feature varies from one region of the parameter space to another, the local sensitivity evaluated at this selected point would not shed much light on the sensitivity of the model over the entire domain of the parameter space. An analysis from global point of view focuses on the general model behaviour over a defined parameter space. Global sensitivity concerns the pattern of change in the model output due to a change in the model input over the entire parameter space (Chang et al., 1993).

In case the model result depends on many model-input parameters, the MSA requires much computation effort and the results are difficult to oversee and to compare. Since each model parameter is varied separately, the effect of mutual correlation on the relative sensitivities is

not considered.

Uncertainty analysis

An uncertainty analysis estimates the stochasticity of the model results, making use of the relationship that the model establishes between its inputs and its outputs. It helps identifying causes and effects of uncertainties in the model outputs. It gives insight into the likelihood of the model output and indicates the domain in which the model is applicable and provides useful output. Subsequently, the analysis provides information with respect to the possible improvement of the model (i.e. reducing the epistemological uncertainty) (Janssen et al., 1990 and Chang et al., 1993).

Uncertainty analysis starts from the probability distribution of each input. In this analysis the entire set of relevant model inputs is considered, the probability distribution function of each model input is determined, including its correlation with other inputs, and the impact of the uncertain model input on the model results is assessed.

Two major concerns in uncertainty analysis are:

1. a priori assumptions concerning the form of dependence and/or correlation structure (see Section 3.2.3) - physical dependency is discerned from correlation in this thesis. Physical dependency means that the form of dependence is based on a physical process, for instance, the hydraulic roughness is related to the discharge stage. Types of correlations that can be distinguished, are (a) correlation between different uncertainty sources, (b) (auto-) correlation in time (c) (auto-) correlation in space.

2. a proper definition of the uncertainty sources (see Section 3.2.4) either by means of classical probability distribution functions, or by applying resampling techniques.

3.2.3   (Auto-)correlation between uncertainties

Several types of correlation can exist between model input. The following types of correlation can be distinguished:

- correlation between model input variables.
- (auto)-correlation in time. This means that the value of a model input variable at an arbitrary point in time is correlated with the value of this variable at a previous point in time. For example, the river discharges in the river Rhine at successive days are mutually dependent.
- (auto)-correlation in space. (Auto)-correlation in space implies that model input variables at a spatial point in the system is correlated to an adjacent point in the system. For instance, the composition of bed material in the Rhine is spatially correlated as a consequence of sorting processes. Examples of sorting processes are river bed armouring, lateral sorting in river bends and downstream fining.

Auto-correlation is often discarded and simplified (Van der Klis, 2003). It has been pointed out that neglecting correlation could have a significant effect on the results (Thoft-Christensen & Baker, 1982). Chang et al. (1994) conclude that excluding correlation among stochastic parameters leads to an overestimation of the uncertainty in the scour depth around a bridge pier. In Duits et al. (2000), the impact of the spatial correlation of the hydraulic roughness in river sections is studied. They conclude that, if the hydraulic roughness in the main channel is highly spatially correlated, the uncertainties in flood levels are larger than if they are uncorrelated. In probabilistic engineering an upper and a lower bound is considered for the reliability of civil engineering structures. The reliability of a structure depends often on more than one system element. Full dependency between system elements results into a lower bound of the probability of failure. This implies that the failure of one system element invokes the failure of the other element(s). The upper bound of the probability of failure exists if the system elements are mutually independent (Ditlevsen, 1979).

The correlation between observations at successive moments in time and between adjacent observations in space gives an indication of the persistence of a data series. Persistence of a data series is considered as the time or space independence of a particular value in this data series. The serial-correlation coefficient is a technique to verify the independence of a particular value in a data series. To determine the correlation between adjacent observations c intervals apart, the *lags c sample serial-correlation coefficient* is given by (Box et al., 1994):

$$r_{\mathrm{c}} = \frac{\sum_{k=1}^{N} \left(F_k - \bar{F} \right) \left(F_{k+c} - \bar{F} \right)}{\sqrt{\sum_{k=1}^{N} \left(F_k - \bar{F} \right)^2}} \tag{3.1}$$

in which F_k is an observation at time t_k. The symbol r is often used as reasonable estimator of mathematical parameter ρ, see Eq. 3.10. The auto-correlation function containing serial-correlation coefficients for different lags shows to what extent data points are still related in time or in space. The correlation coefficient is misleading, as it does not properly indicate the significance of a certain observation for the observation c intervals apart. The coefficient suggests the existence of more dependency than exists, and this problem gets worse as the correlation approaches zero. The squared serial-correlation coefficient, r^2, that describes the proportion of variance in common between the two output samples, is a better measure to indicate persistence. It is called the coefficient of determination. When the serial-correlation coefficient drops below 0.7, the coefficient of determination is approximately 0.5, meaning that the bed level state depends for less than 50% on the bed level state in the preceding period. Below this stage, the mutual dependency is considered moderate to weak.

The *Pearson correlation method* and *Spearman's Rank correlation method* can be used to verify the presence of a statistically significant trend.

The *Pearson correlation method* (Janssen et al., 1990) is a method to verify the presence of a

linear trend. If the data series F consists for instance of a time series of length N, the linear correlation coefficient $r_{t,F}$ indicating the linearity between observations F as a function of time t, can be estimated by:

$$r_{t,F} = \frac{\sum_{k=1}^{N} (t_k - \bar{t}) (F_k - \bar{F})}{\sqrt{\sum_{k=1}^{N} (t_k - \bar{t})^2} \sqrt{\sum_{k=1}^{N} (F_k - \bar{F})^2}} \qquad (3.2)$$

in which F_k is an observation at time t_k.

This methods tends to fail if the relationship (trend) is strongly non-linear. For this reason the method is less applicable to the highly non-linear morphodynamics.

The *Spearman's rank correlation method* is often used to test the presence of a trend. The method is recommended by Dahmen & Hall (1989). The method is simple and distribution-independent, meaning that it does not require the assumption of an underlying statistical distribution. Another advantage is its nearly uniform power for linear and non-linear trends. *Spearman rank correlation method* is based on data ranking. The points of time $t(k)$ with $k = 1, ..., N$ are ranked from the smallest to the largest value. The smallest value is replaced by 1, the consecutive smallest value is replaced by 2, and so on. K_t is the rank of the values $t(k)$. The series of observations $F(k)$ is transformed to its rank equivalent K_F, by assigning the rank number of an observation in the original series to the corresponding order number in the ranked series, $t(k)$. If there are ties (i.e. two or more ranked observations, F, with the same value) the convention is to take K_t as the average rank. Spearman's rank-correlation coefficient is defined as:

$$R_{SP} = 1 - \frac{6 \cdot \sum_{i=1}^{N} (K_{t_i} - K_{F_i}) (K_{t_i} - K_{F_i})}{N \cdot (N \cdot N - 1))} \qquad (3.3)$$

in which N is the total number of data points and i is the chronological order number. This correlation coefficient represents the monotonic relation between t and F. In case the coefficient is close to $+1$ or -1, the value of F will increase or decrease with t, respectively. There is no monotonic relation between t and F, if the coefficient is close to zero.

The null hypothesis, $H_0 : R_{SP} = 0$ (there is no trend), is tested against the alternative hypothesis, $H_1 : R_{SP} <> 0$ (there is a trend), with the test statistics:

$$t_t = R_{SP} \left[\frac{N - 2}{1 - R_{SP} \cdot R_{SP}} \right]^{0.5} \qquad (3.4)$$

in which t_t has Student's t-distribution. The Student's t-distribution is symmetrical around $t = 0$. In other words, according to a 95%-confidence interval, the data series has no trend if:

$$t \{N - 2, 2.5\%\} < t_t < t \{N - 2, 97.5\%\} \qquad (3.5)$$

A data series is stationary if no statistically significant trend is observed and if the variance and the mean of the data series are stable in time. The data series is split up in two non-overlapping subsets of the data series to test the stability of the variance and the mean. The

computed variance and mean of the two sub-sets are compared. The statistical tests can be applied to analyse the stability of the variance and the mean of the two sub-sets.

3.2.4 Definition of the statistics of uncertainty sources

Adequate treatment of uncertainty starts with a good definition of the statistics of the uncertainty source. Probability distribution functions and statistical resampling techniques can be used to do so. These techniques are discussed below.

Use of probability distribution functions

The specification of the probability distribution type and parameters of the stochastic input is often subjective. The specification can introduce statistical uncertainty related to distribution type uncertainty and parameter uncertainty. These uncertainty types cannot be separated. If the probability distribution type is uncertain, the parameters of the distribution function are uncertain too (Slijkhuis et al., 1999). Three methods are available to specify the probability distribution type and estimate its parameters, namely the *classical statistics method*, the *subjective method* and the *Bayesian method*.

For the *classical statistics method* the distribution type and its parameters are estimated on the basis of available data records. Probability distribution types are often characterised by their central moments (Morgan & Henrion, 1990). The mean or expected value of the distribution μ is known as the first central moment. More generally, central moments are defined as the expectation of the kth power of the difference between X and its mean. The k$^{\text{th}}$ central moment of random variable X reads:

$$\mu_k = \int_X (x - \mu)^k f(x)\, dx \tag{3.6}$$

or, for discrete distributions,

$$\mu_k = \sum_X (x - \mu)^k p(x) \tag{3.7}$$

in which μ_k is the k$^{\text{th}}$ central moment of X, μ is the mean of X, $f(x)$ is the probability density function and $p(x)$ is the probability mass function.

The second central moment, μ_2, is more commonly known as the variance and denoted as σ^2. The variance and its square root, σ, the standard deviation, reflect the amount of spread or dispersion in the distribution.

The probability distribution type can be characterised and classified additionally, using dimensionless measures based on the third and fourth central moment, viz. the coefficient of skewness β_1 and the coefficient of kurtosis β_2 of the distribution type:

$$\beta_1 = \frac{\mu_3}{\sigma^3} \tag{3.8}$$

$$\beta_2 = \frac{\mu_4}{\sigma^4} \tag{3.9}$$

The skewness coefficient is a indication for asymmetry of the distribution. Positive skew is commonly observed with highly variable quantities that can take on only positive values. The kurtosis indicates the degree to which the distribution is flat as opposed to having a high central peak.

Pearson & Kendall (1970) introduces a relation between the coefficient of skewness and the coefficient of kurtosis and the corresponding probability distribution type, as shown in Figure 3.1. Moreover, probability plots and goodness-of-fit tests, such as the Kolmogorov-Smirnov-test and the Chi-square test (Benjamin & Cornell, 1970) are commonly used to select an appropriate distribution type and verify its statistical significance.
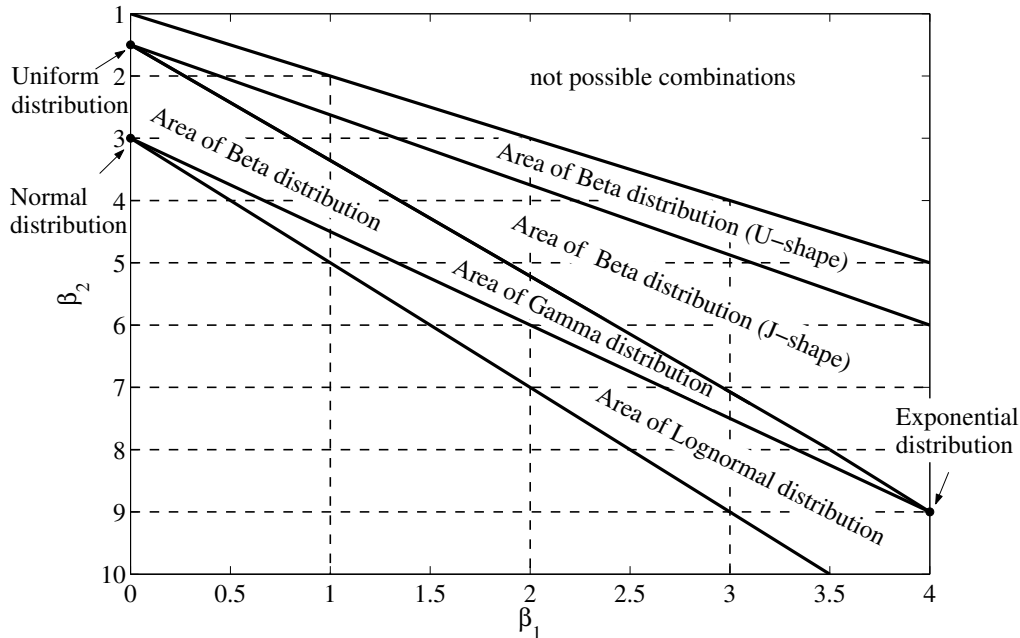
Figure 3.1: Relations between β_1 and β_2 of the different distribution types (Pearson & Kendall, 1970)

Having hypothesised the type of the probability distribution function, various classical parameter estimation methods are available to estimate the statistical parameters of that function using the available data record, such as the methods of moments, maximum likelihood or least squares. Apart from these classical methods, also the method of L-moments, the Bayesian method, the entropy method and non-parametric methods can be used (Van Gelder, 2000). Many attempts (Burcharth & Lui, 1994, Yamaguchi, 1996 and Goda & Kobune, 1990) have been made to assess which method is preferable for the parameter estimation of a particular probability distribution function. The method with the smallest bias and variance is considered to be the best for the particular distribution function.

The main point of interest is the capacity of each method to predict p-quantiles (where $p << 1$). The performance of the parameter estimation method with respect to its small-sample beha-

viour and its under- and overestimation of p-quantiles is analysed in Van Gelder & Vrijling (1997).

The *subjective method* uses experience and intuition from experts and data obtained from literature to estimate the parameters of the probability distribution function. This is called subjective parameter estimation (Cooke, 1991).

A difficulty in fitting probability distributions and estimating their parameters is that there is often a limited amount of data. A major drawback of the classical and subjective method is that statistical uncertainty resulting from this cannot be taken into account. The *Bayesian statistics* (Box & Tiao, 1973) considers the statistical uncertainty and combines the *classical statistics method* and the *subjective method*. We discern two types of statistical uncertainty: parameter uncertainty (when the parameters of a distribution are unknown) and distribution uncertainty (when the type of distribution is unknown). On the basis of theoretical considerations, experience and expert knowledge, an a priori probability distribution function and its parameters are estimated. Using Bayes' Theorem, the prior distribution is updated to the posterior distribution as soon as data becomes available. The Bayesian estimates of the statistical parameters account for the parameter uncertainty. The more data is available, the smaller the parameter uncertainty. Using Bayes' statistics it is possible to discriminate between different distribution types. To that end, the Bayes' factors are used to determine the weights corresponding to how well a probability distribution matches with the data. The probability distribution function for which the bias of its prediction is large should be given less weight than those exhibiting less bias: so the better the fit, the higher the weight.

So far, we focus on the use of univariate distributions, that is, probability distributions of a single-dimension. If two or more model inputs or parameters are stochastically dependent or include a dependence structure in space or time, it may be necessary to model their uncertainty with a multivariate probability distribution function. For the construction of these multivariate distribution functions information about (1) the marginal distribution of each of the components and (2) the correlation among the components is required. Most often it is easier to specify the marginal distributions and correlations than the joint multivariate distributions. Moreover, plausible marginal distributions and correlation frequently imply a joint distribution of unknown functional form. For cases where the marginal distributions are either normal or lognormal, it is rather straightforward to calculate analytically the correlation of the underlying normal distributions to induce the desired correlation between the model inputs (Grimmett & Stirzaker, 1992). It is more difficult in case of arbitrary marginal distributions. Shapiro & Wilcox (1996) propose methods for estimating the multivariate distribution function with specified marginal distributions that are not normal or lognormal for applications in econometrics. Coles & Tawn (1991) and Coles et al. (1999) have also published on methods for estimating non normal multivariate distributions. They focus in particular on modelling extreme events.

Problems concerning environmental extremes are often multivariate in character. Quantifying dependence in extreme data is a central theme in statistical methods for multivariate extreme values. For example, coastal flooding is likely under the combined conditions of extreme surges and wave heights, both processes driven by meteorological conditions. Flooding therefore depends on whether the still-water level and wave processes arise independently or not.

One way of circumventing multivariate problems is to consider a kind of structure function, representing the quantity of interest that depends on other variables. This structure function could range from simple relationships to more complex numerical models. Outputs of the structure function can be constructed using inputs of the basic variables, either obtained from data records, or synthesised from less complex univariate distributions.

Use of statistical resampling techniques

Resampling departs from classical statistics that is largely based on assumptions (often made in an ad-hoc manner) regarding the form of a distribution function and its parameters. Classical statistics usually require a large sample size and physical information on the variable to be statistically described. If one is uncomfortable about the use of theoretical distributions, or the sample size is small and does not conform to the parameterization assumptions, empirical resampling is a good alternative (Efron, 1982). The technique is based upon repeated sampling within the historical data record. A draw-back is therefore, that values beyond the original record are not found.

Various resampling techniques can be discerned, starting from the *Jackknife* and *Bootstrap techniques* (Efron, 1982) to more advanced resampling techniques like the *Nearest-Neighbour technique*. For the Jackknife technique a resample is extracted from the original record by randomly deleting a fixed number of samples. The Bootstrap technique is based on random selecting samples out of the original record. The samples can be arranged randomly to construct new series. Fan & Wang (1996) conclude that the Bootstrap technique provides less biased and more consistent results than the Jackknife technique. The *Jackknife* and *Bootstrap techniques* assume independent and identically distributed data, i.e. data that is not affected by any correlation structure. However, in some cases the dependence structure of successive records in time and/or space, as well as the correlation among other uncertainty sources, should be preserved. The Nearest-Neighbour technique (Lall & Sharma, 1996 and Rajagopalan & Lall, 1999) is a resampling technique that preserves the dependence structure of the original data and considers the statistical correlation among the different variables.

3.2.5   Relative importance of uncertainties

A major source of uncertainty in the prediction of a simulation model arises from uncertainties related to model inputs. Input uncertainty exists independently of any model. In this section we

discuss the importance of input variables for the model outputs of a specified simulation model. Techniques estimating the relative contribution of each model input enables us to discriminate between important and less important sources of uncertainty in input variables. Many of these techniques rely on regression methods that are based on the assumptions of linearity. The validity of these assumptions is of importance to evaluating the appropriateness of the analysis techniques.

Suppose that for a particular model, the output Y is determined by a vector of model inputs $X_1, ..., X_p$. The probability distributions F_X of the model inputs X_i induce on Y the probability distribution F_Y, the prediction distribution.

If the model inputs X_i are mutually independent and the output Y is linear in X_i, the easiest way to represent the importance of uncertainty source X_i for output Y is using the *correlation coefficient*:

$$\rho(Y, X_i) = \frac{Covar(X_i, Y)}{\sigma_{X_i} \sigma_Y} \tag{3.10}$$

in which $Covar(Y, X_i)$ is the covariance between X_i and Y, σ_{X_i} and σ_Y are the standard deviation of uncertainty source X_i and output Y, respectively. The covariance $Covar(X_i, Y)$ is expressed as $E((X_i - \mu_{X_i})(Y - \mu_Y))$.

The percentage of the variance of Y that is explained by the linear model is represented by $R^2 = \sum_{i=1}^{N} \rho^2(Y, X_i)$. If R^2 is less than one, this may be caused either by dependencies in the X_i's or by contributions of higher order terms, i.e. non-linearity in the process.

McKay (1997) proposes a non-parametric analysis of the variance of the model output Y which is based on the properties of variance alone, and not on any particular relationship between model output and input. The prediction uncertainty in Y is characterised by its induced probability distribution, which depends on the uncertain model inputs X_i. Fixing the model inputs at single values reduces the prediction distribution to a single point. The importance of a subset of model inputs with regards to the prediction distribution is investigated. Using variance as indicator of importance, the question is to what extent does the prediction variance decrease when a subset of the model inputs is kept fixed. The prediction variance of the full model and the conditional prediction variance determined by the fixed subset of model inputs are compared. The objective of a variance-based method is to find a subset of the model inputs that drives the prediction variance. The measure of importance of X_i with variance-based methods is the *correlation ratio*:

$$CR_i = \frac{Var(E(Y|X_i))}{Var(Y)} \tag{3.11}$$

in which variance Var is the second central moment, see Section 3.2.4.

Global sensitivity measures like *correlations* and *correlation ratios* may not be appropriate when we are interested in a specific range of the model output. Lack of resolution can limit its usefulness, especially when the effect of a model input X_i on the model output Y varies

drastically over its parameter space. Considering dike ring reliability, for instance, we are not interested in model inputs that drive this reliability on normal days (Cooke & Van Noortwijk, 1999). The interesting driving inputs are those when the dike is near failure. Global measures will be predominantly influenced by regular conditions.

A local sensitivity measure provides a more detailed description of the importance of the model input in a selected range of the output space (Cooke & Van Noortwijk, 1999). Percentile cobweb plotting is a way to represent graphically the relation between the joint probability distribution, in percentiles, of model output Y and a number of explanatory model inputs. The idea of the graphical representation of multi-dimensional distribution via cobweb plots is to take a sample, find percentiles of the variables to which a given sample belongs, and draw lines between the points. Figure 3.2(a) illustrates an example of a cobweb plot. Each vertical line represents the percentile scale of one variable and each broken line represents one sample, intersecting each vertical line in the appropriate (quantile) percentage point. Connecting the lines from left to right we represent the sample path. On the basis of Figure 3.2(a) it is not easy to recognise correlation structures between output and inputs. To make dependence structures more apparent, conditional cobweb plots can be used, where conditioning is done on various values of the model output. Figure 3.2(b) shows the same cobweb plot, where conditioning is applied, selecting on the top 10 percentiles of the output values. This conditional cobweb plot indicates a strong correlation between top percentiles of model output Y and model inputs X_1 and X_2. The correlation between the model output and the other inputs X_3 and X_4 seems to be poor.

(a) Cobweb plot

(b) Conditional cobweb plot. The joint distribution is conditionalised on the top 10 percentiles
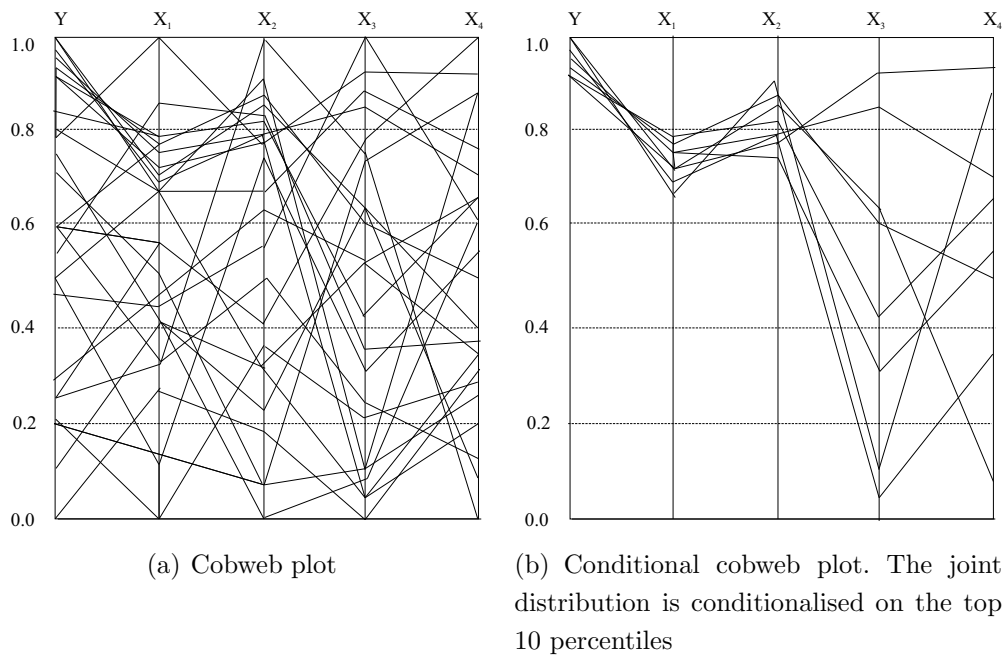
Figure 3.2: Cobweb plots

Morphodynamic systems exhibit the following properties, (1) a strong non-linear behaviour, (2) a time and space dependent signature, (3) model inputs that are mutually correlated, and non-normally distributed, (4) a time lagging effect. Then, it becomes more ambiguous to estimate the relative importance of each individual source to the overall uncertainty. In that case, the relative contribution will probably vary as a function of time and space.

3.3 Uncertainties related to river morphology

Morphological river models are designed to provide insight into the morphological response to human interventions or changes in environmental conditions. Models schematise 'reality', which in case of the river environment is of a dynamic and stochastic nature. Moreover, uncertainties are introduced via the model schematisation and input (see Figure 3.3):

- Model schematisation:
  Uncertainties in model structure are epistemological. They are due to a lack of knowledge of processes, or due to discarding phenomena supposed to be of minor importance. Examples of the latter are one- or two-dimensional modelling, instead of three-dimensional modelling, modelling sediment transport with an empirical formula, and assuming uniform sediment instead of graded sediment.

- Boundary conditions:
  In a morphodynamic model describing a river system of sub-critical flow and carrying non-cohesive bed material, boundary conditions have to be specified for the water motion, e.g. a discharge series at the upstream boundary and a rating curve at the downstream boundary. At the upstream boundary a morphological condition also has to be given, e.g. the sediment supply or the bed level position. Uncertainties in boundary conditions include epistemological uncertainties (as a consequence of limited data available) and inherent uncertainties. Inherent uncertainties exists in the rating curve at the downstream boundary and in the river discharge and the sediment transport at the upstream boundary.

- Initial condition:
  At the beginning of a model simulation the bed level and water level distributions, the river discharge and the bed material composition have to be given. The uncertainties introduced in this stage are inherent and epistemological uncertainties.

- Model parameters:
  The hydraulic roughness, the parameters in the sediment transport formula, and the river geometry are model parameters that have to be specified. Epistemological uncertainties are introduced due to the limited availability of site-specific data. Part of the uncertainties are considered as inherent uncertainties in space.

- Model simulation process:

  The implementation errors of a mathematical model and the truncation error as a result of a numerical approximation are introduced in the model schematisation. Uncertainties in the numerical parameters are characterised as epistemological model uncertainties.

- Input scenarios:

  Input scenarios describe the future conditions. An increase of the river discharge due to climate change is an example. The input scenarios may affect the boundary conditions, initial conditions and model parameters. Uncertainties in input scenarios are considered as inherent.
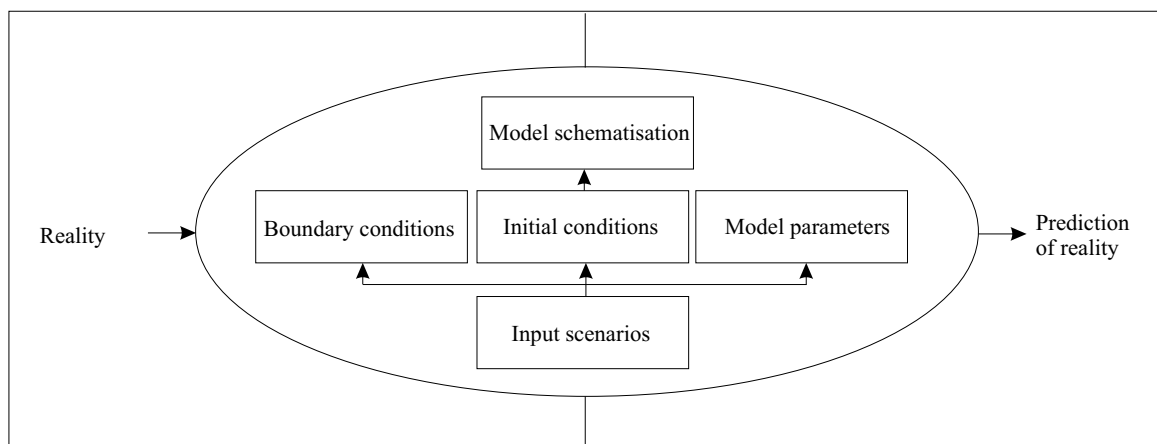
Figure 3.3: Uncertainties introduced via the model schematisation and the specification of model inputs

The way uncertainties in the model input propagate through the model during the simulation affects the uncertainty in the morphological response. It is conceivable that some uncertainties decrease and others increase in time. The relevance of the model input uncertainty may be different for short-term, medium-term and long-term predictions, respectively.

3.4   Stochastic modelling

3.4.1   Stochastic methods

A stochastic method copes with the variability of large complex system behaviour. Mathematical models that provide insight into the processes underlying this system behaviour display many of the following properties (Iman & Helton, 1988):

- many input and output variables;
- model is time-consuming to run on a computer;
- alterations to the model are difficult and time-consuming;

- it is difficult to reduce the model to a single system of equations;
- discontinuities exist in the behaviour of the model;
- correlation exist between the model input variables;
- the associated marginal probability distributions of the model input variables are often non-normal;
- model predictions are non-linear multivariate time-dependent functions of the input variables;
- the relative importance of the individual input variables is a function of time.

The objective of a stochastic method is to quantify uncertainties (statistical characteristics) in the model output. In addition, the method can be applied to estimate the relative contribution of various sources of uncertainty in the model input to the overall uncertainty in the output. Examples of stochastic methods that are commonly used (see Section 1.3 and Section 3.4.2) are Numerical Integration, Monte Carlo Simulation, First Order Reliability Method, Response Surface Replacement Method and Stochastic Differential Equations. A brief description of these methods, along with some applications in research areas adjacent to river hydraulics and morphology, are given in the sections below. The methods are considered potentially suitable to study the stochastic nature of river morphology. Their applicability to river morphology is further discussed in Section 4.4.

The model output Y is assumed to be a function of p stochastic variables X_i:

$$Y = g\left(X_1, X_2, ..., X_p\right) = g\left(\vec{X}\right)|g : \Re^p \to \Re^1 \tag{3.12}$$

The cumulative probability distribution function of Y is defined as a function of the probability density functions of the stochastic variables:

$$F(Y) = \int_{-\infty}^{X_p} \int_{-\infty}^{X_p} ... \int_{-\infty}^{X_1} f_{X_1, X_2, ..., Xp}(X_1, X_2, ..., X_p) dx_1, dx_2, ..., dx_p \tag{3.13}$$

This integral can often not be solved analytically. Numerical methods are useful to estimate the solution.

Numerical Integration uses discretisation to approximate the solution of Eq. 3.13 analytically. Monte Carlo Simulation approximates the output statistics (Eq. 3.13) by running a deterministic model of output Y (approximation of Eq. 3.12) repeatedly, each run with a different set of model inputs which are statistically equivalent. First Order Reliability Method (Morgan & Henrion, 1990) is based on linearising the model output function Eq. 3.12, after which the output statistics are determined. In the Response Surface Replacement a meta-model is developed that replaces the model output function Eq. 3.12. All inferences with respect to uncertainty and sensitivity analyses for the model output function Eq. 3.12 are derived from this meta-model (Iman & Helton, 1988). In the method of Stochastic Differential Equations not only input variables X_i are considered to be stochastic, as well the output function Eq. 3.12 describing the physical system behaviour is a stochastic process.

Numerical Integration

Numerical Integration uses discretisations to approximate the solution of Eq. 3.13 numerically. If the probability distribution function depends on one stochastic variable, it can be estimated by integrating over this particular stochastic variable. It is often not possible to solve these integrals analytically. Therefore, numerical integration methods have been developed (CUR, 1997). A relatively simple numerical integration method is the Riemann integration.

Riemann integration is often used in structural reliability engineering that defines a reliability function, Z, equal to 'Resistance' minus 'Load'. The probability of failure, $Z < 0$ is described as:

$$P_f = \int_{Z<0} f_{\vec{X}}\left(\vec{X}\right) dx_1, dx_2, ..., dx_p = \int_{Z<0} dF_{\vec{X}}\left(\vec{X}\right) = \int_0^1 l\left(Z\right) dF_{\vec{X}}\left(\vec{X}\right) \qquad (3.14)$$

in which $l\left(Z\right)$ is an indicator function, which equals one if the system fails and which equals zero if the system does not fail. This function indicates which part of the integration area contributes to the probability of failure.

In the Riemann procedure the integration domain is divided into grid cells (discretisation). The integration step is constant, which results in a variable step size $dF_X(X)$. In the part of the integration domain with a small probability density the step size is smaller than in the part with a large probability density.

In case of Riemann integration with more than one variable, the multi-dimensional cumulative probability distribution function has to be transformed analytically into independent one-dimensional cumulative probability distribution functions of all stochastic variables. The probability distribution function of the model output can be estimated numerically, based upon the summation of these one-dimensional functions. To make use of the Numerical Integration, the analytical expression of the cumulative probability distribution function of each stochastic variable has to be available. The accuracy of Numerical Integration is relatively high. The smaller the discretisation step, the more accurate the result. The computation effort increases as the discretisation step decreases.

Monte Carlo Simulation

The principle of Monte Carlo Simulation (MCS) (Hammersley & Handscomb, 1964) is to run a deterministic model repeatedly, each run with a different set of model inputs which are statistically equivalent. These sets of model inputs should be randomly generated, according to a proper definition of the statistics of and the correlation structure between the different inputs. To that end, the Crude Sampling technique is most commonly used. On the basis of the set of outputs of all model simulations, the model results can be analysed statistically, in terms of expected value, variance, percentile values and confidence intervals.

A major concern of MCS with crude sampling is the inefficiency of this method. The number of runs that is required for the convergence of the output statistics can be large. This is especially the case if many stochastic model inputs are involved and if computationally intensive numerical models are used. This can make the MCS to a laborious operation. Additionally, the method becomes more complicated with the presence of correlations between model inputs.

The use of efficient sampling techniques may reduce the required number of model runs. An example of such a technique is Latin Hypercube Sampling (Hammersley & Handscomb, 1964). This reduces the sample size by 'stratified' sampling. The domain of the stochastic input is divided into N disjunctive intervals with the same probability of occurrence. Then the crude sampling method is applied to randomly draw one value from each interval. This leads into N sampled values for each model input. The sampled values of the first model input are randomly connected to those of the second model input. These pairs are randomly combined with the samples values of the third parameter, and so on. Eventually, this results in N combinations of p model inputs. This sampling technique results in a reduction of the sample size.

First Order Reliability Method

The First Order Reliability Method (FORM) is based on the linearisation of a model (Morgan & Henrion, 1990). The method is commonly applied in risk evaluation studies of hydraulic structures in hydraulic engineering to assess the reliability of structures under design conditions. The FORM gives an estimate of the probability of failure and also an influence factor of each variable, indicating the variable's importance to the final result (Reeve et al., 2004). Van der Klis (2003) and Maurer et al. (1997) used the method to estimate uncertainties in river morphological responses.

The principle of FORM is briefly described. Consider the model output Y as a function of the stochastic variables X_i, Eq. 3.12. The stochastic variables are assumed statistically independent and Gaussian distributed with mean μ_{X_i} and standard deviation σ_{X_i}. The model can be approximated by its Taylor series expansion:

$$
f\left(\vec{X}\right) = f\left(\vec{X}_0\right) + \sum_{i=1}^{p} \left.\frac{\partial f}{\partial X_i}\right|_{\vec{X}_0} (X_i - X_{0_i}) +
$$
$$
\frac{1}{2!} \sum_{i=1}^{p}\sum_{j=1}^{p} (X_i - X_{0_i})(X_j - X_{0_j}) \left(\left.\frac{\partial^2 f}{\partial X_i \partial X_j}\right|\right)_{\vec{X}_0} + \text{h.o.t.} \qquad (3.15)
$$

in which the subscript X_0 indicates that the derivative is evaluated at this point, and h.o.t. stands for higher order terms.
From this expression the expected value and the variance of Y can be estimated by using the linearity of the expected value μ_Y in its arguments and the relation $\sigma y^2 = \mu_{Y^2} + \mu_Y^2$. In the

FORM, the second and higher order terms in Eq. 3.15 are neglected. The expected value and variance of Y reads:

$$\mu_Y \approx f\left(\vec{X}_0\right) + \sum_{i=1}^{p} \frac{\partial f}{\partial X_i}\bigg|_{\vec{X}_0} (\mu_{X_i} - X_{0_i}) \tag{3.16}$$

$$\sigma_Y^2 \approx \sum_{i=1}^{p} \left(\frac{\partial f}{\partial X_i}\bigg|_{\vec{X}_0} \sigma_{\vec{X}_i}\right)^2 \tag{3.17}$$

The partial derivative term in Eq. 3.16 is called the local sensitivity coefficient. This is an indication for the local sensitivity of stochastic variable X_i around the evaluation point $\vec{X}_0$.

Starting-point of the FORM described above, is that the stochastic variables are Gaussian distributed and mutually independent. Many 'flavours' of FORM are available, that could also deal with non-Gaussian variables and mutual correlation structures, see Thoft-Christensen & Baker (1982) or Reeve et al. (2004).

The FORM is accurate if the relation between model output and input is linear or close to linear. To check the validity of the linear approximation, Beal's non-linearity measure was developed, which measure consists of a statistical test. If the ratio of the error of the first-order approximation and that of the zero-order approximation is large, the first-order term contributes relatively much to the non-linear relationship. The second-order term is expected to be significant and may not be neglected. The Beal's non-linearity measure is discussed in Kuczera (1988).

An advantage of the FORM is that it is easy (a small number of computations is required) to identify which stochastic variables are important. The relative contribution C_i of each stochastic input parameter to the overall uncertainty defined as:

$$C_i = \frac{\left(\frac{\partial f}{\partial X_i}\big|_{\vec{X}_0}\right)^2 \sigma_{X_i}^2}{\sigma_Y^2} \tag{3.18}$$

An disadvantage of this method is that the computation of the derivatives can be time-consuming and difficult for large models. Numerical approximations and the Reduced Rank Square Root can be applied to make this easier. The former method is aimed at the numerical approximation of the derivatives. The latter method reduces the computation effort (Verlaan, 1989).

Response Surface Replacement Method

In the Response Surface Replacement Method a meta-model is developed that replaces the computer model. All inferences with respect to uncertainty and sensitivity analyses for the computer model are derived from this meta-model (Iman & Helton, 1988).

The meta-model, known as the fitted response surface, can be developed on the basis of N model outputs Y_i resulting from deterministic computer simulations driven by a number of selected sets of model inputs $X_1, ..., X_p$. The meta-model is strongly affected by these selected sets of model inputs (Iman & Helton, 1988). The meta-model can be used in a Monte Carlo mode.

The Response Surface Replacement Method is only recommended if the computer model can be adequately replaced by a simplified meta-model.

Stochastic Differential Equations

The time varying behaviour of many physical phenomena is described by deterministic ordinary differential equations. If the state of the physical system at time t is defined as $x(t)$, the time varying behaviour is described with:

$$\begin{aligned} \tfrac{dx}{dt} &= f(x, t) \\ x(t_0) &= x_0 \end{aligned} \qquad (3.19)$$

However, when uncertainties are involved in the physical system behaviour, the state of the physical system should be described in terms of probability. To that end, Stochastic Differential Equations can be used as a model to describe this stochastic process X_t:

$$\begin{aligned} \tfrac{dX_t}{dt} &= f(X, t) + g(X_t, t) N_t \\ X_{t_0} &= X_0 \end{aligned} \qquad (3.20)$$

A stochastic process N_t introduces model uncertainties in the underlying deterministic differential equation. The initial condition X_0 is assumed to be a random variable.

Stochastic partial differential equations are very similar to ordinary partial differential equations. The difference is that stochastic partial differential equations describe stochastic processes, induced by random coefficients, initial values, or forcings. The problem is that many concepts, like differentiation, integration and numerical approximations need to be completely revised. The theory of stochastic (partial) differential equations, their application and numerical solution methods are described by Kloeden et al. (1994) and Jazwinsy (1970).

3.4.2 Stochastic modelling in research areas adjacent to river morphology

A variety of the stochastic methods are applied in different research areas to perform uncertainty analyses. An overview of the application of stochastic methods in the field of river hydraulics and morphology is presented in Chapter 1. An overview in research areas adjacent to river hydraulics and morphology is given below.

Meteorology

In the past, weather forecasts were based on deterministic model computations. The predictability of these models is limited. Deterministic weather forecasting beyond two weeks is not possible due to the chaotic nature of the system, and even weather forecasts one day ahead are not 100% reliable. Small errors in the initial state of the model computation develop within a few days into large errors. In the Netherlands, the Royal Dutch Meteorological Institute uses probabilistic methods to reveal uncertainties in weather forecasts. The probabilistic ensemble method was developed to express weather forecasts in probabilistic terms. Ensemble prediction is a straightforward tool to generate the probability distribution of the weather. In an ensemble system the same forecast is repeated a large number of times from perturbed conditions. In this way, the same model is run many times from slightly different starting points. In order to limit the effort, a special type of perturbations can be calculated which has optimal growth characteristics. An example of such optimal perturbations are the so-called Singular Vectors, for which the growth interval (for example three days), the growth domain (for example the Northern Hemisphere) and a metric property (for example the total energy) have to be specified (Hersbach et al., 1998).

Climatology

In addition to weather forecasts, research at the Royal Dutch Meteorological Institute focusses on climate and climatic changes. The climate is expected to change due to the so-called greenhouse effect. This phenomenon is studied using climate models. By including different scenarios, the climate to be expected is investigated.

In climate research the uncertainty in the state of today's climate and the uncertainty in the climate models is important. With respect to weather forecasts not only a stochastic initial condition is taken into account. Running different models make sure that the model uncertainties are considered, as well. This technique is called 'multi-model ensemble climate prediction' (www.knmi.nl).

Hydrology

In the field of hydrology, the use of rainfall-runoff models in combination with stochastic weather generators is common practice, for instance to obtain insight into river flows under various conditions (Smith & Kojiri, 2003, Lall & Sharma, 1996, Rajagopalan & Lall, 1999, Ten Heggeler et al., 2004, Leander et al., 2004 and Beersma & Buishand, 2004). Most of these studies use resampling techniques in combination with Monte Carlo simulation to reproduce the stochastic nature of rainfall-runoff patterns. For drought assessment Beersma & Buishand (2004) consider the joint probability of precipitation and discharge deficits in the Netherlands. In Smith & Kojiri (2003) and Ten Heggeler et al. (2004) stochastic rainfall patterns are generated with weather

radar data (radar rainfall). These patterns are used as inputs into a distributed rainfall-runoff model, in order to analyse discharge statistics at each reference point in the watershed via Monte Carlo Simulation.

Ecology and Public Health

Ecosystems are complex non-linear and adaptive systems that are inherently chaotic. Problems with regard to environmental hygiene and public health are characterised by lack of knowledge and information about underlying mechanisms and their interactions. The information available about problems regarding ecosystems, atmospheric environment, air pollution, emissions, radioactivity and water quality is usually limited, uncertain and insufficient. Experiments are often not possible and available data is scarce or inadequate. Parameters and variables, like soil characteristics, are subject to inherent natural variability. It is not surprising that sensitivity and uncertainty analyses play an important role in environmental studies. In Janssen et al. (1990) a survey is given of available techniques and methods to perform sensitivity and uncertainty analyses in this research area. The available techniques applied in Janssen et al. (1990) are the individual parameter variation, the differential analyses, the response surface method, the Monte Carlo Simulation with Latin Hypercube sampling and the Hornberger-Spear-Young method, respectively. These methods are evaluated on aspects like application range, assumptions used, ease of use and computational demands. This evaluation showed that in particular the Monte Carlo Simulation combined with the Latin Hypercube sampling technique is a suitable method, even though it can be time-consuming.

Hydraulic engineering

In recent years there has been a growing tendency to carry out risk analyses in hydraulic engineering in order to estimate the (societal) risks involved, to determine the optimum construction process and to guarantee a certain level of safety. Different mathematical methods are used in the probabilistic design of hydraulic structures to provide insight into their reliability. The reliability is often expressed in terms of a limit-state function, representing the margin between 'resistance' against failure and the 'load' mechanisms that cause failure. Resistance (strength) and load are functions of stochastic variables. In constructive hydraulic engineering three types of mathematical models are distinguished (CUR, 1997).

- Level III-methods: the probability distribution functions of all variables (in the 'resistance' and in the 'load') are considered when determining the probability of failure. The reliability of a construction is directly related to this probability of failure. Two types of Level-III methods are Numerical Integration and Monte Carlo Simulation.
- Level II-method: the probability of failure is determined by linearising the reliability function ('resistance' minus 'load') around a certain point. The probability distribution

function of each variable is approximated by a standard normal distribution function. The First Order Reliability Method is a level-II method.

- Level I-method: the probability of failure is not determined. In the design stage the margin between the 'resistance' against failure and the 'load' mechanisms is taken into account by the introduction of partial safety factors.

Both First Order Reliability Method and Monte Carlo Simulation are applied in Cooke & Van Noortwijk (1999), a study of dike ring reliability that identify the principal driving forces when the dike is close to failure.

Chapter 4

Methodology

4.1 Introduction

This thesis combines two research fields, namely the field of river morphodynamics and stochastic modelling. Background information on both research fields has been provided in the previous two chapters. This chapter has a methodological character: it includes the choice of the methods, models and tools that will be used in the remainder of this thesis and the justification of these choices.

We restrict ourselves to non-tidal lowland rivers with fixed banks and subcritical flow, carrying non-cohesive sediment. Throughout this dissertation, the non-tidal part of the Rhine in the Netherlands is used as a study case. Therefore, the chapter starts with a brief description of the study area (Section 4.2). Morphological phenomena are distinguished at various scale levels in the Rhine, according to De Vriend's (1999) scale cascade (Section 4.3).

The applicability of stochastic methods to study the stochastic nature of river morphology is discussed in Section 4.4. Since existing deterministic morphodynamic models are important and widely-used tools in present-day engineering practice, preference is given to stochastic methods that make use of such models. Monte Carlo Simulation (MCS) with crude sampling appears to be a robust and suitable method to quantify uncertainties involved in morphodynamic predictions. Therefore, this method will be used in this thesis.

The principle of MCS is to run a deterministic model repeatedly, each time with a different set of model inputs which are statistically equivalent. We have a choice of deterministic numerical process-based morphodynamic models, ranging from 1-D to more sophisticated 2-D and 3-D models. The applicability of these models depends amongst other factors on:

- the type of engineering problems in design, operation and maintenance of the river system,
- the aspects of the morphodynamic behaviour of a lowland river that are important to these engineering problems,
- the model's appropriateness to be run in a stochastic mode, using MCS.

In principle, river morphology concerns a 3-D process, but most problems do not need to be tackled by means of a 'complete' 3-D description (De Vries, 1993). A major concern regarding MCS is the inefficiency of the method. Computationally intensive numerical models in combination with a large number of simulations (required for convergence of the output statistics) can make MCS to a laborious operation. The computational effort per individual numerical simulation differs considerably between 1-D and multi-dimensional models. Therefore, preference is given to a 1-D approach. This approach is assumed to be appropriate to illustrate the potential of a stochastic approach in river management practice. Two different 1-D models are used in this thesis, viz. (1) a simple hypothetical model having dimensions similar to those of the Waal (Section 4.5.3), and (2) a more realistic, but also more complex Rhine model that incorporates the branches Niederrhein, Waal and IJssel (Section 4.5.4). The latter model has been set-up, calibrated and validated by Jesse & Kroekenstoel (2001).

A question that needs to be answered of course, is to what extent the relevant phenomena can be modelled and predicted with a 1-D numerical model. A justification of using this 1-D Rhine model is given in Section 4.6, where the 1-D model is validated against a quasi-3D model of the Waal. The quasi-3D Waal model has been developed by Sloff (2004).
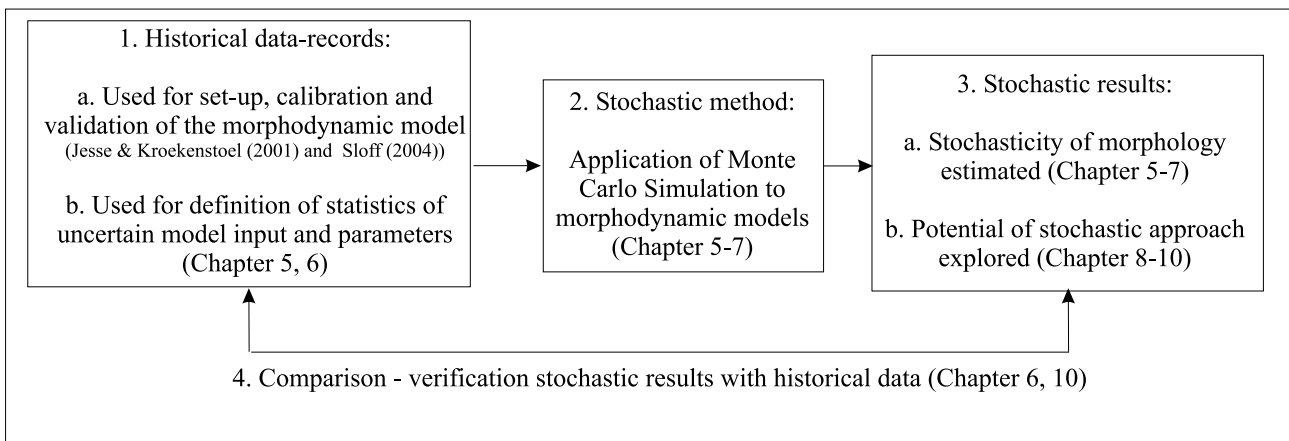

Figure 4.1: Research methodology

In summary, the research methodology is visualised in Figure 4.1. First, historical data is used for (a) the set-up, calibration and validation of morphodynamic models[1], and (b) the definition of input statistics and correlation structures. The application of Monte Carlo Simulation to morphodynamic models follows. On the basis of the set of outputs of all model simulations, the stochasticity of the river bed is estimated in the next step. This step contains also an inventory of (a) the uncertainty sources that contribute most to this stochasticity, and (b) the potential of the stochastic approach. Finally, a comparison of the stochastic outputs with historical data follows to produce insight into relation between model versus reality. Regarding the latter, we

---

1.   This part has been done by Jesse & Kroekenstoel (2001) and Sloff (2004)

have to realise that historical data does not cover the full range of possible conditions, but reflects only a single realisation. In Section 5.5, we focus on the question whether a single realisation can be used to reveal the ensemble statistics.

4.2 The Rhine in the Netherlands

4.2.1 The Rhine as study case

The principal aim of this thesis is to find out how to analyse the stochasticity of morphodynamics at various scale levels in non-tidal lowland rivers and on how to use this kind of analysis to support river engineers and managers in their every-day practice. We choose to consider a single river, viz. the Rhine in the Netherlands, and more specifically the Niederrhein, Waal and IJssel branches. A thorough analysis of the non-tidal lowland part of the Rhine in the Netherlands will improve the knowledge on how to cope with the stochastic nature of morphodynamics of the Rhine in particular, but may also produce generic knowledge on stochastic morphodynamics in general. We expect that the answers to questions such as: 'How to do stochastic analysis in river morphodynamics?' and 'What kind of information and data should be available?', will apply to other non-tidal lowland river systems, as well.

Stochastic analysis usually requires a large amount of data and physical information, in order to obtain a good definition of the statistics of the uncertainty sources involved and to validate in the end the estimated stochastic parameters concerning the morphodynamics. Therefore, the availability of (1) an impressive database comprising data on e.g. discharges, bathymetry, composition of bed material, water levels, water depths, dredging activities and navigation draughts, and (2) various numerical morphodynamic models of the river, make the Rhine an appropriate study case. Moreover, the Rhine in the Netherlands is a multi-functional river in a densely populated area, which offers the opportunity to expose the potential of stochastic methods in present-day river management practice.

4.2.2 Description of the Rhine

The Rhine is a large river in Western Europe and has a total length of 1,320 km. It rises in Switzerland as a snowmelt-fed mountain river and eventually debouches as a rain- and snowmelt-fed lowland river in the North Sea in the Netherlands. In the 19$^{\text{th}}$ and early 20$^{\text{th}}$ centuries, the Rhine was heavily trained for the purpose of safe discharge of water, sediment and ice, and of a better navigability. The large-scale river training resulted in the 'present-day' appearance of the river (Figure 4.2): fixed planform, non-permeable groynes, a single main channel intensively used for navigation, low levees ('summer dikes') that protect floodplains from frequent flooding, silted up flat floodplains used as meadows and high dikes acting as a main flood defence. These dikes protect a dense riparian population.

The Netherlands

North Sea

Germany

Belgium

IJssel

Lek

Lower-Rhine

Pannerdensch Kanaal

Waal

Niederrhein

Outline of the river

Polder

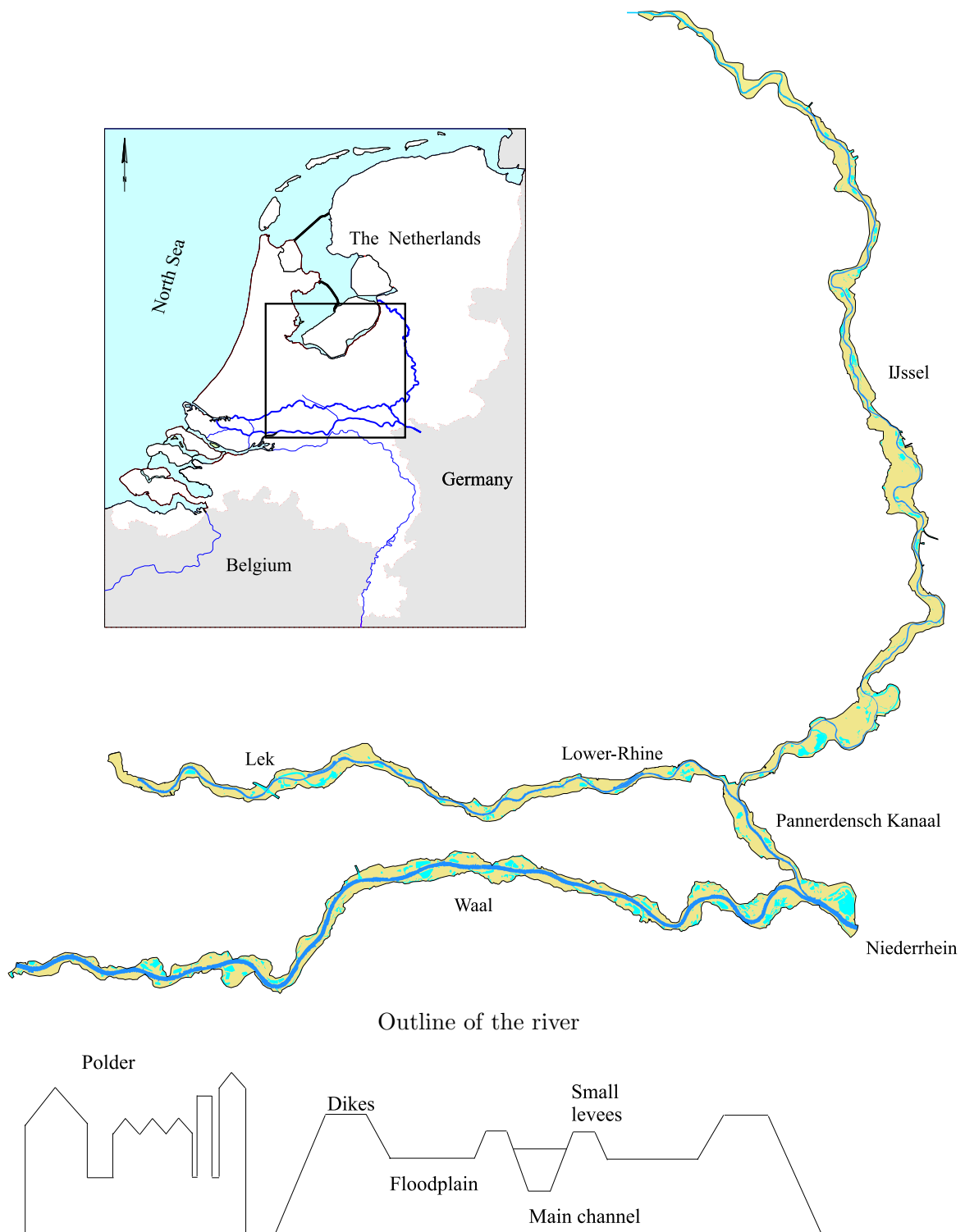Dikes

Small
levees

Floodplain

Main channel

Figure 4.2: The Rhine branches in the Netherlands and the outline of the river

In the Netherlands six main branches can be distinguished: Niederrhein[2], Waal, Pannerdensch Kanaal, IJssel, Lower-Rhine and Lek. There are two bifurcations: the Pannerdensche Kop and the IJsselkop. At the Pannerdensche Kop bifurcation approximately 66% of the Rhine discharge is directed to the Waal. The remaining 34% flows into the Pannerdensch Kanaal, and at the IJsselkop bifurcation two thirds of this is directed into the Lower-Rhine and one third into the IJssel. Under low and intermediate flow conditions, the distribution is controlled by a weir in the Lower-Rhine.

Geometry and bed slope vary between the different Rhine branches. All branches have a cross-section in which different zones can be distinguished: the main channel bed, the groyne section, the flow-conveying floodplains and the storage area. The width-relation between the main channel and the floodplain, the level of the floodplains compared to that of the main channel, the presence (or absence) of summer dikes and the storage capacity in the floodplains differ per branch. On average, the bed slope, the floodplain width and the grain size of the bed material decrease in the direction of the North Sea and the IJssel Lake, whereas the width of the main channel increases in downstream direction. The mean width of the IJssel increases in downstream direction from some 75 m at the IJsselkop bifurcation to 175 m at the outlet in Lake IJssel, for instance.

Even within a branch differences in geometry exist. Wide and narrow floodplains are located alternately at the left and the right side of the river (see Figure 4.3), variation exist in levee height and vegetation cover, storage and conveyance capacity of floodplains, radius of curvature, etc. Crossings between bends are found. Complex flow patterns vary along and across the branch. This leads to transverse bed slopes and asymmetric cross-sectional shapes, and to accretion and erosion patterns migrating through the system. In general, these perturbations will decay while migrating downstream, and interfere with bottom waves generated elsewhere in the river.

Despite the extensive spatial variability within each branch, Table 4.1 gives an indication of dimensions and characteristics of the Niederrhein, Waal and IJssel in the Netherlands. On the basis of the figures in Table 4.1 and the equations Eq. 2.1-2.7, the morphological time-scales of the Rhine branches can be estimated. It appears that these scales differ between the Rhine branches, in particular as a consequence of differences in sediment transport rate. The morphological time-scale of the IJssel, for instance, is much larger than the ones for the Niederrhein and the Waal. This means that the large-scale river morphology in the IJssel responds slower to the changes in the river regime than that in the Niederrhein and the Waal.

---

2.   Part of the Niederrhein that is situated in the Netherlands is also known as the Bovenrijn ('Upper-Rhine')

dimensions and characteristics	symbol	Rhine branch			unit
		Niederrhein	Waal	IJssel	
length	L	5	83	93	km
width main channel[1]	B_{m}	330/440	260/370	90/120	m
width floodplain	B_{f}	850	550	550	m
bed slope	i_{b}	0.13	0.12	0.10	m/km
average Chézy coefficient main channel	C_{m}	40	40	40	$\sqrt{\mathrm{m}}$/s
average Chézy coefficient floodplain	C_{f}	35	35	35	$\sqrt{\mathrm{m}}$/s
grain size of bed material	D_{50}	0.005	0.001	0.001	m
mean discharge	Q_{mean}	2220	1480	317	m³/s
mean annual sediment load	S_{yr}	570,000	507,000	37,000	m³/yr

[1] width of main channel excluding/including groyne section

Table 4.1: Indicative dimensions and characteristics of the Niederrhein, Waal and IJssel
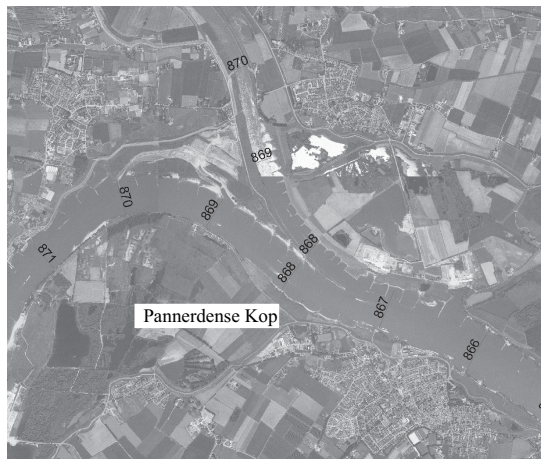
(a) Bifurcation Point Pannerdensche Kop
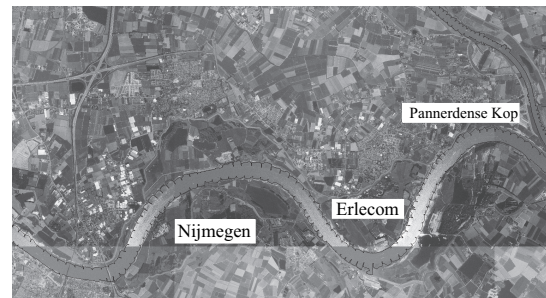
(b) River bends Erlecom and Nijmegen

(c) Variation in floodplain width near Ochten km 907

Figure 4.3: Aerial photographs of the Rhine (courtesy of Rijkswaterstaat)

4.3   Relevant morphological phenomena

Morphological changes take place at a wide variety of spatial and temporal scales, from individual grain motion to the evolution of the entire river system. River training works have resulted in a more or less fixed planform of the Rhine branches. Fixed river banks, groynes and dikes prevent free meandering and braiding. According to the scale-cascade in Section 2.2.3, three scale levels of morphological phenomena are discerned for the Dutch part of the Rhine, see Table 4.2.

scale levels	morphological phenomena
micro	- bedforms, such as ripples and dunes - vertical segregation of sediment fractions
meso	cross-sectional profile evolution: - transverse bed slope and pointbar/pool formation in bends - crossings between opposite bends - formation of shallow and deep parts in geometrically complex reaches - bank erosion - overbank sand deposition - local scour in groyne fields and formation of so-called groyne flames - local scour e.g. around bridge piers
macro	- longitudinal profile evolution - evolution of geometry at river bifurcations

Table 4.2: Morphodynamic scale levels in the Rhine in the Netherlands

This section proceeds with a description of the morphological phenomena at each scale level. Information on how these phenomena are dealt with (or not) in the morphodynamic Rhine models is given in Section 4.6.1.

4.3.1   Mirco-scale

Bedforms

Different types of bedforms are distinguished in the Rhine, ranging from small ripples to large river dunes. Bedforms tend to develop due to the interaction between flow and river bed (Van Rijn, 1993). Ripples are bedforms of small dimensions (height and length in the order of centimetres, respectively decimetres) and occur in hydraulically calm conditions. Their dimensions are strongly related to the grain size of bed material and much less to water depth and flow velocity. Dunes in river channels are asymmetrical transverse bedforms with a gentle stoss side slope and a steep lee side slope. They may evolve into large features that are in the order of hundreds of metres long and several metres high. Grain size of bed material is not as important

as for ripples, water depth and flow velocity appear to be more important. In the Rhine, ripples and small dunes are superimposed on larger dunes. Growth and decay of dunes is related to discharge variation: dunes increase in height and in length as a function of the discharge. The maximum dune dimensions are reached some days after the peak discharge. Wilbers (2004) observed a difference in bedforms located left and right of the river axis in the Waal. He indicated that bedforms right of the axis are larger than the ones at left side. Also, the median grain size is larger in the right part of the channel. This is explained by the fact that ships navigating upstream towards Germany carry more cargo than those going the other way. Vessels sailing either way induce currents in between the groynes that are strong enough to erode fine-grained sediments and transfer these to the river bed (Yossef, 2005 and Ten Brinke et al., 1998). These currents are stronger for loaded vessels, resulting in finer grained sediment near the left bank. Furthermore, navigation-induced currents appear to flatten the dune-tops.

Segregation of sediment

In the Rhine significant downstream fining and vertical segregation of fine and coarse sediment are observed (e.g. Kleinhans, 2002, Julien et al., 2002, Blom, 2003). Bend effects, bifurcation points, bedforms and navigation cause lateral variation in grain size. The combination of spiral flow and down-hill gravity forces in bends is the dominating mechanism for transversal grain sorting, yielding relatively coarse sediment in the outer bend and fine sediment in the inner bend. Bed armouring, with coarser particles covering the finer ones, are important segregation processes in the Niederrhein, Pannerdensch Kanaal and the areas close to the bifurcations (Jesse & Kroekenstoel, 2001).

4.3.2   Meso-scale

At meso-scale the main focus is on the cross-sectional profile evolution. This includes transverse bed slope and pointbar/pool formation in bends, alternate bars in straight reaches and stable shallow and deep parts in geometrically complex reaches (e.g. with one-sided floodplains, located alternately at left and the right side of the river) and at crossings between two opposite river bends. It also includes phenomena like overbank sand deposition during high floods, bank erosion and local scour around bridge piers and in groyne fields, and the formation of so-called groyne flames (e.g. Yossef & Klaassen, 2002).

Transverse bed slope and pointbar/pool development

Struiksma et al. (1985) and Talmon et al. (1995) studied the bed deformation in river bends. Curvature-induced secondary flow in a river bend results in a transverse bed slope and point-bar and pool development in the inner- and outer bend, respectively. The transverse slope is

determined by local parameters such as water depth, bed-shear stress, bend curvature and sediment properties. The equilibrium slope depends on the balance between the upslope drag force induced by spiral flow and the downslope gravitational force, both acting on the grains moving along the bed. Struiksma et al. (1985) approximate the axi-symmetrical lateral bed slope for infinitely long bends of constant curvature as follows:

$$\frac{\partial z_{\mathrm{b}}}{\partial y} = -A f_{\mathrm{s}}(\theta) \frac{h}{R_{\mathrm{b}}} \tag{4.1}$$

in which z_{b} is the bed level [m], A is the secondary flow direction coefficient [-], $f_{\mathrm{s}}(\theta)$ is a function of the Shields parameter θ [-], h is the water depth [m] and R_{b} is the radius of curvature [m]. The secondary flow direction coefficient is defined as (De Vriend, 1977):

$$A = \frac{2\epsilon}{\kappa^2} \left(1 - \frac{\sqrt{g}}{\kappa C} \right) \tag{4.2}$$

in which ϵ is a tuning coefficient [-], κ is the Von Karmann coefficient (≈ 0.4) [-], C is the Chézy coefficient [m$^{1/2}$/s] and g is the acceleration due to gravity [m/s^2].
The function $f_{\mathrm{s}}(\theta)$ can be approximated as (Talmon et al., 1995):

$$f_{\mathrm{s}}(\theta) = 9 \left(\frac{D_{50}}{h} \right)^{0.3} \sqrt{\theta} \tag{4.3}$$

in which D_{50} is the median grain size of the bed material [m].
The axi-symmetrical situation described by Eq. 4.1, though an important system property, is hardly ever reached in natural rivers, since river bends are limited in length and do not have a constant radius of curvature. Moreover, transverse slopes tend to lag behind variation in flow conditions. Lateral re-distribution of flow and sediment motion appear to be important for the bed development. The bed development in a bend is influenced by transitional effects due to a difference between the conditions upstream and those in the bend. The change of curvature induces a change in secondary flow. Struiksma et al. (1985) showed that the transverse bed slope in a bend cannot be predicted solely from local conditions, since non-local effects due to the re-distribution of flow and sediment in the first part of the bend can lead to a significant 'overshoot' of the lateral bed slope.

Crossings between opposite bends

At crossings between two opposite bends the bed deformation is affected by the flow conditions in the upstream bend, since the flow pattern lags behind the variation of the channel curvature. In the transition zone between two bends a shoal may be formed in the middle of the river. The size of this shoal depends on the discharge and the hydraulic roughness. At low-flow stages scour occurs at crossings, resulting in an increase of the water depth. At high-flow stages the opposite is observed.

Formation of shoals and deep parts in geometrically complex reaches

The Rhine contains various geometrically complex reaches, including width variations (flood-plain widening or constriction) and man-made structures for instance. These will influence the water motion, thus producing spatial gradients in the sediment flux, hence morphological chan-ges. Accretion and scour patterns may migrate downstream, (partly) decay and interfere with bottom waves initiated elsewhere in the river.

Overbank sand deposition

(Ten Brinke et al., 1998)
Overbank deposits are sediments accumulated on the floodplain during periods of high-flow. Using aerial photographs and field measurements, sandy overbank deposits formed by the high floods of 1993/94 and 1995 were quantified along the Waal and IJssel . Deposits were forming patchy sand splays on the top and landward slope of the natural levees, and covered about 4% of the embanked floodplain on the Waal and about 1% on the IJssel.
The total volume of sand deposits was estimated at 169,000 and 217,000 m^3 for the Waal in 1993/94 and 1995, respectively. The averaged yearly transport of bed material in the Waal is roughly 500,000 m^3. Along the IJssel about 46.000 m^3 was deposited, which exceeds the averaged annual sediment load of 37,000 m^3. The overlap of the deposition areas in both years was between 55% and 70%. The volumes deposited on the left bank of the Waal were larger than those on the right bank. For the IJssel the difference between both banks was negligible. In bends, the volumes of overbank deposits on the inner bank are much larger than those on the outer bank, both in the Waal and in the IJssel.
The controlling mechanisms of overbank deposition are (1) pointbar formation and (2) lateral flow exchange between main channel and floodplains. Curvature-induced secondary flow in river bends results in sediment transport from the outer bend to the inner bend. During high floods these helicoidal currents are important for overbank sand transport. The flux of sand from the main channel into the floodplains is much larger in a sinuous section of the river than in straight reaches. Moreover, the relatively high frequency and magnitude of overbank flows induced at geometrically complex locations, especially in combination with large amounts of suspended material, leads to patchy sand splays. Deposition of sandy sediments in between the groynes and on the floodplains behind them appears to be more significant at the left bank. This may be attributed to a larger amount of suspended fine sediments at the left bank, due to navigation-induced erosion of the groyne fields under low-flow conditions.

Local scour and formation of 'groyne flames' near groynes

Groynes have been constructed in the Rhine to restrict the main channel and to provide an inland waterway of sufficient depth and width. The presence of these groynes appears to have

a significant morphological impact. Vortex shedding from the groyne head causes scour holes that protrude into the main channel and fade out in downstream direction. Downstream of the scour holes deposition areas are formed, which are often referred to as 'groyne flames'. These flames usually extend some tens of metres into the main channel and may become critical to navigability under low-flow conditions (Yossef & Klaassen, 2002).

4.3.3 Macro-scale

Longitudinal profile evolution

At this scale-level, the longitudinal profile of a river branch responds to natural changes or training schemes. The regulation measures in the Rhine in the 19th and 20th century have largely affected the longitudinal profile evolution.

The river training works induced a large-scale tilting of the river bed in the Waal. Large-scale erosion is observed in the Niederrhein (1.3 m over a period of 50 years) and the upstream part of the Waal (0.8 m over a period of 50 years)(Visser et al., 1999). Near Tiel (km 915), there is a hinge point, downstream of which long-term sedimentation takes place. This implies an overall reduction in bed slope. The river regulation measures also led to a gradual siltation of the floodplains.

The morphological response of the IJssel induced by the regulation works is similar to that of the Waal, but less pronounced (0.4 m bed degradation over a period of 50 years). A typical cross-section in the IJssel contains a narrow main channel and wide floodplains. The ratio of the floodplain width to the main channel width is much larger for the IJssel than for the Waal. The floodplain level in the IJssel is relatively high when compared to that of the main channel. Large-scale dredging activities have been undertaken in the Rhine since the end of the 19th century. The dredging was aimed to accelerate the 'desired' impact of the river regulation works, viz. bed level degradation to obtain a larger navigation depth in the river. Most of this dredging took place 'uncontrolled' without permits and regulation. As a result, it is unknown whether the impacts of the regulation works on the longitudinal profile evolution have been realised to their full extent, or that the adaptation process is still going on (Visser et al., 1999).

Morphological evolution at bifurcations

Bifurcations play a central role in the distribution of water and sediment over the bifurcated branches. The morphological stability of the bifurcations in the Rhine system is relevant for the maintenance of the river branches, as well as for the long-term prediction of the system (Sloff et al., 2003). River bifurcations are known to exhibit an unstable morphological behaviour under certain conditions. The stability is of interest in the Rhine case, because the present management policy is to maintain the discharge distribution at the bifurcations under all discharge

conditions. Yet, the discharge discharge distribution varies slightly in time, as a result of time-dependent morphological changes around the bifurcation point. This may lead to substantial differences in extreme flood levels, thus endangering the system's safety (see Section 9.4.3).

At bifurcations, the discharge distribution is governed by the conveyance and the available total difference in head over the outflowing branches to the base of the river. The distribution of sediment is usually not governed by the discharge distribution, but rather by the local 2-D or 3-D flow pattern. Hence, the geometry at bifurcations is of great importance. In the simplest way, a bifurcation is represented by a simple 1-D branch model. This type of model requires additional input in the form of an empirical nodal-point relation that specifies how sediment transport rates are divided over the outflowing branches of the bifurcation. The predictive capacity of such a model strongly depends on the quality of the empirical relation. In a 2-D and 3-D model, sediments are distributed automatically according to the geometry, flow conditions and sediment characteristics at the bifurcation. Inclusion of physical mechanisms for grain sorting and alluvial roughness and a realistic representation of sediment and flow interaction at the bifurcation appears to be important (Mosselman et al., 1999).

Using a dune tracking technique, Wilbers (2004) showed that approximately 90% of the sediment transport in the Rhine at the Pannerdensche Kop goes to the Waal. The remaining 10% goes to the Pannerdensch Kanaal. This implies that the ratio of sediment transport rates is different from the ratio of discharges (66/34%). This is partially explained by the Bulle effect (Bulle, 1926). Spiral motion deflects the water near the surface away from the centre of curvature and near the bed towards this centre. As most of the sediment is transported on or close to the river bed, a relatively large part of the sediment transport is directed into the Waal (see Figure 4.3(a)). Horizontal and vertical sorting of graded sediments appears to be another important factor in the sediment distribution over the branches.

At the IJssel Kop, 60% of the sediment transport of the Pannerdensch Kanaal is directed into the Lower-Rhine (located at the inner bend) and 40% into the IJssel (located at the outer bend) (Ten Brinke et al., 2001).

4.4   Stochastic method

Morphodynamic models are effective tools to provide insight into the physical system behaviour. Parameter setting and input representation depend on the phenomena to be reproduced. This turns out to be not entirely trivial, especially in case of non-linear models, where the expected value of a prediction based on randomly varying inputs is not equal to the prediction based on the expected value of each input quantity (Gardner & O'Neill, 1983).

Predictability is furthermore restricted by the various uncertainty sources involved, such as uncertainties that are inherent to nature, those introduced during the modelling process (choice

of model concept and specification of boundary conditions, initial conditions and model para-
meters) and those due to the lack of understanding of the physical processes. Regarding the
latter, one may even argue whether the physical processes and phenomena of a natural river
system can be described, at all, by models using a set of deterministic differential equations,
empirical sediment transport formulae and a number of adjustable model parameters.

Background information on stochastic methods (Numerical Integration, Monte Carlo Simula-
tion (MCS), the First-Order Reliability Method (FORM), Response Surface Replacement and
Stochastic Differential Equations) and their applicability in various research fields is already
presented in Section 3.4. The applicability of these stochastic methods to study the stochastic
nature of river morphology depends on how well the methods deal with the strong non-linearity
and complexity of river morphodynamics. Since existing deterministic morphodynamic models
are important and widely-used tools in engineering practice, stochastic methods that make use
of such models are preferred.

On the basis of these criteria many stochastic prediction methods can be eliminated from the list
of potentially suitable methods for river morphology. Numerical Integration is not considered
any further, as the method requires too many model evaluations. Response Surface Replacement
is not recommended, as morphodynamic models are too complex to adequately be replaced by a
simplified meta-model. Stochastic Differential Equations is a technique that deals with irregular
stochastic processes, meaning that the state and the physical system behaviour is described in
terms of probability. The problem is that many concepts, like differentiation, integration and
numerical approximations need to be completely revised. As a consequence, existing morpho-
dynamic models cannot be used as a basis of such a stochastic analysis. For this reason, the
method is not considered any further.

Van der Klis (2003) investigated the applicability of three potentially suitable methods, namely
(1) FORM, (2) MCS with crude sampling, and (3) MCS with Latin Hypercube sampling.
The applicability of FORM has been examined, mainly because of its good reputation in civil
engineering. The attractive property of this method in risk assessments of hydraulic structures,
is the small number of computations required. Van der Klis (2003) showed FORM to be less
suitable to river morphology. The combination of non-linearity and large uncertainties leads to
inaccurate results. FORM is not suitable for practical problems in river morphology that are
space or time dependent. For instance, predicting where, when and how frequently navigation
channel requirements are not fulfilled, is necessary for the timely deployment of dredging or
scour protection measures. This requires information about the probability of a particular state
of the river bed for several locations or moments in time. For each location or each point in
time, FORM requires a large number of simulations to locate a design point, and thus annihila-
ting the potential advantage of a small sample size. The only type of problem for which FORM
might be applicable is the probability of occurrence of an extreme state of the river bed that is
space and time independent. This is the case, for instance, if one is interested in erosion close

to hydraulic structures, which may undermine and destabilise banks and foundations.

MCS with crude sampling and Latin Hypercube sampling give both accurate results for river morphology, as long as the sample size is large enough and the description of the input uncertainties adequate. MCS is suitable for a wider range of applications than the FORM. Therefore, preference is given to MCS. Running numerical models in a stochastic mode using MCS is usually rather time-consuming. An advantage of MCS with crude sampling over Latin Hypercube sampling is the possibility to estimate the required sample size beforehand and verifying the sample size conveniently afterwards. Van der Klis (2003) concluded that MCS with crude sampling is a robust and suitable (though laborious) method to quantify the uncertainty involved in morphodynamic predictions. Therefore, this method will be used in this thesis. A detailed description of the principle of MCS with crude sampling is presented in Section 3.4.1. In this thesis, three numerical morphodynamic models are run in an MCS-setting. If a model simulation in the MCS-procedure gets unstable, either due to physically impossible conditions or incorrect model settings, the results of that particular simulation are excluded from the set of outputs that are considered in the statistical analyses afterwards, even if the simulation gets unstable halfway through the computation period.

4.5   Numerical model concept

4.5.1   1-D model concept

The need for uncertainty analysis using morphodynamic models of lowland rivers including the real-life geometrical complexity, is explained in Sections 1.3 and Section 4.4. The underlying deterministic model can be spatially one- or multi-dimensional. Numerical model simulations with complex morphodynamic models are usually time-consuming. The computational effort per individual numerical simulation differs considerably between 1-D and multi-dimensional models. Moreover, this effort will increase substantially when running these models in an MCS-setting. For practical reasons, we will mainly utilise the 1-D numerical morphodynamic modelling software package SOBEK, because this requires less computational effort than a 2-D approach. In Section 4.6, we will introduce a quasi-3D approach as a way to validate this 1D-concept.

The 1D-concept in general (e.g. constituting equations, boundary and initial conditions) will be described in Section 4.5.2. Two different 1-D models are used in this thesis, viz. (1) a hypothetical model having dimensions similar to those of the Waal (Section 4.5.3), and (2) a more realistic, but also more complex Rhine model that incorporates the branches Niederrhein, Waal and IJssel (Section 4.5.4).

The hypothetical model is used to get insight into the morphological response to isolated geometrical variations or human interventions. The main disadvantage of the hypothetical model

is that it concerns a rather idealised situation. Therefore, this model is of little use to the operation and maintenance practice of real-life rivers. In reality, a river consists of a network of branches and bifurcations, it will contain man-made structures, variations in geometry and flow resistance, etc. They act upon the river hydrodynamics and will lead to a bed level response. Different sources of bed level variations act simultaneously, with different intensities and different response times. The resulting shoals and pools tend to migrate downstream, (partly) decay and interfere with morphological changes initiated elsewhere in the river. These effects can only be described with a more realistic model based on the actual river geometry, such as the Rhine model. The reason for still using the hypothetical model is that the potential of a stochastic approach can best be investigated by first examining simple cases in which the morphological processes are fully transparent. Van der Klis (2003) concludes that the experience gained with hypothetical models enables the interpretation of uncertainty estimates in more complex situations.

4.5.2 Numerical software package SOBEK

SOBEK is a 1-D modelling system for open-channel networks. It can be used to simulate unsteady and steady flow, (uniform and graded) sediment transport, morphology, salt intrusion, and water quality. SOBEK is developed by WL|Delft Hydraulics and Rijkswaterstaat RIZA, in The Netherlands. The morphodynamic SOBEK software package consists of decoupled equations describing flow, sediment transport and bed level changes.

Flow equations

The water flow is computed by solving the 1-D cross-sectionally integrated shallow-water equations (Saint Venant-equations), representing the conservation of cross-sectionally integrated mass and momentum. These equations read:

$$\frac{\partial A}{\partial t} + \frac{\partial Q}{\partial x} = q_{\text{lateral}} \tag{4.4}$$

$$\frac{\partial Q}{\partial t} + \frac{\partial}{\partial x}\left(\alpha_{\text{b}}\frac{Q^2}{A_{\text{f}}}\right) + gA_{\text{f}}\frac{\partial(h+z_{\text{b}})}{\partial x} + A_{\text{f}}\frac{\tau_{\text{b}}}{\rho R} = 0 \tag{4.5}$$

in which A is the total cross-sectional area [m^2], A_{f} the cross-sectional flow area [m^2], Q the discharge [m^3/s], q_{lateral} the discharge added to the river per unit length [m^2/s], α_{b} the Boussinesq constant [-], g the acceleration due to gravity [m/s^2], h the water depth [m], z_{b} the bed level [m], ρ the mass density of water [kg/m^3], τ_{b} the bed-shear stress [kg/m/s^2] and R the hydraulic radius [m]. Time and space are represented by t and x, respectively.

The bed-shear stress τ_{b} is expressed by the Chézy formula:

$$\frac{\tau_{\text{b}}}{\rho} = \frac{gQ\left|Q\right|}{C^2 A_{\text{f}}^2} \tag{4.6}$$

in which C the Chézy coefficient [m$^{1/2}$/s]

Transport and Morphology equations

The sediment transport field and the sediment balance equation determine the morphological changes. Empirically derived sediment transport formulae are used to estimate the sediment transport in rivers. Each transport formula has its own field of application - bedload (Meyer-Peter & Müller, 1948), suspended load (Van Rijn, 1993) or total load (Engelund & Hansen, 1967). The sediment transport capacity depends on the flow conditions and on sediment characteristics such as density, grain size distribution and shape. Spatial gradients in sediment transport will lead to morphological changes. These changes can be incorporated in SOBEK via the continuity equation for bed material:

$$\frac{\partial A_{\mathrm{s}}}{\partial t} - \frac{\partial S}{\partial x} = -s_{\mathrm{lateral}} \tag{4.7}$$

in which A_{s} is the sediment-transporting cross-sectional area [m^2], S is the sediment transport rate through the cross-section, expressed in deposited volume (i.e. including pores) per unit time [m^3/s], and s_{lateral} is the lateral sediment supply per unit river length [m^3/m/s].

Boundary and initial conditions

The fully time-dependent morphodynamic system has three bundles of characteristics: two describing the propagation of flow disturbances and the third describing the propagation of bed disturbances. In a fully dynamic system, the characteristics of water and bed will mutually influence each other and are generally too complex to be separated.

At low Froude numbers, however, the propagation speed of a disturbance in the water surface is larger than the flow velocity and much larger that the propagation speed of a bed disturbance. Therefore, a decoupled system is applicable: when computing the water motion, the bed is held fixed, and when computing the bed level changes, the water motion is kept invariant to changes in the bed level.

In order to have a mathematically well-posed system, fixed-bed flow computations require one boundary condition at the upstream boundary (usually the discharge) and one at the downstream boundary (often the water level or a stage-discharge relationship). Two initial conditions are usually needed, which are usually given in terms of the dependent variables h and Q. If the bed is mobile, one extra boundary is required at the upstream boundary, usually given in terms of bed level or sediment transport rate. One extra initial condition is needed, which concerns the bed topography at the beginning of the model run.

4.5.3   A hypothetical 1-D model of dimensions similar to those of the Waal

The 1-D morphodynamic simulation package SOBEK is used to simulate the morphological processes in a highly simplified river of similar dimensions as the Waal. It concerns a prismatic

channel with an initially plane sloping bed. The morphological response to isolated variations in geometry, such as a constriction or a widening, or human interventions can be investigated with this model.

For the purpose of illustration, we consider an instantaneously applied floodplain lowering. The case concerns a straight compound channel of 180 km length. Over a distance of 10 km the floodplains are lowered by 1 m (see Figure 4.4). The floodplains are assumed to be non-alluvial, bank erosion and lateral sediment transport between the main channel and floodplains are neglected. We use the sediment transport formula of Engelund & Hansen (1967), which computes the total sediment load and is usually applied for rivers with a relatively fine sediment. The dimensions, model inputs and parameter settings are chosen according to the river Waal conditions (Table 4.3).
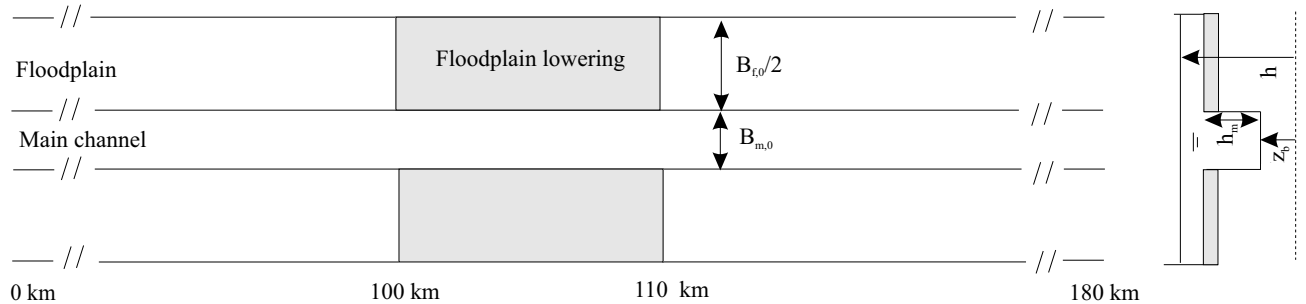
Figure 4.4: A prismatic channel of 180 km length with a composite cross-section: over a distance of 10 km the floodplains are lowered by 1 m

description	symbol	value	unit
bed slope	i_b	0.11	m/km
width main channel	B_m	260	m
width floodplain	B_f	1100	m
height bank main channel	h_m	6 (5)	m
Chézy coefficient main channel	C_m	40	$\sqrt{\mathrm{m}}$/s
Chézy coefficient floodplain	C_f	35	$\sqrt{\mathrm{m}}$/s
grain size bed material	D_{50}	0.001	m
numerical grid size	Δx	500	m
numerical time step	Δt	10	days
computation period	T	20	years

Table 4.3: Dimensions in the case study of a highly simplified floodplain lowering

4.5.4   1-D Rhine model

The Rhine model based on the 1-D morphodynamic simulation package SOBEK has been
developed by Jesse & Kroekenstoel (2001). For the Rhine model the quasi-steady approach
is used, meaning that the flow module iterates until the flow pattern reaches a steady state
solution, after which the sediment transport rates are estimated and the bed levels are updated.
With the model, we make dynamic simulations, each covering a period of 20 years, with a
morphological time step of 10 days and a grid size of 500 m. The model has been calibrated on
the basis of hydraulic and bathymetric data and data on sediment transport rates in the period
1987-1997. The hydraulic roughness, the nodal-point relation (describing sediment distribution
at bifurcations), the sediment transport formula and the parameters in the sediment transport
formula are used as tuning parameters in the calibration process of the model.

Schematisation of planform

Topologically speaking, the Rhine model consists of a network of nodes and branches. It includes
six main branches of the Rhine - Niederrhein, Waal, Pannerdensch Kanaal, Lower-Rhine, Lek
and IJssel (bifurcates into Keteldiep and Kattendiep near the downstream end) - and the
bifurcation points Pannerdensche Kop and IJssel Kop (see Figure 4.5).

At each spatial grid point a cross-sectional profile is defined, distinguishing between the main
channel, the groyne section, the flow-conveying floodplain and the storage area. The morpho-
logically active part of the cross-section is restricted to the main channel and is indicated by the
transport width. Lateral sediment transport from the main channel into the floodplains or vice
versa is neglected. All sediment transport and all morphological changes therefore occur in the
main channel. For the initial bed topography (cross-sectional profiles), use is made of digital
elevation maps and bathymetric soundings. Since we deal with a 1-D model the geometrical
information left and right of the river axis is averaged. Thus we neglect, for example, 2-D phe-
nomena, such as asymmetrical cross-sections. Each cross-sectional profile is described with 15
points: 5 points for the main channel, 3 for the groyne section and 7 for the floodplain section
(see Figure 4.5). For each point the bed level position with respect to a reference level, the
total width and the flow-conveying width are specified. The height of summer levees and the
flow-conveying and storage area behind the summer levees are defined separately in the model.
Due to gradients in the sediment transport, the bed level positions in the alluvial part of the
cross-sections will change. Erosion and sedimentation are distributed proportional to a local
reference depth across the sediment transport width of the cross-section.

Bottom protection structures in the sharp bends near Erlecom (km 873-876), Nijmegen (km
882-885) and St. Andries (km 925-928) have been constructed for navigation purposes, so as to
enlarge the navigable width. In the model these structures are schematised as fixed bed layers
imposing a lower bound on the bed level and an enhanced hydraulic roughness. Weirs have

been constructed in the Lower-Rhine and Lek near Driel (891 km), Amerongen (922 km) and Hagestein (947 km). These weirs are schematised in the model as structures with hydraulic controllers.

In addition to the initial condition that is given in terms of bed topography, two initial conditions are imposed in terms of water level and discharge at the beginning of the model run.
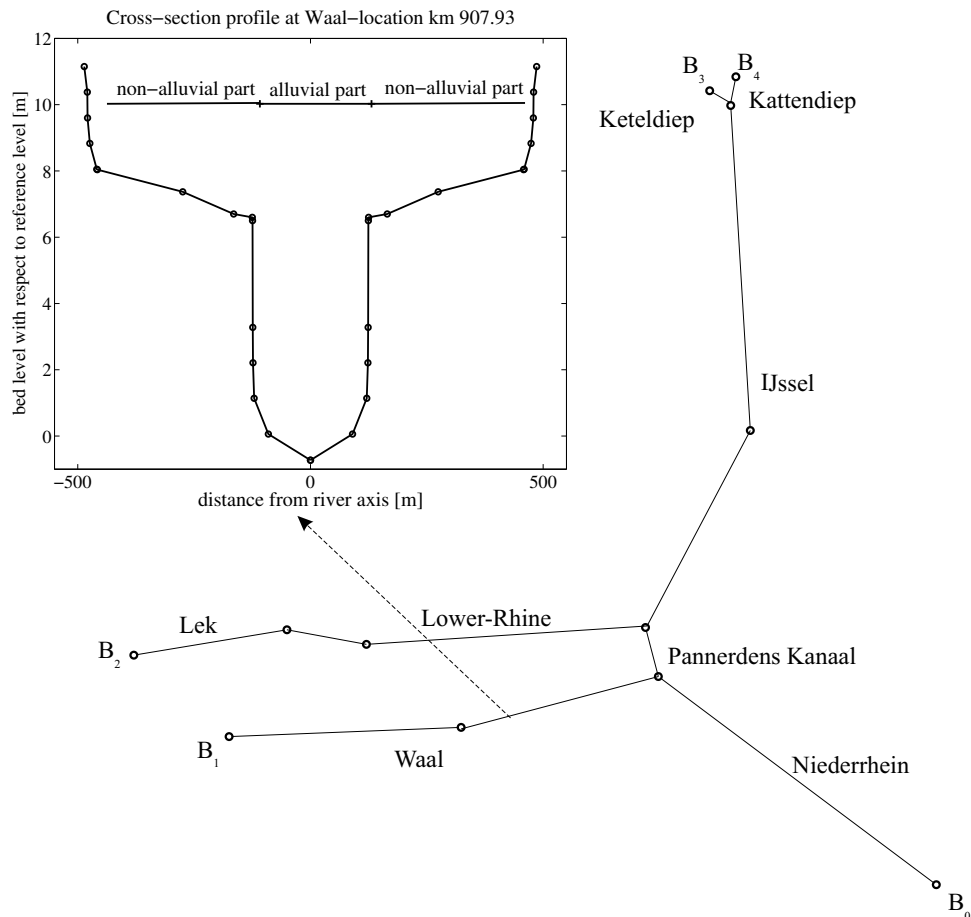

Figure 4.5: Schematisation Rhine branches in the model as a network of nodes and branches and an example of the cross-section schematisation

Upstream boundary conditions

The following upstream boundary conditions are imposed:

- The hydraulic condition is a discharge time series.
- The morphological condition is that at any point in time the incoming sediment transport rate equals the local transport capacity at the boundary.

Regarding the hydraulic boundary condition at the upstream boundary, the quasi-steady approach allows discharge time series to be represented by a piecewise constant function, such

that during one computational time step the discharge is constant. The existing 100-year daily discharge record taken in the Niederrhein near Lobith is the data source. In order to match the discharge time series with the numerical time step applied in the simulation, these data are averaged over intervals of approximately 10 days, such that 36 of these intervals form a year. For each of them, the weighted average, Q_{w}, of the daily discharges, Q_{d}, is estimated, such that the expected total volume of transported sediment, V, in each interval T_{w}, remains unchanged:

$$V = T_{\mathrm{w}} \cdot S\left(Q_{\mathrm{w}}\right) = T_{\mathrm{w}} \cdot E\left(S\left(Q_{\mathrm{d}}\right)\right) = T_{\mathrm{w}} \cdot \frac{\sum_{d=1}^{N} S\left(Q_{\mathrm{d}}\right)}{N} \tag{4.8}$$

in which S the sediment transport volume per second [m^3/s], and N the number of daily discharges averaged (10 or 11 days) [-].

If the sediment transport formula is a general function of the depth averaged flow velocity u to the power n, the following calculation for the sediment transport and representative discharge can be made:

$$S\left(Q_{\mathrm{w}}\right) = B_{\mathrm{s}} m u^{n} = m B_{\mathrm{s}}^{1-n} Q_{\mathrm{w}}^{n} h^{-n}, \;\; \text{so that} \;\; Q_{\mathrm{w}} = B_{\mathrm{s}} h \left(\frac{E\left(S\left(Q_{\mathrm{d}}\right)\right)}{m B_{\mathrm{s}}}\right)^{1/n} \tag{4.9}$$

in which B_{s} is the width of the sediment transporting zone [m], m a multiplier [-], h the water depth [m].

If in the definition of Q_{w} the bed slope would be taken constant, instead of using the water depth, we would have:

$$S\left(Q_{\mathrm{w}}\right) = m B_{\mathrm{s}}^{1-n/3} Q_{\mathrm{w}}^{n/3} i_{\mathrm{b}}^{n/3} C^{2n/3} \;\; \text{so that} \;\; Q_{\mathrm{w}} = \left(\frac{E\left(S\left(Q_{\mathrm{d}}\right)\right)}{m B_{\mathrm{s}}}\right)^{3/n} \frac{B_{\mathrm{s}}}{C^2 i_{\mathrm{b}}} \tag{4.10}$$

So, for the conversion from daily discharge to discharges per intervals of approximately 10 days, we could use either Eq. 4.9 or Eq. 4.10. The conversion results in 36 intervals of 100 data points. For illustration, the resulting discharge series for each year in the period 1900-2000 and its overal statistics are shown in Figure 4.6.

About two thirds of the Rhine discharge flow into the Waal. A more accurate scaling-factor for different discharge regimes, determined on the basis of (1) discharge measurements at Pannerdensche Kop and (2) Rhine model computations, is shown in Figure 4.6(e). This scaling-factor is used in the hypothetical model in which the Waal discharge has to be imposed at the inflow boundary.

Downstream boundary conditions

Hydraulic conditions in the form of rating curves (stage-discharge relationship) are imposed at each of the downstream boundaries - B$_1$ Waal (Werkendam), B$_2$ Lek (Krimpen aan de Lek), B$_3$ IJssel (Kattendiep) and B$_4$ IJssel (Keteldiep), see Figure 4.5 and 4.7. Rating curves are deduced from measurements, viz. water level, cross-sectional geometry and flow velocity measurements.
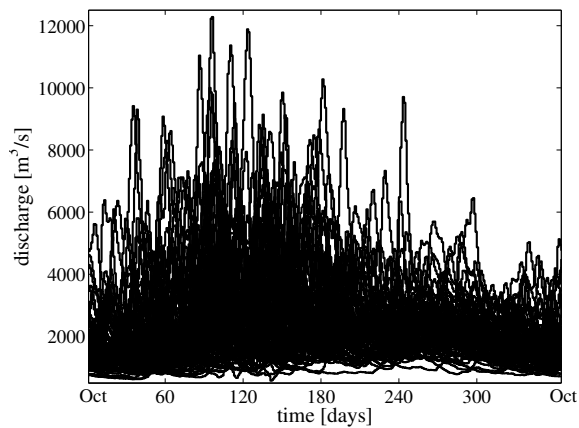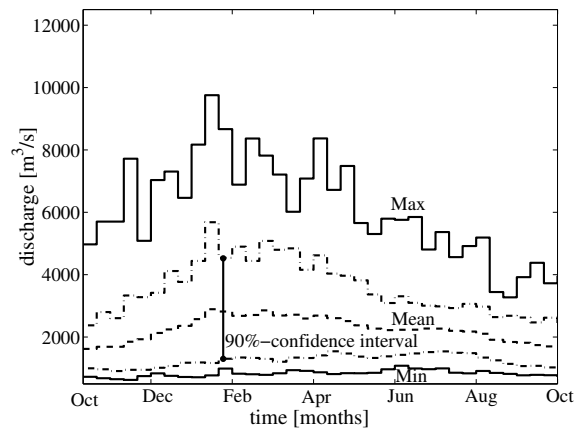
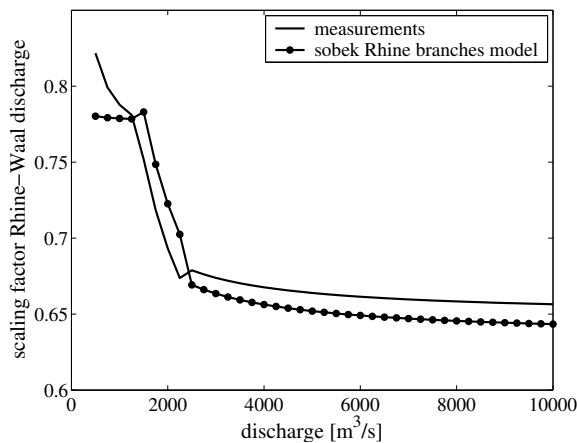(a) Yearly discharge time series with daily records
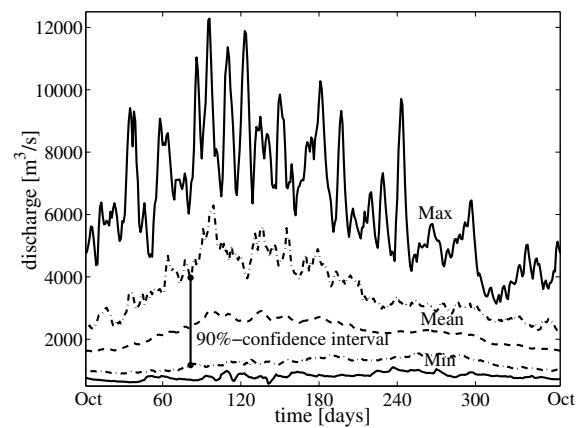
(b) Statistics of the daily discharge through the hydrological year
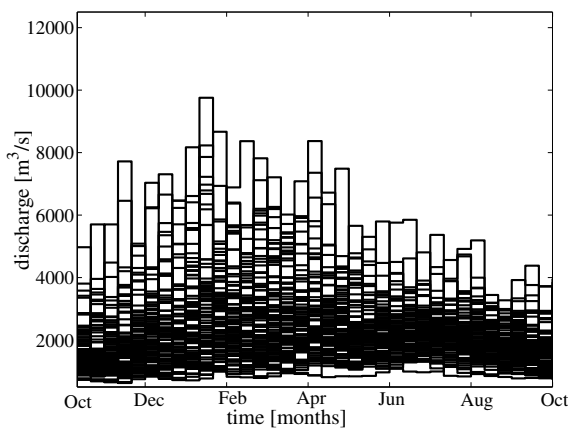
(c) Yearly discharge time series, averaged over intervals of approximately 10 days

(d) Statistics of the discharge over 36 intervals through the hydrological year

(e) Scaling-factor Rhine-Waal discharges for different discharge regimes

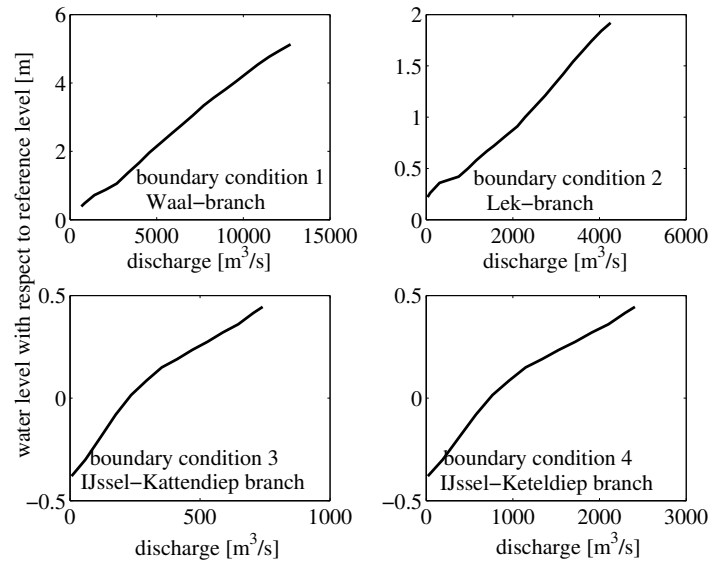**Figure 4.6:** Discharge record and statistics at Lobith for the period 1900-2000

Figure 4.7: Rating curves at downstream boundaries: B_1 - Waal, B_2 - Lek, B_3 - IJssel (Kattendiep) and B_4 - IJssel (Keteldiep)

Conditions at bifurcations

At the Pannerdensche Kop bifurcation the discharge distribution fully depends on the conveyance and the available total difference in head over the outflowing branches to the base of the river. The discharge distribution at the IJsselkop is controlled by a weir in the Lower-Rhine for Rhine discharges in the Niederrhein below a threshold value of 2400 m^3/s. For discharges above this threshold value the weir does not operate, meaning that the discharge distribution is governed by the conveyance and resistance of the branches.

The distribution of sediment at the bifurcations is expressed by means of the following nodal-point relation:

$$\frac{S_1}{S_2} = \alpha \frac{Q_1}{Q_2} + \beta \tag{4.11}$$

So, the ratio of sediment load of the two outflowing branches, S_1/S_2, is expressed as a linear function of the water distribution over these branches, Q_1/Q_2. The coefficient α is used as a tuning coefficient in the calibration process of the model, and equals 3 and 1.5 for the Pannerdensche Kop and IJsselkop bifurcation, respectively. The coefficient β equals zero.

This relation can be rewritten in the following format:

$$S_1 = \frac{F}{1+F} S_{\mathrm{t}}$$
$$S_2 = \frac{1}{1+F} S_{\mathrm{t}} \tag{4.12}$$

This means: $F = \alpha \dfrac{Q_1}{Q_2}$

in which S_t is the total sediment volume entering the bifurcation [m³/s]. Thus, when at the Pannerdensche Kop bifurcation 66% of the Rhine discharge is directed into the Waal and the remaining 34% flows into the Pannerdensch Kanaal, then 85% of the sediment load is directed into the Waal and 15% goes towards the Pannerdensch Kanaal. This ratio corresponds more or less with the ratio derived by Wilbers (2004).

Hydraulic roughness

The hydraulic roughness of the main channel is often composed of separate contributions for the grains of the bed material and for the bedforms that cover the riverbed. In the model use is made of the roughness predictor of Vanoni & Hwang (1967):

$$C^{-2} = C_g^{-2} + C_{bf}^{-2} \tag{4.13}$$

in which C_g and C_{bf} are the Chézy coefficients for the grain size and the bedforms, respectively [m$^{1/2}$/s].

The Chézy coefficient for the grain size is given by the White-Colebrook formula (Jansen et al., 1979):

$$C_g = ln\,(10)\,\kappa^{-1}g^{1/2}\log\frac{12R}{k_m} \approx 18\log\frac{12R}{k_m} \tag{4.14}$$

in which κ is the Von Karmann coefficient [-], g the acceleration due to gravity [m/s²], R the hydraulic radius [m] and k_m the roughness height [m]. The Nikuradse roughness height of the main channel k_m is expressed as $3.5D_{90}$ in the model, in which D_{90} is the grain size diameter which is not exceeded by 90% of the bed material [m].

The Chézy coefficient related to the bedforms is described as (Vanoni & Hwang, 1967):

$$C_{bf} = (8g)^{1/2}\left(3.3\log\frac{Lh}{H_d^2} - 2.3\right) \tag{4.15}$$

in which g the acceleration due to gravity [m/s²], L the dune length [m], h the water depth [m] and H_d the dune height [m].

Model units have been defined for which the Chézy coefficients are estimated as a function of the river discharge via the Vanoni & Hwang (1967) hydraulic roughness predictor (see Figure 4.8).

The hydraulic roughness of the floodplains is related to the various ecotypes and their spatial distribution over the floodplains. Nikuradse roughness coefficients of the floodplain k_{fp} are chosen with the help of roughness tables. The White-Colebrook formula (Eq. 4.14) is used to transform the Nikuradse coefficients into Chézy coefficients. The roughness of the floodplain cover is however not always a fixed value, but may depend on the inundation depth of the floodplain. The dependency on the inundation depth is, for instance, significant for floodplain

shrubs and forest ecotypes. However, with the application of the White-Colebrook formula this dependency is not considered.

Subsequently, all 'estimated' Chézy coefficients are used as tuning parameters in the calibration process of the model. As a consequence, these coefficients are slightly adjusted by Jesse & Kroekenstoel (2001), thus losing part of their physical meaning. This may have its impact on the computed transport rates. Figure 4.8 shows the calibrated Chézy coefficients of the main channel as a function of discharge (for different model units) and Nikuradse hydraulic roughness lengths of the floodplains of the Niederrhein and the Waal.

(a) Chézy coefficients of the main channel as a function of the local discharge

(b) Nikuradse coefficient of the floodplains
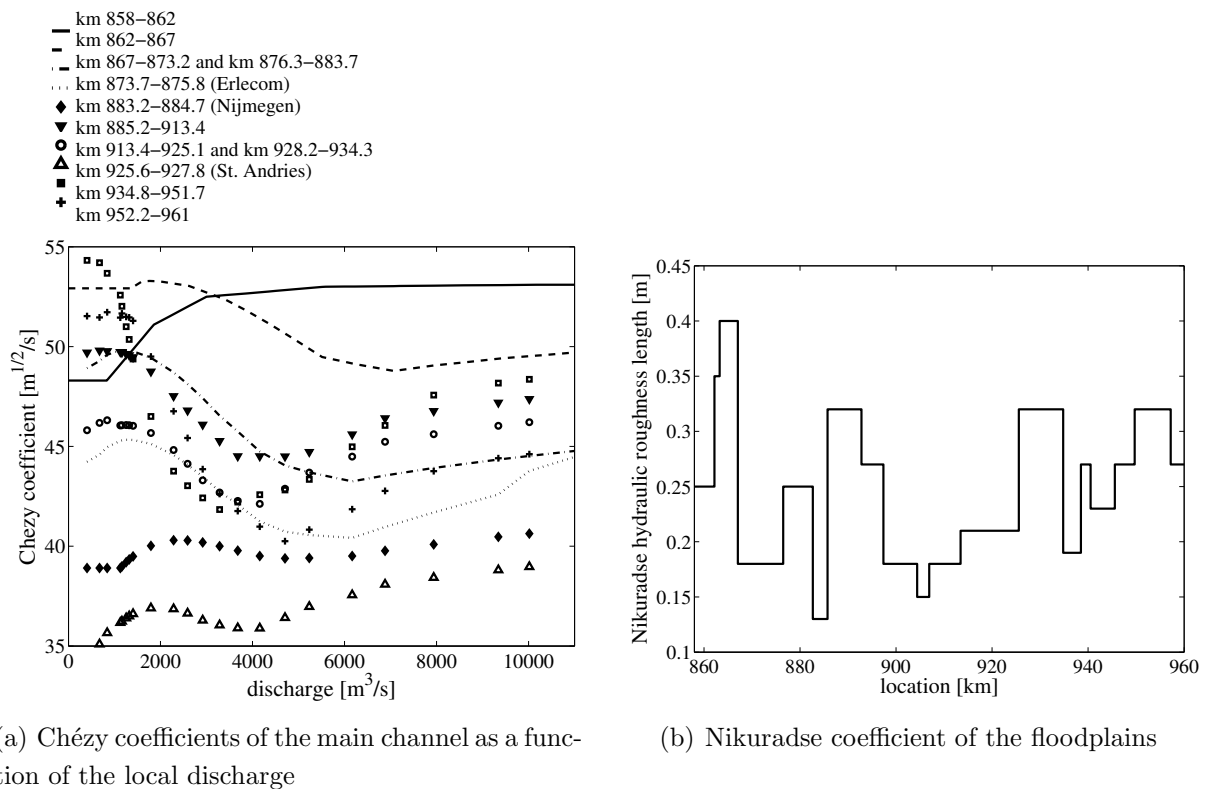
Figure 4.8: Chézy coefficients of the main channel and Nikuradse hydraulic roughness lengths of the floodplains of the floodplains in the Niederrhein and the Waal

Grain size of the bed material

The Rhine is characterised by non-uniform sediment (e.g. Kleinhans, 2002 and Julien et al., 2002). In the Rhine significant downstream fining and vertical segregation of fine and coarse sediments are observed. Bend effects, bifurcation points, bedforms and navigation cause lateral variation in grain size. Vertical grain sorting and bed armouring, with coarser particles covering the finer ones, are important segregation processes in the Niederrhein, Pannerdensch Kanaal and the areas close to the bifurcations (Jesse & Kroekenstoel, 2001).

In a morphodynamic model system for non-uniform sediment, the bed could be schematised into homogeneous top layer, the active layer (of a certain thickness and sediment size fraction) and a non-moving homogeneous substrate (Hirano, 1971). In this kind of model system, detailed information on sediment layers, their thickness and size fractions is required. This data is not available for the Dutch Rhine. Moreover, the vertical sorting processes are less important in the Waal and IJssel, branches that are considered more specifically in this thesis. Therefore, uniformity of the bed material is assumed in the model. The model somehow accounts for the longitudinal sorting process (downstream fining) by specifying the uniform grain size of the bed material at each location. Four sediment measuring campaigns are used as a data source. Information from the grain size distribution curves that are deduced from the data, viz. the D_{50} and the D_{90} grain size characteristic is used in the model (see Figure 4.9).

(a) Grain size characteristics D_{50} (b) Grain size characteristics D_{90}
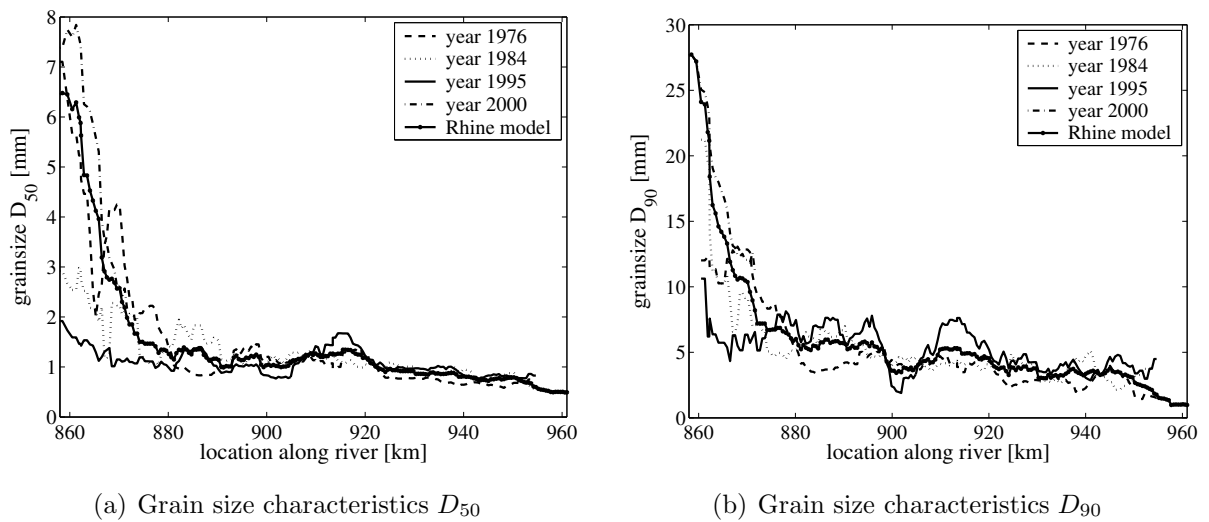
Figure 4.9: Spatial distribution of grain size characteristics in Niederrhein and Waal - four sediment measuring campaigns (1976, 1984, 1995, 2000) and values set in the Rhine model

Sediment transport formula

The bedload sediment transport formula of Meyer-Peter & Müller (1948) is incorporated in the model. The formula reads:

$$s = A \cdot \frac{8\sqrt{g\Delta_{\mathrm{d}}D_{50}^3}}{1-\epsilon} \left(\frac{u^2}{C_{90}^{3/2}C^{1/2}\Delta_{\mathrm{d}}D_{50}} - \theta_{\mathrm{c}} \right)^{\alpha} \tag{4.16}$$

in which s is the bedload sediment transport rate per unit width, expressed in deposited volume (including pores) [m³/m/s], A is a multiplier used for calibration purposes [-], g the acceleration due to gravity [m/s²], Δ_{d} the relative density of the sediment [-], D_{50} the median grain size of the bed material [m], ϵ the porosity of the bed [-], C_{90} the hydraulic roughness Chézy coefficient related to the bed material [m¹ᐟ²/s], C the Chézy coefficient [m¹ᐟ²/s], u the depth averaged flow

velocity in the main channel [m/s], θ_c the critical Shields parameter (equal to 0.047) [-] and α a constant exponent (equal to 1.5) [-].

The Rhine is characterised by non-uniform sediment. Nonetheless, uniformity in the bed material is assumed in the model. When significant vertical segregation of fine and coarse sediment occurs, the finer sediment particles will be in motion at low-flow, whereas the coarser ones are not transported. To account for the transport of fine sediment under low-flow conditions, the critical Shields parameter is reduced to 0.025. Justification of this reduction and the choice for using the Meyer-Peter & Müller (1948)-formula is given by Jesse & Kroekenstoel (2001).

4.6   Model justification

4.6.1   1-D approach vs quasi-3D approach

A major concern with MCS with crude sampling is the inefficiency of the method. Computationally intensive numerical models in combination with a large number of simulations (required for convergence of the output statistics) can make MCS a laborious operation. The computational effort per individual numerical simulation differs considerably between 1-D and multi-dimensional models. Therefore, preference is given to a 1-D approach. We expect to produce generic knowledge on the use of stochastic methods in river morphology that holds for multi-dimensional model approaches as well. The potential of a stochastic model approach in river management practice can be explored with a 1D-approach. A question that needs to be addressed, however, is to what extent the relevant morphological phenomena can be modelled and predicted with the 1-D models.

The 1D Rhine model, which was described in the previous chapter, approximates the river as a network of branches and nodes, including man-made structures and variations in geometry and flow resistance. Table 4.4 gives an overview on how the model deals with the morphological phenomena at various scale-levels that were discussed in Section 4.3. The calibrated 1-D Rhine model is valuable to gain insight into the morphological processes at macro-scale level, thus the longitudinal profile evolution. Moreover, the geometrically induced bed variability along the river is incorporated.
Since the model is purely 1-D, there is no distinction between the left and the right side of the river. Thus, the 1-D model gives a width-averaged representation of the morphodynamics of the river bed, meaning that 2-D phenomena, such as cross-sectional profile evolution imposed by the river alignment, are neglected. This means that 2-D features, such as alternate bars, or transverse slopes in bends, are not considered. Neither is the fact that large floodplain areas are located alternately at the right and left side of the river, which under flood conditions may lead to strong 3-D cross-flows over the main channel (Knight, 2001 and Shiono & Muto, 1998).

For 2D-effects analytically based post-processing should be applied (see Section 4.3.2), or the step to 2-D or 3-D modelling should be made.

scale levels	morphological phenomena	1D-Rhine model	Quasi-3D Waal model
micro	- bedforms, such as ripples and dunes	±	±
	- vertical segregation of sediment fractions	-	-
meso	cross sectional profile evolution:		
	- transverse bed slope and point-bar/pool formation in bends	-	+
	- formation of shallow and deep parts in geometrically complex reaches	a	+
	- crossings between opposite bends	-	+
	- bank erosion	-	-
	- overbank sand deposition	-	-
	- local scour e.g. around bridge piers	-	-
	- local scour in groyne fields and formation of so-called groyne flames	-	-
macro	- longitudinal profile evolution	+	+
	- evolution of geometry at river bifurcations	±	+

- = not dealt with; + = dealt with; ± = dealt with parametrically;
a = formation of shallow and deep parts is width-averaged

Table 4.4: Overview on how the 1D Rhine model and the quasi-3D Waal model deal with morphological phenomena at various scale-levels

We have the impression that the Rhine model is representative of reality as long as multi-dimensional effects do not dominate the morphological processes to be modelled. Moreover, we expect that in that case the estimated uncertainty, when running this model in a stochastic mode, is representative as well. If multi-dimensional processes are predominant, the uncertainty in the width-averaged quantity per cross-section is expected to be smaller than that in individual points in this cross-section, because of the averaging out of the relatively large anomalies. In that case, the Rhine model results are expected to be less representative and they probably may lose part of their physical meaning.

For the purpose of validating the 1D approach and testing the above-mentioned hypotheses, a model will be used that is capable of describing multi-dimensional phenomena. In principle, river morphology concerns a 3-D process, however, most problems do not need to be tackled by means of a 'complete' 3-D description (De Vries, 1993). In river morphological practice, quasi-

3D models, i.e. 2D depth-averaged models with parametrised curvature-induced secondary flow, are frequently used. For the Niederrhein and the Waal, for instance, a number of models based on the numerical software package Delft3D have been developed by WL|Delft Hydraulics (Sloff et al., 2003, Sloff & Jagers, 2004, Sloff, 2004). Apart from these models, an impressive database on flow, sediment transport and bathymetry is available for the Rhine. Lambeek et al. (2004) ran one of the Delft3D-models in a stochastic mode. Using this type of model in a Monte Carlo-setting is considered promising. Therefore, we use one of these models to explore the ensemble dimensions.

The quasi-3D model of the Waal (Sloff, 2004) is appropriate for the purpose of validating the 1D approach, since the model area considered is characterised by large variations in geometry (such as floodplain widenings and constrictions alternately located left and right of the river axis), bends of moderate curvature and crossing between opposite bends. Morphodynamic phenomena at meso and macro-scale are considered in this model, see Table 4.4. This includes the simulation of transverse bed slope formation (pointbar and pool combinations in bends) and the formation of shallow and deep parts alternately at the left and the right side of the river. The formation of bedforms, such as dunes and ripples, is not explicitly simulated in the Delft3D model, but is included parametrically via an alluvial bed roughness predictor. Descriptions of the numerical software package Delft3D-MOR and the model of the Waal will be given in the next sections. The actual validation of the 1-D model concept against the quasi-3D model will be described in Section 4.6.4.

4.6.2   Numerical software package Delft3D-MOR

The Delft3D-MOR program of the Delft3D software package has been designed to simulate morphodynamic behaviour of rivers, coasts and estuaries at time scales of days to years. It describes the complex interaction between waves, currents, sediment transport and bathymetry. Each of these processes is dealt with in a separate module. These modules are operated in sequential or cyclic (iterative) modes, using each others results. Delft3D-MOR is a finite-difference system in which the processes are simulated on an orthogonal curvilinear grid, allowing for an efficient and accurate representation of complex domains. The computational grid is staggered, meaning that not all quantities are defined at the same location in the numerical grid. The principal constituents of a Delft3D-MOR model are the flow module (Delft3D-FLOW), the sediment transport module (Delft3D-TRAN) and the bottom change module (Delft3D-BOTT).

Flow equations

The hydrodynamic module Delft3D-FLOW solves the unsteady shallow water equations in two (depth-averaged) or in three dimensions. The 2-D flow mode is applicable in vertically well-mixed nearly-horizontal flow regimes and is often combined with a parametrisation for

curvature-induced secondary flow (quasi-three dimensional). The depth-averaged equation of continuity reads:

$$\frac{\partial \left(h + z_b\right)}{\partial t} + \frac{\partial hu}{\partial x} + \frac{\partial hv}{\partial y} = 0 \tag{4.17}$$

The depth-averaged equations of motion (in their commonly used form):

$$\frac{\partial u}{\partial t} + u\frac{\partial u}{\partial x} + v\frac{\partial u}{\partial y} + g\frac{\partial \left(h + z_b\right)}{\partial x} + \frac{\tau_{bx}}{\rho h} = \frac{1}{\rho h}\frac{\partial \left(hT_{xx}\right)}{\partial x} + \frac{1}{\rho h}\frac{\partial \left(hT_{xy}\right)}{\partial y} \tag{4.18}$$

$$\frac{\partial v}{\partial t} + u\frac{\partial v}{\partial x} + v\frac{\partial v}{\partial y} + g\frac{\partial \left(h + z_b\right)}{\partial y} + \frac{\tau_{by}}{\rho h} = \frac{1}{\rho h}\frac{\partial \left(hT_{xy}\right)}{\partial x} + \frac{1}{\rho h}\frac{\partial \left(hT_{yy}\right)}{\partial y} \tag{4.19}$$

in which h is the water depth [m], z_b the bed level [m], u and v the depth-averaged velocity in x and y-direction [m/s], g the acceleration due to gravity [m/s^2], τ_{bx}, τ_{by} the bed-shear stress in x and y-direction [kg/m/s^2], T_{xx}, T_{xy} and T_{yy} the horizontal exchange of momentum through viscosity [kg/m/s^2], turbulence, spiral flow, wave action and non-uniformity of velocity distribution.

The bed-shear stresses are expressed by the 2D version of Chézy's law:

$$\tau_{bx} = \frac{\rho gu\sqrt{u^2 + v^2}}{C^2} \ \ \text{and} \ \ \tau_{by} = \frac{\rho gv\sqrt{u^2 + v^2}}{C^2} \tag{4.20}$$

Transport and Morphology equations

A number of empirical formulae for sediment transport are incorporated in the Delft3D-TRAN module. Gradients in the sediment transport field give rise to bed level changes. The development of the bed level, z_b, is computed in the Delft3D-BOTT module and is based on the conservation of sediment mass:

$$\frac{\partial z_b}{\partial t} + \frac{\partial s_{bx}}{\partial x} + \frac{\partial s_{by}}{\partial y} + E - D = 0 \tag{4.21}$$

in which s_{bx} and s_{by} are the bedload sediment transport rates per unit of width in x and y-direction (i.e. including pores) [m^3/m/s], while E is the entrainment rate and D the deposition rate of suspended sediment [m/s].

The bedload transport components are computed as follows:

$$s_{b,x} = s_b\cos\left(\alpha_s\right) \ \ and \ \ s_{b,y} = s_b\sin\left(\alpha_s\right) \tag{4.22}$$

in which α_s is the transport direction indicated by an angle relative to the x-direction and s_b is the bedload transport magnitude [m^3/m/s].

For time-dependent 2-D river bed deformation, the deviation of the bedload transport vector from the main flow direction has two constituents, viz. (1) the influence of the spiral motion (due to the curvature of the flow) and (2) the influence of the sloping bed.

In a bend, the flow direction near the bed, and thus the bed-shear stress direction, deviates from the depth-averaged flow direction due to the spiral flow effects:

$$tan\left(\alpha_\tau\right) = \frac{v - \alpha_I \frac{u}{|u|} I}{u - \alpha_I \frac{v}{|u|} I} \tag{4.23}$$

in which $|u|$ is the depth-averaged velocity magnitude and I is the spiral motion intensity. α_I is given by:

$$\alpha_I = \frac{2}{\kappa^2} E_s \left(1 - \frac{1}{2} \frac{\sqrt{g}}{\kappa C}\right) \tag{4.24}$$

in which E_s is a calibration coefficient [-].

Van Bendegom (1947) gives the following direction formula for sediment grains moving along a sloping bed:

$$\tan\left(\alpha_s\right) = \frac{sin\left(\delta\right) - \frac{1}{f(\theta)} \frac{\partial z_b}{\partial y}}{cos\left(\delta\right) - \frac{1}{f(\theta)} \frac{\partial z_b}{\partial x}} \tag{4.25}$$

in which $f\left(\theta\right)$ is the slope factor (assumed to be a function of the Shields parameter θ), α_s the direction of the sediment transport and δ the angle of direction of the near-bed flow, or the bed-shear stress.

The transverse slope effect is given as:

$$f\left(\theta\right) = a_s \theta^{b_s} \tag{4.26}$$

The function was approximated by Talmon et al. (1995), see Eq.4.3. In practice often the function is written as $f\left(\theta\right) = 0.85\sqrt{\theta}$ for natural channels.

4.6.3 Quasi-3D Waal model

For the analysis of time-dependent 2-D river bed deformations in the Waal, a detailed quasi-3D Delft3D model has been developed by Sloff (2004). The hydraulic roughness, the parameters in the transport formula and those related to the direction of bedload sediment transport are used as tuning parameters in the model.

Schematisation of planform

The Waal model area covers the reach from km 886 (Nijmegen) to km 923 and has a total length of 37 km. The model area is characterised by large variations in geometry, bends of moderate curvature and crossing between opposite bends. This is clearly illustrated in Figure 4.10, showing the model topography.

The curvilinear computational grid consists of 370 by 70 cells, with the grid lines (almost) perpendicular to each other. The initial bed topography is based on bed elevation maps and

bathymetric soundings. A distinction is made between main channel, groyne section and flood-plains. The alluvial part of the river is restricted to the main channel (cell row 29-40). This means that accretion and erosion processes on the floodplains or in the groyne sections are not considered. The averaged cell width and length in the main channel are 22-27 m and 90-110 m, respectively. Groyne fields, summer levees and steep obstacles in the floodplains are schematised by 2D-weirs.
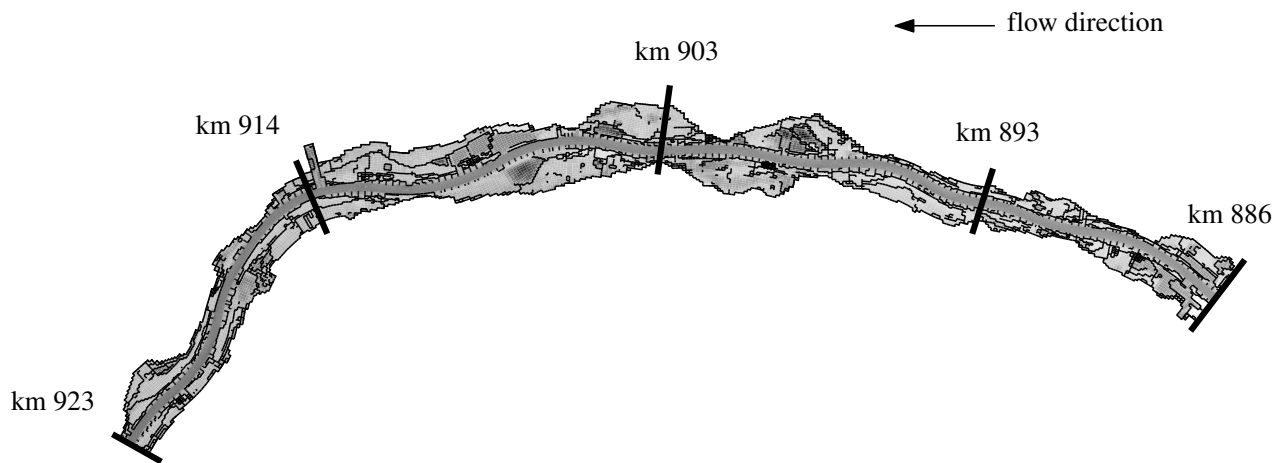

Figure 4.10: Bed topography in the Waal model

Figure 4.11 shows the initial bed topography of different cross-sections along the Waal. It becomes clear that each cross-section exhibits a certain degree of asymmetry. Deep ponds (usually sand mining pits) and narrow and wide cross-sectional profiles are located alternately in the floodplains at the left and the right side of river.

Figure 4.12 shows the curvilinear grid for four subsections, viz. (a) km 893-903, (b) km 903-913, (c) km 913-918, and (d) km 918-923. Km-locations of the cross-sections are indicated by bold lines perpendicular to the main channel axis. The other bold lines represent groynes, summer levees and steep obstacles. The dashed lines indicate the boundaries of the main channel.

Boundary conditions

The boundary conditions consist of a hydraulic and a morphological condition at the upstream boundary and a hydraulic condition at the downstream boundary. At the inflow boundary a discharge time series is imposed (see Section 4.5.4). For every discharge value, a discharge distribution over the grid cells of the upstream boundary is required. For discharges below the threshold value of 1693 m^3/s all water will flow via the main channel resulting in a discharge distribution over grid cells 29-40. At flow regimes above this threshold value floodplains are inundated and the discharge is distributed over the entire cross-section. The morphological condition at the upstream boundary is that the incoming sediment transport per unit width equals

the local transport capacity at the boundary. The hydraulic downstream boundary consists of a rating curve.
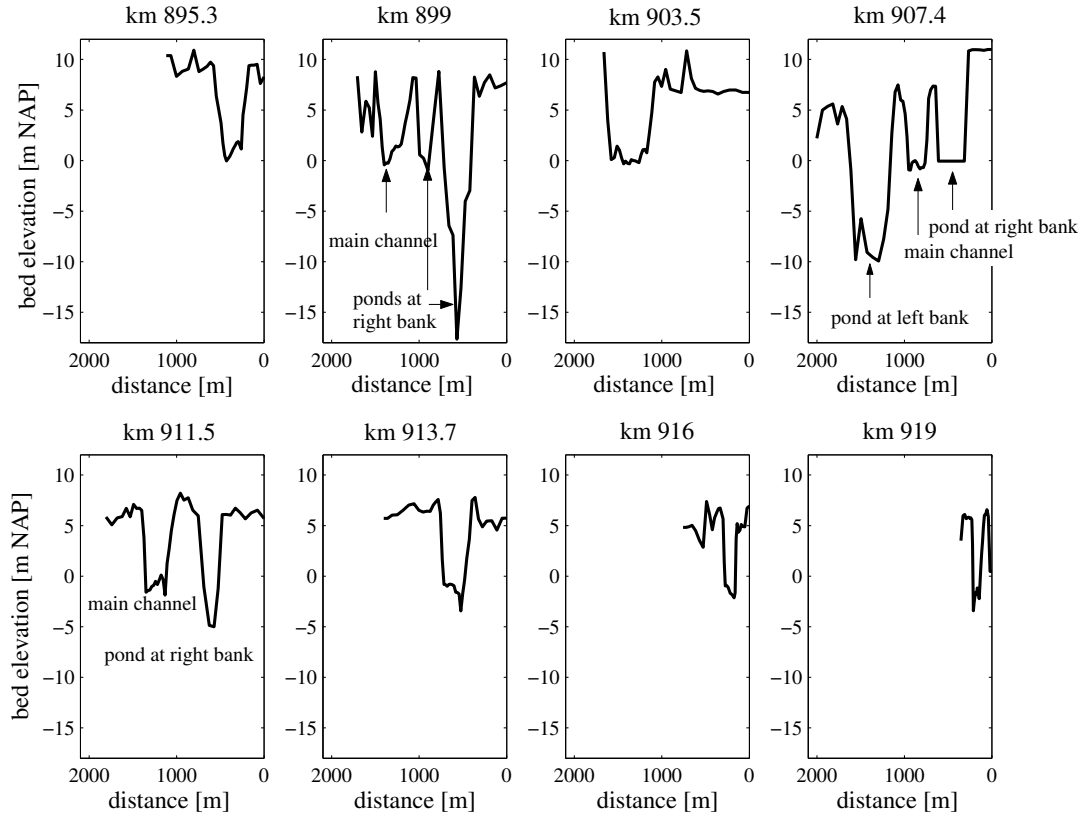
Figure 4.11: Initial bed topography in various cross-sections, along the Waal river

Hydraulic roughness

Nikuradse roughness coefficients that vary in longitudinal and in transverse direction in the main channel, are incorporated in the model. To that end, an adapted version of the Van Rijn (1984)-roughness predictor is used. This predictor accounts for variation in hydraulic roughness at different flow conditions, since bedforms tend to develop and affect the bottom roughness. The hydraulic roughness of the floodplains is related to the various ecotypes and their spatial distribution over the floodplains. Nikuradse roughness coefficients k are chosen with the help of roughness tables. The roughness of floodplain cover is however not always a fixed value, but may depend on the inundation depth of the floodplain. For floodplain shrub, forest ecotypes and fencings, for instance, this dependency on the inundation depth is significant and may even turn the Chézy coefficient from an increasing into a decreasing function of the water depth (Baptist, 2005). An analytical model for hydraulic roughness of submerged vegetation is incorporated in the model (Klopstra et al., 1997).
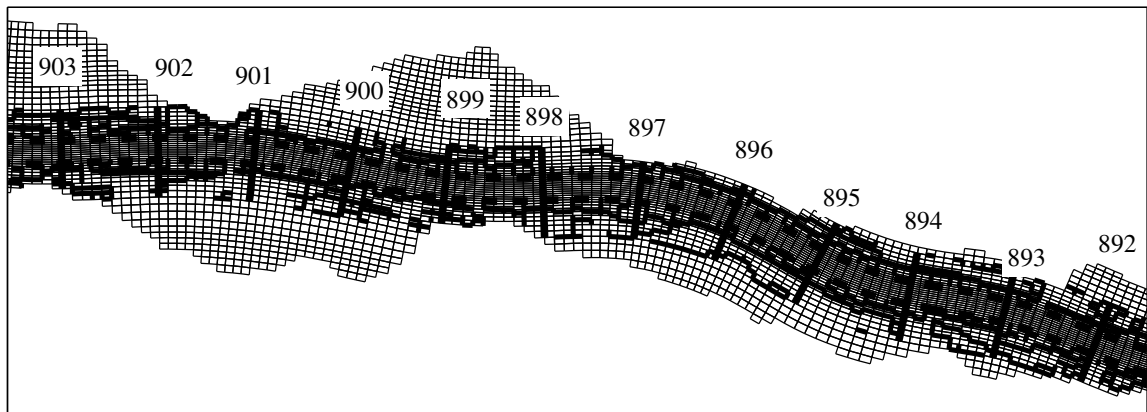
(a) Section km 893-903
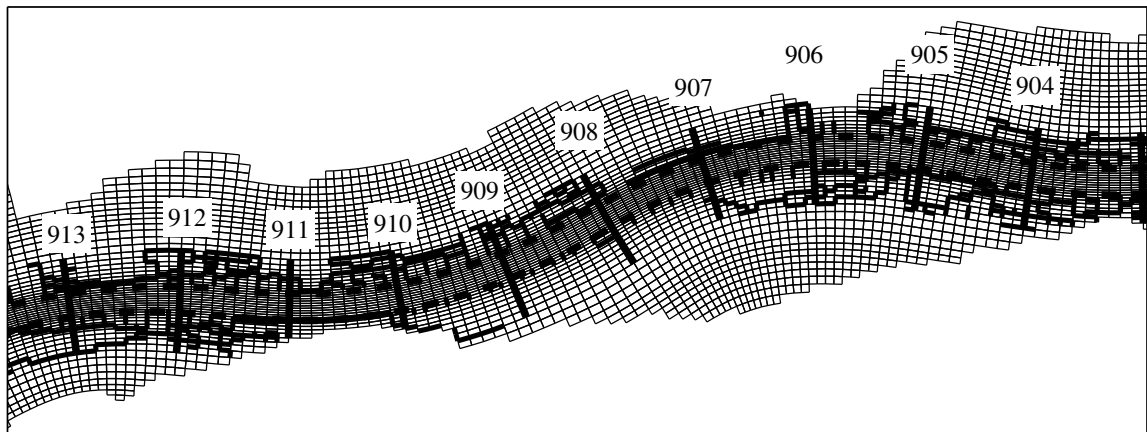
(b) Section km 903-913
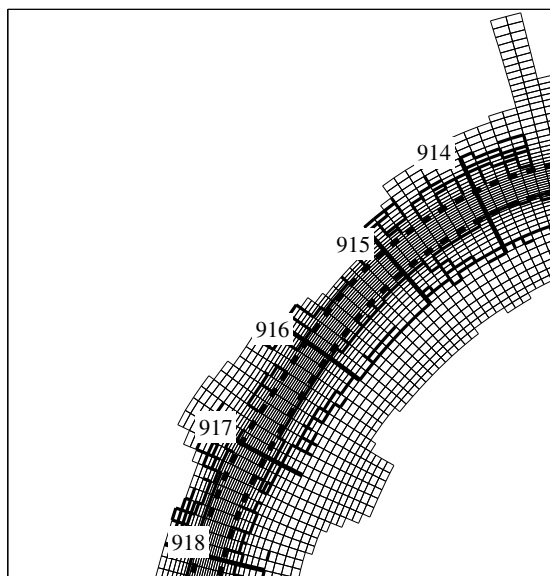
(c) Section km 913-918
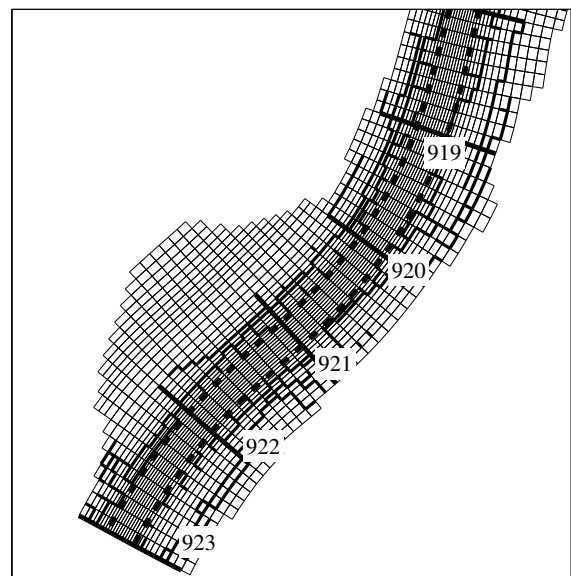
(d) Section km 918-923

Figure 4.12: Curvilinear computational grid of four subsections of the Waal model

Sediment transport related choices and parameters

The Meyer-Peter & Müller (1948) formula has been extensively tested and used for rivers with coarse bed material in which suspended load was absent. The Engelund & Hansen (1967) formula has been found to give a fair prediction for fine sandy rivers with substantial suspended load. The formula of Engelund and Hansen concerns the total load, including bed load and suspended load of the bed material, and reads

$$s = A \frac{0.05 u^5}{(1 - \epsilon)\, \sqrt{g} C^3 \Delta_\mathrm{d}^2 D} \tag{4.27}$$

in which s is the sediment transport rate per unit width (i.e. including pores) [m^3/m/s], u the depth-averaged flow velocity in the main channel [m/s], ϵ the porosity of the bed [-], g the acceleration due to gravity [m/s^2], C the Chézy coefficient [m$^{1/2}$/s], Δ_d the relative density of the sediment [-] and D the median grain size of the bed material [m]. A is a multiplier used for calibration purposes, and is chosen equal to 0.5 [-].

In the calibration process of the model, the Engelund and Hansen formula was found to be more appropriate than the Meyer-Peter & Müller formula, as it better corresponds to the physical conditions in the Waal. Sediment segregation processes are significant in the upstream regions of the Rhine system, but are of minor importance in the Waal branch. As a consequence of downstream fining of sediment, suspended load is of major importance in the Waal. Therefore, the Engelund and Hansen formula is incorporated in the model.
In the study area uniformity of the bed material is assumed. Lateral sorting of sediment is neglected. The bed material is characterised using the D_{50} characteristic, which is taken equal to 0.001 m.

In the quasi-3D model, the direction of the bedload sediment transport is split into two components, viz. the influence of the spiral motion and the sloping bed. The calibration coefficient E_s in the spiral flow effect on transport direction (Eq. 4.24) is taken equal to 1. The coefficients for a_s and b_s in the bed slope effect (Eq. 4.26) are chosen 0.6 and 0.5, respectively.

Morphodynamic process tree

Delft3D-MOR is composed of separate modules - viz. Delft3D-FLOW, Delft3D-TRAN, Delft3D-BOT - which are operated alternately, using each others results. A steering module controls the interaction between these modules, known as the process tree. At every moment of the simulation process only one module is active, which means that the various physical processes are computed as if they were uncoupled. The modules are executed consecutively in a loop. Each execution uses the most recent morphological state. The user can specify the order in which the modules are executed and the number of time steps to be run in each module. In

that way, the user may vary the coupling frequency between the physical modules, from an almost fully coupled approach to a quasi-steady approach.

For the Waal model the quasi-steady approach is used. The computational effort of the morphological simulation primarily depends on the effort required in the flow module. A reduction of the computational effort of the time-consuming flow module is obtained in the following way:

1. the discharge hydrograph is discretised into constant values $500 \text{ m}^3/\text{s}$ apart, which yields 16 different discharge stages (see Figure 4.13). Prior to the morphodynamic simulation, for each of these discharge stages the flow module is iterated until the flow pattern reaches equilibrium. The resulting stabilised flow patterns are stored in a database and are used as initial 'guesses' of the flow field on other bed topographies during the morphodynamic simulations.

2. Next, the stabilised flow patterns in the database are used as starting points for executing the flow module, at each discharge level during morphodynamic simulations. In this way, the flow pattern iterates quickly towards its new steady state and the number of time steps in the time-consuming flow module may be reduced significantly.
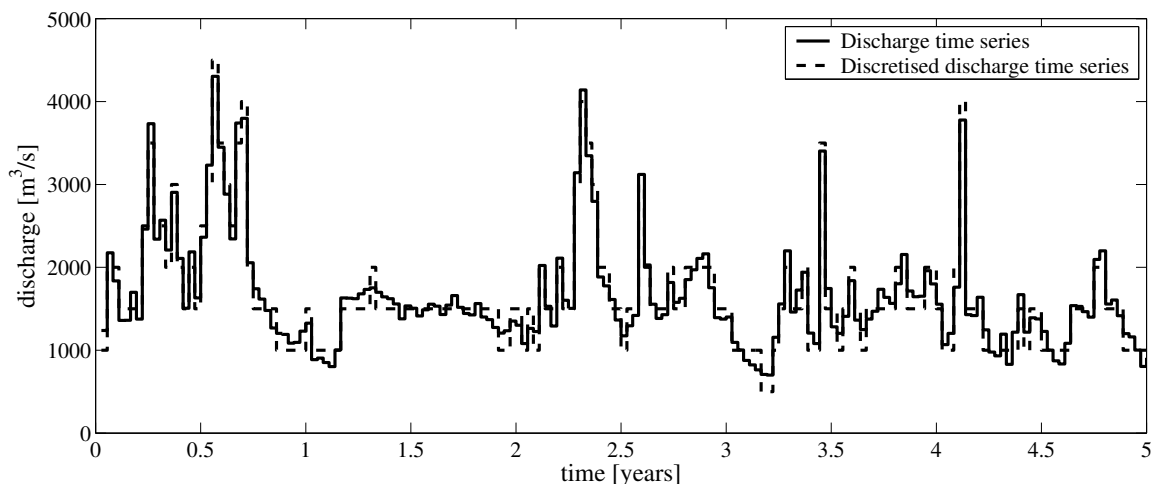
Figure 4.13: Discretisation of discharge time series

The computation simulates a period of 5 years. Figure 4.14 shows the switching between modules as a process tree. For the discharge time series a stepwise approximation is taken, with a new discharge level every 10 days. Each level starts with the stabilised hydrodynamics corresponding with the initial morphological state. The flow conditions are updated next, while using the most recent morphological state. The internal time step in the flow module is 6 seconds. The transport and bottom modules are updated after every 100 time steps of the flow computation. The transport and bottom modules are executed 5 times with a morphological step of 1 day. As long as the bed level changes are relatively small, one can assume that the spatial distributions of water level and discharge remain unaffected. This means that it is possible to compute new flow velocities using $\vec{u} = \vec{q}/h$, where $\vec{q}$ is the local unit discharge vector

and h is the local adjusted water depth. This 'continuity correction' allows us to continue with another morphological step without running the flow module in between the transport and bottom module. After executing the transport and bottom modules 5 times, an update of the hydrodynamics follows. This loop is repeated two times thus covering a period of 10 days. For the computation period of 5 years, the entire flow chart is run through 180 times.
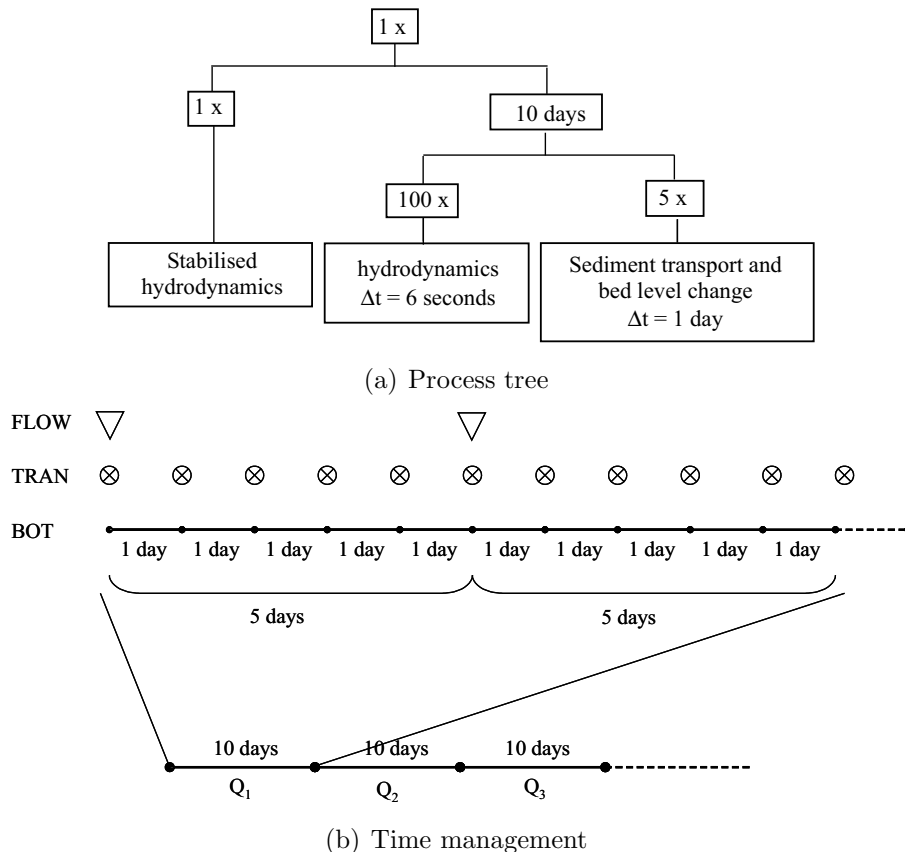

(a) Process tree

(b) Time management

Figure 4.14: Process tree used in the simulation - each simulation period starts with the stabilised hydrodynamics. Subsequently, the sediment transport rates and bed levels are iterated for 5 days. After 5 days, the flow conditions are updated. The latter loop is repeated two times, thus covering a period of 10 days

4.6.4 Validation

The actual justification of using the 1-D Rhine model is described in this section. Model simulations driven by the discharge hydrograph in Figure 4.13 form the basis of this validation. The validation is restricted to the results over the period 1-5 years in the model section km 893-923. One year spin-up is considered sufficient to dissipate errors induced by the initial bathymetry and model settings. Table 4.5 gives a brief overview of the model inputs and parameter settings in the two models.

For the purpose of validation, we focus on the following questions:

- Does the 1-D model provide a good representation of the bed level variability if multi-dimensional processes do not dominate the morphological processes?
- Do the computed width-averaged accretion and erosion patterns (1-D model) imposed by river alignment give a proper distinction between locations that are sensitive to the bed level variability and those that are not?
- Could the 1-D model be used in combination with analytically based post-processing to account for 2D-effects such as transverse bed slopes (for instance by using the axi-symmetrical approximation for lateral bed slopes by Struiksma et al. (1985))?

description	1-D SOBEK model	quasi-3D Delft3D model
flow equations	○ shallow water equation solved in one-dimension	○ shallow water equation solved in 2-dimensions ○ parametrisation for curvature-induced secondary flow
grid size Δx	○ 500 m	○ 90-110 m
time step Δt	○ 10 days	○ 1 day
upstream boundary	○ discharges per interval of $\pm$ 10 days	○ discharges per interval of $\pm$ 10 days, which are discretised into constant values 500 m³/s apart
downstream boundary	○ stage-discharge relationship	○ stage-discharge relationship
roughness main channel	○ roughness predictor Vanoni & Hwang (1967)	○ roughness predictor Van Rijn (1984)
roughness floodplain	○ constant values from roughness table	○ constant values from roughness table ○ analytical model for submerged vegetation
grain size bed material	○ uniform at each location	○ uniform in entire model
sediment transport formula	○ Meyer-Peter&Müller (1948) with a reduced critical Shields parameter	○ Engelund & Hansen (1967)

Table 4.5: Overview of the model inputs and parameter settings in the 1-D SOBEK model and the quasi-3D Delft3D model

Sediment transport volume per year

For a proper validation, the speed at which morphodynamic processes takes place is important. This speed can be characterised by a so-called morphological time-scale (see Section 2.2.5). A

large (small) morphological time-scale implies that the river morphology reacts slow (fast) to changes in the river regime. Thus, the morphological time-scale is an indicator for the amount of bed level variability, given the variability of the input (especially the discharge hydrograph). The morphological time-scale is inversely proportional to the sediment transport rate. Figure 4.15 shows the sediment transport volume per year along the Waal for the 1-D and quasi-3D model and two approximations on the basis of measurements in the period 1970-1990 and 1990-2000.

The transport formula incorporated in the 1-D model differs from the one incorporated in the quasi-3D model. The Engelund & Hansen (1967)-formula has been included in the latter, whereas Meyer-Peter & Müller (1948)-formula is utilised in the former model. Running the quasi-3D model with the Meyer-Peter & Müller (1948)-formula demonstrates that the uncertainty introduced by using a different type of transport model, is negligible.
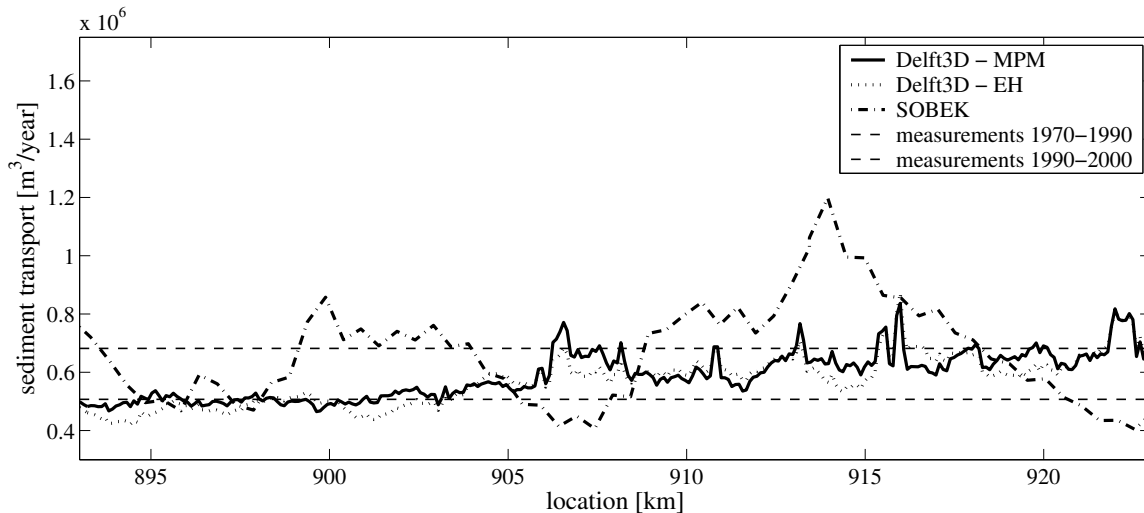
Figure 4.15: Sediment transport volume per year along the Waal, as computed with the 1-D and quasi-3D model and two approximations on the basis of measurements in the period 1970-1990 and 1990-2000

The figure shows that the computed sediment transport rates in the models are of the same order of magnitude as those observed in nature. We elaborate on this in Section 7.4. Therefore, the time-scale at which morphodynamic processes takes place are assumed to be more or less the same in both models.

Variation in floodplain width and bend radius of curvature

In contrast to the quasi-3D model, in the 1-D model there is no distinction between the geometrical information left and right of the river axis and the effect of bends is not considered. Moreover, the grid resolution in the 1-D model is much lower. Figure 4.16(a) shows the variation
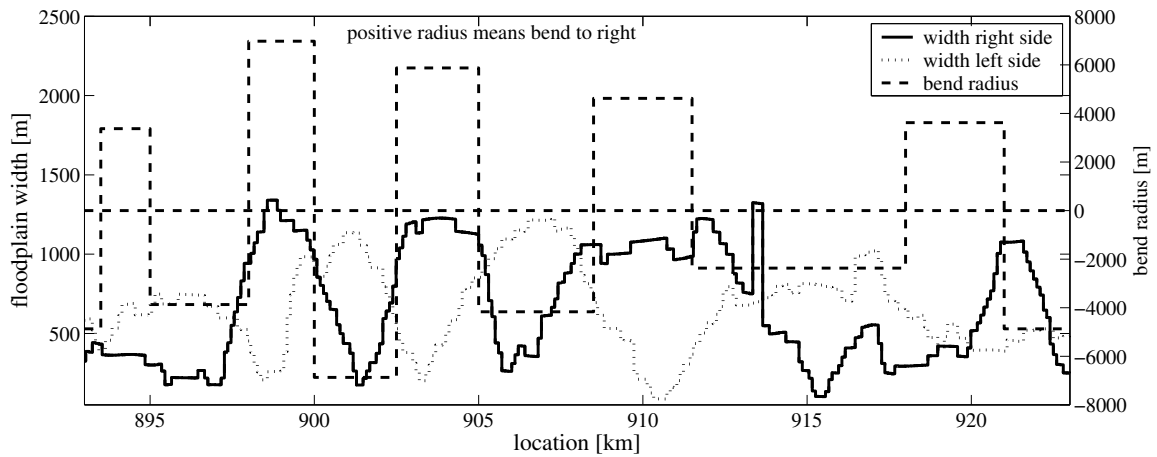
(a) Floodplain width at left and right side of the river and bend radius in the quasi-3D model
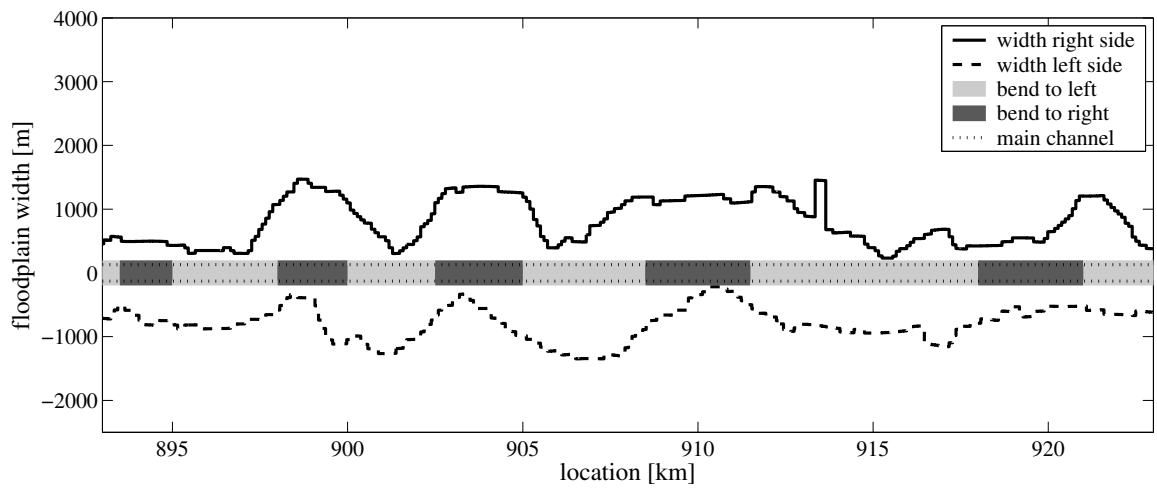
(b) Floodplain width at left and right side of the river in the quasi-3D model
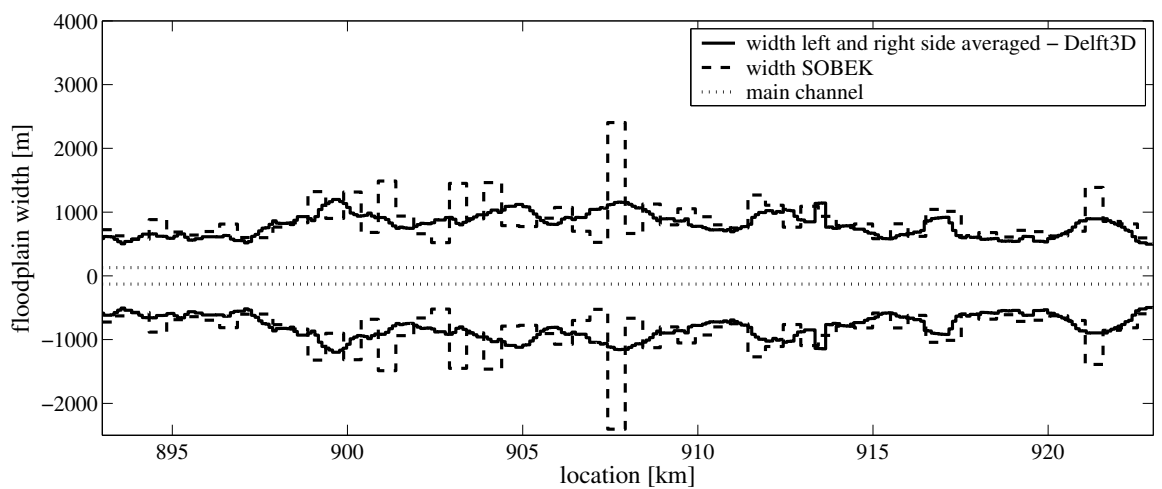
(c) Cross-sectionally averaged floodplain width in the 1-D model and derived from the quasi-3D model

Figure 4.16: Floodplain width and bend radius

in floodplain width left and right of the axis and bend radius along the Waal, as incorporated in the quasi-3D model. We can clearly notice that bends turn alternately to the left and to the right. Moreover, it appears that bends to the right (left) and one-side floodplain located at the right side (left side) occur simultaneously.

Figure 4.16(b) illustrates that floodplains are confined in narrow sections alternately located at the left and the right side of the river. As a consequence of averaging geometrical information, these strong confinements are not incorporated in the 1-D model, see Figure 4.16(c). Apart from km 908, the cross-sectionally averaged values of these quasi-3D model-quantities are of the same order of magnitude as the floodplain widths incorporated in the 1-D model, but the variations along the river are much smaller.

Representation of morphology

With respect to the representation of morphology, Figure 4.17 clearly illustrates the impact of bends in Delft3D computations, since the bed level in the outer bends is much lower that that of the inner bends.
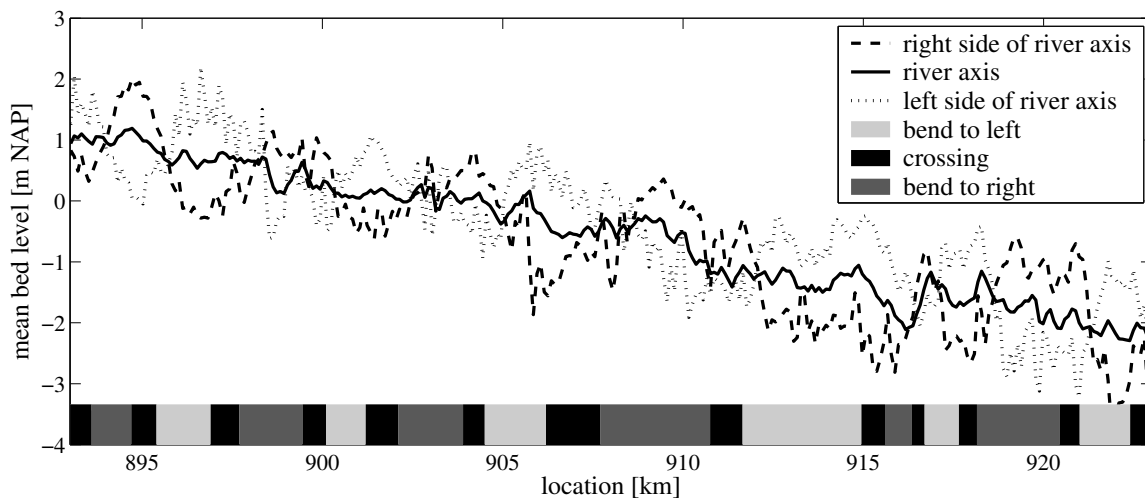
Figure 4.17: Time-averaged bed level over the four-year period, as computed with the quasi-3D model

Figures 4.18 and 4.19 show the space-plot of standard deviations of the time-averaged bed levels over the four-year period for the two model approaches. Note that these values are derived from one model simulation. Natural variation due to bedforms or variation resulting from uncertainty in model parameters and boundary conditions are not expressed in these values. The influence of width fluctuations, bends and crossings between bends alongside the river is noticeable. These effects are not evenly distributed, but vary over the cross-section (see Figure 4.19).

The standard deviation in individual longitudinal profiles of the quasi-3D model, for instance,

left and right of the axis, is larger than after width-averaging. This is most probably due to the averaging-out of the relatively large transversal variations in the river bed.

The bed level variability according to the 1-D model is much smaller than that resulting from the width-averaged quantities of the quasi-3D model. However, the computed width-averaged quantities of the 1-D model give a proper distinction between locations that are sensitive to bed level variability imposed by river alignment and those that are not. This becomes more evident in Chapter 6, when the entire Niederrhein and Waal stretch is considered.
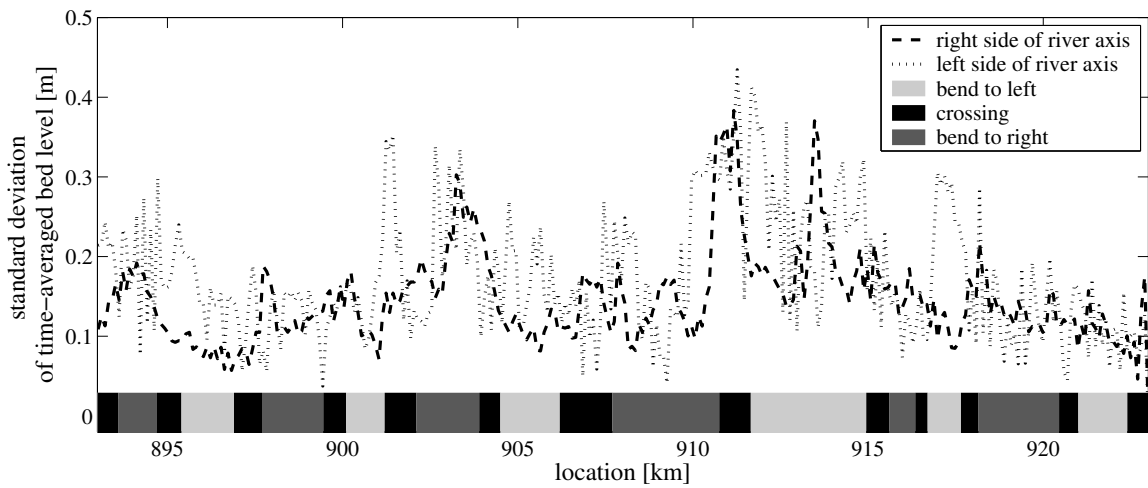
(a) Standard deviation of time-averaged bed level, as computed with the quasi-3D model
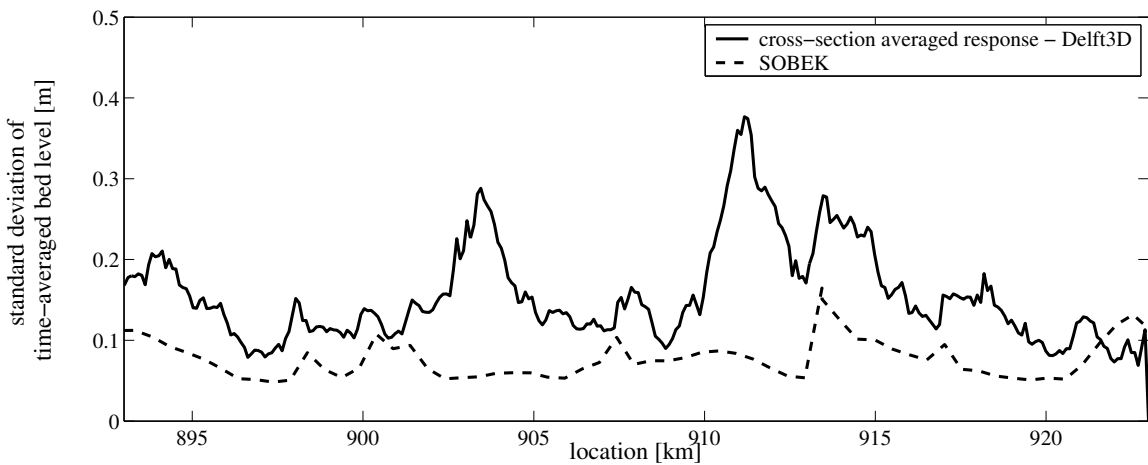
(b) Standard deviation of time-averaged cross-sectionally averaged bed level, as computed with the 1-D model and quasi-3D model

Figure 4.18: Standard deviation of time-averaged bed level over the four-year period, as computed with the 1-D model and quasi-3D model
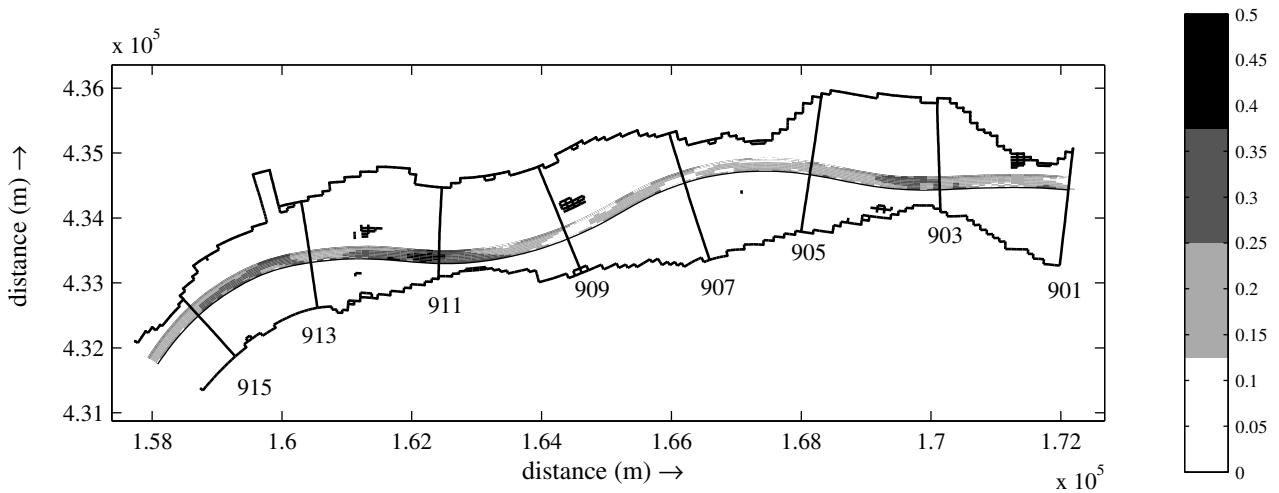
Figure 4.19: Standard deviation of time-averaged bed level over the four-year period at section km 913-923, as computed with the quasi-3D model

Curvature-induced transverse slopes

Cross-sectional profile evolution imposed by the river alignment, such as transverse slopes in bends, is not considered in the 1-D model. However, the axi-symmetrical approximation for lateral bed slopes given by Struiksma et al. (1985) can be used to account for this 2D-effect, via post-processing of the 1-D model results. Transverse slopes are approximated by using the 1-D model results as inputs for the axi-symmetrical solution in Eq. 4.1. To that end, the 1-D model is driven by a characteristic constant Waal discharge of 1800 m^3/s. The resulting slopes and the transverse slopes in the initial bathymetry in the quasi-3D model are shown in Figure 4.20.
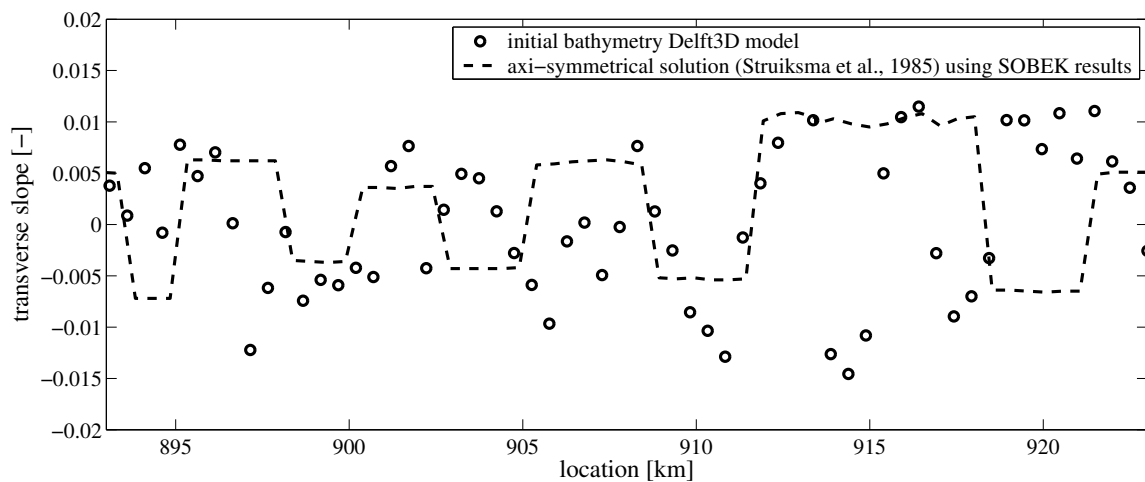
Figure 4.20: Transverse slopes (1) approximated by the axi-symmetrical solution via post-processing of the 1-D model results; and (2) in the initial bathymetry of quasi-3D model
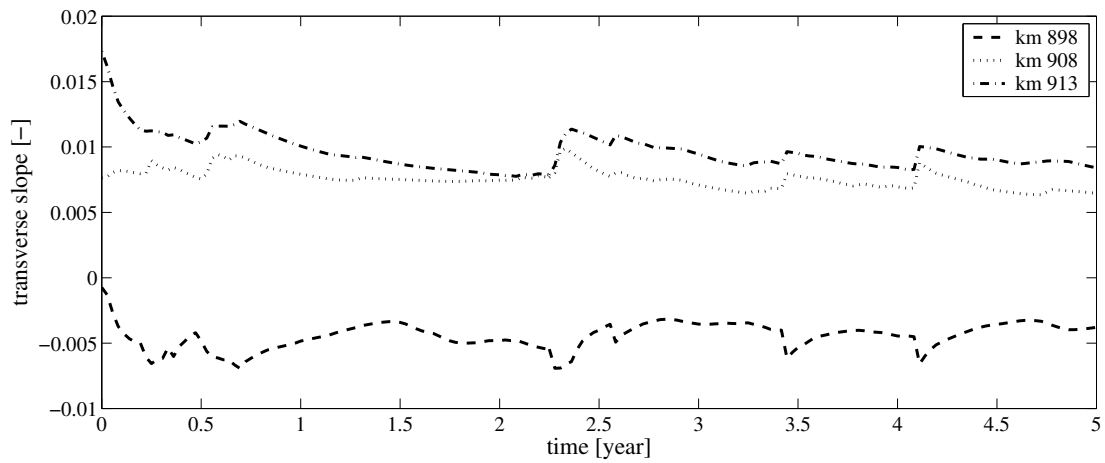
The 1-D model and quasi-3D model results during the 5-year simulation period are used to estimate the time evolution of the transverse slopes. For three different locations, this time evolution is shown in Figure 4.21. The axi-symmetrical solution (Figure 4.21(c)) strongly oscillates due to fluctuations in river discharge (see Figure 4.13). In natural rivers this axi-symmetrical solution will hardly ever be reached, since river bends are limited in length and do not have a constant radius of curvature. Moreover, the flow conditions are not constant in time. Transverse slopes tend to lag behind discharge variations. This becomes clear from Figure 4.21(a) showing that the transverse slopes quickly respond to discharge peaks (small morphological time-scale), after which they slowly reduce during moderate and low discharges (large morphological time-scale).

If we want to account for the transverse-slope effect in a 1-D model via post-processing of results, the axi-symmetrical solution for a characteristic discharge of 1800 m^3/s gives a reasonable approximation for the averaged transverse slope, but it is not suitable for estimating the slope variations in response to a varying discharge. In that case, it is rather recommendable to use a relaxation model driven by the axi-symmetrical solution.

4.6.5   Conclusion of model justification

The calibrated 1-D SOBEK Rhine model is purely 1-D, i.e. there is no distinction between the left and the right side of the river. Thus, the model produces a width-averaged representation of the morphodynamics of the river bed, meaning that 2-D phenomena within the cross-section, such as curvature-induced profile evolution, is not described. In this section we showed that, as a consequence of the averaging-out effect, the bed level variation decreases significantly. However, the computed width-averaged profiles still provide a first indication of locations that are susceptible to geometrically induced bed level variability and those that are not. It is possible to some extent to account for 2D-transverse slope effects by post-processing the numerical model results.

Considering that the computational effort per individual numerical simulation differs considerably between the 1-D and the quasi-3D model, preference is given to the 1-D approach. We expect to produce generic knowledge on the use of stochastic methods in river morphology that also holds for multi-dimensional model approaches. The potential of a stochastic model approach in river management practice can be explored much more easily with a 1D-approach, whereas this would require too much computational effort for a quasi-3D approach.

(a) Quasi-3D model simulation
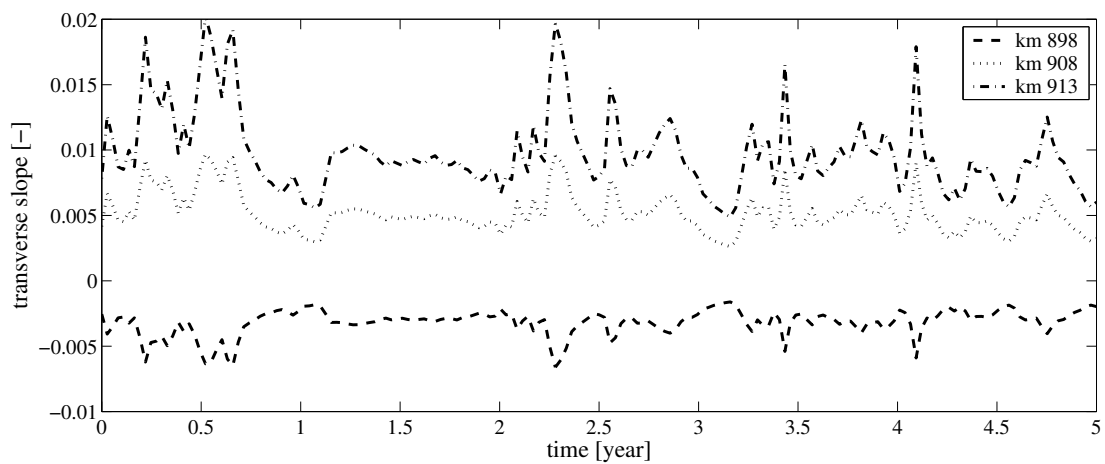
(b) 1-D model simulation
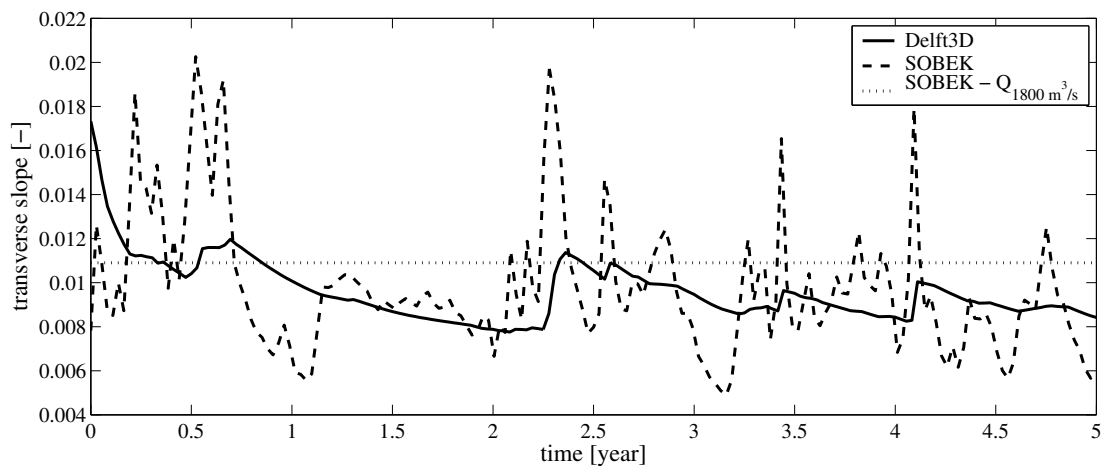
(c) Transverse slope at location km 913 derived via post-processing the 1-D model results with (1) a constant discharge of 1800 m³/s and (2) a discharge time series; and (3) the quasi-3D model simulations

Figure 4.21: Time evolution of the transverse bed slope at three locations km 898, 908 and 913

Part two: Application of Monte Carlo Simulation to morphodynamic models

Chapter 5

Hypothetical 1-D model of dimensions similar to those of the Waal

5.1 Introduction

In Part two of this thesis, three different models are run in a stochastic mode using MCS with crude sampling, viz. a simple 1-D Waal model, a more complex 1-D model of multiple Rhine branches and a quasi-3D Waal model. We start with a simple hypothetical model of dimensions similar to those of the Waal. It concerns a highly idealised situation in which the river is schematised as a prismatic channel with an initially plane sloping bed. The morphological response to isolated geometrical variations or human interventions can be investigated with this model. For the purpose of illustration, we consider a flood protection measure as proposed in the Room for the River-scheme[1]. Over a distance of 10 km the floodplains are lowered by 1 m, as indicated in Figure 5.1. This case study is also presented in Van Vuren et al. (2002). The simple 1-D model is further described in Section 4.5.3.
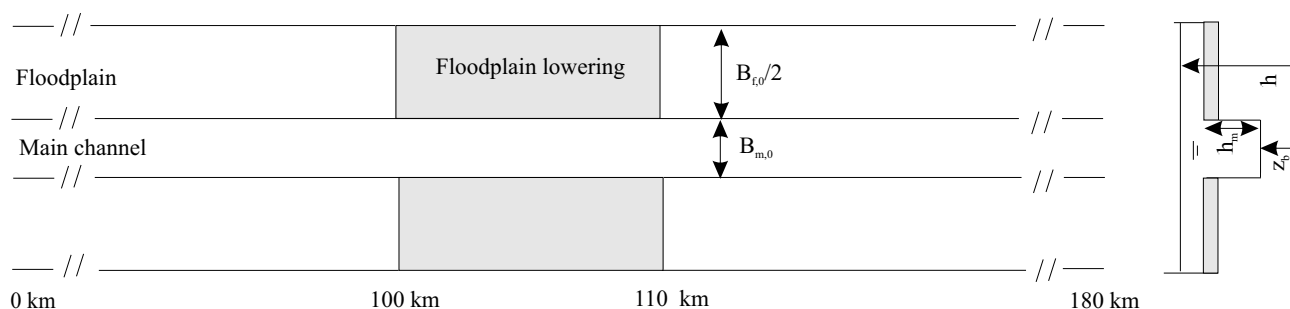

Figure 5.1: A prismatic channel of 180 km length with a composite cross-section: over a distance of 10 km the floodplains are lowered by 1 m

The main advantage of the hypothetical model is that the potential of the stochastic approach can best be understood by first examining simplified cases in which the morphological processes

---

1. A Dutch river improvement scheme for the Rhine branches, meant to cope with increasing design discharges (see Chapter 8)

are fully transparent (Van der Klis, 2003). This provides rapid insight into the physical system behaviour and the uncertainties involved.

In this chapter we start with the deterministic approach. In case of a constant discharge through a straight river reach, the system evolves towards an equilibrium state. Theory on static equilibrium profiles for a channel with a rectangular cross-section and a compound channel is presented in Section 5.2.1. A static equilibrium state will, however, never be reached, since variation in the river discharge leads to a continuous adaptation of the river bed. The step towards a dynamic approach is made in Section 5.2.2.

Since we know neither the river discharge time series, nor the exact values of other model inputs involved on beforehand, a stochastic approach follows in Section 5.3, in which the impact of three uncertainty sources (viz. river discharge, hydraulic roughness and grain size of bed material) on the evolution of the river bed is considered. Results and findings are discussed in Section 5.4.

It is often suggested that a very long deterministic model run reveals most of the output statistics of interest, and that there is no reason for doing computationally intensive Monte Carlo Simulations. Section 5.5 focuses on this subject. The chapter ends with conclusions.
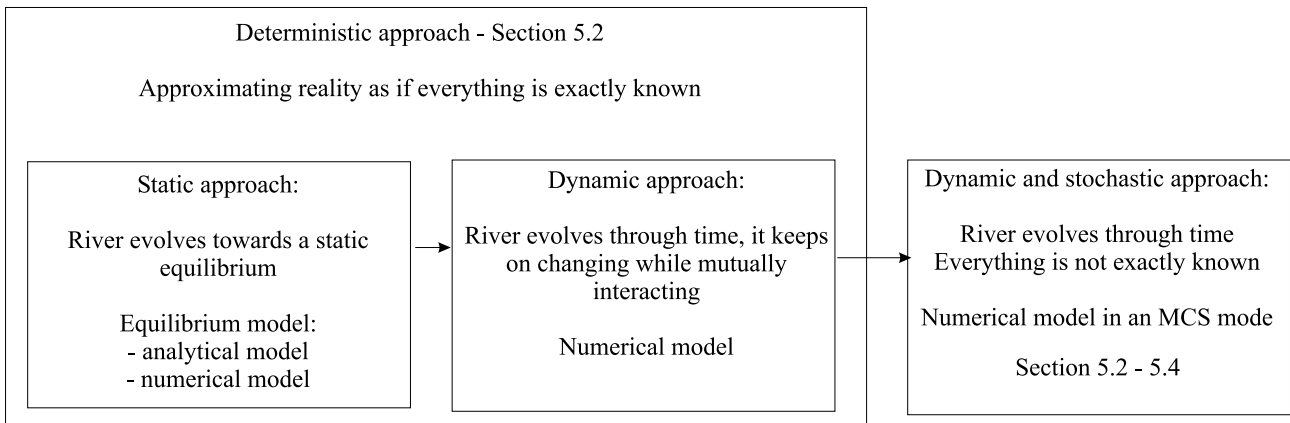

Figure 5.2: From a deterministic static and dynamic approach toward a stochastic dynamic approach

5.2   Deterministic approach

5.2.1   Static equilibrium approach

A first indication of the morphological response can be derived from a highly simplified model. In case of a constant discharge through a straight river reach with a rectangular cross-section without floodplains, the bed level will approach an equilibrium state that can be derived from (Jansen et al., 1979):

$$Q = B_{\mathrm{s}} u h \tag{5.1}$$

$$u = C\sqrt{hi_{\mathrm{b}}} \tag{5.2}$$

$$S = B_{\mathrm{s}}s = B_{\mathrm{s}}mu^n \tag{5.3}$$

in which Q is the discharge [m^3/s], u the flow velocity [m/s], B_{s} the sediment transporting width [m], h the water depth [m], C the Chézy coefficient [m$^{1/2}$/s], i_{b} the bottom slope [-], s the bedload sediment transport per unit width (i.e. including pores) [m^3/m/s], m and n parameters in the sediment transport formula [-] and S the total amount of sediment transported per unit time through the river cross-section [m^3/s].

The equilibrium state is described by the following formulae for the water depth h_{eq} and the bed slope i_{eq}:

$$h_{\mathrm{eq}} = \left(\frac{S}{mB_{\mathrm{s}}}\right)^{-1/n} \frac{Q}{B_{\mathrm{s}}} \tag{5.4}$$

$$i_{\mathrm{eq}} = \left(\frac{S}{mB_{\mathrm{s}}}\right)^{3/n} \frac{B_{\mathrm{s}}}{C^2 Q} \tag{5.5}$$

In principle, this equilibrium approach is only valid for straight channels without floodplains. For a river with a compound channel the static equilibrium profile appears to be essentially different from the one for a river without floodplains. For rivers with a composite cross-section more equilibrium profiles can exist, depending on the boundary conditions. Moreover, it appears that the equilibrium profile may be curved (Eerkens, 1996). However, given the conditions, there is a unique equilibrium state.

For three distinct discharge levels - (1) constant below bankfull, (2) constant intermediate, meaning that the discharge is below bankfull upstream and downstream of the lowered reach, but above within this reach, and (3) constant above bankfull in all sections - the equilibrium state in our case study 'floodplain lowering' is determined with:
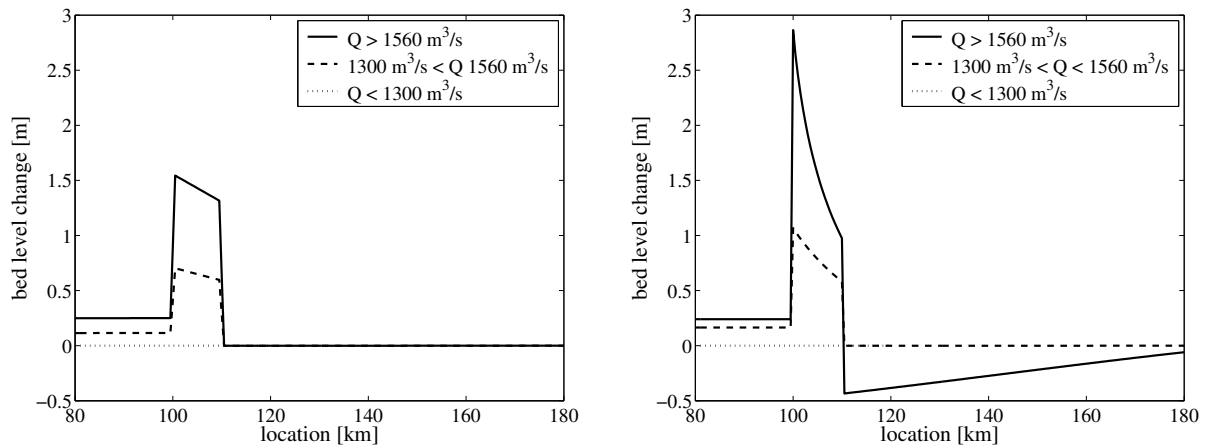
- the analytical equilibrium model (Eq. 5.4-5.5);
- the numerical 1-D model (Figure 5.1 and Section 4.5.3).

When the discharge stays below the bankfull discharge, floodplain lowering has no morphological effect.

Equilibrium state according to the analytical equilibrium model

We assume that the sediment transport only takes place within the main channel. Therefore, depending on the flow stage, the lateral discharge into the lowered floodplains is schematised as a concentrated water extraction at the upstream end of the lowered floodplain reach. The discharge back into the main channel is schematised as a concentrated water supply at the downstream end of the lowered floodplain reach. The expressions for h_{eq} and i_{b} (Eq. 5.4-5.5) imply an increasing bed slope and a decreasing water depth (see Figure 5.3(a)). Thus, the

bed level of the main channel in the lowered floodplain reach becomes steeper and increases. Upstream of the lowered floodplain reach the bed level in the main channel will rise. The equilibrium state under a constant discharge above bankfull is more or less similar in shape as the one for an intermediate discharge, but the accretion is more pronounced and the bed slope becomes steeper.

(a) Equilibrium states according to the analytical equilibrium model

(b) Equilibrium states, as derived with the numerical model

Figure 5.3: Equilibrium states under a constant discharge for three distinct discharge levels

Equilibrium state, as derived from the numerical 1-D model

In reality, the this lateral discharge into and from the floodplains will not be concentrated at two points, but rather distributed over a substantial part of the lowered floodplain reach. This effect is considered in the numerical simulation, resulting in an equilibrium state that differs substantially from the one obtained from the equilibrium model (see Figure 5.3(b)). For the constant intermediate discharge, the equilibrium profile is curved. This can be explained by the feedback between the morphological changes in the main channel and the discharge distribution between the main channel and the floodplains. Accretion in the main channel induces a re-distribution of river discharge between main channel and floodplains. A higher percentage of the river discharge will flow via the floodplains. In fact, the discharge extraction, which schematises the interaction in the river, is not constant, but a function of the morphological change in the main channel. This feedback results in more accretion than expected on the basis of the analytical equilibrium model. As a consequence, the water depth decreases and the bed slope increases.

If the discharge exceeds the bankfull discharges in the entire reach, the equilibrium profile is not only curved, but it also shows systematic erosion in the reach downstream the lowered floodplains. Part of the river discharge flows via the floodplains in the lowered reach, but

further downstream the whole discharge is diverted back into the main channel. Due to a local gradient in the sediment transport, erosion waves are initiated and propagate downstream. This erosion induces a re-distribution of the river discharge between the main channel and the floodplains. A higher percentage will flow via the main channel. This feedback results in more erosion, which results eventually in water being transported entirely through the deepened main channel. This means that, due to the floodplain lowering, the downstream section tends towards an equilibrium state that is essentially different from the one suggested by the analytical model. Clearly, the extra degree of freedom constituted by the discharge distribution makes this difference.

5.2.2   Dynamic approach, fluctuations in the river discharge

In fact, the river discharge is not constant, but a function of time. The variation in the river discharge leads to a continuous adaptation of the river bed. With each new discharge new bottom waves are initiated, which start migrating downstream. Figure 5.4 shows that each discharge time series results in a different morphological response, which differs from the equilibrium state described in Section 5.2.1.
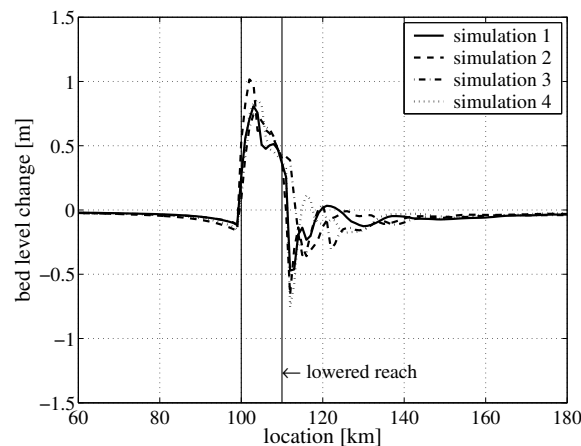

Figure 5.4: Effect of a variable discharge after a simulation period of 20 years, as computed with the 1-D model for four different time series

A notable feature of Figure 5.3 and Figure 5.4 is that the dynamic approach after 20 years shows upstream scour, while the equilibrium approach after 100 years shows accretion in the main channel upstream of the lowered reach. The scour in the dynamic approach, must be attributed to the consistent set-down of the water level in this area, when the water can go around the shallow part in the main channel via the lowered floodplains. Under a constant discharge, this set-down gradually turns into a set-up of the water level on the long run, as a consequence of accretion in the main channel of the lowered reach. The river bed evolves slowly to its equilibrium state, as is shown in Figure 5.3. In the dynamic approach the height of

the accretion and erosion peaks is discharge-dependent. At discharges above bankfull, bottom waves are initiated in the main channel. These bottom waves migrate downstream and (partly) decay during discharges below bankfull, when the flow stays within the main channel. Thus, a static equilibrium state as discussed in the previous section will never be reached, as long as the discharge keeps on varying.

The decay of bed perturbations while migrating downstream is clearly visualised in Figure 5.5. The figure shows the morphological effect of floodplain lowering as a function of time and space. The black spots indicate accretion and erosion patterns initiated at discharge peaks. While migrating downstream through the system, the disturbances propagate (diagonal streaks) and tend to spread out and smooth (transition from black into grey-shaded spots).
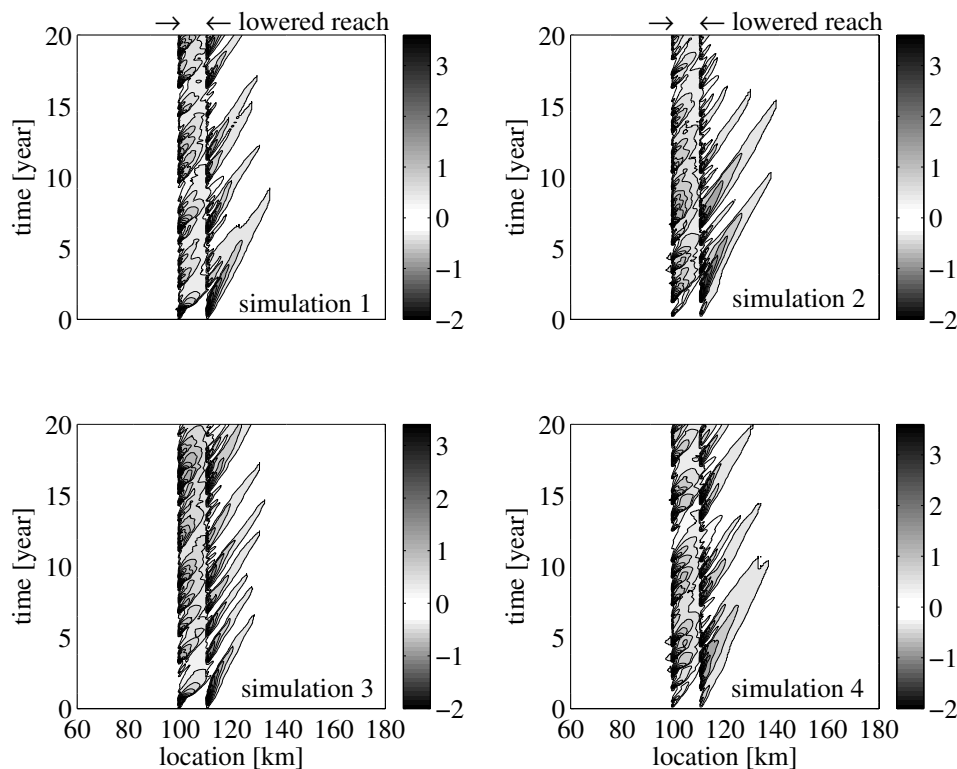
Figure 5.5: Time-stack plots of the morphological effect of a variable discharge, as computed with the 1-D model for four different time series

5.3   Stochastic approach

Purely deterministic predictions may result in an incomplete picture. As indicated in the previous section, deterministic predictions using different discharge time series results, for instance, in a different morphological response. The morphological response to floodplain lowering is to some extent uncertain, due to uncertainty in model schematisation and the specification of the

model input (see Section 4.4 and 3.3). In a stochastic prediction, the bed level variability (in space and time) is made explicit.

The stochastic variability of the morphological response to floodplain lowering due to uncertainties in the river discharge at the upstream boundary, the hydraulic roughness of the main channel and the median grain size of the bed material is assessed below. The other model inputs are included as deterministic values.

A key source of uncertainty is the choice of the statistical model to come up with a good definition for the uncertainties considered. For instance, when using classical probability distributions, the choice of distribution type and its parameters is often subjective. This source of uncertainty is not considered in this chapter. In Chapter 6, we investigate the impact of different definitions for uncertainty sources, by using amongst others different distribution types and parameters. In addition to classical probability distributions, use is made of resampling techniques, and even a combination between the two.

Assumptions regarding the landscaping of the floodplain after lowering, such as design of the new floodplain and the time-evolution of the hydrodynamic properties of the lowered reach, are considered separately, as they may affect the morphological response.

5.3.1   Uncertainty sources

River discharge

In practice, we do not know the river discharge time series on beforehand. On the basis of the historical discharge data, different discharge times series that are equally likely to occur can be predicted with the help of stochastic methods. An extensive overview of methods that have been proposed in literature to model the natural randomness of discharge time series is presented in Section 6.4. Duits (1997) and Van Vuren & Van Breen (2003) derive a method to randomly synthesise discharge time series. The generation of the discharge time series is based on 100 years of daily discharge measurements in the Rhine at Lobith (see Section 4.5.4). The method accounts for the seasonal dependency of the discharge and the correlation of the discharges in successive time intervals. Discharge peaks far beyond the physical limit of the Rhine system can be easily synthesised. Therefore, we truncated discharge peaks at the design discharge of 15.000 m^3/s^2. In this study, all discharge time series of 100 years duration have been synthesised with this statistical method.

---

2.   the discharge on which the design of the Dutch Rhine flood defence used to based until 2001. In 2001, the design discharge has been raised from 15.000 to 16.000 m^3/s

Hydraulic roughness of the main channel

In reality, the hydraulic roughness of the main channel depends on the river discharge and the changing bedforms. Here this dependency is neglected. The hydraulic roughness is presented by a constant Chézy coefficient in each part of the model. The hydraulic roughness is given a lognormal probability distribution, with a mean value of 40 $m^{1/2}$/s and a standard deviation of 5 $m^{1/2}$/s (Van der Klis, 2003).

Median grain size of the bed material

The uncertainty in the grain size of the bed material originates from small-scale spatial and temporal variations. Spatial variations occur as a result of bedforms, local armouring and bend effects. Spatial and temporal variations are due to graded-sediment processes (sorting). In this case study a uniform grain size is assumed, and this grain size is assumed to have a lognormal probability distribution function, with a mean value of 1 mm and a standard deviation of 0.5 mm.

5.3.2   Design aspects of the floodplain lowering

The morphological response to the large-scale floodplain lowering and (re-)landscaping project along the river Waal is affected by three design aspects:

- Lowering the floodplains: Depending on the flow stage, lowering the floodplains will influence the discharge distribution between the floodplains and the main channel: a greater part of the discharge will be conveyed through the floodplains. These changes in the discharge distribution inevitably affect the morphology. If sediment is transported through the floodplains, the sediment transport distribution between the floodplains and the main channel may even be changed. This distribution is probably not proportional to the discharge distribution. It seems logical to assume that the morphological response will increase in magnitude as the floodplains are lowered more.
- Rate of accretion in the floodplain: The rate of accretion in the floodplain may increase, due to the increased lateral sediment transport into the floodplains caused by changes in the discharge distribution, and due to the increased trapping efficiency of the lowered floodplains. Therefore, floodplain lowering is not a self-sustaining measure. Without any countermeasures, the situation preceding the floodplain lowering is likely to be restored in the long run. Morphological changes in different parts of the cross-section will influence each other.
- Nature development and (re-)landscaping in the floodplains: Nature development is another important activity that takes place in the floodplains. Nature development is incorporated in the (re-)landscaping programs. In these programs the traditional

agricultural land in the floodplains is replaced by forest and various types of nature. This entails an enhanced hydraulic roughness, which increases further as the vegetation grows. This will influence the discharge distribution between the main channel and the floodplains in a way that counteracts the effects of lowering.

5.3.3   Cases for Monte Carlo Simulations

Van der Klis (2003) applied MCS to estimate the morphological response to a constriction in the main channel of the Waal. A rough sensitivity analysis gave a first distinction between important and less important inputs. She concluded that the morphological response is most sensitive to river discharge variations.

Given the aforementioned uncertainty sources and design factors and in line with the findings in the study of Van der Klis, MCS is applied to four different cases (Table 5.1), the first of which will serve as a reference case. The impact of the uncertain discharge is included in all cases. Case 2 includes additional uncertainties. The impacts of floodplain accretion and an enhanced hydraulic roughness of the floodplains are analysed in Case 3 and Case 4.

Case 1: Uncertain discharge

The level of the lowered floodplains is maintained and the lateral sediment transport into and from the floodplains is neglected. All sediment transport therefore occurs in the main channel. The type of vegetation in the floodplains is the same before and after the lowering. Only uncertainties in the river discharge are considered.

cases for Monte Carlo Simulation	case 1	case 2	case 3	case 4
uncertainty sources:				
- discharge	X	X	X	X
- hydraulic roughness	-	X	-	-
- grain size	-	X	-	-
floodplain accretion	-	-	X	-
nature development	-	-	-	X

Table 5.1: Cases for Monte Carlo Simulation

Case 2: Uncertain discharge, hydraulic roughness of the main channel and grain size

The same situation as described for Case 1, but now uncertainties in the hydraulic roughness of the main channel and the grain size of the bed material are also taken into account.

Case 3: Accretion in the floodplains

Lateral sediment transport from the main channel into the floodplains is taken into account. Part of this sediment will deposit on the floodplains. The net sediment transport into the floodplains is modelled as a sediment extraction from the main channel. This sediment extraction is given as a function of the discharge:

$$\Delta S\left(t\right) = \begin{cases} \frac{Q_{\text{floodplains}}}{Q_{\text{total}}} \cdot S\left(Q\left(t\right)\right) & \text{if } Q\left(t\right) > Q_{\text{bankfull}} \\ 0 & \text{otherwise} \end{cases} \tag{5.6}$$

The reduction in sediment transport in the main channel has morphological impacts. The resulting bed level changes in the floodplains, due to accretion in the floodplains, will affect the discharge distribution between the main channel and the floodplains. This will have a morphological impact. Yet, this feedback is not considered in this case.

Case 4: Nature development in the floodplains

We assume nature development to entail an instantaneous increase in the hydraulic roughness of the floodplains, which remains unaltered thereafter. The new hydraulic roughness of the floodplains is equal to 30 m$^{1/2}$/s.

5.3.4   Sample size for Monte Carlo Simulations

Computationally intensive numerical models, in combination with the large number of simulations required for convergence of the output statistics, can make MCS with crude sampling a laborious operation. Information on the estimation of a plausible sample size is required beforehand, to avoid either pointless expenditure of computational effort, or an unacceptable reduction of the sample size. The appropriate sample size depends on the desired degree of accuracy. The accuracy of an MCS can be increased simply by increasing the sample size.

Morgan & Henrion (1990) describe a method to estimate the sample size required for a specific degree of accuracy. In their method, the precision of the estimate of a fractile (Y_{p}) that must be estimated, is expressed as the allowed deviation in terms of an interval of fractiles (Δp). The sample size N required to be α confident that the actual p$^{\text{th}}$ fractile, Y_{p}, lies between the estimates of the $p - \Delta p^{\text{th}}$ and $p + \Delta p^{\text{th}}$ fractiles, is:

$$N = p\left(1-p\right)\left(\frac{c_{\alpha}}{\Delta p}\right)^{2} \tag{5.7}$$

where c_{α} is the deviation that encloses probability α of a random variable with unit normal distribution ($P\left(-c_{\alpha} < \Phi < c_{\alpha}\right) = \alpha$).

Van der Klis (2003) extended this method to make it correspond better with the present river management practice. The desired accuracy can be expressed as an allowed deviation from an estimated fractile, in metres of bed level change. The distribution type of the model output is assumed to be known, otherwise a Gaussian distribution can be utilised as a first assumption. To estimate the required sample size, the next steps have to be made:

1. Specify the desired degree of accuracy of a fractile p that should be estimated and the width of the α confidence interval that should contain the actual value of p.

2. Roughly estimate the statistical parameters of the presumed distribution type, based on a small sample of outputs, that is in the order of a few tens of runs.

3. Estimate the fractile (p_1, p_2) of the assumed output distribution that corresponds to the confidence interval defined in step 1, utilising the inverse probability distribution with the estimated parameters of step 2. This results in the fractile interval of width $2\Delta p = p_2 - p_1$.

4. Now we have sufficient information to estimate the sample size using Eq. 5.7.

Van der Klis (2003) noted the importance of checking the accuracy afterwards, since this method gives only an estimate of the required sample size, based on an assumed distribution function with roughly estimated parameters. When the desired accuracy is not yet reached, additional samples should be added to the MCS.

Morgan & Henrion (1990) describe a method to estimate the α confidence interval of the pth fractile, for a random sample of N values Y. This interval is determined by two values, Y_i and Y_k, that contain the pth fractile with confidence α. The order numbers (ranks) defining this interval are:

$$i = \left\lfloor Np - c_\alpha \sqrt{Np(1-p)} \right\rfloor \tag{5.8}$$

$$k = \left\lceil Np + c_\alpha \sqrt{Np(1-p)} \right\rceil \tag{5.9}$$

in which Np is the estimated p[th] fractile, $\sqrt{Np(p-1)}$ an estimate of its standard deviation, and c_α the deviation enclosing probability α in a unit normal distribution. The notation $\lfloor \, \rfloor$ and $\lceil \, \rceil$ indicates that we round off these two quantities to the nearest lower and higher whole number, respectively.

The method of Van der Klis (2003) is used to roughly approximate the sample size in our case study on beforehand. Suppose we are interested in the maximum accretion. We want to be 95% confident that the actual 90th fractile Y_p of the maximum accretion (p=0.90) has a precision of plus or minus 10 cm. To solve this problem, we consider the bed level response to floodplain lowering in Case 1 through a computation period of 20 years. Since there is no information available on the probability distribution of the maximum accretion, we assume the maximum accretion to be Gaussian distributed. From a first set of 50 simulations, we estimate the mean and the standard deviation of the assumed Gaussian distributed maximum accretion.

This results in a mean value of 3.93 m and a standard deviation of 0.54 m. Assuming that the output distribution is Gaussian distributed, the 90th percentile of the maximum accretion is approximately 4.62 m (see Figure 5.6(a)).
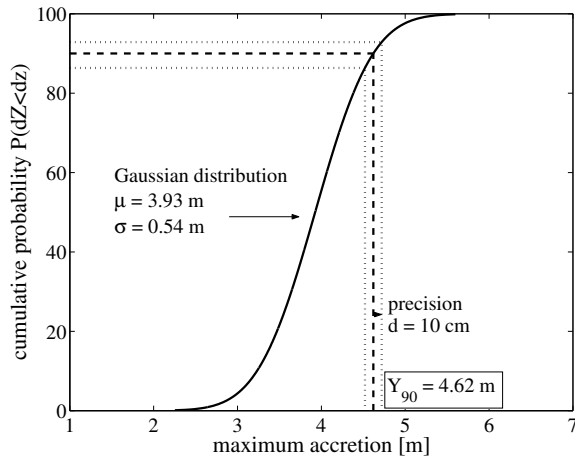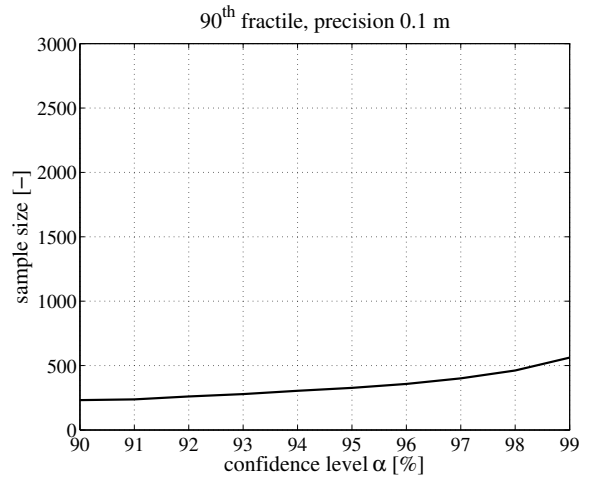

(a) Cumulative probability distribution of Gaussian distributed maximum accretion with $\mu = 3.93$ m and $\sigma = 0.54$ m)
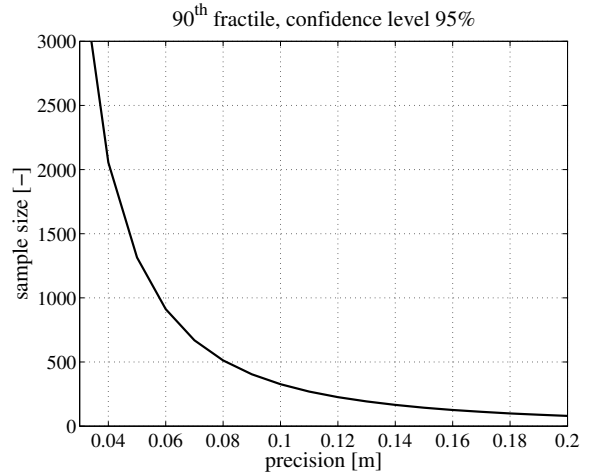
(b) The required sample size as a function of the desired precision (90th fractile Y_{p}, and a 95% confidence level)
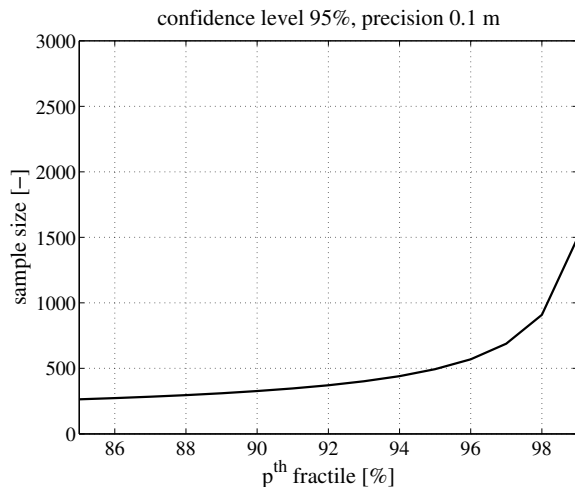
(c) The required sample size as a function of the fractile number p (95% confidence level, and precision of 0.10 m)

(d) The required sample size as a function of confidence level α (90th fractile Y_{p}, precision of 0.10 m)

Figure 5.6: Sensitivity of the required sample size to desired degree of precision, confidence level and fractile number

The allowable confidence interval would be [4.52 m, 4.72 m], which corresponds with the 86th and 93th percentiles respectively ($\Delta p = 0.033$). The sample size to reach this degree of accuracy is

$$N = p\,(1-p)\left(\frac{c_\alpha}{\Delta p}\right)^2 \approx 0.9\,(1-0.9)\left(\frac{1.96}{0.033}\right)^2 \approx 320 \qquad (5.10)$$

The size of the first set of simulations on the basis of which the distribution parameters of the Gaussian distributed maximum accretion are roughly estimated, appears to be important. If we derive, for instance, the distribution parameters from a first set of 20 simulations (instead of 50), the mean value and standard deviation would be 1.18 m and 0.48 m, respectively, resulting in a required sample size of 250. This sensitivity can be considered as the major drawback of the method. In fact, the method provides an estimation of the order of magnitude (viz. whether tens, hundreds, or thousands of samples are required), rather than the 'exact' number of samples that is required for a certain accuracy. There is no guideline on how to set the number of realisations of the first set.

From Eq. 5.7 it follows that the required sample size N is inversely proportional to the square of the desired degree of accuracy ($N \propto \frac{1}{\Delta p}^2$). Figure 5.6(b) shows the required sample size as a function of the desired precision of the 90th fractile Y_{p} and a 95% confidence level. If we want to be 95% confident that the actual 90th fractile Y_{p} of the maximum accretion lies within an estimated interval of maximum 10 cm, instead of 20 cm, the required samples size should be a factor 4 larger. Figure 5.6(c)-(d) show the sensitivity of the required sample size to the chosen confidence level and fractile number. The figure underlines the importance of a careful consideration of the desired degree of precision and the fractile number.

Van der Klis (2003) notes that it is pointless to demand a very high precision of the output statistics, as the uncertainty in the model input is known only roughly. Moreover, she argues to focus on more precise estimates of extreme fractiles only if this is inevitable and meaningful with respect to the accuracy with which the input uncertainties are described. Bearing this in mind, we use a sample size of 400 in this case study. An accuracy check follows in Section 5.4.5, using the standard statistical techniques of Morgan & Henrion (1990) a posteriori.

5.4 Results

5.4.1 Use of stochastic predictions

One may wonder how to use the results of stochastic predictions in practice. River morphodynamics may influence many functions of the river, like safe discharge of water, ice and sediment; safe and efficient navigation; land-use in the floodplains; ecological functions and recreational functions.
For example, the river manager has to ensure a particular navigation depth. Close to hydraulic structures, erosion may undermine and destabilise banks and foundations. Predicting where,

when and how frequently the bed reaches a critical level is necessary for the timely deployment of dredging or scour protection measures. Both the spatial and the temporal variation of the morphological response statistics are important. The presentation of the response statistics at different points along the river provides insight into potential bottlenecks. At these bottleneck locations the temporal variation of the statistical properties gives information about how frequently the river does not meet the required conditions and when (how many years ahead, in which season of the year) this is likely to happen the first time.

5.4.2   Spatial variation of morphological response statistics

The four MCS-cases are meant to investigate the stochastic nature of the morphological response in the main channel to large-scale floodplain lowering and (re-)landscaping programs. The set of outputs resulting from all model runs in each case is used in each case to estimate the statistical properties of the bed level response.
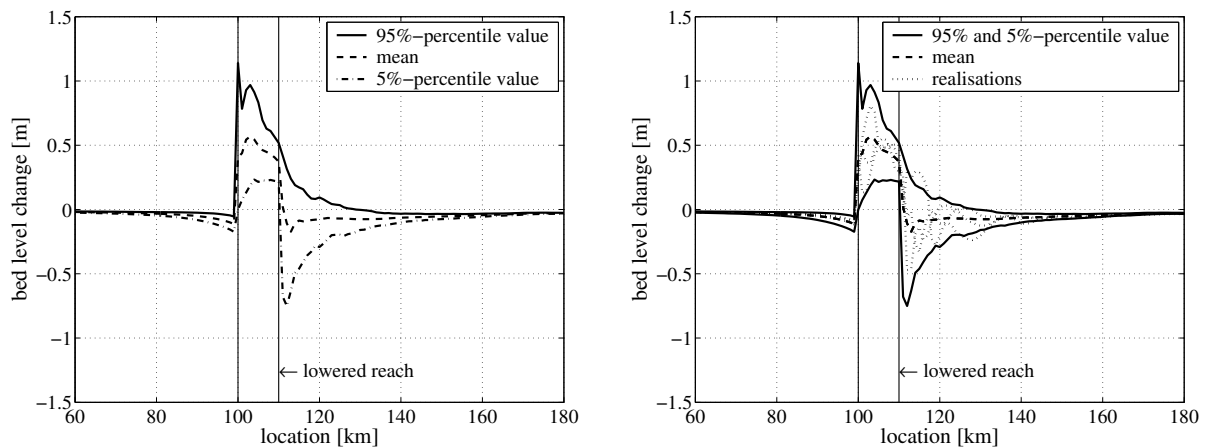
(a) Morphological response statistics for Case 1 after 30 years, expressed in terms of its mean and its 90% confidence interval

(b) Actual realisations versus the statistical characteristics expressed in terms of its mean and its 90% confidence interval (the envelopes of all realisations)

Figure 5.7: Morphological response statistics for Case 1 after 30 years in December, as computed with the simple 1-D model

Figure 5.7(a) shows the morphological response in the main channel for Case 1, in December of the 30th simulated year. In this figure the mean bed level and the 95%- and 5%-percentile values are presented. The 95%- and 5%-percentile values span the 90% confidence interval, i.e. the bed level changes have a probability of 90% the bed level changes of falling within this range. Note that the lines represent the envelopes of all realisations and cannot be considered as actual realisations (Figure 5.7(b)). The latter exhibit much stronger variations, representing the individual bed waves that are caused by the varying discharge in the lowered reach.

The envelope, especially in the downstream reach, rather indicates the spatial variation of the maximum wave amplitude.

The figure illustrates that the largest uncertainty in the main channel occurs at the upstream and downstream ends of the lowered floodplain reach. It is shown that the mean response over all realisations is rather moderate, but that there may also be strong morphological impacts on the main channel. Note that the bed level just upstream of the lowered reach is consistently lower than the initial bed. This must be attributed to a consistent set-down of the water level in this area, when the water can go around the shallow part in the main channel via the lowered floodplains.

The morphological response statistics differs from the equilibrium state described in Section 5.2.1. The variation in the river discharge leads to a continuous adaptation of the river bed. Bottom waves, initiated with each new discharge stage, are noticed in the stochastic response, even after 30 years (Figure 5.7(b)). The long-term average response is rather similar to the deterministic equilibrium response as shown in Figure 5.3.

A Monte Carlo prediction for a much longer period must show whether the 90% confidence interval further decreases. The degree to which the bottom waves disappear in the longterm statistics shows to what extent it can be seen as a 'memory' effect. A Monte Carlo prediction over a period of 100 years is shown in Figure 5.8. This figure illustrates that the morphological response statistics at the beginning of year 20, 40, 60, 80, 100, respectively are more or less equal. The response statistics have converged to a stable state in a period of less than 20 years.
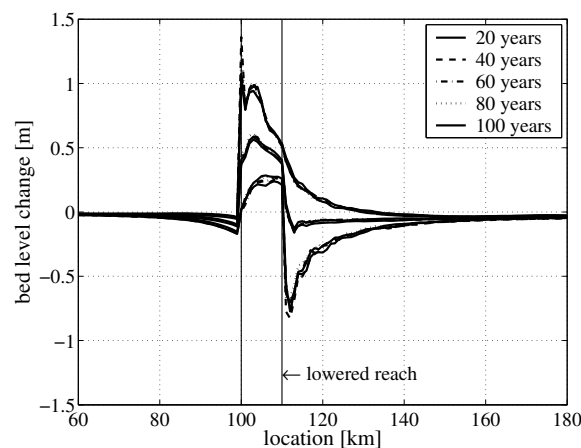

Figure 5.8: Morphological response statistics after 20, 40, 60, 80, 100 years (in December), respectively, as computed with the simple 1-D model

The spatial variation of the response provides insight into the probability of bottleneck formation in the river. As illustrated in the figure the maximum accretion probability is found at the upstream end of the lowered floodplain reach, the maximum erosion probability just downstream of it.

5.4.3   Temporal variation of morphological response statistics

The temporal variation of the response statistics provides information about when and how often the bed exceeds a particular level. The temporal variation of the statistical properties of the morphological response is illustrated in Figure 5.9 and Figure 5.10. Especially at the transition points (the upstream and downstream end of the lowered floodplain reach), the seasonal fluctuation of the 90% confidence interval is significant. The largest interval is found in the period right after the period with the highest flood probability (2-6 months, March to June). The computations start in January.

Figure 5.10 provides insight into the temporal variation of the response statistics at the upstream end (location 100 km) and downstream (location 120 km) of the lowered floodplain reach. The statistics converge quickly to a stable state and show a periodic oscillation, which reflects the seasonal variation. This variation is considerable. Especially the maximum accretion has a strong seasonal signature.
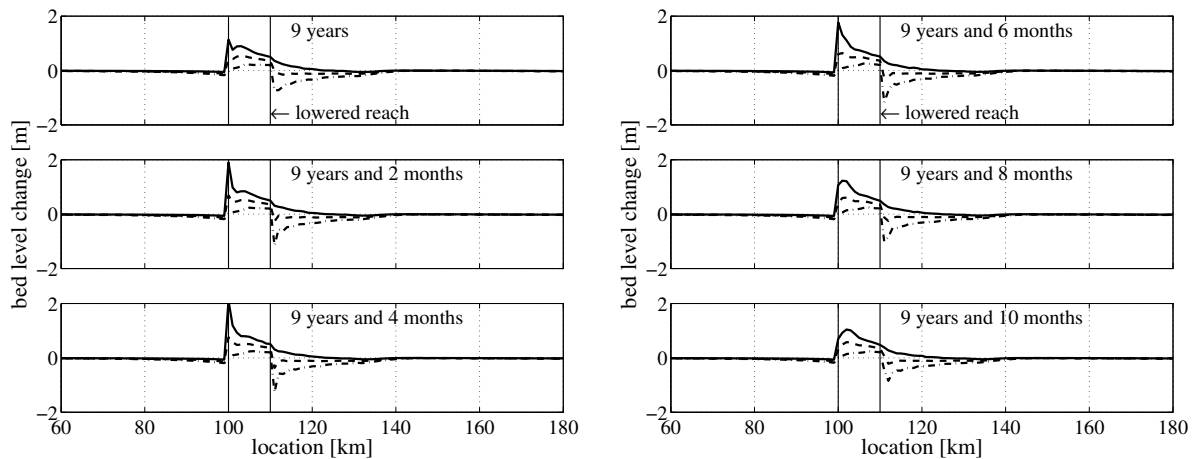

Figure 5.9: Temporal variation of the morphological response statistics during the 9th year of the simulation for Case 1, as computed with the simple 1-D model

Another interesting aspect is the asymmetry in the seasonal variation of the 95%-percentile and the 5%-percentile. The 95% percentile has a larger amplitude than the 5% percentile. This can be explained from the gradients in sediment transport. At the location of the floodplain lowering the current velocity will decrease extremely if the discharge exceeds the bankfull discharge. Sedimentation bottom waves will be initiated. These bottom waves will migrate downstream and (partly) decay during discharges lower than bankfull. At low water, the river stays within the main channel and the floodplain lowering will have no influence. Therefore, there will be no net erosion at this location. This is why the 5% percentile shows much less seasonal variation than the 95% percentile.
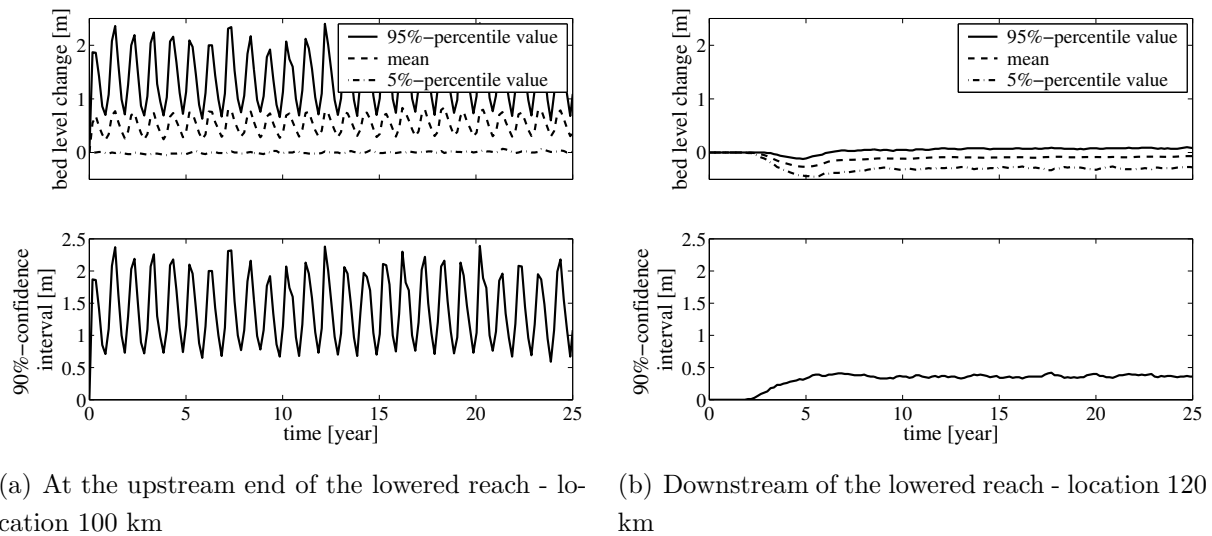
(a) At the upstream end of the lowered reach - location 100 km

(b) Downstream of the lowered reach - location 120 km

Figure 5.10: Temporal variation of the morphological response statistics during a 25-year period, as computed with the simple 1-D model

5.4.4 Comparison between the four Cases

In Figure 5.11 the morphological responses after 30 years for Case 1 - Case 4 are expressed in terms of the mean and the 90% confidence interval.

Figure 5.11(a) shows the effect of taking some other uncertainties into account (Case 2). Uncertainties in the hydraulic roughness of the main channel and the grain size of the bed material are taken included. Apparently, the effects of these additional uncertainties are small compared to those of the uncertainties in the discharge time series.

Figure 5.11(b) shows the effect of including lateral sediment transport from the main channel into the floodplains (Case 3). Part of this sediment will be deposited on the floodplains. The net sediment transport into the floodplains is modelled as a sediment extraction from the main channel, prescribed as a function of the discharge. The plot shows that the effect of this extension is quite a bit stronger than that in the previous case. Also note the systematic large-scale tilting of the bed. This indicates another period of 'autonomous' bed degradation if the floodplains along the Waal are to be lowered systematically and the summer levees are to be removed.

In Figure 5.11(c) we assume nature development to entail an instantaneous increase in the hydraulic roughness of the floodplains, which remains unaltered thereafter. The morphological response is less pronounced. The accretion in the main channel is slightly smaller.

In conclusion, the small adaptations to the reference case (Case 1) show that:

- The morphological response statistics are the most sensitive to river discharge variation. The contribution of the uncertainty in discharge variation to uncertainty in morpholo-

gical predictions is dominant.

- The morphological response is less pronounced if floodplain accretion (Case 3) and nature development in the floodplains (Case 4) are taken into account.

- As compared to Case 1, the size of the 90% confidence interval is slightly larger for Case 2 and is more or less the same for Case 3 and Case 4.
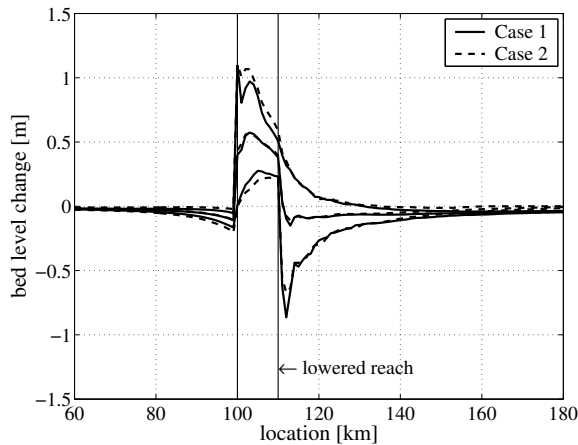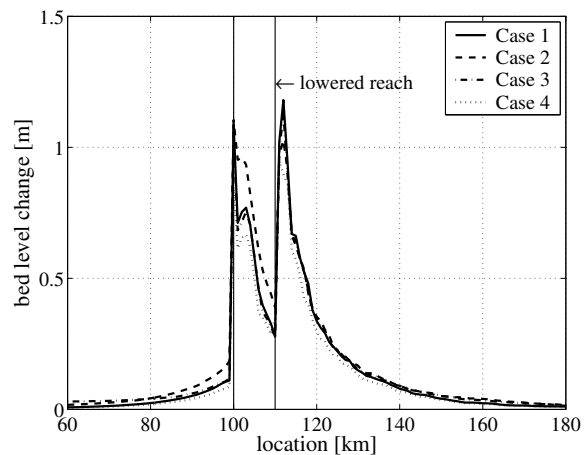

(a) Comparison of the morphological response statistics between Case 1 (uncertain discharge) and Case 2 (uncertain discharge, hydraulic roughness, grain size)
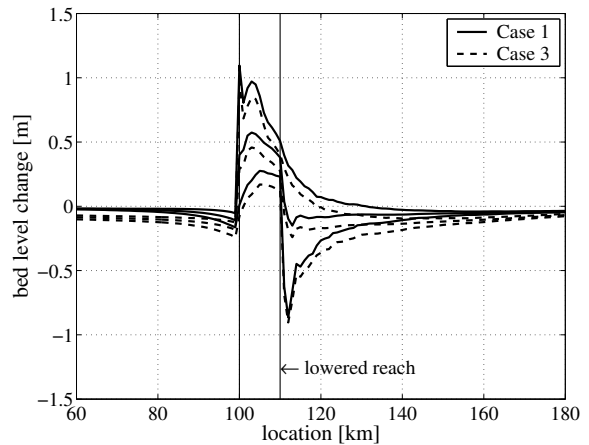
(b) Comparison of the morphological response statistics between Case 1 (uncertain discharge) and Case 3 (uncertain discharge and accretion in the floodplains
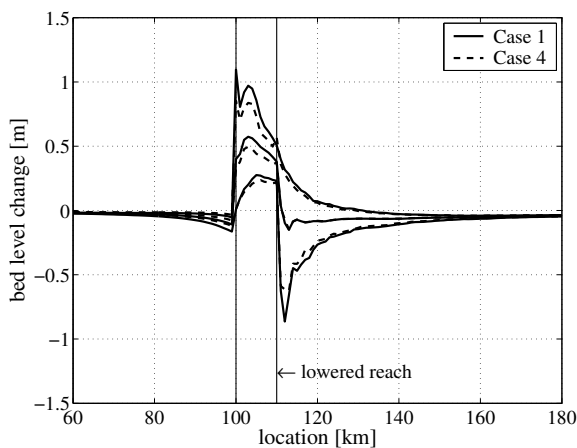
(c) Comparison of the morphological response statistics between Case 1 (uncertain discharge) and Case 4 (uncertain discharge and nature development in the floodplains)

(d) Size of the 90% confidence interval in Case 1 - Case 4

Figure 5.11: Morphological response statistics for Case 1 - Case 4, as computed with the simple 1-D model

### 5.4.5 Convergence of statistical properties

The accuracy of the MCS results can easily be estimated using standard statistical techniques afterwards. Moreover, the accuracy can also be checked by plotting estimates of the pth fractile against the number of simulations performed.

We check the convergence of the 90th fractile Y_{90} of the maximum accretion in Section 5.3.4. An approximation of the sample size is given that is required to be 95% confident that the actual 90th fractile Y_{90} of the maximum accretion (p=0.9) has a precision of plus or minus 10 cm. The enclosures of this confidence interval can be estimated afterwards using Eq. 5.8 and Eq. 5.9. The confidence interval of the 90th fractile of the maximum accretion is enclosed by Y_i and Y_k, with

$$i = \left\lfloor Np - c_\alpha \sqrt{Np\,(1-p)} \right\rfloor = \left\lfloor 400 \times 0.9 - 1.96 \sqrt{400 \times 0.9\,(1-0.9)} \right\rfloor = 348 \qquad (5.11)$$

$$k = \left\lceil Np + c_\alpha \sqrt{Np\,(1-p)} \right\rceil = \left\lceil 400 \times 0.9 + 1.96 \sqrt{400 \times 0.9\,(1-0.9)} \right\rceil = 372 \qquad (5.12)$$

For Case 1, this resulted in the confidence interval [4.57 m, 4.69 m]. The width of this interval (12 cm) is smaller than the desired precision (20 cm). Thus the desired accuracy is reached, meaning that the sample size of 400 is sufficient. Figure 5.12(a) shows the convergence of the estimate of the 90th fractile of the maximum accretion against the number of simulations performed. The dotted lines represent the enclosures of the confidence interval of the 90th fractile of the maximum accretion. The plot shows that the desired precision in the maximum accretion is reached with a sample size of 150 (Figure 5.12(b)).
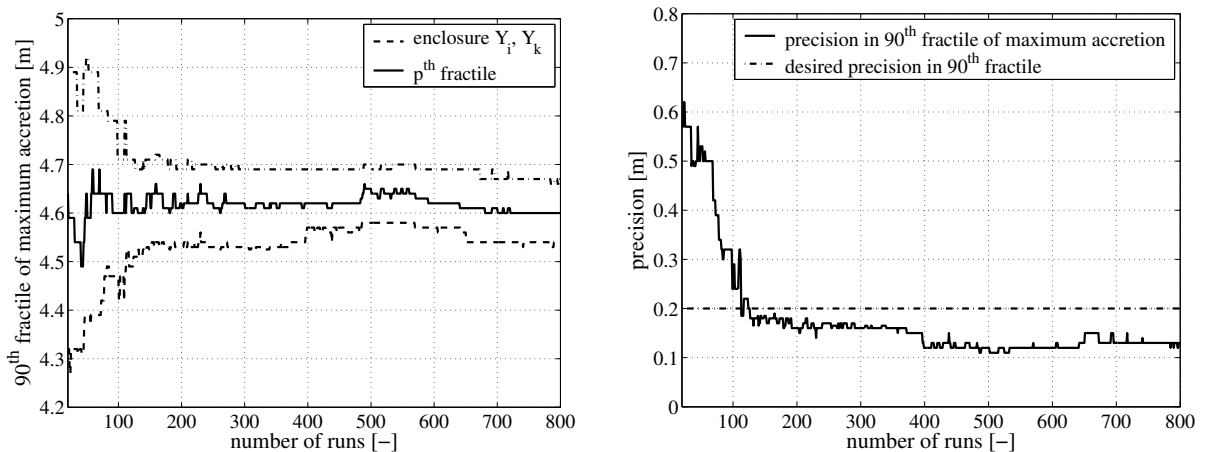
(a) Convergence of the 90th fractile of the maximum accretion

(b) Convergence of the precision in the 90th fractile of the maximum accretion

Figure 5.12: Convergence of the statistical characteristics against the number of simulations, as computed with the simple 1-D model

The convergence of the results appears to depend on the point at which convergence is studied. The mean accretion at the upstream end of the lowered reach will converge after a smaller

number of runs than a more extreme percentile, like the maximum accretion. The more extreme the situation, the more the probability depends on extreme events and the slower the convergence. Furthermore, the convergence seems to be affected by the distribution type of the morphological quantity observed. If the distribution of the quantity is extremely skewed, the required sample size to obtain a sufficiently converged estimate of an extreme percentile would be significantly larger.

5.5   Time series analysis versus Monte Carlo Simulation

While doing all these computationally intensive simulations, it is often suggested that, instead of doing a large number of model runs in a MCS-procedure, a record that is long enough, either obtained from historical data, or obtained from a single deterministic model run, already reveals part of the output statistics of interest. In other words, could the dynamics of a physical system be reconstructed from a time series? In fact, the underlying concept is that of ergodicity, meaning that a system tends in probability to a limiting form that is independent of the initial conditions, i.e. if a system is followed long enough, then all possible states will occur.

In this section, we gather output samples over time, instead of over separate simulations, in order to assess whether a single time series can be used to estimate the ensemble statistics. We did not use an existing historical record, but a 'record' obtained from the results of a model run (Case 1) over a period of 1000 years, so as to make sure we observe the system for a sufficient long period. The imposed 1000-year discharge time series at the inflow boundary, is arranged from the first 50 discharge time series of 20 years duration that were synthesised for the MCS. A time-stack plot of the resulting morphological response of the first and the last 100 years is shown in Figure 5.13. We have to bear in mind, that for this analysis, the output samples must be stationary, homogeneous and mutually independent.

Knowledge gained with this exercise, can be applied when utilising historical records for validation proposes of the stochastic results, later on in this thesis. Historical records can only reveal the ensemble dimension, when we can invoke the principle of ergodicity. In that case, the historical records should (1) cover a sufficiently long period, i.e. that gives a proper reflection of the population statistics, and (2) preserve homogeneity, persistency and stationarity.

Stationarity and homogeneity

The output samples should be strictly stationary, meaning that its statistical properties are unaffected by the choice of the time horizon and are free from a significant trend in time. Moreover, homogeneity should be preserved. Homogeneity does not hold during transition periods, for instance in a river reach, in which the river adapts to new river works. Stationarity does not

hold for rivers affected by systematic long-term changes of the bed topography. This is the case in the Dutch Rhine branches, which are undergoing long-term longitudinal profile evolution (see Section 4.3.3).

For the hypothetical 1-D model of floodplain lowering a transition period of 5 years is taken into account. The output samples of the remaining 995 years are used in the time series analysis (TSA). The Spearman's rank correlation method (Dahmen & Hall, 1989) is utilised to assess the degree of stationarity of the output samples. First, the Spearman's rank correlation coefficient is computed with Eq. 3.3. Subsequently, for each river location, we test if a significant trend is observed or not, by using Eq. 3.4-3.5. Since the test value t_t (Eq. 3.5) stays within the 95%-confidence interval, we say that no statistical siginificant trend is observed.
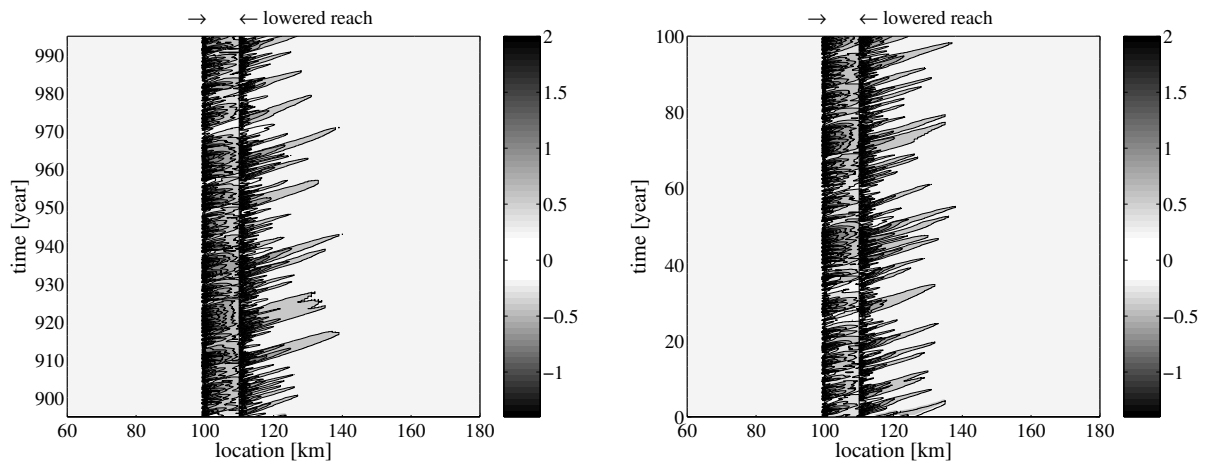
(a) First one hundred years of the 1000-year run   (b) Last one hundred years of the 1000-year run

Figure 5.13: Time-stack plot of the morphological effect, as computed for the first and last hundred years of the 1000-year deterministic model run

Mutual independency

Persistence of the data series is considered as the time independence of a particular value in the data series. The correlation between output samples at successive moments in time gives an indication of the persistence of the output samples. For river morphology, bed level states at a particular location at different time steps are mutually independent if the period in between is large enough.

The serial-correlation coefficient can help to verify the independence of the output samples (Box et al., 1994). The autocorrelation function, containing serial-correlation coefficients for different lags, shows to what extent output samples are still related in time (see Section 3.2.3). The squared serial-correlation coefficient, r^2, describes the proportion of variance in common between the two output samples. It is called the coefficient of determination. When the serial-correlation coefficient drops below 0.7, the coefficient of determination is approximately 0.5,

meaning that the bed level state depends for less than 50% on the bed level state in the preceding period. Below this stage, the mutual dependency is considered moderate to weak.

The autocorrelation function in Figure 5.14 illustrates that bed levels in periods close to each other are strongly correlated (correlation close to 1). This correlation reduces if the interval between successive output samples increases.

If the period in between successive bed level states is large enough, the output samples are considered as mutually independent. The length of this period depends on the activity of the bed at a particular location. This becomes clear from Figure 5.14(a), showing the autocorrelation function at different locations. At the upstream end of the lowered reach (km 100), the bed activity is large, resulting in a rapid decrease of the serial-correlation coefficient. The bed activity reduces in downstream direction, leading to an increase in correlation. The periodic oscillation of the autocorrelation function at location km 100, resembles the seasonal correlation of the bed level states that results from seasonal fluctuations in discharge. If r drops below the threshold value of 0.7, the bed level states at different time steps are assumed to be mutually independent. This corresponds with a lag of 5-25 periods of approximately 10-day (see Figure 5.14(b)).
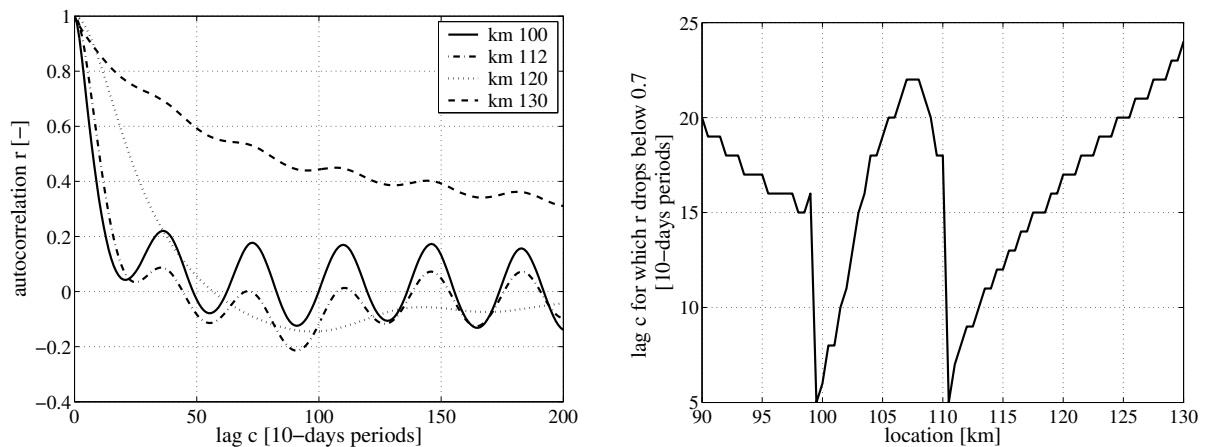
(a) Autocorrelation function containing serial-correlation coefficients for different lags at different locations

(b) Time-lag c as a function of river location for which the serial-correlation coefficient r drops below 0.7

Figure 5.14: Autocorrelation, illustrating the correlation between bed levels in successive periods

Statistics derived from time series analysis (TSA)

The stochastic prediction provides insight into when, where and with what frequency required conditions will not be fulfilled. Bottlenecks and critical time intervals can be identified. If we want to use output samples over time to obtain similar information as with the application of MCS, we choose a lag of at least 36 periods (a one-year period) to discriminate between

bed level states that are mutually independent. The appropriateness of using time series ana-lysis (TSA) in order to do stochastic predictions is assessed by the following aspects, (1) its spatial representation of morphological response statistics, (2) its temporal representation of morphological response statistics, and (3) its use in river management practice.

Figure 5.15 shows the spatial response statistics at different points along the river that provides insight into potential bottlenecks. The left panel presents the estimates of the mean bed level change and the 95%- and 5%-percentiles values after a period of 20 years in the high-water sea-son, as obtained from the MCS. The grey areas represent the uncertainty around the estimates of the statistical properties. The right panel shows the statistics of the bed level changes from the single simulation of 1000 years duration, by taking the bed level states in the high-water season of each year. A slight difference in height of the percentile values is noticed at the up-stream and downstream ends of the lowered floodplain reach. The envelopes of the MCS show more fluctuations than those of the TSA. In general, however, the figure illustrates that the spatial response statistics are more or less equal, meaning that the TSA reveals similar output statistics of interest, namely information on potential bottlenecks.
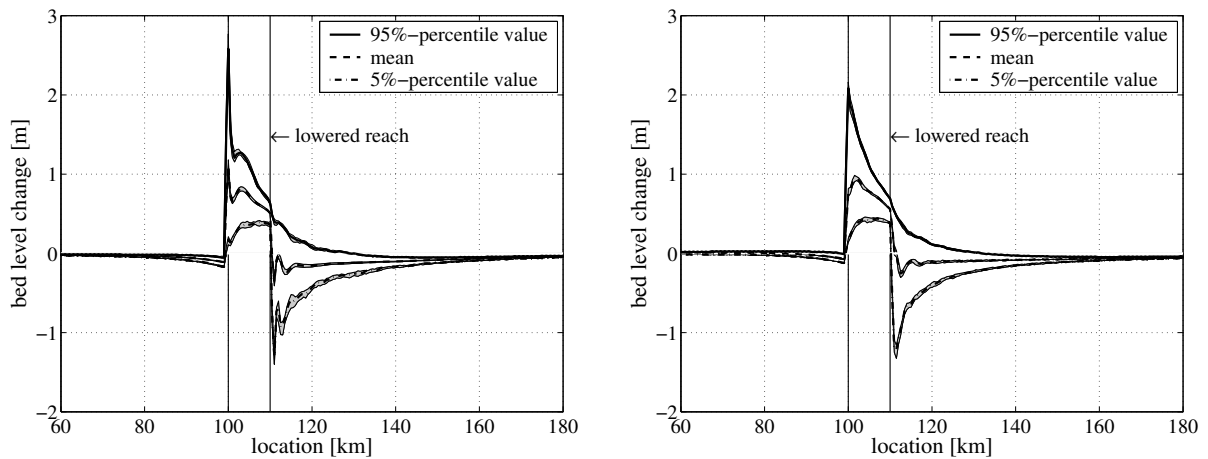
(a) Morphological response statistics for MCS, ex-pressed in terms of the mean and the 95%- and 5%-precentile values. The grey areas indicate the 90%-confidence interval of the corresponding sta-tistical properties

(b) Morphological response statistics for TSA, ex-pressed in terms of the mean and the 95%- and 5%-precentile values. The grey areas indicate the 90%-confidence interval of the corresponding sta-tistical properties

Figure 5.15: Spatial variations in morphological response statistics, as computed with the simple 1-D model using MCS and TSA

At bottleneck locations the temporal variation of the statistical properties gives information about when and how frequently the river does not meet the required conditions. Since we can use only the output samples at time-lags of at least 5-25 periods of approximately 10 days (in order to have bed level states that are mutually independent), we choose to cut the 1000-year output series into 50 parts of 20-years each. The 50 time series are considered mutually

independent and are used to estimate the temporal response statistics as shown in Figure 5.16. The figure is more or less equal to the one derived for MCS (based on 400 model runs), see Figure 5.10. But, a sample size of 50 appears not to be sufficient to let the statistics converge.
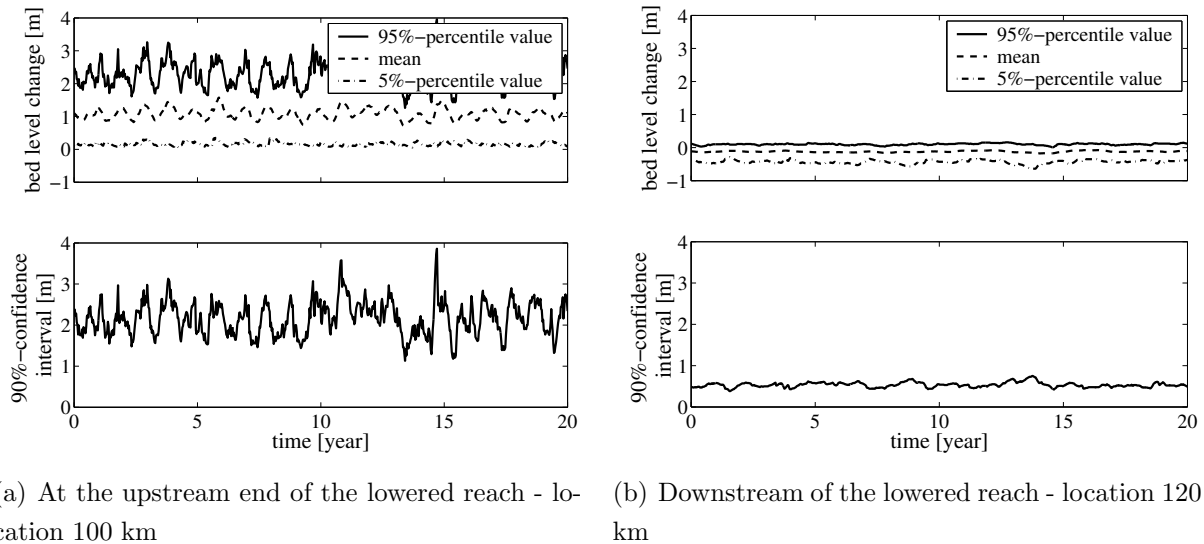

(a) At the upstream end of the lowered reach - location 100 km

(b) Downstream of the lowered reach - location 120 km

Figure 5.16: Temporal variation of the morphological response statistics during a 20-year period, as computed with the simple 1-D model using TSA

Insight in the morphological response statistics both in time and in space, is obtained with time-stack plots in Figure 5.17. The figure shows the mean value and the standard deviation of the bed level response as a function of time and space, for MCS and TSA. Again, the response statistics computed with MCS and TSA are more or less similar.

For some applications information of the response statistics in time and space is necessary. The frequency of reaching a critical level somewhere in the river, for instance, is important when the river manager has to ensure a certain navigation depth. Predicting where, when and how frequently the bed level reaches a critical level is necessary for the time deployment of dredging measures. TSA might be suitable to provide a rough indication of the navigability of a river under uncertain conditions. To that end, the deterministic time series should be split into short parts, that are treated as separate simulations, like in MCS. The deterministic run should, however, be long enough to get sufficient separate time series for convergence of the response statistics. A deterministic model run of 1000 years duration is probably too short.

We elaborate on the use of time series analysis versus MCS in river management practice, using the following example. Suppose a hydraulic structure is located just downstream the lowered floodplain reach (km 111). Erosion may undermine and destabilise its foundation. Therefore, we are interested in the maximum erosion depth at this location over the lifespan the hydraulic structure. Each simulation of the MCS yields a single value of maximum erosion depth. Figure 5.18 shows the cumulative probability distribution function of the maximum erosion depth in a

period of 20 years for 400 model simulations. The grey area indicates the statistical uncertainty around this probability distribution plot. From the single simulation of 1000 years duration, the maximum erosion depths of each 20 year-period (meaning 50 periods of 20 years) is estimated. The dashed line in Figure 5.18 represents the cumulative probability distribution function that is derived from the 50 depth values. A shift to the left of the distribution function derived with output samples over time is noticed, indicating an underestimation of the maximum erosion depth at location km 111. Underestimating the erosion may jeopardise the design of a stable hydraulic structure. This underestimation can be attributed to the fact that during MCS a larger number of discharge time series has been included, namely 400 times 20 years ($\sim$ 8000 years), whereas for TSA the statistics are based on 50 times 20 years ($\sim$ 1000 years).

(a) Mean bed level response - MCS

(b) Standard deviation of bed level response - MSC

(c) Mean bed level response - TSA

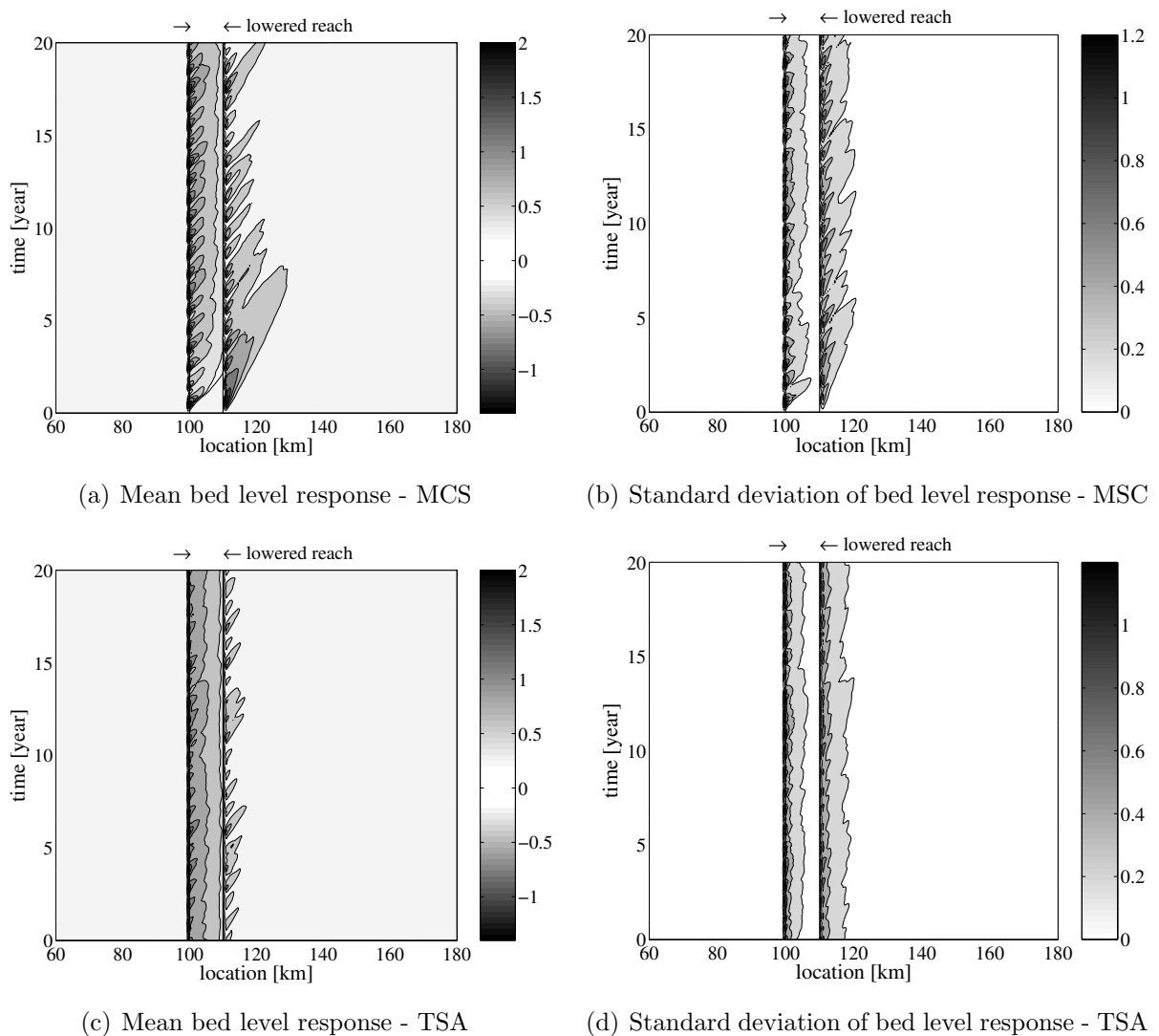(d) Standard deviation of bed level response - TSA

Figure 5.17: Morphological response statistics as a function of time and space, as computed with the simple 1-D model using MCS and TSA
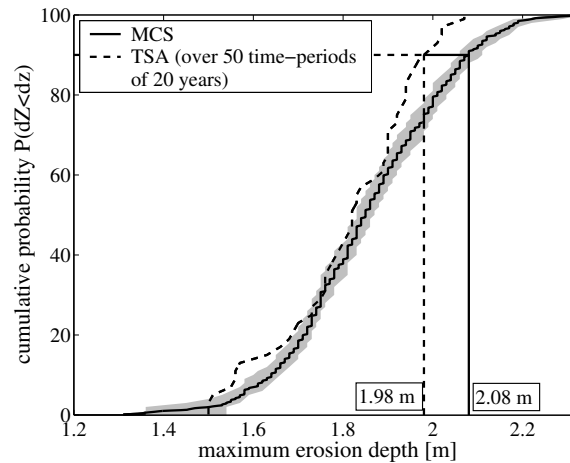
Figure 5.18: Maximum erosion depth just downstream the lowered floodplain reach at km 111, as computed with the simple 1-D model using MCS and TSA

We did not use an existing record obtained from measurements, but a 'record' obtained from the results of a model run to determine to what extent a long-term record can reveal the ensemble statistics. The discharge series imposed at the inflow boundary of this model, has been synthesised by using the lognormal multivariate distribution. In that way, values beyond the historical discharge record are incorporated in the analysis. If, in the previous example, a historical record was used for the model input setting in the TSA, the difference between TSA and MCS would probably have been larger. A historical record is often too short to properly reflect the 'population' statistics. Extreme conditions may well have been missed, whereas extreme inputs, beyond the historical record, significantly influence the output statistics. The potential of TSA would have been even less, if one was interested in the maximum erosion over a shorter time interval. In that case, the impact of random behaviour becomes more evident.

5.6   Conclusions

The hypothetical model of dimensions similar to those of the Waal is used to get insight into the morphological response to floodplain lowering. The underlying rationale is that the potential of a stochastic approach is best understood by first examining a simplified case in which the morphological processes are fully transparent.

The stochastic predictions of the main channel morphology show that the mean response to floodplain lowering over all realisations is rather moderate, but that extreme accretion or accretion may also occur. The presentation of the response statistics at different points along the river provides insight into potential bottlenecks. At these bottleneck locations the temporal variation of the statistical properties gives information about when and how frequently the

river does not meet the required conditions. Especially at the transition points of the lowered floodplain reach, the seasonal variation of the response statistics is large.

The morphological response statistics are most sensitive to river discharge variation. The effect of taking some other uncertainty sources into account is small. The morphological response to floodplain lowering is less pronounced if floodplain accretion and nature development in the floodplains are taken into account. The impact of floodplain accretion and nature development in the floodplains on the uncertainty in the morphological predictions is negligible.

As compared with the results of single deterministic model runs, the stochastic predictions indicate a considerable uncertainty in the river's response to floodplain lowering. It is often suggested that a very long deterministic model run reveals most of the output statistics of interest. It would mean that output samples can be gathered over time, instead of over separate simulations, like in MCS. This chapter shows that time series analysis (TSA) reveals part of the output statistics. It provides similar information on the location of potential bottlenecks (e.g. nautical bottlenecks or locations with an enhanced danger of destabilisation of hydraulic structures). Yet, it is not straightforward to produce, for instance, information about when and how frequently the river does not meet the required conditions.

The potential of TSA in river maintenance practice is illustrated with an example of the maximum erosion depth just downstream the lowered reach. As compared with MCS, the maximum erosion tends to be underestimated with TSA, which may lead to stability problems for construction works (like groynes). The potential of TSA may be less, if one is interested in the maximum erosion over a shorter time interval.

TSA is not suitable for river systems in transition periods, for instance, for rivers that adapt to new river works or that are affected by systematic long-term changes. This is often the case in natural rivers. We therefore expect TSA to be therefore less suitable in maintenance practice of real-life rivers. This underpins the importance of stochastic methods.

In order to use the type of information obtained from stochastic analysis, river managers have to quantify the required morphological conditions. Contact with these potential users is relevant to get more insight into their interests. It is important to be critical on the demanded degree of precision, since it is pointless to demand a high precision if uncertainty in model input is known only roughly. Users should focus on precise estimates of extreme percentiles only if it is meaningful for the accuracy of the input statistics. A careful consideration on the desired precision is important, if it were only because it determines the required samples size.

The main disadvantage of the hypothetical model is that it concerns a rather idealised situation, as the river is schematised to a straight compound channel excluding summer levees. Therefore, the model is of little use to operation and maintenance practice of real-life rivers. The experience gained with simplified cases, however, will support the interpretation of uncertainty estimates in the more complex situations considered in the next two chapters.

Chapter 6

1-D Rhine model

6.1 Introduction

River models are usually simplified representations of reality, assuming, for instance, a prismatic channel with a plane sloping bed, like in Chapter 5. The hypothetical model contributed to a quick understanding of the physical system behaviour and the potential of the stochastic model approach. The main disadvantage of such a model is that it concerns a rather idealised situation. Therefore, the hypothetical model is of little use to operation and maintenance practice of real-life rivers. The step to a more complex model of the Rhine incorporating man-made structures and variations in geometry and flow resistance, is made in this chapter. We focus in particular on how uncertain model inputs and parameters influence the uncertainty in the outputs of the 1-D Rhine model. To that end, the model is run in an MCS-setting. The potential of using this model in a stochastic mode in river management practice is explored in Chapters 8 through 10.

The 1-D Rhine model is described and discussed in detail in Chapter 4. Running this model in an MCS-setting is rather time-consuming. Therefore, the number of branches incorporated in the model has been reduced in order to reduce the computational effort per individual simulation. The adapted version of the Rhine model includes the branches Niederrhein and Waal. We have kept the discharge distribution at the Pannerdensche Kop bifurcation fixed at 66-34% under all discharge conditions. The research area is restricted to the section downstream of Pannerdensche Kop up to Nijmegen (km 867-915).

It is worthwhile to put effort into determining the relative contribution of each uncertainty source to the overall uncertainty in the model output. Prior to the uncertainty analysis, a first selection between important and less important uncertainty sources is obtained with a sensitivity analysis. Among these most important uncertainty sources are parameters that are used as tuning parameters in the calibration process. The following uncertainty sources are addressed individually:

- river discharge - Section 6.4;
- grain size of bed material - Section 6.5;

- parameters in calibration process - Section 6.6:
    - hydraulic roughness of the main channel;
    - parameters playing a role in the sediment transport formula.

MCS gives accurate results, as long as the sample size is large enough and the description of the input uncertainty adequate. The appropriate sample size depends on the desired degree of accuracy. The method described in Section 5.3.4 is used to roughly approximate the sample size on beforehand. Background information on the statistical description of uncertainty is provided in Section 3.2.4 and is used in combination with field observations and measurements, literature and expert opinions to statistically describe the above-mentioned uncertainty sources.

The relative contribution of the uncertain model inputs and parameters to the overall uncertainty is discussed in Section 6.7. The MCS with the uncertainty sources addressed individually are used to that end. Moreover, an MCS is performed in which the above-mentioned uncertainty sources are included simultaneously. Estimating this relative contribution appears not to be straightforward, since morphodynamic systems exhibit a strong non-linear behaviour, a time and space dependent signature, model inputs that are mutually correlated and a time-lagging effect.

Finally, a bathymetric database of the Rhine is used to compare the bed level variability observed in nature with the estimated stochasticity of the MCS-results. The chapter ends with some conclusions.

6.2   Sensitivity analysis

Insight into the model sensitivity is often obtained by systematically and deterministically varying the model input quantities one by one and estimating their impact on the model results. Since the 1-D Rhine model contains many input and output variables that have a strong time and space dependency, this insight is not easily achieved. Apart from this, the presence of correlations and the fact that we deal with a calibrated model, make a sensitivity analysis less straightforward.

The 1-D Rhine model is affected by various uncertainties, including those in the model schematisation and in the specification of model input (for example boundary conditions, initial conditions) and the model parameters. Uncertainties introduced by the model schematisation, numerical solution technique and the specification of future scenarios are left out of consideration, here.

As noted in Section 3.2.2, a sensitivity analysis can be performed from a local or a global point of view. We will apply a global sensitivity analysis, in order to have a first indication of model inputs and parameters that contribute most to the output uncertainty. Therefore, various model

inputs are perturbed one by one around their pivot value over 80% of what is considered to be the physically realistic range. In order to estimate this range, use is made of field observations and measurements, expert opinions and literature. The large range of variation probably yields a poor estimate of the possible deviation from the local pivot point of the results, given the non-linear character of the system. Apart from this, perturbing each model input or parameter over 80% of its physically realistic range makes the results easy to oversee and compare.

The following list of the model inputs and parameters is considered in the sensitivity analysis. Information on their pivot values is provided in Section 4.5.4.

Upstream boundary condition - river discharge

Uncertainty in river discharge is inherent to nature, it cannot be reduced, unless large interventions are undertaken (e.g. a dam in the river). To test the model's sensitivity to discharge variations, use is made of the range of 100 years of discharge measurements at Lobith. Out of this range, the 90%-percentile and 10%-percentile values of the discharges are derived for each of the 36 periods of approximately 10 days in the hydrological year (see Figure 4.6(b)). The 90th and 10th percentile series are arranged to construct two extreme time series of 20 years duration, in order to investigate the impact of extreme discharge events that holds for a longer period by means of sensitivity analysis.

*Downstream boundary condition - stage-discharge relationships*

Stage-discharge relationships are deduced from measurements. Uncertainty results amongst others from measurement errors. Moreover, the evolution of the river system due to human interventions also induces a gradual change in the relationships. The uncertainty in the stage-discharge relationships is reflected by giving the stage for each discharge value as a normal probability distribution function with the pivot values as mean values and a standard deviation 0.15 m. A perturbation over the 80%-confidence range, implies that for each discharge level the corresponding stages are lowered and raised by 0.19 m.

Conditions at Pannerdensche Kop bifurcation

We have kept the discharge distribution at the Pannerdensche Kop bifurcation fixed under all discharge conditions. The actual discharge distribution is, however, governed by the conveyance and resistance of the branches. Local morphological changes around the bifurcation may lead to variations in discharge distributions. Daily discharge measurements at the Pannerdensche Kop in the period 1961-2000 show variations in Waal discharges between tens and hundreds of cubic metres per second (Figure 6.1(a)).
Figure 6.1(b) shows this variation in percentage terms for three discharge regimes in a box plot.

The box has lines at the lower quartile, median, and upper quartile values. The whiskers are lines extending from each end of the box to show the extent of the rest of the data. Outliers are data with values beyond the ends of the whiskers. The length of the 'whiskers' equals 1.5 times the inter-quartile range. For discharges below a threshold value of 1400 m^3/s, the discharge distribution at the Pannerdensche Kop is largely influenced by the weir operation at Driel in the Lower-Rhine, which is indicated by the highest deviation in discharge distribution. In the sensitivity analysis, the discharge distribution is varied with $\pm$ 6%.
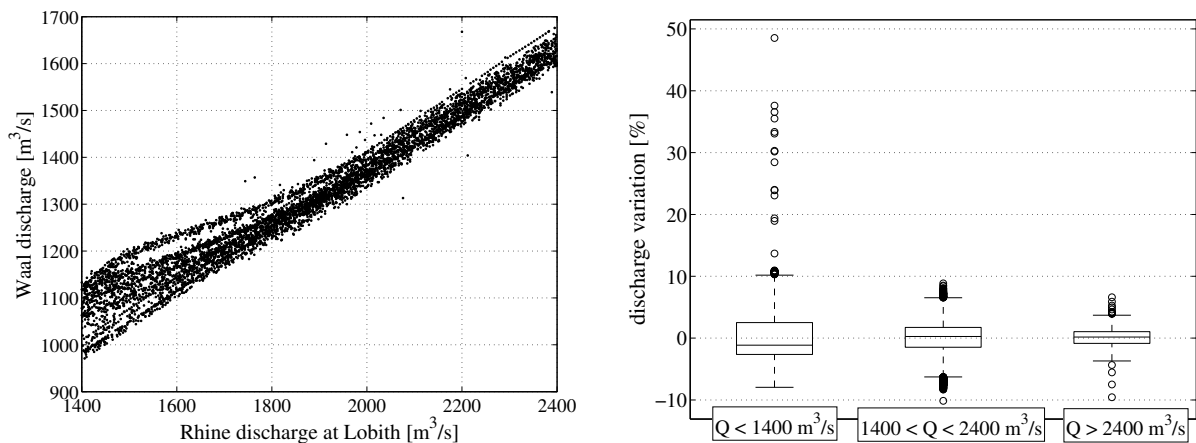
(a) Waal discharge as a function of the Rhine discharge at Lobith (1400 < Q < 2400 m^3/s)

(b) Variation in discharge distribution at Pannerdensche Kop bifurcation for three discharge regimes in a box plot

Figure 6.1: Discharge distribution at the Pannerdensche Kop bifurcation on the basis of daily discharge measurements in the period 1961-2000

In the 1-D Rhine model, a nodal point relation, Eq. 4-12, describes the sediment distribution at the bifurcation. The ratio of sediment load over the outflowing branches is expressed as a linear function of the water distribution over these branches. The pivot value of coefficient α is 3; and is varied over the range 2.5 - 3.5.

Hydraulic roughness of the main channel and the floodplain

The hydraulic roughness of the main channel is related to grain size and bedforms. The hydraulic roughness of the floodplain is related to the various ecotypes and their spatial distribution over the floodplains (Baptist, 2005). Uncertainties in the hydraulic roughness are inherent to natural variability, e.g. of the spatial grain size distribution, bedforms (shape and height) and seasonal and spatial variation in floodplain vegetation. An additional source of model uncertainty originates from the fact that the hydraulic roughness values are used as hydraulic calibration parameters. Johnson (1996a) gives a literature review on uncertainty in hydraulic roughness coefficients. She expresses the uncertainty by means of the coefficient of variation,

ν. This coefficient is defined as the ratio of the standard deviation to the mean. We fixed ν at 0.15. When using the pivot values of the hydraulic roughness coefficients of the main channel (see Figure 4.8) as mean values, the standard deviation varies within the range 5-8 $m^{1/2}/s$. For the Nikuradse coefficients of the floodplain, this results in a standard deviation in the range 0.02-0.06 m.

Grain size of the bed material

The Rhine is characterised by non-uniform sediment. The (time-dependent) lateral and vertical sorting processes of fine and coarse sediment are important to its morphological behaviour. Nonetheless, the Rhine model assumes uniformity in the bed material (see Section 4.5.4). Longitudinal sorting effects are to some extent included as the D_{50} and D_{90} are given as functions of location along the river. Four measuring campaigns are used as a data source. Sampling - i.e. sampling instruments, location, timing and sample size - and analysis (sieving) introduce model uncertainty in the grain size distribution curves and the D_{50} and D_{90} characteristics that are deduced from these curves. Figure 6.2 shows the pivot values of the spatial distribution of the grain size characteristics (solid lines). The dashed lines enclose 80% of the parameter range.
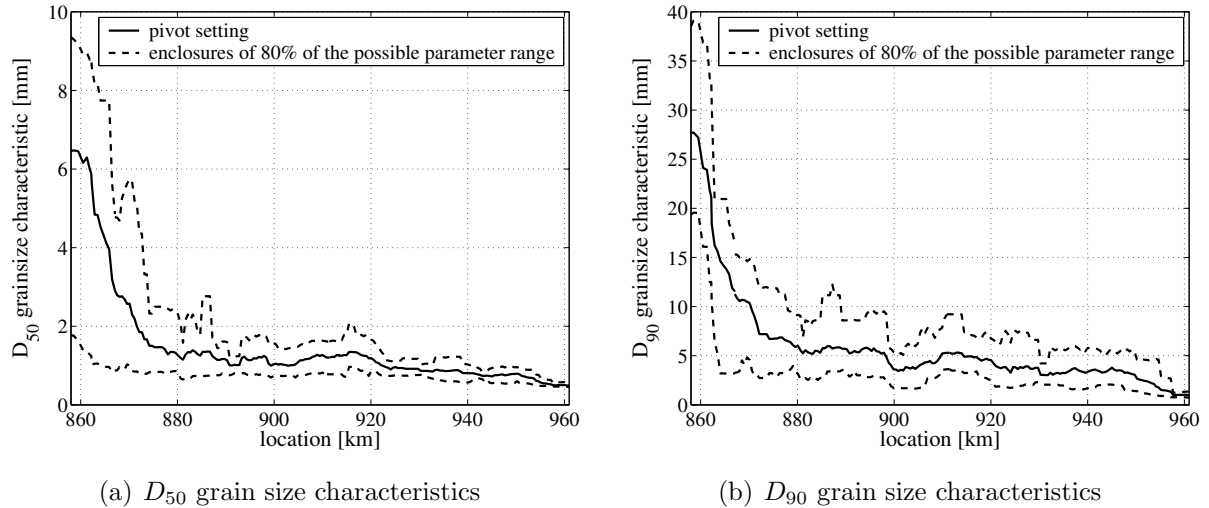

(a) D_{50} grain size characteristics   (b) D_{90} grain size characteristics

Figure 6.2: Spatial distribution of the D_{90} and D_{90} grain size characteristics in Niederrhein and Waal

Parameters in the sediment transport formula

A number of formulae have been developed to compute the amount of sediment transport as a function of various flow parameters and sediment properties. None of these formulae have gained universal acceptance in confidently predicting sediment transport rates (Yang, 1996). Uncertainty is inherent, since the formulae and their parameters are empirically derived. With

the choice of the Meyer-Peter & Müller (1948)-formula in combination with a reduced value of
the critical Shields parameter, model uncertainty is involved in the Rhine model that reflects the
inability to represent the true physical behaviour of the river. The sensitivity of two parameters,
namely the critical Shields parameter θ_{cr} and the exponent of the bed shear stress α, is analysed.
The pivot values ($\theta_{cr} = 0.025$ and $\alpha = 1.5$) are varied with 0.02 and 0.3, respectively.

Conclusions sensitivity analysis

Figure 6.3 illustrates the sensitivity of the morphological response to the above-mentioned
model inputs and model parameters. The sensitivity is shown at five different locations in
the high-water season. The morphological response appears to be the most sensitive to the
parameters of the sediment transport formula, viz. the exponent of the bed shear stress and the
critical Shield parameter. Moreover, sensitivity to the river discharge, the grain size of the bed
material and the hydraulic roughness of the main channel, is clearly noticed. The remainder
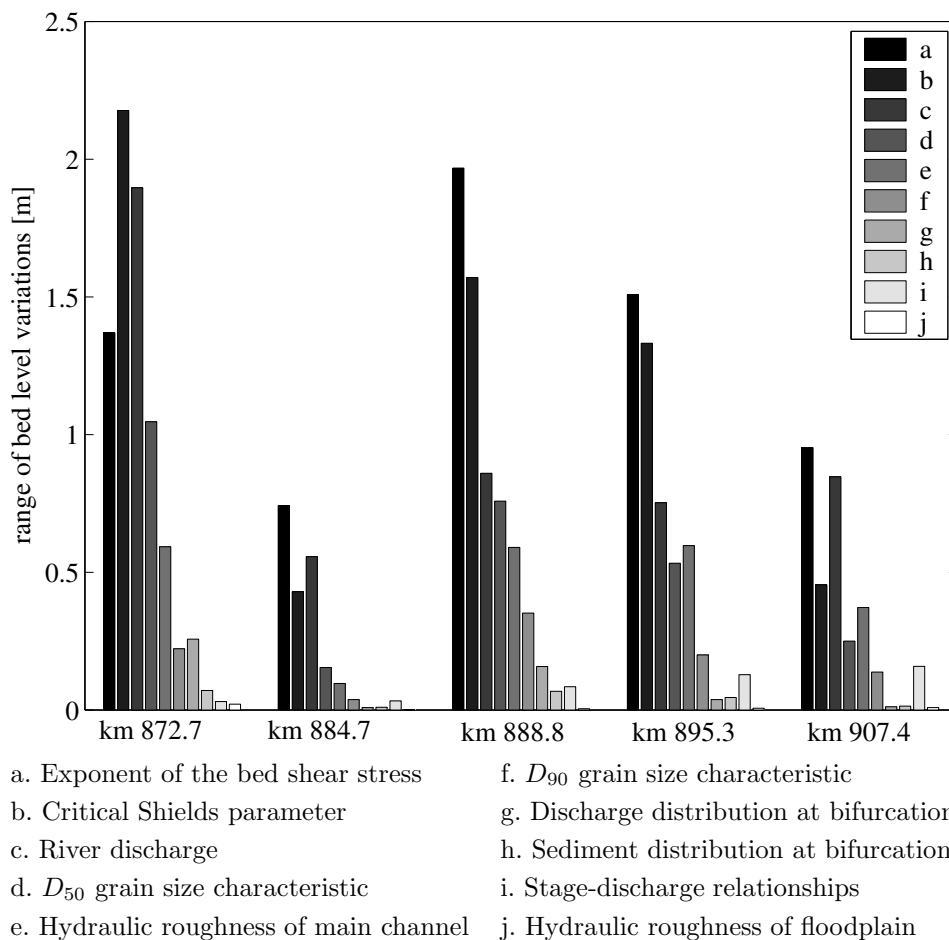inputs and parameters seem to be of minor importance.

a. Exponent of the bed shear stress   f. D_{90} grain size characteristic
b. Critical Shields parameter   g. Discharge distribution at bifurcation
c. River discharge   h. Sediment distribution at bifurcation
d. D_{50} grain size characteristic   i. Stage-discharge relationships
e. Hydraulic roughness of main channel   j. Hydraulic roughness of floodplain

Figure 6.3: Sensitivity of the cross-sectionally averaged bed level response at five different locations
in the high-water season, as computed with the 1-D Rhine model

6.3   Sample size for Monte Carlo Simulations

In the previous section, we have taken a deterministic approach to perform a traditional sensitivity analysis. In sections to follow, we address the impact of different uncertainty sources individually, using MCS. The sensitivity of morphology to the various uncertainty sources is investigated, while comparing the mean, the 95% and 5%-percentile values and the corresponding 90%-confidence interval of the bed level response with respect to the initial situation. We roughly approximate on beforehand the sample size N for a specific degree of accuracy, using the method presented in Section 5.3.4:

$$N = p\left(1 - p\right)\left(\frac{c_\alpha}{\Delta p}\right)^2 \tag{6.1}$$

in which p is the fractile number of interest, Δp the allowed deviation in terms of an interval of fractiles, and c_α is the deviation that encloses probability α of a random variable with unit normal distribution $(P\left(-c_\alpha < \Phi < c_\alpha\right) = \alpha)$.

The desired accuracy is expressed as an allowed deviation from an estimated fractile, in metres of bed level change. In this case, we want to be 90% confident that the actual 95% and 5% fractiles, $Y_{0.95}$ and $Y_{0.05}$ of the bed level response with respect to the initial situation, have a precision of at least 10 cm. An approximation of the sample size to obtain this precision in the computation of the 95% and 5% fractiles of the morphological response at five different locations, is given in Table 6.1. The required sample size is approximated for the different uncertain input sources, from a first set of 50 simulations.

Location	$Q\left(t\right)$	D	C	θ_{cr}	α	all sources
km 872.7	135	100	215	280	25	640
km 884.7	10	5	5	10	5	25
km 888.8	30	50	55	280	65	440
km 895.3	5	25	80	125	40	230
km 907.4	215	5	245	40	15	400

Table 6.1: An approximation of the sample size to be 90% confident that the actual 95% and 5% fractiles of the bed level response after 20 years in the high-water season, have a precision of at least 10 cm

The approximations of the sample size differ strongly between locations and between uncertainty sources. As we will see at the end of this chapter, this can probably be explained by the fact that the morphological response statistics vary in time and space, and in a different way for each uncertainty source. For all MCS, we use a sample size of 500.

6.4   Uncertainty in river discharge

6.4.1   Statistical description of the discharge uncertainty

We cannot predict the exact future discharge hydrograph. But, on the basis of the historical discharge data, different discharge times series that are equally likely to occur can be synthesised with the help of stochastic methods. The generation of the discharge time series in this section is based on 100 years of daily discharge measurements in the Niederrhein near Lobith. The conversion from daily discharges to discharges per interval of approximately 10 days is required in order to match the discharge time series with the numerical time step applied in the simulation. This conversion is presented in Section 4.5.4 and results for the Rhine dataset in 36 intervals of 100 data points.

For each model run in the MCS, we need a time series of discharges as a an upstream hydraulic boundary condition. Each series, however, yields a different morphological response. Van der Klis (2003) showed the sensitivity of this response to the height, duration and chronology of flood events and the magnitude of low and moderate discharges in the hydrograph. Flood events of relatively short duration have a relatively strong effect on the morphology, especially in non-prismatic channels. At discharges above bankfull, bottom waves (due to consecutive sedimentation and erosion) are initiated in the main channel. These bottom waves migrate downstream and (partly) decay during discharges lower than bankfull, when the flow stays within the main channel. Roughly speaking, flood events give rise to intermediate-scale bed disturbances, whereas the average features of the hydrograph determine the overall large-scale evolution. Moreover, the correlation structure in the discharge time series, such as the seasonal dependency and the correlation of discharges in successive time intervals, seem to be important.

In this section, we discuss the use of four stochastic methods that are proposed in literature to model the natural randomness of time series, such as discharge time series.

Method 1 - Multivariate lognormal distribution

Duits (1997) and Van Vuren & Van Breen (2003) derived a statistical description of the aforementioned 10-day discharge time series in three consecutive steps. First, they describe each of the '10-day'-intervals of 100 data points with a marginal probability distribution function. Since the discharges in successive time intervals are mutually correlated, the autocorrelation function is estimated in addition. Finally, a multivariate distribution function is constructed on the basis of the marginal distribution functions for each period and the autocorrelation function. This multivariate distribution function is used for the random generation of discharge time series. According to Bayesian statistics, the lognormal probability distribution function provides the best fit to the data. A three-parameter (or shifted) lognormal distribution is formulated with the third parameter representing the minimum possible observation. This parameter is referred

to as the location parameter.

The parameters of the lognormal distribution function are given in Figure 6.4(a). The autocorrelation function in Figure 6.4(b) illustrates that discharges in periods close to each other are strongly correlated (correlation coefficient close to 1). This correlation decreases if the interval between successive discharges increases. Therefore, the correlation between three successive 10-day intervals is taken into account.
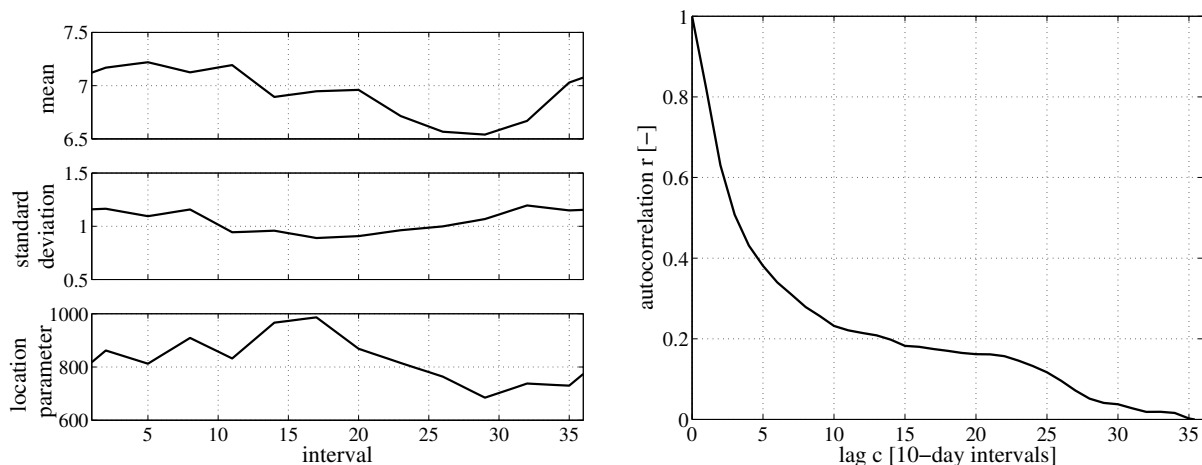
(a) Parameters of the lognormal distribution for 36 intervals of 100 data points (January (1) - December (36))

(b) Autocorrelation function containing serial-correlation coefficients for different lags

Figure 6.4: Statistical parameters of multivariate lognormal distribution function

Method 2 - Bootstrap resampling

Bootstrap resampling can be applied to construct a new time series by resampling from the original data set (Efron, 1982). A convenient characteristic of resampling is that no assumptions have to be made about the underlying distributions of the discharge in each 10-day interval. The Bootstrap technique is suitable if data points are not affected by any correlation structure. However, discharge time series of the Rhine show a strong seasonal dependency. Furthermore, the correlation of discharges in periods close to each other is significant. Therefore, we do not randomly sample discharges from the entire historical record, but short discharge time series of one-year duration are randomly selected from the 100-year data record. Subsequently the one-year discharge time series are arranged at random to construct new time series. Thus, the impact of reordering historical 10-day intervals within a hydrological year is not considered.

Method 3 - Nearest-Neighbour resampling

Nearest-Neighbour resampling is a strategy that preserves the dependence structure of the time series while bootstrapping (Lall & Sharma, 1996). The underlying concept is that resampling is

restricted to the historical values that have similar characteristics as those of the latest selected value. One of these historical values, also known as nearest neighbours, is selected at random and its historical successor is the next value to be added to the sequence.

The resampling strategy for discharge time series consists of the following steps:

1.   The discharge time series is denoted by Q_t, t=1,....,n. We assume that the serial dependence in discharge time series is limited to the two previous lags of approximately 10 days. So, the future discharge Q_t depends on the two prior values Q_{t-1} and Q_{t-2}. This set is known as a feature vector (or state vector) D_t of dimension d

$$D_t : (Q_{t-1}, Q_{t-2}) ; \quad d = 2 \tag{6.2}$$

2.   The next step is to find the k historical nearest neighbours of the current feature vector, i.e. we are looking for k patterns in the historical data that have similar characteristics as those of the current pattern, and then resample from their successors. The search for the k nearest neighbours was restricted to a 7 interval wide 'moving window', centered on the interval t of interest. In this way, we impose a realistic seasonal cycle upon the synthesised time series. For the 100-yr historical record, the nearest neighbours are selected from $n = 7 \times 100 = 700$ intervals. The k nearest neighbours of D_t are selected using the weighted Euclidean distance. For two d-dimensional vectors D_t and D_u, this distance is defined by

$$\delta \left(D_t, D_u \right) = \left(\sum_{j=1}^{d} w_j \left(v_{tj} - v_{uj} \right)^2 \right)^{\frac{1}{2}} \tag{6.3}$$

where v_{tj} and v_{uj} are the jth components of D_t and D_u. The scaling weights w_j are determined for each of the feature vector elements as the inverse of their sample variance (i.e. the mean squared deviation with respect to the total mean).

3.   A decreasing discrete kernel is defined for resampling one of the k nearest neighbours

$$p_j = \frac{1/j}{\sum_{j=1}^{k} 1/j} \tag{6.4}$$

where p_j is the probability that the jth closest neighbour is resampled. This resampling kernel gives more weight to closer neighbours.

4.   The discrete probability function (Eq. 6.4) is used to select at random one of the k nearest neighbours. The historical successor of the sampled nearest neighbour, Q_t, is the next value to be added to the sequence. The current feature vector is updated, and step 2-4 is repeated as long as additional simulated values are needed.

The choice of the number of nearest neighbours, k, depends on the type of kernel function $\{p_j\}$ for resampling, the number n of values from which the nearest neighbours are selected, and

the dimension d of the feature vector (Buishand & Brandsma, 2001). Lall & Sharma (1996) propose to use $k = n^{1/2}$ for $1 \leq d \leq 6$ and $n \geq 100$. In our case, this yields in $k = 27$.

A draw-back of resampling is that values beyond the historical record are not found. However, for periods longer than a 10-day interval, the generated series can be more extreme (in the sense of more dry or wet) than the historical records, because of rearranging the historical 10-day intervals.

Method 4 - Statistical description of the Rhine discharge by four parameters

In Van der Klis (2003), the discharge time series are schematised by averaging the periods of low discharges, and representing all floods in a year by a single flood event. The low and moderate discharges beneath a certain threshold value are replaced by their weighted average over the year. All floods above this threshold are combined into a single flood event per year, occurring at the same time as the flood with the maximum peak. This resulted in a statistical description of the discharge in a hydrological year by four parameters: the flood height H, the flood duration D, the time of occurrence of the peak of the flood T and the magnitude of the low discharge L. The flood events are schematised with a triangular peak or a trapezoidal peak as illustrated in Figure 6.5.

(a) Trapezoidal flood events   (b) Triangular flood events
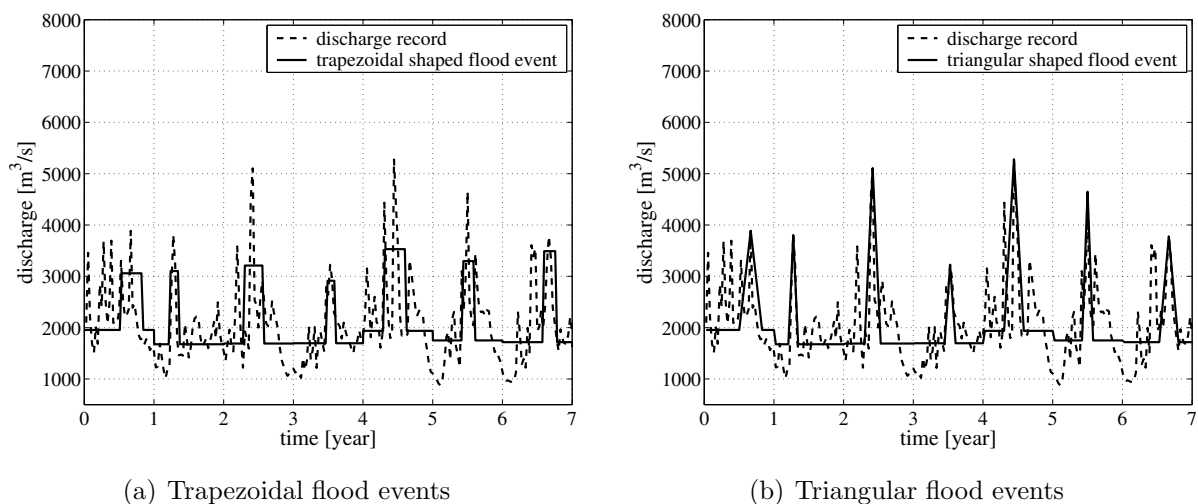
Figure 6.5: A statistical description of the Rhine discharge in a hydrological year by four parameters: flood height H, flood duration D, time of occurrence of the peak of the flood T and magnitude of the low discharge L, after Van der Klis (2003)
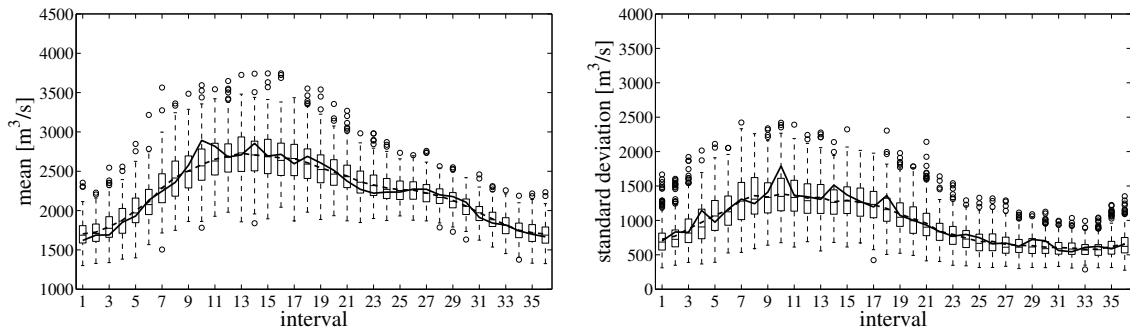
The four parameters in the statistical model are described with Gaussian probability distribution functions. By random sampling from these distribution functions, discharge time series are synthesised.
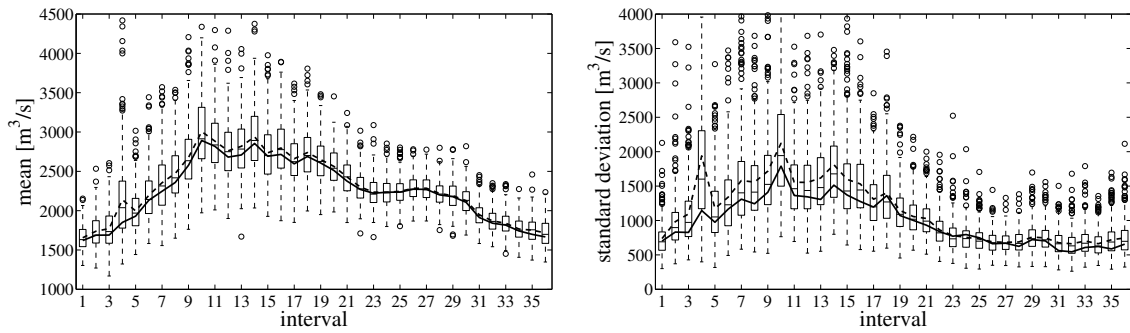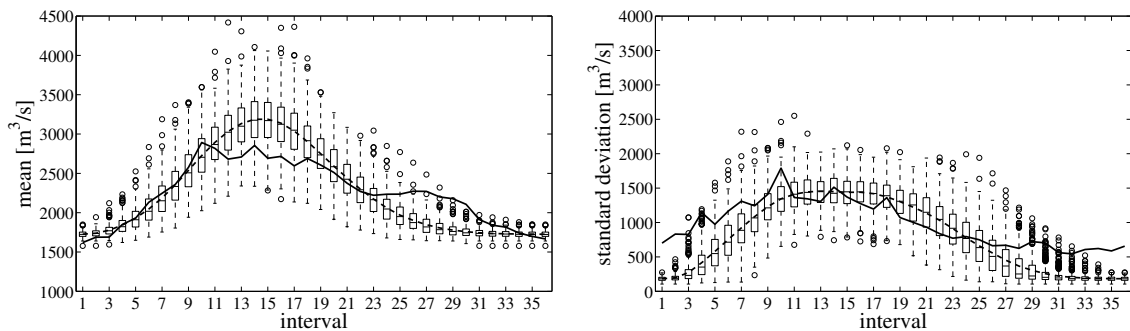
(a) Method 1 - Multivariate lognormal distribution
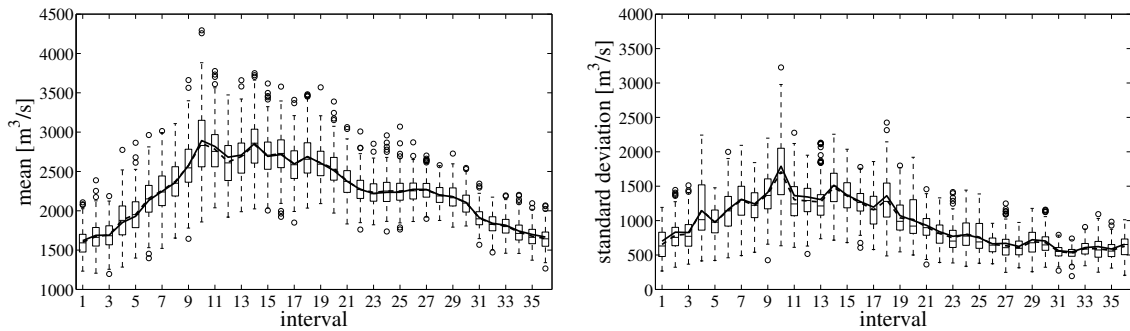
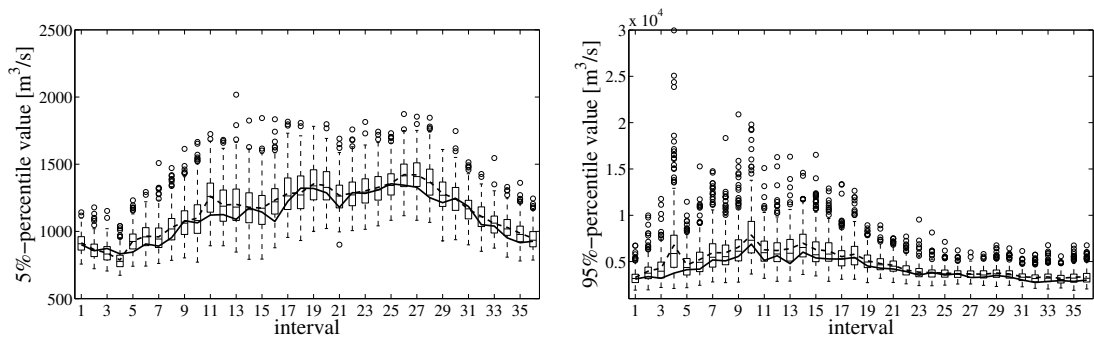(b) Method 2 - Bootstrap resampling technique

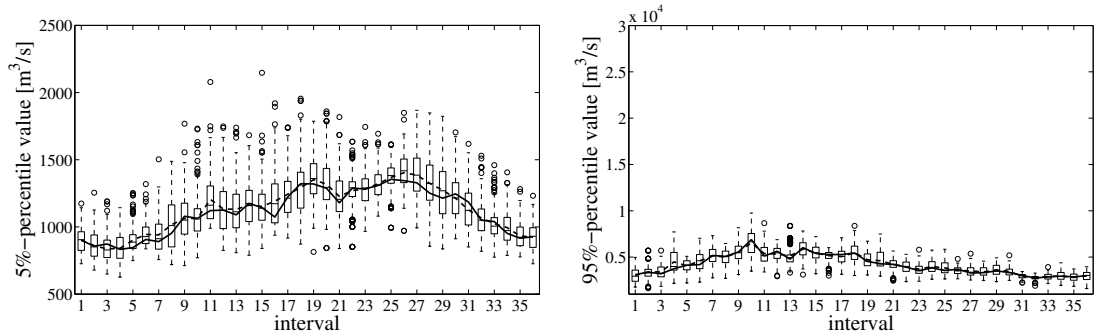(c) Method 3 - Nearest-Neighbour resampling technique

(d) Method 4 - Statistical description of the Rhine discharge by four parameters

The solid lines represent the estimates of historical data. The dashed lines show the mean values of the estimates of each methods. The box plots give an impression of the uncertainty in these estimates. Outliers are indicated by circles.
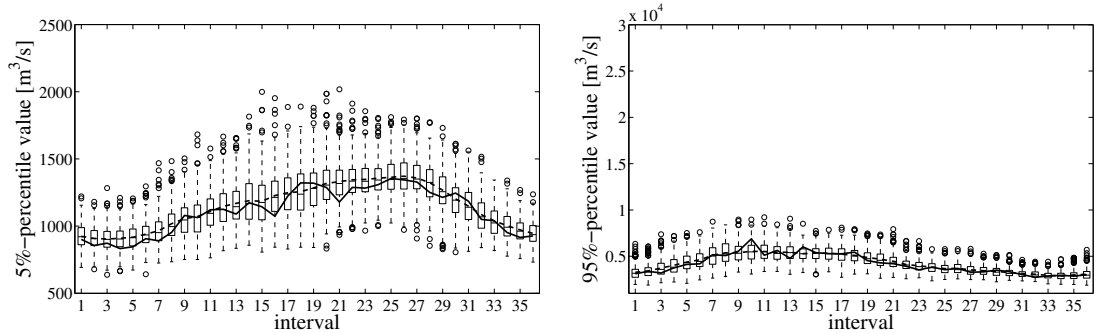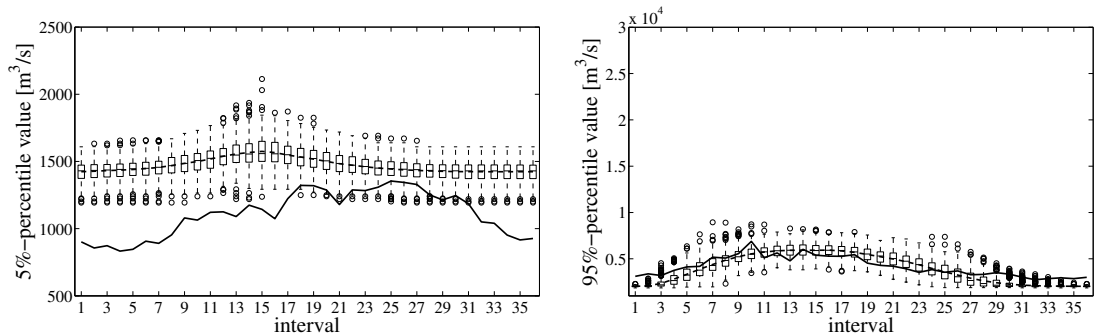
Figure 6.6: Statistics of the discharge over 36 intervals through the hydrological year for four statistical methods and historical data (left panel: mean value, right panel: standard deviation)

(a) Method 1 - Multivariate lognormal distribution

(b) Method 2 - Bootstrap resampling technique

(c) Method 3 - Nearest-Neighbour resampling technique

(d) Method 4 - Statistical description of the Rhine discharge by four parameters

The solid lines represent the estimates of historical data. The dashed lines show the mean values of the estimates of each method. The box plots give an impression of the uncertainty in these estimates. Outliers are indicated by circles.

Figure 6.7: Statistics of the discharge over 36 intervals through the hydrological year for four statistical methods and historical data (left panel: 5%-percentile value, right panel: 95%-percentile value)

With each of these four methods, 500 discharge time series have been generated. Figure 6.6 and 6.7 show the statistics of the discharge (mean value, standard deviation and 95%- and 5%-percentile values) over 36 intervals through the hydrological year for the four statistical methods and the historical data. The solid lines represent the estimates of historical data. The dashed lines show the mean values of the estimates of the four methods. The box plots give an impression of the uncertainty in these estimates. The box has lines at the lower quartile, median, and upper quartile values. The whiskers are lines extending from each end of the box to show the extent of the rest of the data. The length of the whisker equals 1.5 times the inter-quartile range. Outliers are data with values beyond the ends of the whiskers.

The major disadvantage of Method 1 - Multivariate lognormal distribution functions - is that the tails of the lognormal distribution functions do not properly fit the extreme values of the historical data record. The generation of discharge time series resulted in peak discharges that are too large in magnitude and occur too often, whereas in practice the Rhine discharge in the Netherlands is physically bounded. Method 4 that describes the hydrological year by four parameters does worse for the low and moderate discharges, but performs reasonably well for the flood events.

The statistics of discharge time series generated by resampling (Method 2 and Method 3) perfectly match the historical data. By definition, however, extreme discharges that have not occurred in the past 100 years are not included in the synthesised series. A draw-back of Bootstrap resampling in comparison with Nearest-Neighbour resampling, is that the dependence structure is only preserved if we randomly select periods of one year.

Method 5 - Bootstrap resampling in combination with a flood event predictor

To allow the synthesis of discharge peaks outside the range of historical observations, we use Bootstrap resampling in combination with a flood event predictor. The flood event predictor allows the generation of peaks outside the range of historical observations. The resulting statistics of the discharge over 36 intervals through the hydrological year are shown in Figure 6.8. The consecutive steps are followed in this method:

1. A one-year discharge time series is randomly selected from the 100-year historical record with the help of Bootstrap resampling.
2. Subsequently, a discharge peak Q_H is at random selected from a Weibull probability distribution function that statistically describes the yearly discharge peak. The Weibull function and its parameters are derived from the historical data, and reads:
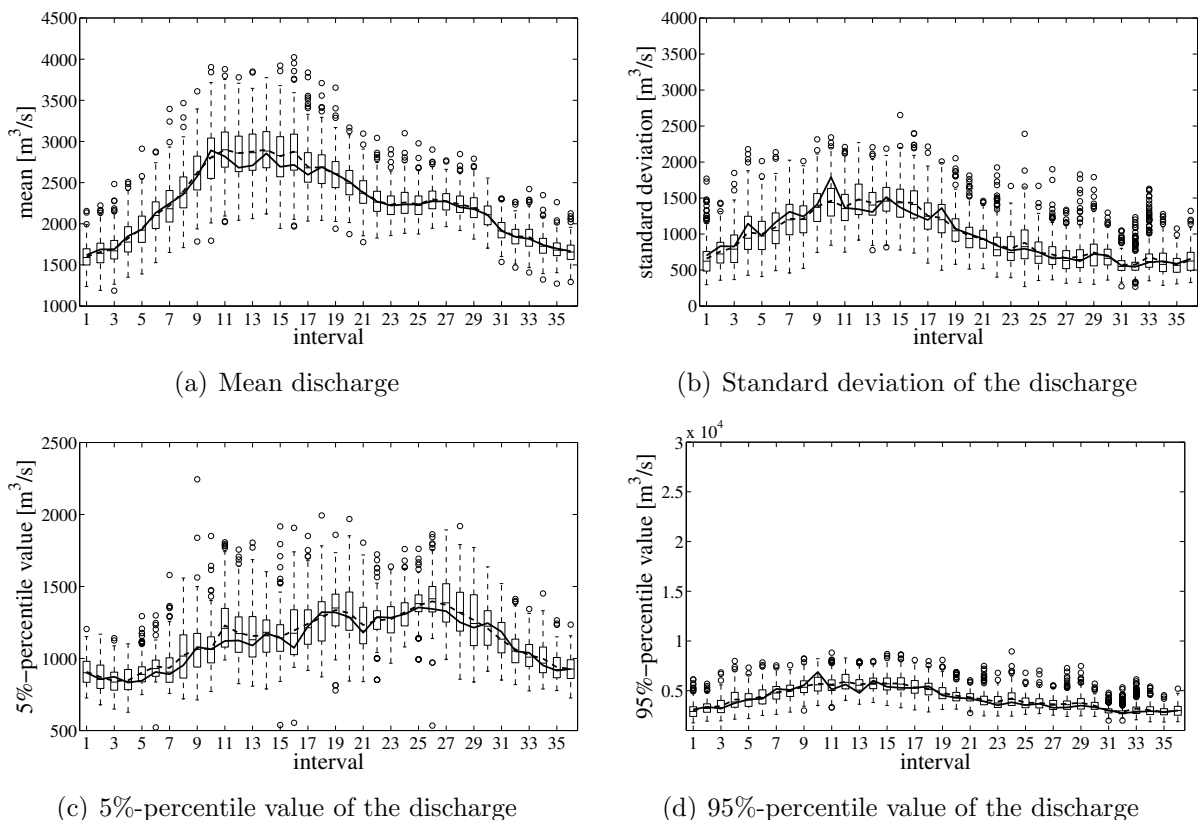
$$f(Q_H) = a \cdot b \cdot Q_H^{b-1} \cdot e^{-a \cdot Q_H^b} \tag{6.5}$$

in which the scale and shape parameters a and b are $8.5 \cdot 10^{-14}$ and 3.5, respectively. Next, the corresponding flood wave with discharge peak Q_H is constructed. To that end,

use is made of a standard wave shape, obtained by amplifying historical flood waves until they reach a standard peak value and taking the mean of all these normalised shapes, as shown in Figure 6.9. The variation in this average shape is not considered.

3.   The highest flood event in the selected one-year discharge time series using the Bootstrap resampling technique is replaced by the synthesised yearly flood event with the sampled discharge peak

4.   Finally, steps 1 - 3 are repeated and the synthesised one-year discharge time series are connected to form new discharge hydrographs.

The statistics of the low and moderate discharge in Figure 6.8 coincide with the lines of the historical data. The synthesis of discharge peaks outside the range of historical observations is a clear advantage of this method compared with the Bootstrap resampling method. Bootstrap resampling in combination with a flood event predictor is used in the section below to estimate the uncertainty in morphology induced by discharge uncertainty.

(a) Mean discharge

(b) Standard deviation of the discharge

(c) 5%-percentile value of the discharge

(d) 95%-percentile value of the discharge

The solid lines represent the estimates of historical data. The dashed lines show the mean values of the estimates of the method. The box plots give an impression of the uncertainty in these estimates. Outliers are data with values beyond the ends of the whiskers and are indicated by circles.

Figure 6.8: Statistics of the discharge over 36 intervals through the hydrological year for Bootstrap resampling in combination with a flood event predictor and historical data
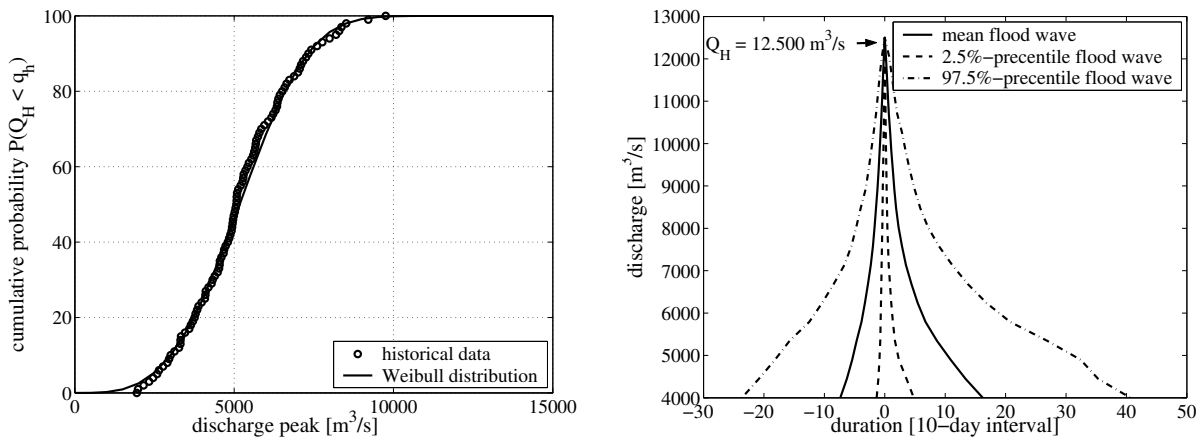
(a) Weibull distribution function that statistically describes the yearly discharge peak

(b) Statistics of the standard wave shape, obtained by amplifying historical flood waves until they reach a standard peak value of $Q_\mathrm{H} = 12.500 \ \mathrm{m^3/s}$

Figure 6.9: A statistical description of the yearly flood event

6.4.2   Stochastic morphological response to uncertainty

Spatial variation of morphological response statistics

The stochastic nature of the morphological evolution in the main channel of the Waal is analysed on the basis of 500 model runs, each covering a period of 20 years. Each run is driven by one of the discharge time series synthesised with Bootstrap resampling in combination with the flood event predictor. It results in a computed bed topography after 20 years for each model run, reflecting one possible future state. The lines in Figure 6.10 represent the morphological response of two model runs after a period of 20 years.
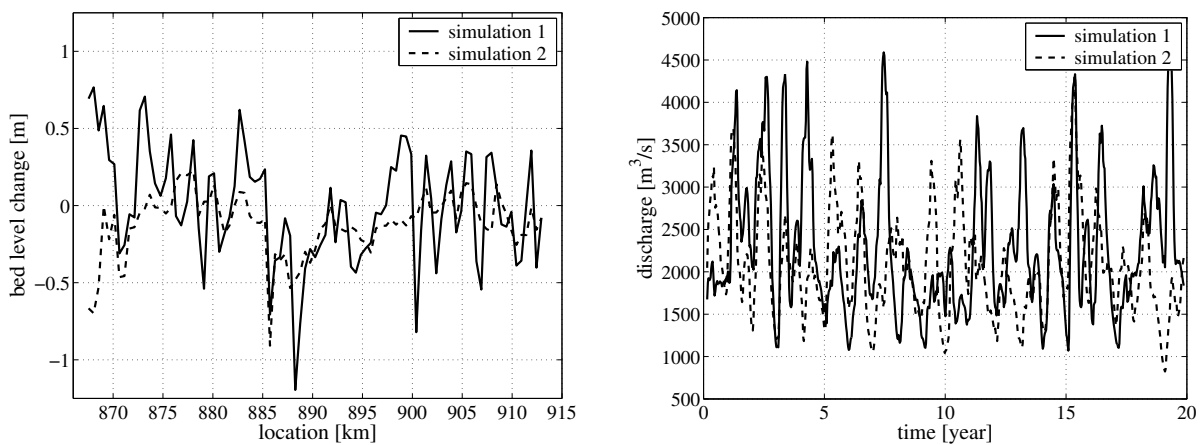
(a) Morphological response

(b) Discharge time series

Figure 6.10: The cross-sectionally averaged bed level response in the Waal after 20 years in the high-water season for two runs and the moving-average discharge over a time-window of 3 months

The moving-average discharge over a time-window of 3 months of the two model runs is shown in the same figure. It becomes clear that the morphological state at any particular moment in time depends on the short-term history of the discharge time series. Simulation 1, for instance, ends with relatively high discharges in the last three years, resulting in bed level variations. Hence it makes a difference whether the 20-year time series ends in the high-water season or in the dry season.

In the last century large-scale tilting of the river Waal is observed. Large-scale erosion is found in the upstream part of the Waal. Near Tiel there is a hinge point, downstream of which long-term sedimentation occurs. Long-term Rhine model computations show a continuation of this large-scale tilting. Figure 6.11 shows a prediction of general scour in the upstream part of the Waal after a period of 20 years.
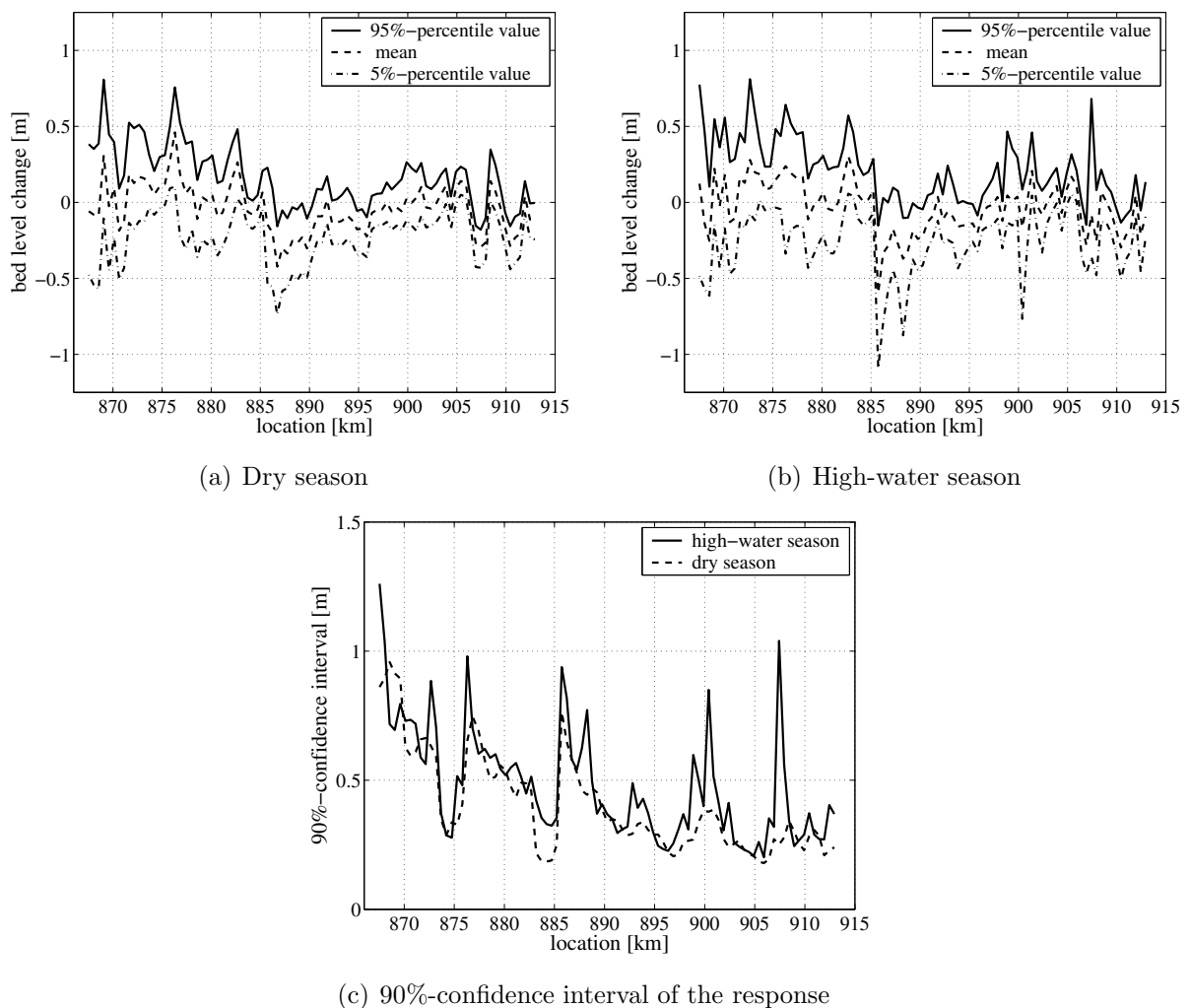

(a) Dry season

(b) High-water season

(c) 90%-confidence interval of the response

Figure 6.11: Spatial variation of the statistical properties of the cross-sectionally averaged bed level response in the Waal after 20 years, as computed with the 1-D Rhine model

On top of that, the lower panel of the figure illustrates that the varying discharge, in combination

with non-uniformities in the river geometry (width variation and man-made structures) leads to a specific morphological response. Each non-uniformity in the river geometry acts as a generator of new bottom waves, each of which travels downstream. Given the uncertainty in the discharge hydrograph, this may lead to large uncertainties in the morphological prediction.

At locations with strong geometrical non-uniformities, a peak in the confidence interval of the bed level is observed (see Figure 6.11(c)). This phenomenon is more pronounced in the high-water season than in the dry season. This is clearly illustrated in Figure 6.12, which shows the cumulative probability distribution functions for two different locations, one near a place where the floodplain geometry strongly varies (km 907.4) and one in a more or less prismatic channel reach (km 895.3).
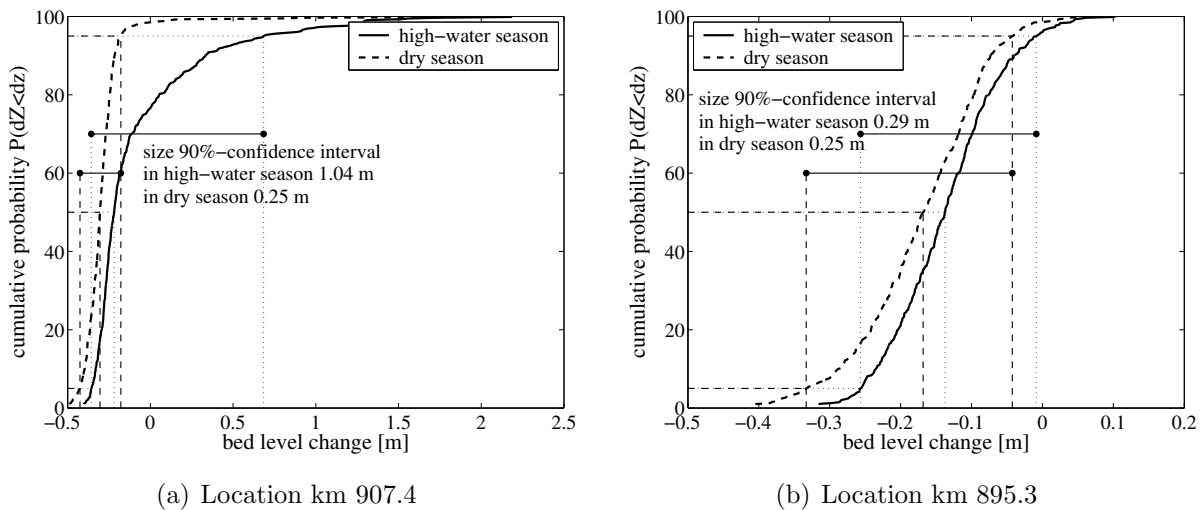

(a) Location km 907.4   (b) Location km 895.3

Figure 6.12: Cumulative probability distribution of the cross-sectionally averaged bed level response at two river locations after 20 years in the dry and high-water season, as computed with the 1-D Rhine model

Examples of locations where changes in river geometry cause a wide range of bed level changes are:

- The bottom protection structures at Erlecom (km 873-876) and at Nijmegen (km 882-885). These structures, designed for navigation purposes, prevent the riverbed from scouring. In the model the structures are schematised as fixed layers imposing a lower bound on the bed level. At both locations the morphological response after 20 years shows a threshold in the overall eroding riverbed and a dip in the confidence interval. The fixed layers prevent further erosion, but they lead to extra scour and bed level variability immediately downstream.

- Locations with a large variation in the floodplain width: Hiensche Waarden and Afferdensche Waarden (km 898-901), Ochtense Buitenpolder (km 902-906) and Willemspolder and Drutense Waard (km 906-913). At these locations an increase in the size of the

confidence interval is noticed. For example, there is a large open water area between km 906 and km 908 in the floodplain 'Willemspolder', followed by a sudden width-reduction just beyond km 908 (Figure 4.3(c)). An increase in flood-conveying width results in sedimentation; a decrease leads to erosion in the main channel. At the transition points this results in an increase in bed level variability, hence a larger size of the confidence interval.

• The Pannerdensche Kop bifurcation (km 867). The actual discharge distribution and the sediment distribution at this point depend on the local morphological situation, which is strongly variable (as indicated by the large confidence interval).

Temporal variation of morphological response statistics

The results described above concern the spatial morphological response statistics after a period of 20 years, ending in the high-water season and the dry season, respectively. The temporal variation of the response statistics is analysed for two locations (see Figure 6.13): one in a river section with a large change in river geometry (km 907.4) and another in a more or less prismatic river section (km 895.3).
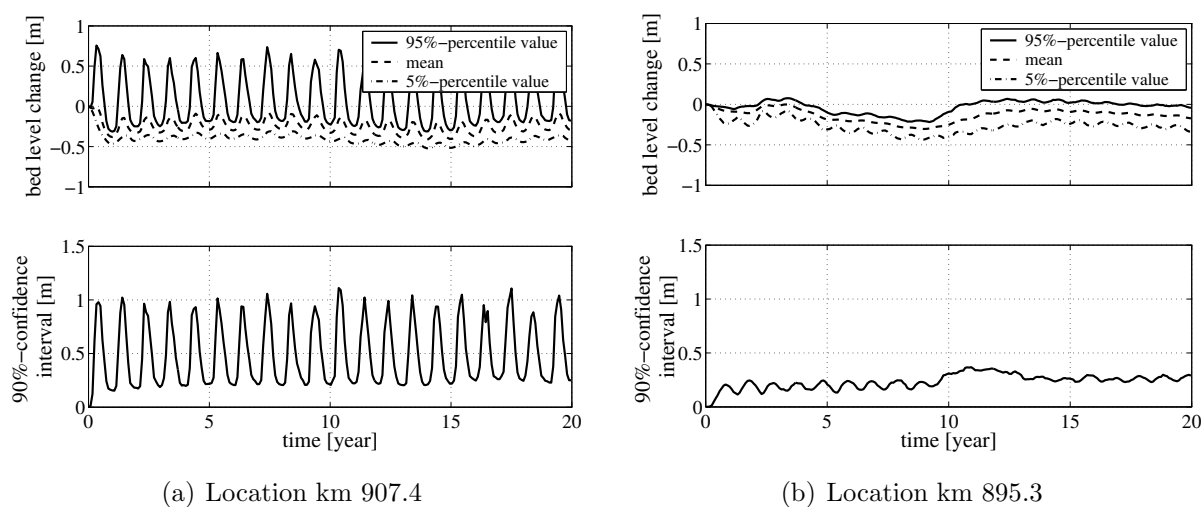

(a) Location km 907.4   (b) Location km 895.3

Figure 6.13: Temporal variation of the statistical properties of the cross-sectionally averaged bed level response at two locations in the Waal, as computed with the 1-D Rhine model

In the section with the large change in river geometry (the transition from a narrow to a wide cross section), the seasonal variation in the morphological response statistics is considerable (Figure 6.13(a)). It reflects the seasonal variation in river discharge. The seasonal fluctuation of the standard deviation is significant, with the largest values found in the high-water season and the smallest ones in the dry season. The 95%-percentile strongly oscillates, and the 5%-percentile much less so. This can be explained by the fact that at discharges above bankfull bottom waves (sedimentation) are initiated in the main channel. These bottom waves migrate

downstream and (partly) decay during discharges below bankfull, when the flow stays within the main channel. Therefore, the seasonal variation in the 5%-percentile is limited.

At km 895 the seasonal signature is much less pronounced (Figure 6.13(b)). The uncertainty in the bed level change at this location is affected by the bottom waves initiated at other locations in the river, which propagate downstream and at a certain moment pass by this location.

The largest uncertainty in bed level variability in the study area occurs in the high-water season in the Willempolder (km 907.4): the size of the confidence interval is approximately 1.5 m. The smallest uncertainty is predicted for the Waal bend at Nijmegen (km 884) in the low water season. The size of the confidence interval is less than 0.15 m, due to the bed protection applied there.

6.4.3   Comparison of the discharge synthesisation methods

The capability of different discharge synthesisation methods to reproduce the historical discharge statistics was discussed in Section 6.4.1. Here, we rather focus on the comparison of the discharge synthesisation methods by their morphological impacts. Figure 6.14(a) shows the spatial variation of the response statistics - mean response and the 95%- and 5%-percentile values - for the different methods. The 90% confidence interval for the discharge synthesisation methods is presented in Figure 6.14(b). Figure 6.15(a) gives the change of the confidence interval (in percentage terms) as compared with Bootstrap resampling.

The response statistics of the multivariate lognormal distribution show a slight increase in the confidence interval in comparison with Bootstrap resampling. From figure 6.14 it appears that the tail of the multivariate lognormal distribution does not fit the extreme values of the historical discharge record very well. Discharge peaks far beyond the physical limit of the Rhine system can easily occur. Therefore, we truncated discharge peaks at the design discharge of 15.000 m^3/s[1]. The point at which the discharges are truncated appears to affect the morphological response statistics. The confidence interval increases as a function of the truncation level. Figure 6.15(b) illustrates that the confidence interval is larger for the simulation with the discharge truncated at the design discharge than the one truncated at a lower level, namely the maximum discharge in the historical record. It should be noticed that the number of model simulations that get unstable increases substantially with the truncation level.

The morphological response statistics from the MCS with time series generated by Nearest-Neighbour resampling do not significantly differ from those obtained from MCS with standard Bootstrapping. For the inclusion of seasonal dependency and correlation between discharges in successive periods, standard Bootstrapping implies a random selection of one-year records that

---

1.   the discharge on which the design of the Dutch Rhine flood defence used to based until 2001. In 2001, the design discharge has been raised from 15.000 to 16.000 m^3/s

(a) Statistical properties   (b) 90%-confidence interval
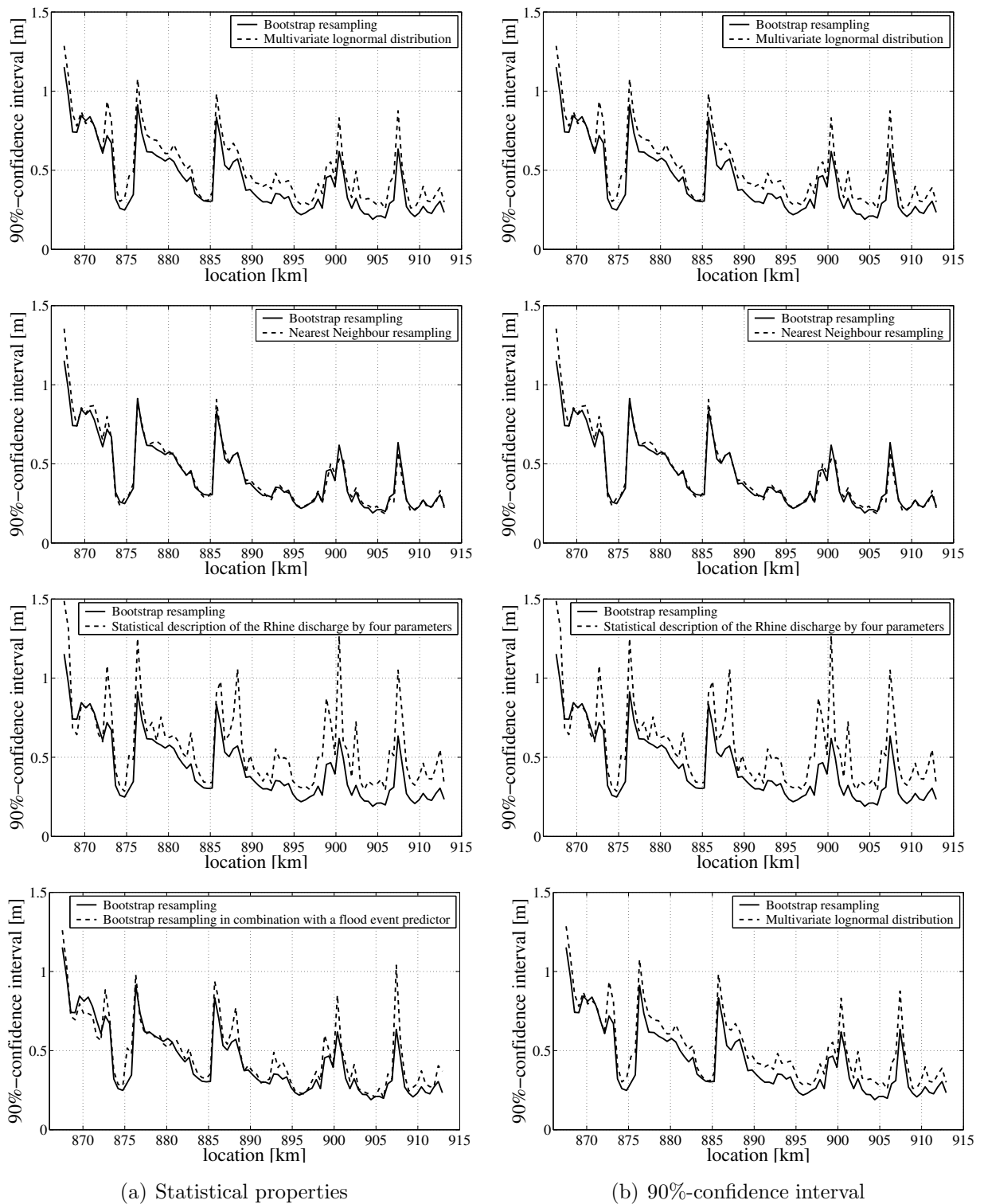
Figure 6.14: Spatial variation of the statistical properties of the cross-sectionally averaged bed level response in the Waal after 20 years in the high-water season, as computed with the 1-D Rhine model for the different discharge synthesisation methods
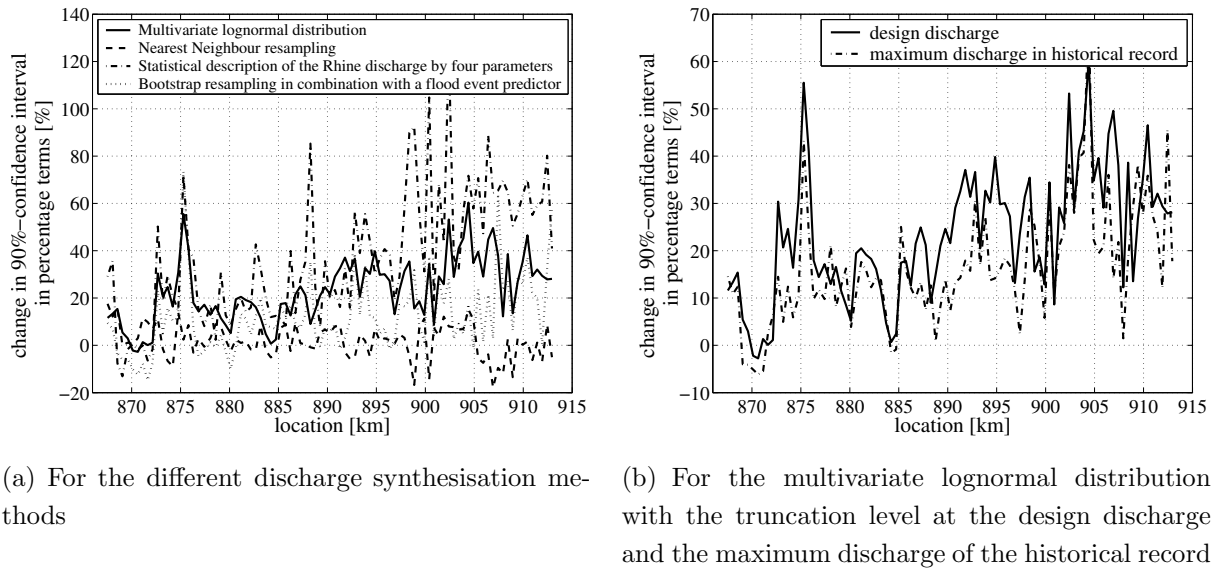
(a) For the different discharge synthesisation me-
thods

(b) For the multivariate lognormal distribution
with the truncation level at the design discharge
and the maximum discharge of the historical record

Figure 6.15: Change in the 90%-confidence interval of the cross-sectionally averaged bed level res-
ponse, in percentage terms, after a period of 20 years in the high-water season, for different MCS, as
compared with Bootstrap resampling

were subsequently arranged to construct new time series. Nearest-Neighbour resampling is a
strategy that preserves the dependence structure of the historical record, while bootstrapping
from historical 10-day interval records. Thus, the impact of reordering historical 10-day intervals
within a hydrological year turns out to be only marginal.

The statistical description of the Rhine discharge by four parameters suggested by (Van der Klis,
2003), performs not too well. This can be explained by the fact that the discharge time series
are too strongly schematised. The low and moderate discharges beneath a certain threshold
value are replaced by their weighted average over the hydrological year. Fluctuations in low
and moderate discharges appear to be important for morphological predictions. All floods above
this threshold are combined into a single flood event per year, occurring at the same time as
the flood with the maximum peak. In reality, floods may occur at different moments in time,
and they may occur more than once a year. The simplification of combining all flood events in
one flood per year, results in a wrong description of the sediment transport variation through
the year. The succession of discharge peaks through the year turns out to have an important
effect on the morphological response. This is especially the case in a river like the Rhine, which
contains non-uniformities in river geometry that act as generators of bottom waves when the
discharges exceeds bankfull.

Bootstrap resampling in combination with a flood event predictor is used to ensure the synthesis
of peak discharges outside the historical range. On average, the inclusion of discharge peaks
outside the range of historical observations hardly affects the morphological response in this
particular river. There is only a small increase in the confidence interval, indicating a slightly

larger possible variation of this response.

It becomes clear from the above that resampling is a robust, adequate and efficient technique to model the natural randomness of discharge time series when considering river morphology. It requires less computational effort to construct time series than the other methods. By definition, however, values beyond the historical record are not found in the new generated series. To allow the synthesis of discharge peaks outside the range of historical observations, we decided to use a resampling technique in combination with a flood event predictor. The flood event predictor allows the generation of peaks outside the range of historical observations. Resampling in combination with a flood event predictor probably better represents the discharge statistics, but resampling as such only slightly underestimates the possible variation of the morphological response. The multivariate lognormal distribution function and the statistical description of the Rhine discharge by four parameters turn out to be less suitable for the present purpose. Preference is given to the use of resampling techniques. There is not much difference between the resampling techniques investigated, viz. standard bootstrapping and Nearest-Neighbour resampling.

6.5 Uncertainty in grain size of the bed material

6.5.1 Statistical description of uncertainty

Uncertainty involved in the specification of D_{50} and D_{90} is inherent to the complexity of the morphodynamic river system, comprising the strong spatial and temporal variation of the bed material. A drawback to this is the ambiguity of sediment measurements, since each measurement is affected by the river's conditions at the moment of measuring and those prior to measuring (e.g. discharge level). Moreover, uncertainty is introduced due to the sampling - instruments, location, timing, sample size - and the sieving analysis.

In literature, the uncertainty in sediment particle size is often described by a uniform distribution function (Johnson & Ayyub, 1992, Yeh & Tung, 1993 and Chang et al., 1993). A uniform distribution provides one of the simplest means of representing uncertainty in model input (Morgan & Henrion, 1990). Its use is appropriate when we are able and willing to identify the range of possible values, but unable to decide which values within this range are more likely to occur than others. The statistical parameters of the uniform distribution may be estimated from measurements or can be determined using physical or subjective reasoning to determine the minimum and the maximum possible values of the random variable.

The grain size statistics of the bed material is described here with a uniform distribution function. Figure 6.16(a) shows the upper and lower bounds of this distribution function for D_{50}, as derived from four measuring campaigns.
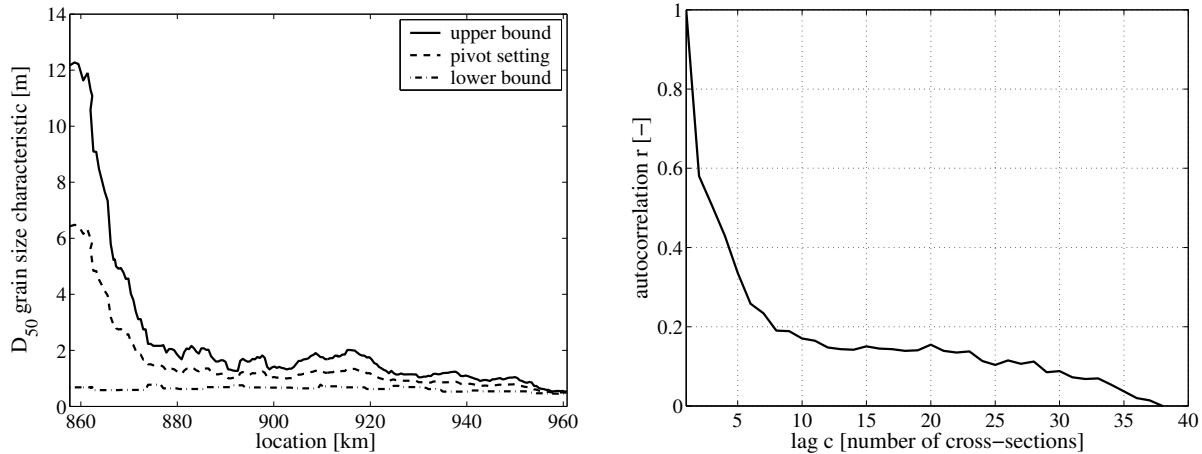
(a) Uniform distribution function of the D_{50} grain size characteristic

(b) Autocorrelation function containing serial-correlation functions for different lags

Figure 6.16: Sensitivity of the response statistics to (1) the size of the model units, (2) the correlation coefficient, and (3) the coefficient of variation

The significant downstream fining of the bed material is clearly illustrated by the input statistics of the bed material. Apart from the longitudinal sorting effect, the smoothness of the grain size series is important. To account for this, we consider the mutual correlation of grain sizes in adjacent cross-sections. The serial-correlation coefficient provides information about the mutual dependency of the grain size at adjacent river locations. The autocorrelation function in Figure 6.16(b) containing the serial-correlation coefficients for different lags shows to what extent the grain size characteristic in a certain cross-section depends on the characteristics in preceding cross-sections. The figure shows a strong correlation between the D_{50} in adjacent cross-sections (r at lag 1 is 0.6, $r^2 = 0.36$, so approximately 36% of the grain size depends on the grain size in the preceding location). The serial-correlation coefficient decreases rapidly for lags larger than 1. The serial-correlation at lag 1 is incorporated in the sampling procedure, via the use of a bivariate uniform distribution function. Sampling from this bivariate function is not straightforward, and is, therefore, illustrated in Figure 6.17. The procedure for the statistical description of uncertainty in D_{50} is repeated for D_{90}.

In Johnson & Ayyub (1992), Yeh & Tung (1993) and Chang et al. (1993), the uncertainty in the grain size of the bed material is described with uniform distribution functions with coefficients of variation 0.05, 0.02 and 0.08, respectively. Figure 6.18 gives the coefficients of variation as a function of location along the Waal that are deduced from the statistical description of the D_{50} of the bed material. It can be noticed that on average the values are slightly larger than those in the above-mentioned literature. This tend to increase the estimated confidence interval.
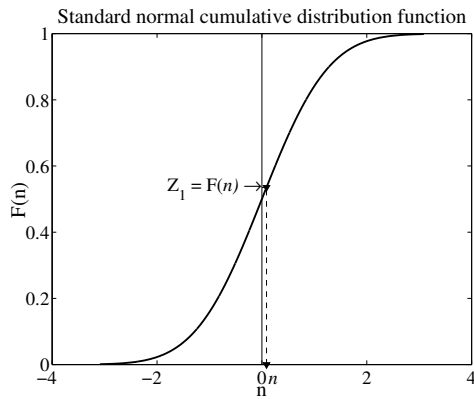
(a) A number Z_1 is drawn from the standard uniform distribution and is transformed into a number n of the standard normal distribution
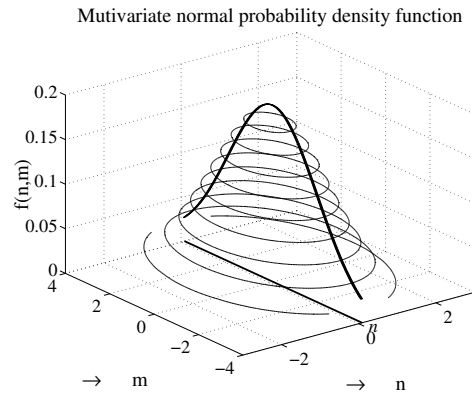
(b) Given autocorrelation $\rho(1)$, the bivariate normal distribution is derived, from which the conditional normal distribution is deduced, given n
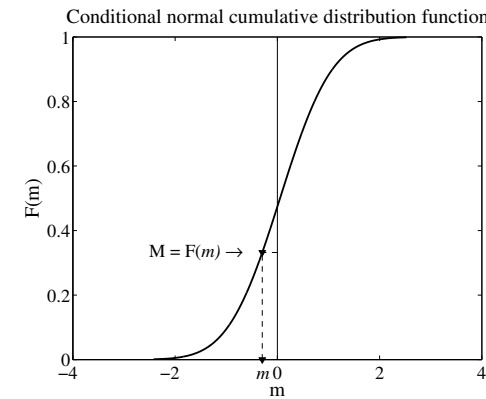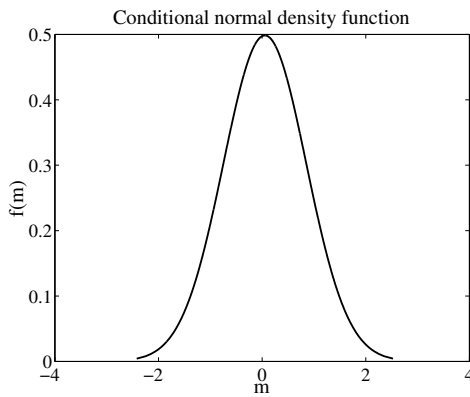
(c) Subsequently, a number M is randomly drawn from the standard uniform distribution and is transformed into a number m of the conditional normal distribution
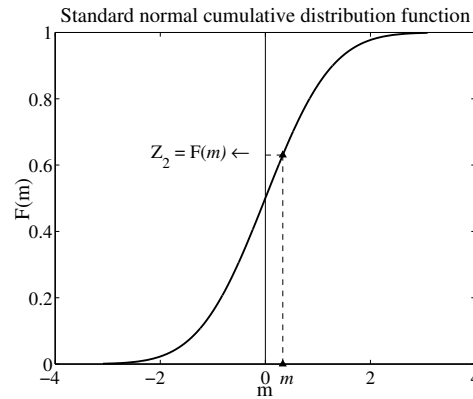
(d) This number m is transformed into a number Z_2 of the conditional standard uniform distribution

Step a-d is repeated N-times in order to sample for each cross-section i a number Z_i of the conditional standard uniform distribution. The numbers Z_i are transformed into a D_{50_i} grain size characteristic using the following equation $D_{50_i} = Z_i(b_i - a_i) + a_i$, in which a_i and b_i represent the lower and upper bound of the uniform distribution.

Figure 6.17: Procedure to randomly generate samples of D_{50} bed characteristics from a bivariate uniform distribution function
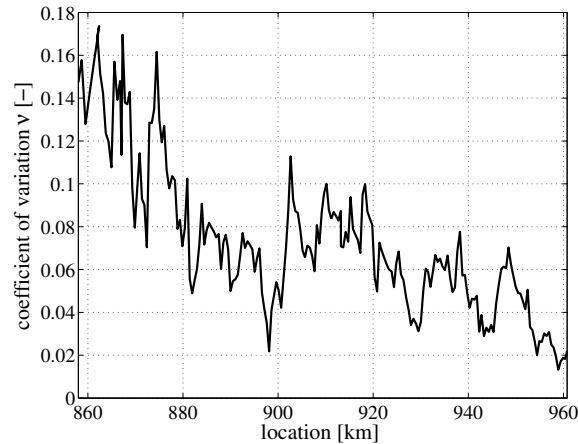
Figure 6.18: Coefficients of variation along the river Waal for the D_{50} grain size characteristic, as computed with the 1-D Rhine model

6.5.2   Stochastic morphological response to uncertainty

A decrease (increase) of the grain size results in a reduction (increase) of the expected long-term erosion in the Waal section between km 867 and km 915, leading to a steeper (flatter) bottom slope. As illustrated by Figure 6.16(a), a significant downstream fining of the bed material is found. As a consequence, the bed level confidence interval resulting from the uncertainty in grain size also decreases in the downstream direction, as is shown by the response statistics of the grain size characteristic D_{50} in Figure 6.19(a). The morphological response statistics appear not to exhibit the seasonal variation as observed from the MCS with the randomly varied river discharge.

In case only the uncertainty in the grain size characteristic D_{50} in the Waal is considered (so we ignore the uncertainty in the grain size in the Niederrhein), the confidence interval decreases significantly (Figure 6.19(a)). This is attributed to the fact that the amount of sediment that flows into the Waal depends very much on the coarseness of the bed material upstream. In the Niederrhein processes such as vertical grain sorting and bed armouring, with coarser particles covering the finer ones, are significant, which result in a large uncertainty in the D_{50} of the bed material. The sediment inflow in the Waal exhibits large fluctuations and thus affect the morphological response statistics in the Waal.

Figure 6.19(b) shows that the uncertainty induced by the uncertain D_{90} is much smaller than that resulting from the uncertain D_{50}. When considering the uncertainties in D_{50} and D_{90} simultaneously, the confidence interval hardly increases with respect to that resulting from the MCS with uncertain D_{50} only. Apparently, the contribution to the variance does not add up accordingly to the rules of linear error propagation.
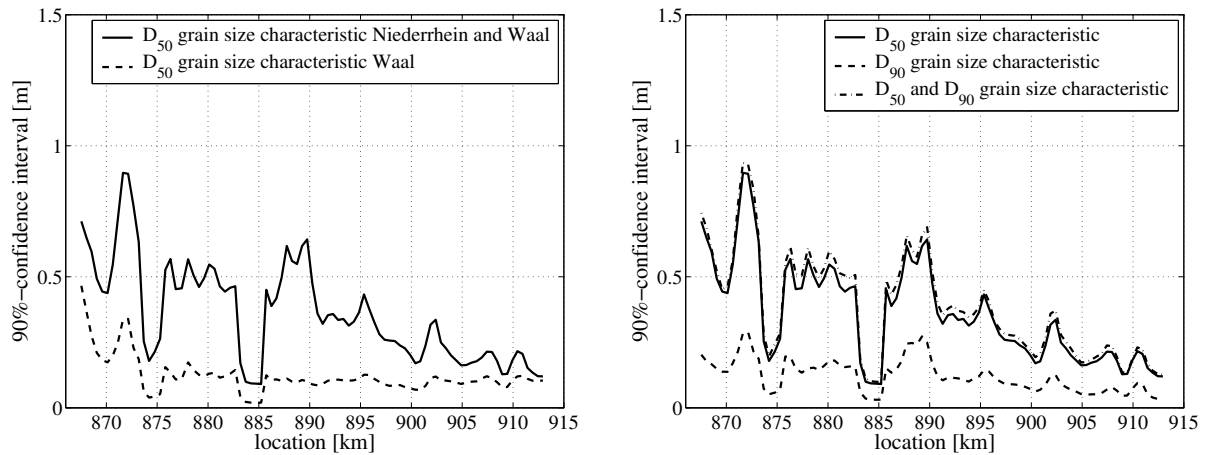
(a) 90%-confidence interval for the MCS with the uncertainty in D_{50} in the Niederrhein and Waal, and in the Waal only

(b) 90%-confidence interval for the MCS with the uncertainty in D_{50} and D_{90} in the Niederrhein and Waal

Figure 6.19: 90%-confidence interval of the cross-sectionally averaged bed level response in the Waal after 20 years in the high-water season, as computed with the 1-D Rhine model - uncertainty source: grain size of the bed material

6.6   Model calibration and uncertainty

6.6.1   Model calibration

Successful application of a physically based model, like the 1-D Rhine model, depends much on how well the model is calibrated. Model calibration is known as the process whereby free parameter values are selected, such that the model optimally reproduces the behaviour of the actual physical system. To calibrate the unknown values of the model parameters, we want to find those values that minimise the error between the model prediction and the observations (Werner, 2004). This error arises from the existence of model errors, i.e. the difference between the model structure and the physical system being modelled, and uncertainty in the available calibration data set (Aronica et al., 1998). Not only the model and data error (quality of data) is important, the success of the calibration process also depends on the quantity of calibration data.

Parameter calibration can either be done manually, or automatic calibration procedures can be used. In the traditional approach an appropriate objective function (a measure of the match between the model output and the observations) is chosen to find the model parameter set that optimises this objective function (Sorooshian et al., 1993). The optimal parameter set appears to be sensitive to factors such as data error, model error, quantity and quality of calibration data and the chosen objective function.

In highly non-linear models, however, there may be many different parameter sets that fit the calibration data equally well, i.e. that have the same or very similar values of the objective

function. Moreover, different calibration data sets can give a different performance for the same parameter sets. In this case, the concept that, for a given model structure, an optimal parameter set exists loses credibility. There is rather an equifinality of parameter sets, where different different parameter sets exhibit equal or near-equal performance to the optimal parameter set (Beven, 1993). With the non-uniqueness of the optimal parameter set, uncertainty inherent to the calibration process is introduced. The inability to place a reasonable degree of confidence on the estimated calibration parameter values leaves considerable uncertainty in the model forecasts (Aronica et al., 1998).

The 1-D Rhine model is calibrated on the basis of hydraulic and bathymetric data in the period 1987-1997. Among the tuning parameters in the calibration process are some of the parameters to which morphology appears to be most sensitive, namely:

- the hydraulic roughness of the main channel;
- the parameters in the sediment transport formula.

Taking notice of the above uncertainty in the morphological response due to the uncertainty in the hydraulic roughness of the main channel and the parameters in the sediment transport formula is considered below.

6.6.2   Hydraulic roughness as uncertainty source

Calibration and shortcomings in definition

The hydraulic roughness parameters are used as tuning parameters in the hydraulic calibration process of the model. The hydraulic roughness of the floodplain appears to be of minor importance to morphology and is therefore not considered herein. We mainly focus on the hydraulic roughness of the main channel.

Model units have been defined for the main channel, for which Chézy coefficients are estimated as a function of the river discharge, using the roughness predictor of Vanoni & Hwang (1967). In the calibration process, the parameters D_{90}, L and H_d in this roughness predictor (see Eq. 4.13-4.15) are changed within physically realistic bounds, until the differences between water level predictions and observations have sufficiently converged. The model units cover the distance between successive gauging stations. To account for a local increase of the hydraulic roughness at locations with bottom protection structures, some model units are added. Nonetheless, the subdivision of the model units has no real physical background, but relies on the positioning of the gauging stations. Just for the Waal branch, the calibration boils down to approximately 370 tuning parameters (16 model units times 23 discharge stages).

Considering the previous section, the resulting optimal roughness parameter set shows a degree of non-uniqueness. Different parameter sets might produce equally acceptable model results. This phenomenon is referred to as equifinality (Beven, 1993). From a mathematical point of

view, one can say that the originally designated roughness values computed via the Vanoni-Hwang roughness predictor are multiplied with an uncertain model factor, $m(x,t)$.

On the one hand, the calibration process makes the model produce the desired results, which may reduce the output uncertainty. On the other hand, the calibration may attempt to reduce discrepancies due to other sources via the roughness coefficients, which leads to additional uncertainty and loss of predictive skill (over-calibration). This involves a risk especially if the model is extrapolated to events that are more extreme than the ones observed so far.

Besides parameter uncertainty introduced during the calibration, shortcomings in the roughness predictor and the implementation of roughness values in the model result in model uncertainties.

The hydraulic roughness values are implemented in the model in such a way, that for a certain discharge level, the hydraulic roughness in a particular model unit is always the same. In reality, however, the magnitude of the roughness coefficient depends also on the recent discharge history, since every river bed state, including bedforms (ripples, dunes), is the result of an evolution process.

Part of the hydraulic roughness is related to the size and shape of the bedforms. The effect of the superposition of bedforms of different size, on the hydraulic roughness is left out of consideration in the roughness predictor. Through this effect the hydraulic roughness is underestimated (Wilbers, 2004).

Another aspect that is recognised as being incorrect is the way the contribution of the grain roughness to the total roughness is modelled. It is assumed that this contribution is the same for the situation with and without bedforms, while in fact it depends on the region of flow separation and the bedforms, themselves (Wilbers, 2004).

Statistical description of uncertainty

Johnson (1996b) gives a review of literature published on uncertainty in the hydraulic roughness. In most of these publications the hydraulic roughness is given as a Manning coefficient, of which the uncertainty is expressed by the coefficient of variation and the type of probability distribution function. The coefficients of variation presented in Table 6.2 are estimated on the basis of measured data and expert opinions.

Duits et al. (2000) express the uncertainty in Chézy coefficients in a 1-D hydrodynamic model of the Rhine by a lognormal probability distribution and a coefficient of variation that varies between 0.05-0.15.

In this study, the coefficient of variation of the Chézy coefficient is fixed at 0.15. The mean values are equal to the pivot setting of the Chézy coefficients in the Rhine model. Using the definition of the coefficient of variation, the standard deviations can be easily estimated. The physical dependency of the hydraulic roughness on the discharge is incorporated in the

model by including a table with roughness coefficients as a function of the discharge level derived
via the Vanoni & Hwang (1967)-predictor. Another point of interest is the correlation of the
hydraulic roughness between two points along the river. This correlation decreases with the
distance between those points. The serial-correlation coefficient depends on the length of the
model units for which roughness coefficients are specified. In our case, these model units vary
in length from several kilometres up to tens of kilometres, see Figure 4.8. A serial-correlation
coefficient at lag 1 of 0.5 is taken.

coefficients of variation	distribution function type	reference
0.15	normal	Cesare (1991)
0.08	uniform	Chang et al. (1993)
0.08	triangular	Yeh & Tung (1993)
0.20-0.35	lognormal	Hydraulic Engineering Center (1986)
0.28, 0.18	uniform	Johnson (1996b)

Table 6.2: Uncertainty in hydraulic roughness (Johnson, 1996b)

The lognormal distribution appears to be a good representation for many physical quantities,
such as the hydraulic roughness. If the Manning coefficient is lognormally distributed, the Chézy
coefficient is also lognormally distributed. The conversion of the central moments to the sta-
tistical parameters of the lognormal probability function is straightforward. For the conversion
of the serial-correlation coefficient to the lognormal distribution, the following equation is used
(Shapiro & Wilcox, 1996):

$$\rho\left(C_{\mathrm{i}}, C_{\mathrm{i}+1}\right) = \frac{e^{\rho \sigma_{C_{\mathrm{i}}} \sigma_{C_{\mathrm{i}+1}}} - 1}{\sqrt{\left(e^{\sigma_{C_{\mathrm{i}}}^2} - 1\right)\left(e^{\sigma_{C_{\mathrm{i}+1}}^2} - 1\right)}} \tag{6.6}$$

Impact of uncertainty in the hydraulic roughness on morphology

The impact of uncertainty in the roughness coefficients on morphology is shown in Figure 6.20.
The results show a significant fluctuation of the spatial response statistics at the locations of the
bottom protection structures at Erlecom (km 873 - 876) and at Nijmegen (km 882 - 885). After
20 years, a bar in the river bed develops, since the bottom protection structures prevent further
erosion. A dip in the confidence interval indicates a low bed level variability at these locations.
The fixed layers lead to extra scour and bed level variability immediately downstream.
The figure illustrates that the morphological response statistics do not exhibit the seasonal
variation as observed in those resulting from the MCS with the randomly varied river discharge.

The sensitivity of the response statistics to (1) the size of the model units; (2) the correlation
coefficient; and (3) the coefficient of variation, can now be analysed.
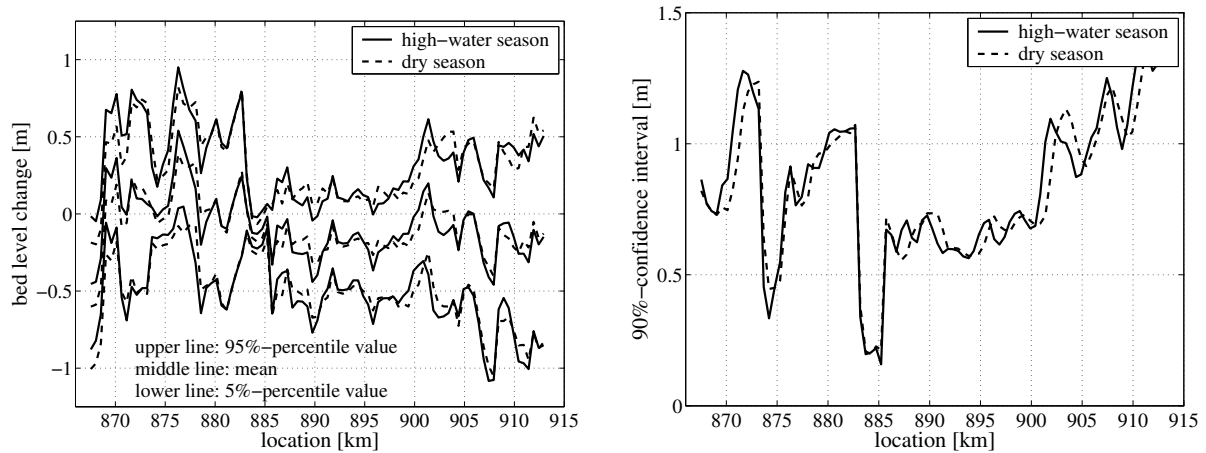
(a) Response statistics in the high-water and dry season

(b) 90%-confidence interval of the response

Figure 6.20: Spatial variation of the statistical properties of the cross-sectionally averaged bed level response in the Waal after 20 years in the high-water season, as computed with the 1-D Rhine model - uncertainty source: roughness coefficient

- Size of the model units - In the 1-D Rhine model, model units have been defined, for which the roughness coefficients are set such, that the error between water level predictions and observations, at several gauging stations in the river and under various discharge conditions, is minimised. The model units have no real physical background, but relies on the positioning of the gauging stations. To test the sensitivity to this choice, the Rhine is subdivided into model units that have a more physical background, viz. model units that exhibit more or less similar morphological behaviour. These units are relatively short, with an averaged length of 2 km.

  Figure 6.21(a) shows that the confidence interval is sensitive to the size of the model units. In the case of relatively short model units high and low roughness values will be sampled, which tends to decrease the size of the confidence interval of the morphological changes.

- Correlation coefficient - The serial-correlation coefficient depends on the length of the model units, for which roughness coefficients are specified. The correlation in roughness coefficients between two points along the river decreases with the distance between those points. Figure 6.21(a) shows that the sensitivity to the correlation coefficient, by raising the correlation coefficient to 0.8, is low, though slightly more pronounced in the case of larger morphological units. This is probably due to the fact that the relatively short model units are only mutually correlated, implying that the hydraulic roughness values between model units at a mutual distance larger than a few kilometres are considered as independent.

- Coefficient of variation - The choice of coefficient of variation appears to have a signifi-

cant effect on the size of the confidence interval. A decrease of this coefficient, meaning a decrease of the standard deviation, yields a decrease of the confidence interval, as is shown in Figure 6.21(b).
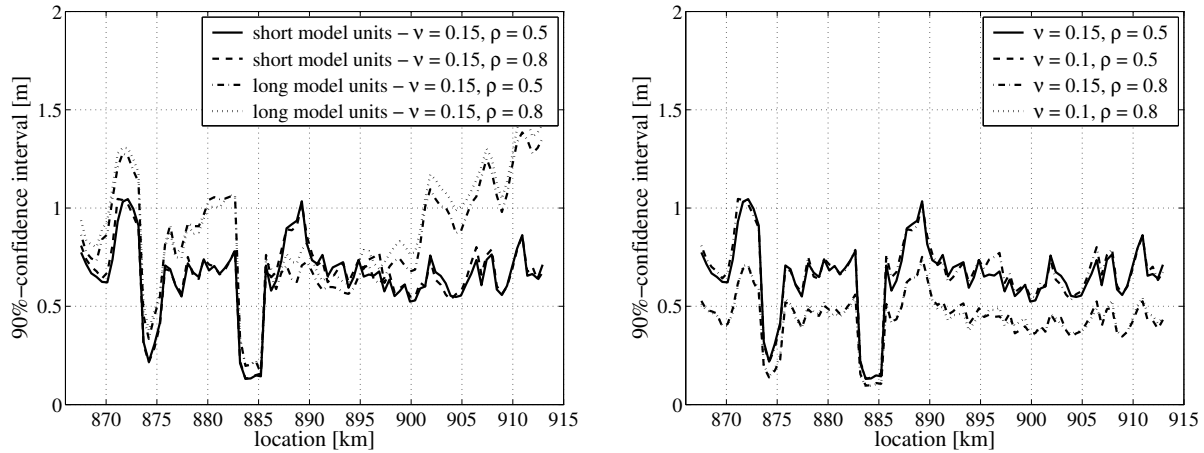
(a) Sensitivity to coefficient of variation ν and serial-correlation coefficient ρ for short model units that exhibit more or less similar morphological behaviour

(b) Sensitivity to size of model units and serial-correlation coefficient ρ

Figure 6.21: Sensitivity of the cross-sectionally averaged bed level response statistics after 20 years in the high-water season to (1) the size of the model units, (2) the correlation coefficient, and (3) the coefficient of variation, as computed with the 1-D Rhine model

6.6.3   Parameters in the sediment transport formula as uncertainty sources

From a physical point of view, the sediment transport rate is directly related to the flow intensity and the grain size of the bed material. Hence, sediment transport formulae have been derived experimentally by including the flow and sediment properties based on physical laws and available observations. Uncertainty is inherent to these formulae, since the formula itself, as well as its parameters are uncertain.

The largely empirical transport formula of Meyer-Peter & Müller (1948) is incorporated in the 1-D Rhine model. We only consider the uncertainty that is involved with the inability to accurately evaluate some model parameters, namely the critical Shields parameter θ_{cr} and the exponent of the bed shear stress α. The critical Shields parameter (tuning parameter) has been reduced during the calibration of the Rhine model from 0.047 to 0.025 (see Section 4.5.4).

Statistical description of uncertainty in critical Shields parameter, θ_{cr}

The stability of non-cohesive sediment particles on the riverbed, their initiation of motion, depends on the forces acting on it, such as the submerged weight, drag forces and lift forces

(Jansen et al., 1979). Various methods can be used to define the critical conditions for initiation of motion. The most common method is the Shields diagram, which gives the dimensionless critical shear stress as a function of the particle Reynolds number for uniform sediments. From this diagram the critical shear stress, known as critical Shields parameter, can be deduced for different flow conditions. If the shear stress exceeds the critical Shields parameter, the bed is in motion. For non-uniform sediments other methods are available (for instance, see Wiberg & Smith, 1989). Yet, many authors question the concept of critical mean flow conditions for initiation of sediment motion (Van Rijn, 1993). The stochastic nature of the driving and resisting forces makes it difficult to define a deterministic critical bed-shear stress for the initiation of motion. Therefore, the critical shear stress is best described stochastically.

Johnson (1996a) discusses the uncertainty involved in the estimation of the excess shear stress that is used to determine the sediment transport capacity and the bedforms that occur under various conditions. She applied MCS to determine the uncertainty in the excess shear stress, which is amongst others affected by the critical shear stress. The critical shear stress is statistically described by a normal distribution function with coefficient of variation 0.5. In order to avoid problems with negative values for the critical shear stress, the normal distribution is truncated at zero. As a result the area under the truncated probability density curve A* is less than one. The area remaining after truncation should be normalised, to ensure that the area A* is again one. To that end, the probability densities for the critical shear stresses are multiplied with a factor $1/(1 - A^*)$.
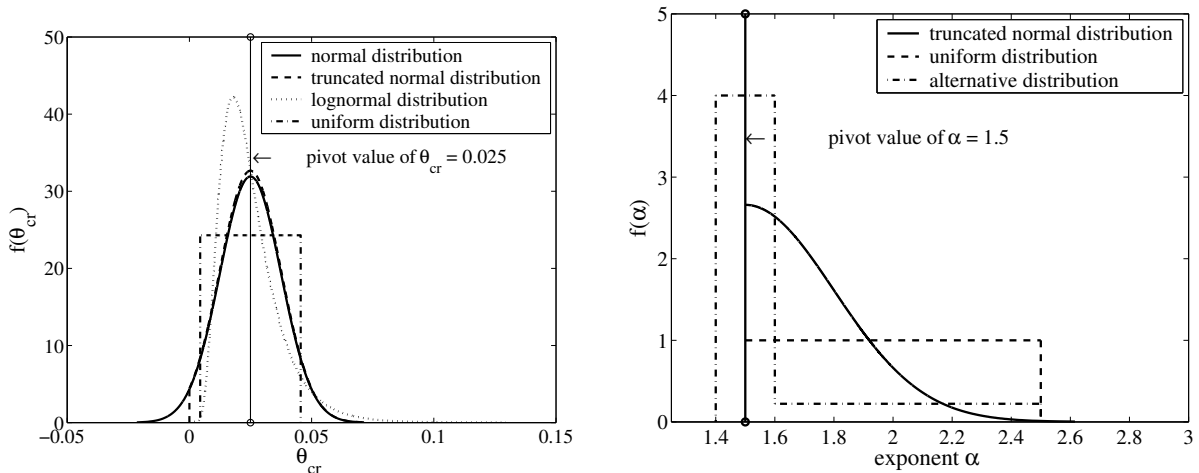
(a) Statistical description of the critical Shields parameter θ_{cr} in the Rhine model

(b) Statistical description of the exponent of the bed shear stress α in the Rhine model

Figure 6.22: Statistical description of the parameters θ_{cr} and α in the transport formula

In accordance with Johnson (1996a), we use a truncated normal distribution with coefficient of variation of 0.5 to statistically describe the critical Shield parameter (see Figure 6.22(a)). The pivot value of the critical Shields parameter, 0.025 (see remark on a reduced value of θ_{cr} in the

Rhine model in Section 4.5.4), is taken as the mean value in this distribution. In addition, MCS is done with a lognormally distributed critical Shield parameter. The statistical parameters of this distribution function are derived from the central moments. The lognormal distribution is much more 'tail-heavy' than the normal distribution. As a consequence, it attributes a higher probability to extreme values in the tail of the distribution. Finally, a uniform distribution function is used to describe the uncertainty in the critical Shields parameter. The range of possible values of θ_{cr}, 0.004 - 0.046, is deduced also from the central moments. The uniform distribution expresses that we are unable to say which values within this range are more likely to occur than others. To make sure that the expected yearly sediment volume remains unchanged, the calibration factor A (see Eq. 4.16) is changed simultaneously with θ_{cr} in the MCS.

Statistical description of uncertainty in the exponent of bed shear stress, α

The bed load transport rate can be expressed in two ways, namely as a function of the flow velocity to the exponent n and as a function of the bed shear stress to the exponent α. The exponent n lies in the range of 3-5 and the exponent α is in the order of 1.5 (Van Rijn, 1993). The latter is used in the Meyer-Peter & Müller (1948)-formula. The exponent of the bed shear stress in this formula is constant and equal to 1.5. Generally speaking, the exponent can be in the range of 1.5-2.5[2].

The exponent of the bed shear stress α is statistically described with (1) a uniform distribution between 1.5 and 2.5, (2) a normal distribution with a mean value of 1.5 and a standard deviation of 0.3, truncated at 1.5 and (3) a distribution function that attributes a probability of 80% in the range 1.4-1.6 and 20% in the range of 1.6-2.5 (see Figure 6.22(b)). The second and the third statistical description prevent a shift of the central point of the distribution away from the pivot value 1.5.

Impact of uncertainty in the sediment transport formula on morphology

For the separate simulations in MCS, the critical Shields parameter θ_{cr} is changed during the entire computation period. Because of the significant downstream fining of sediment, θ_{cr} decreases in the downstream direction. If the bed shear stress is approximately constant, a smaller critical Shields parameter enhances the sediment transport capacity. As a consequence, a milder bottom slope would develop. The morphological response statistics are shown in Figure 6.23. The nature of the θ_{cr}-uncertainty does not significantly influence the mean morphological response, but the uncertainty, as such, leads to a large 90%-confidence interval (see Figure 6.23(a)).

---

2.   If the shear stress is extremely large, the critical shear stress term can be neglected in the transport formula. In that case, the bed load transport rate can be expressed as a function of the flow velocity to the power n. According to Van Rijn (1993) this exponent is in the range of 3-5. Therefore, the exponent of the bed shear stress α can be in the range of 1.5-2.5
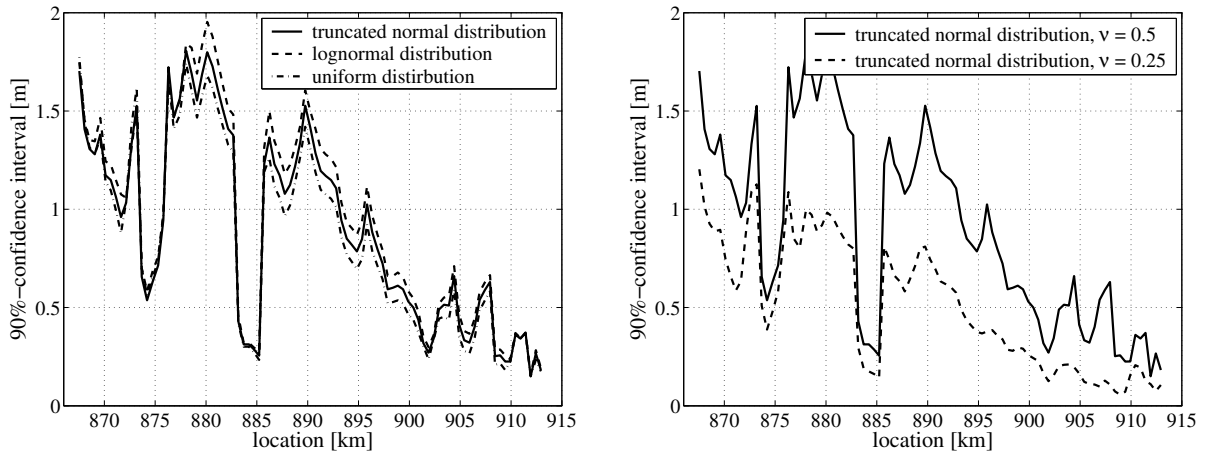
(a) 90%-confidence interval for three statistical descriptions of θ_{cr}, viz. (1) normal distribution, truncated at 1.5, (2) uniform distribution, and (3) alternative distribution

(b) 90%-confidence interval for the normal distribution, truncated at 1.5, with $\nu = 0.5$ and 0.25, respectively

Figure 6.23: Spatial variation of the statistical properties of the cross-sectionally averaged bed level response in the Waal after 20 years in the high-water season, as computed with the 1-D Rhine model - uncertainty source: the critical Shields parameter, θ_{cr}

The size of the confidence interval decreases towards the hinge point near Tiel. If we reduce the coefficient of variation ν from 0.5 to 0.25, the 90%-confidence interval reduces significantly, as is shown in Figure 6.23(b).
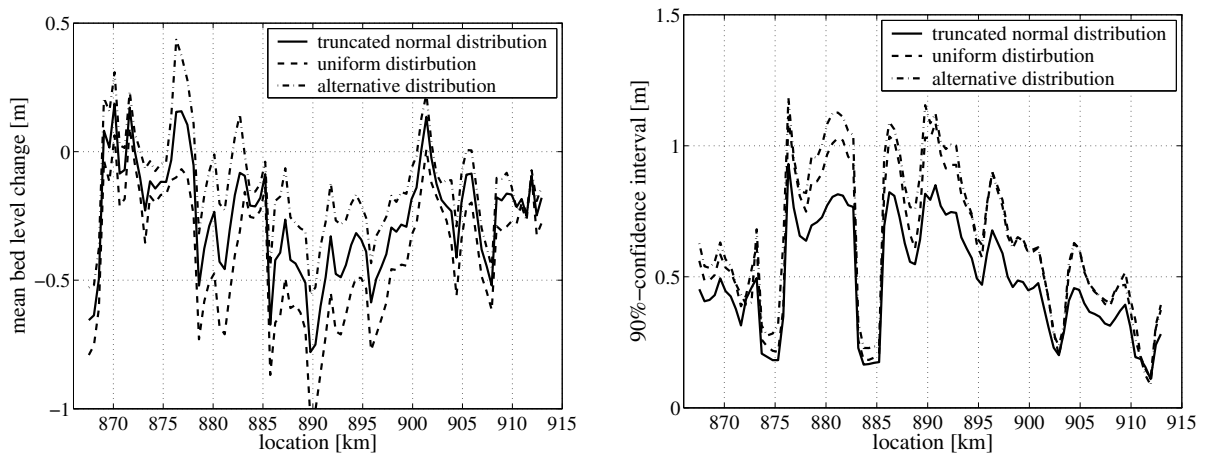
(a) Mean response

(b) 90%-confidence interval of the response

Figure 6.24: Spatial variation of the statistical properties of the cross-sectionally averaged bed level response in the Waal after 20 years in the high-water season, as computed with the 1-D Rhine model - uncertainty source: the exponent of the bed shear stress, α

Figure 6.24 shows the morphological impact of the uncertainty in the exponent of the bed shear stress. The mean responses strongly differ, for the three statistical descriptions and the same

goes for the confidence intervals. We attribute most significance to the results of the normal distribution, truncated at 1.5, and the alternative distribution, since the central point of these distributions is close to the pivot value of α.

6.7   Relative importance of uncertainty sources

The relative contribution of the various uncertain model inputs and parameters to the overall uncertainty is discussed here. Use is made of the MCS with the uncertainty sources included individually. In addition, an MCS is performed with the following uncertainty sources are included simultaneously:

- river discharge - Bootstrap resampling in combination with a flood event predictor;
- grain size of the bed material - D_{50} and D_{90} in Niederrhein and Waal, bivariate uniform distribution, $\rho = 0.6$;
- hydraulic roughness of the main channel of short model units - bivariate lognormal distribution, $\nu = 0.15$ and $\rho = 0.5$;
- parameters in the sediment transport formula
    - θ_{cr} - truncated normal distribution, $\nu = 0.5$;
    - α - truncated normal distribution, $\mu = 1.5$, $\sigma = 0.3$.

Figure 6.25 shows the morphological response statistics from each MCS after a period of 20 years in the high-water season. The temporal variation of these statistics is presented for two different locations in Figure 6.26, viz. for a location in a river section with a large change in river geometry (km 907.4) and a location in a more or less prismatic river section (km 895.3). Figure 6.27 gives the spatial variation of the 90%-confidence interval from each MCS after a period of 5, 10, 15, and 20 years in the high-water season, and so, provides insight into the temporal evolution over a period of years. We will discuss these results in the following subsections.

### 6.7.1   Overall uncertainty when combining all sources

It appears that the various contributions to the overall uncertainty do not add up according to the rules of linear error propagation. This may probably be an indication for the degree of non-linearity of morphodynamic river system. However, it may also refer to the presence of correlation structures among the different model inputs. The non-linear behaviour of morpho-dynamic systems, combined with the time and space dependent signature and the time-lagging effect, presumably results in complex interactions of the various uncertainty sources, ultimately tending to reduce the overall uncertainty.

Figure 6.26 shows that the amplitude of the seasonal fluctuation of the confidence interval resulting from the MCS with all uncertainty sources included, for instance, is much smaller

than that when the uncertainty in the discharge is considered on its own. The reduction of the seasonal effect indicates that the other uncertainty sources have a damping effect on this seasonal feature. The error propagation for the combination of all uncertainty sources will be substantiated further later on.
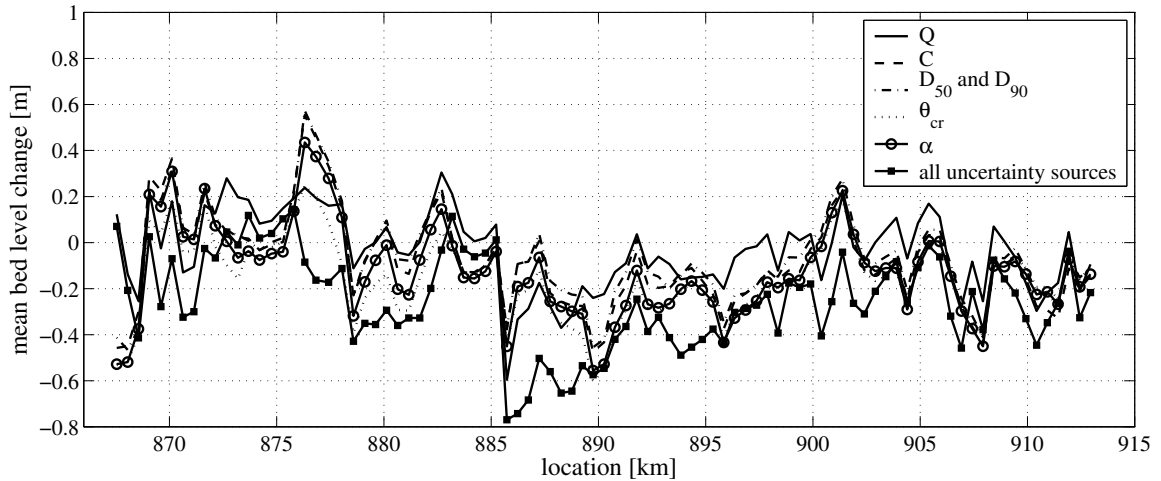
(a) Mean response
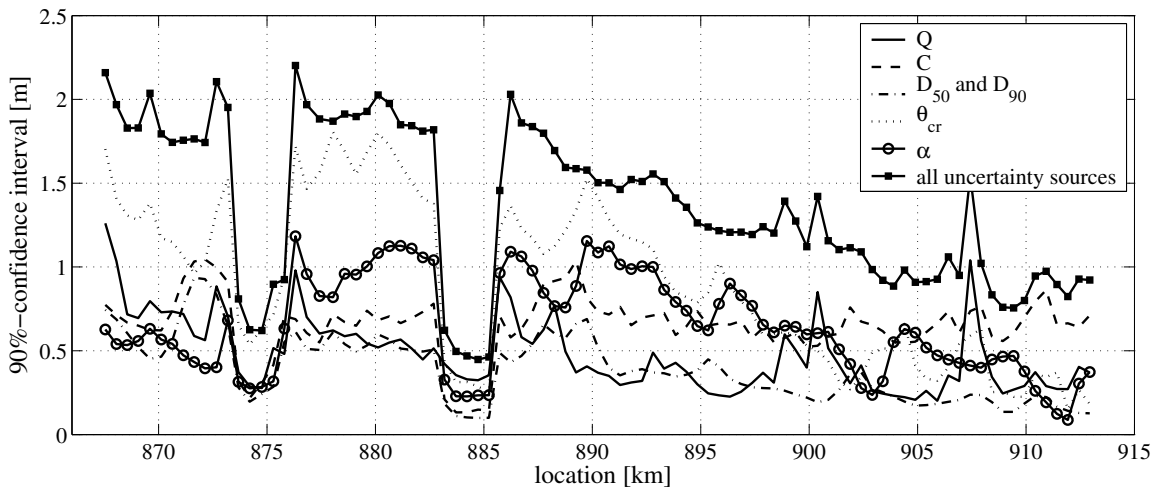
(b) 90%-confidence interval of the response

Figure 6.25: Spatial variation of the statistical properties of the cross-sectionally averaged bed level response in the Waal after 20 years in the high-water season, from each MCS, as computed with the 1-D Rhine model

6.7.2 Relative contribution of each uncertainty source

Figure 6.25-6.27 illustrate that the morphological response statistics in the Waal exhibits a strong spatial and temporal variation. The response statistics does not only show that many possible morphological states can occur. They also show that in some reaches the spatial and

temporal bed level variations are more pronounced than in others. These variations turn out
to be different for each uncertainty source. As a consequence, the relative contribution of each
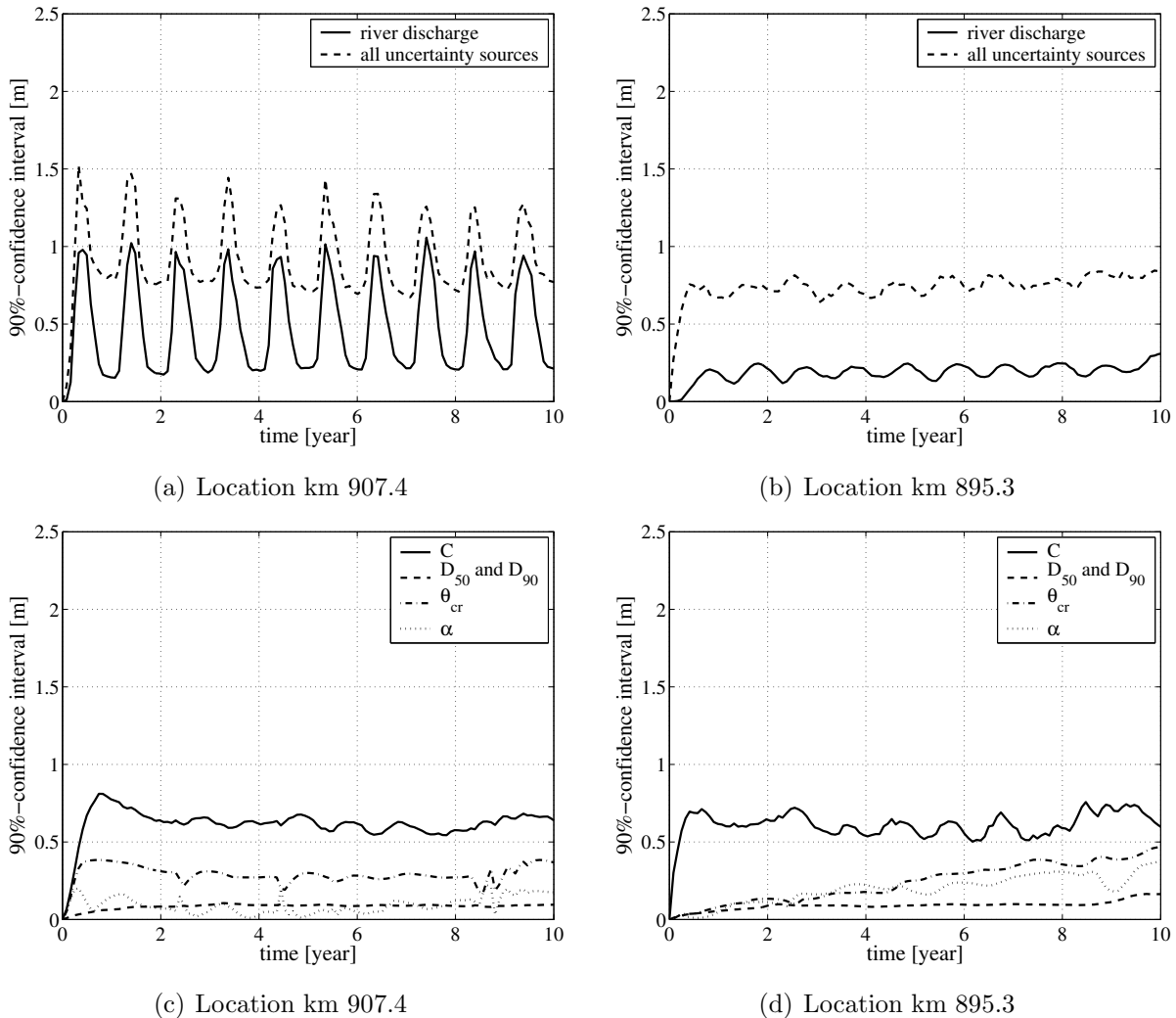uncertainty source is a function of time and space.

(a) Location km 907.4

(b) Location km 895.3

(c) Location km 907.4

(d) Location km 895.3

Figure 6.26: Temporal variation of the statistical properties of the cross-sectionally averaged bed
level response at two locations in the Waal, from each MCS, as computed with the 1-D Rhine model

For instance, the uncertainty in the critical Shields parameter and the exponent of the bed shear
stress are dominant in the section between km 867 and km 895, whereas they are less important
in the downstream part. The importance of the uncertainty in the hydraulic roughness of the
main channel seems to increase in the downstream direction. The uncertainty in the grain size
of the bed material turns out to be of minor importance. The importance of the river discharge
exhibits a seasonal variation. As becomes apparent from Figure 6.26, this is most significant at
locations with non-uniformities in the river geometry, whereas at locations in a uniform river
reach it is less pronounced. The seasonal dependency is not noticed in the response statistics
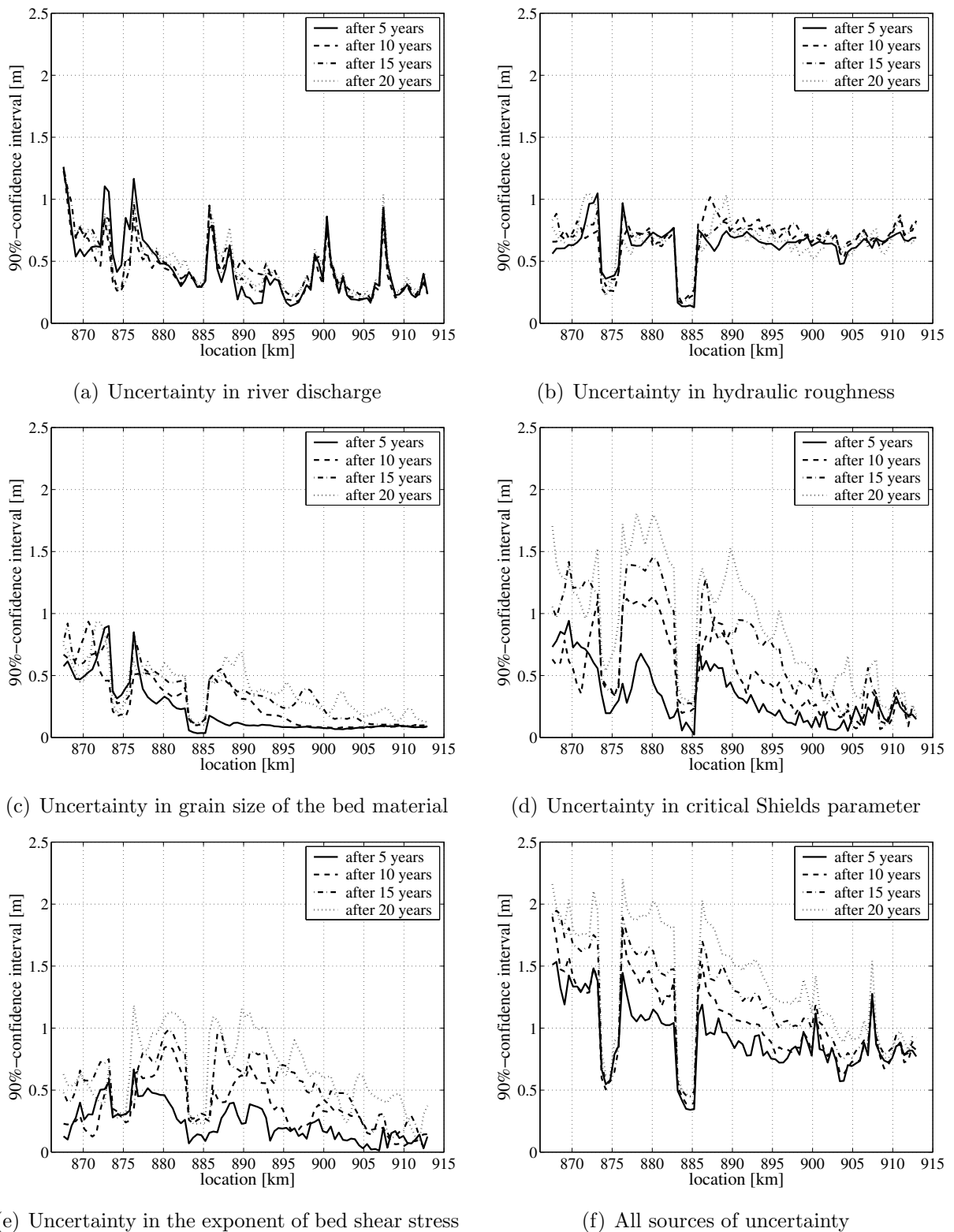from other MCS. For some of the MCS, the response statistics do exhibit however some temporal

(a) Uncertainty in river discharge

(b) Uncertainty in hydraulic roughness

(c) Uncertainty in grain size of the bed material

(d) Uncertainty in critical Shields parameter

(e) Uncertainty in the exponent of bed shear stress

(f) All sources of uncertainty

Figure 6.27: Spatial variation of the 90%-confidence interval of the cross-sectionally averaged bed level response after a period of 5, 10, 15, and 20 years in the high-water season, from each MCS, as computed with the 1-D Rhine model

variation, viz. they evolve in time, over a period of several years (see Figure 6.27). This temporal evolution is the most significant for the parameters in the sediment transport formula, θ_{cr} and α. The 90%-confidence interval from the MCS with the uncertain θ_{cr}, increases as a function of time, to a decreasing extent in the downstream direction. Over a period of several years, the response statistics in the downstream parts are likely to be affected by those of the locations further upstream, as bottom waves initiated at the upstream locations, propagate downstream and pass at a certain moment the locations downstream, if they have not decayed to almost zero by that time. For the river discharge and the hydraulic roughness of the main channel, the temporal evolution over a period of years seems to be insignificant, since their response statistics are more or less constant over a period of years.

Techniques to quantify the relative contribution

Techniques to quantitatively estimate the relative importance of uncertain input variables to the total uncertainty in the model output have been presented in Section 3.2.5. Techniques, like (1) Correlation coefficient analysis, (2) Correlation ratio analysis, and (3) Percentile Cobweb plotting may help to discriminate between important and less important sources of uncertainty. The relative importance of the model inputs X_i (river discharge, grain size of the bed material, hydraulic roughness of the main channel and parameters in the sediment transport formula θ_{cr} and α) to the model output Y (the cross-sectionally averaged bed level response) is investigated below by using these techniques. The suffix i stands for the discriminator of the model input source.

For a first indication of model inputs that contribute most to the output uncertainty, the correlation coefficient r is considered. The method of correlation coefficients relies, however, on the assumptions that Y is linear in X_i and that the model inputs X_i are mutually independent. The squared correlation coefficient, r^2, is known as the coefficient of determination, and describes the percentage of variance of output Y. Figure 6.28 shows the coefficient of determination at four different locations, for the morphological response after 5 and 20 years in the high-water and dry season.

It can be noticed that the coefficient of determination varies per location and per moment in time. For the upstream locations, the hydraulic roughness of the main channel turns out to have the highest contribution to the variance in the morphological response. However, this contribution decreases over the years, since the relative contribution of the critical Shields parameter increases significantly. The latter is not noticed at the more downstream situated locations, km 907.4 and km 911.4. At location km 907.4, the impact of the seasonal signature of the discharge is clearly visible in the coefficient of determination. In the high-water season, a larger percentage of the variance of output Y is explained by the discharge. At all locations, the relative importance of the uncertainty in the grain size of the bed material is very low.
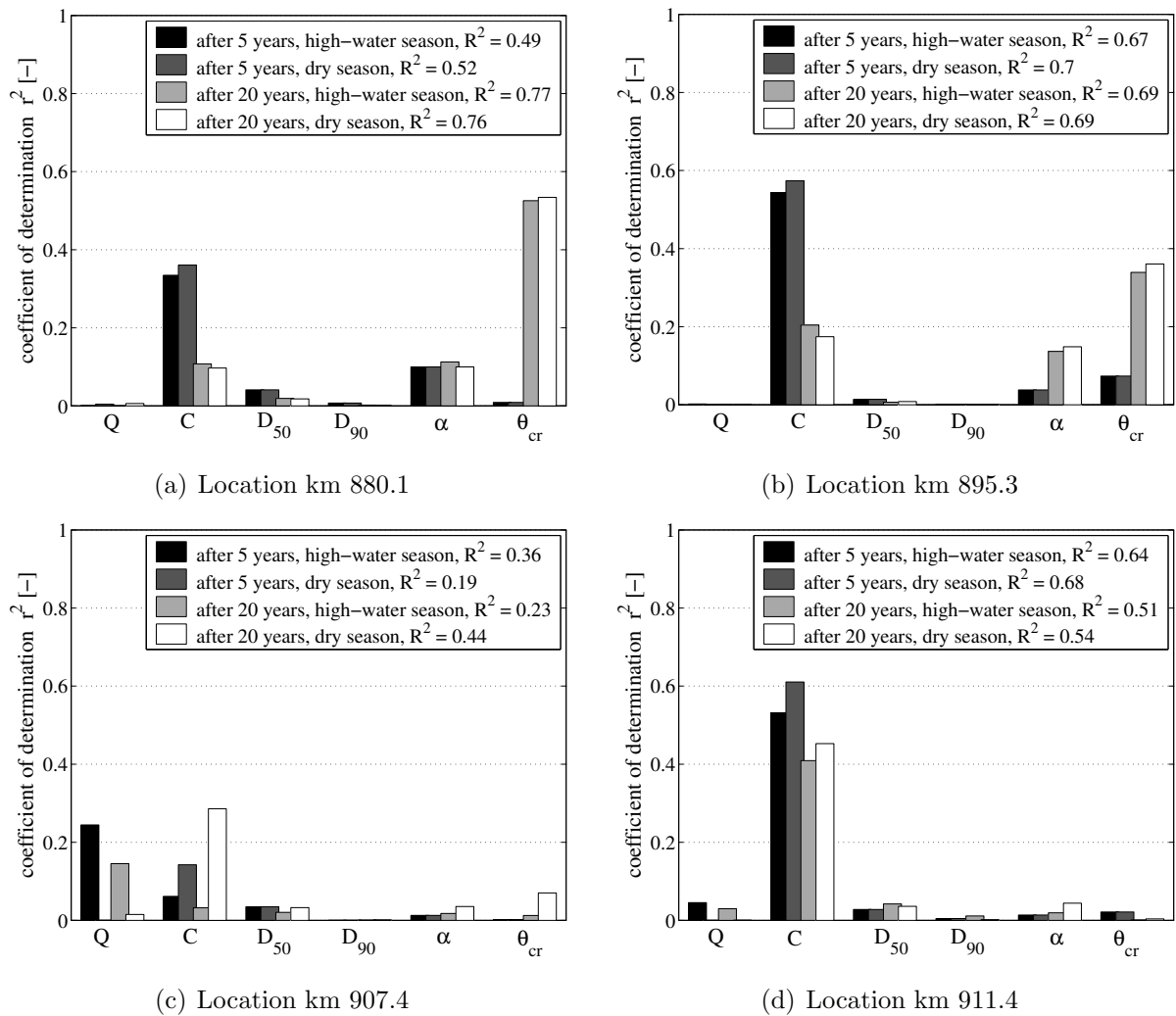
Figure 6.28: Coefficient of determination, r^2 at four different locations, after a period of 5 and 20 years in the high-water and dry season

Adding up the coefficients of determination of the model inputs gives the percentage of the variance of Y that is explained by the linear model. As shown in the labels of Figure 6.28, in all cases, R^2 is much smaller than one. This may refer either to correlations and dependencies between model inputs, or to contributions of higher order terms, i.e. non-linearity in the morphological process.

The correlation ratio, CR, is another measure to express the importance of model input X_i to model output Y. This measure does not rely on the assumption of linearity. The objective is to find a subset of the model inputs that drives the variance of Y. The variance is used as an indicator of importance. The prediction variance when combining all uncertainty sources in one MCS is compared with the conditional prediction variance that is determined by an MCS

driven by a subset of uncertain model inputs:

$$CR_i = \frac{Var\left(E\left(Y\,|X_i\right)\right)}{Var\left(Y\right)} \tag{6.7}$$

In the case where the correlation ratio, CR, is close to 1, the prediction variance is driven largely by that particular subset. Figure 6.29 gives the CR_i's at four different locations, for the morphological response after 5 and 20 years in the high-water and dry season.
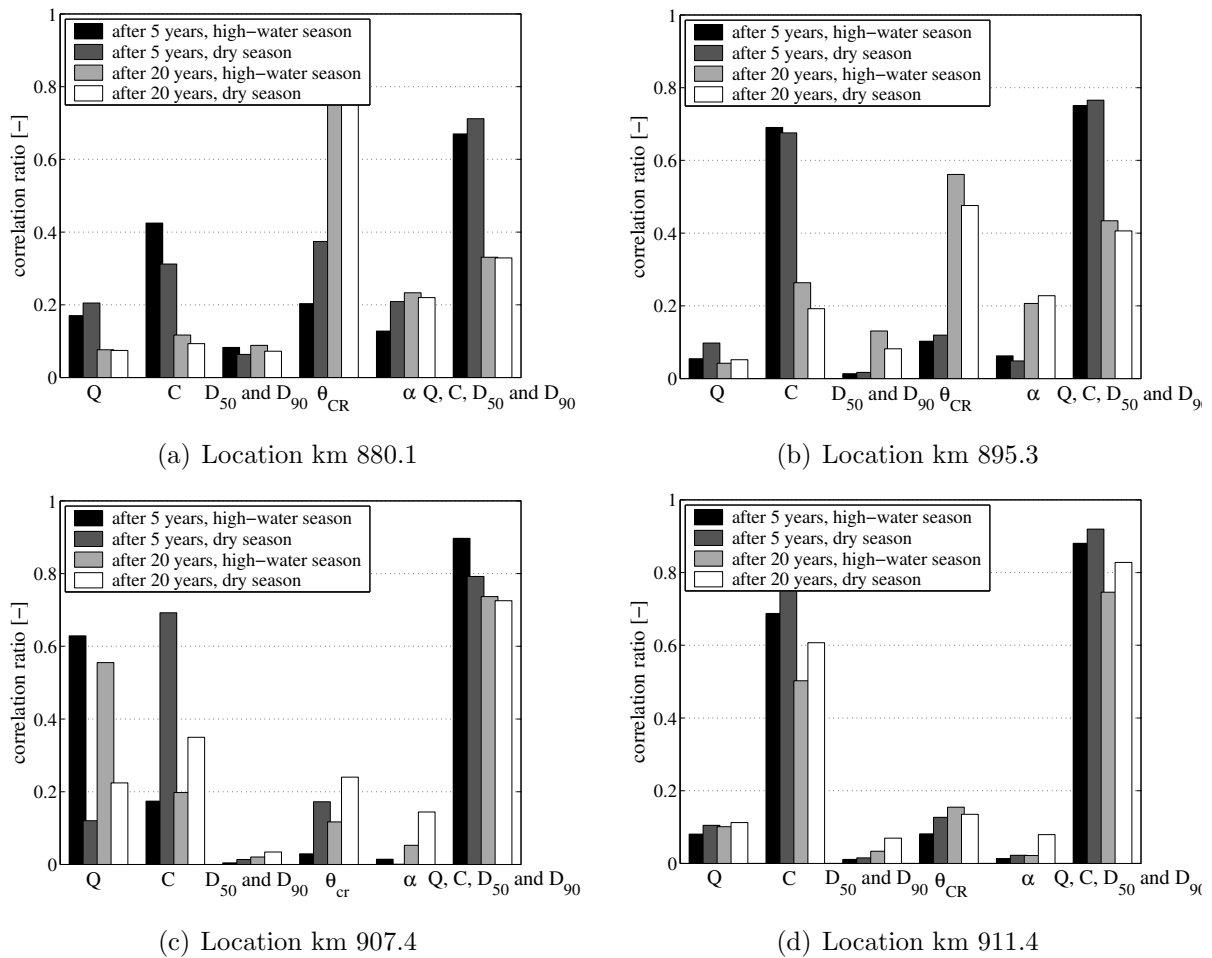

(a) Location km 880.1

(b) Location km 895.3

(c) Location km 907.4

(d) Location km 911.4

Figure 6.29: Correlation ration at four different locations, after a period of 5 and 20 years in the high-water and dry season

The correlation ratio, CR, is derived from the MCS with the uncertainty sources included individually, and an MCS with the uncertainty in the river discharge, the hydraulic roughness of the main channel and the grain size of the bed material included simultaneously. Figure 6.29 shows a more or less similar picture as that of the correlation coefficients in Figure 6.28.

In general, the contribution of the grain size of the bed material to the uncertain morphological response is negligible. At the upstream locations, the importance of the critical Shields parameter for the prediction variance is quite large and seems to increase even over the years. Further

increase of the θ_{cr}-variance requires more investigation. In the downstream direction, this relative importance of the critical Shields parameter decreases, whereas the hydraulic roughness of the main channel becomes more important. At location km 907.4 and 911.4, the prediction variance is mostly driven by a combination of uncertainty in river discharge, hydraulic roughness of the main channel and grain size of the bed material.

The global measures, like correlations, or correlation ratios may not be appropriate when we are interested in a specific range of the model output (Cooke & Van Noortwijk, 1999). Their usefulness is limited, especially when the effect of an input on the model output is drastically different in different parts of the parameter space. In that case, the cobweb plotting technique (see Section 3.2.5) is appropriate.

A cobweb plot provides a graphical representation of the relation between the joint probability distribution of output Y and a number of explanatory model inputs X_i. When normalised by various values of output Y, these plots provide insight into the importance of the model inputs for a selected range of the output space. Figure 6.30 and Figure 6.31 show cobweb plots of the joint distribution, in percentiles of the output Y at locations km 880.1 and km 907.4 and 6 explanatory variables, the river discharge, the hydraulic roughness of the main channel, the D_{50} grain size characteristic, the D_{90} grain size characteristic, the exponent of the bed shear stress, the critical Shields parameter. On the basis of the general cobwebs (upper panels), we conclude that there is no strong evidence of correlation between output, (1), and model inputs (2-7). However, if the joint distributions are conditionalised on the top (or bottom) 10 percentiles of the output, we can clearly notice that some of the model inputs differ strongly from uniform.

From Figure 6.30 we conclude that at location km 880.5:

- Y is positively correlated to the roughness coefficients of the main channel. The top 10 percentiles of Y (1) are associated with high roughness coefficients (3), whereas low values of Y link to low roughness coefficients;
- Y is slightly negatively correlated to the exponent of the bed shear stress (6);
- after a period of 5 years, the top (or bottom) 10 percentiles of Y end up more or less uniformly for the river discharge (2), the grain size of the bed material (4) and (5), and the critical Shields parameter (7), which indicates unconditional uniformity. However, after a period of 20 years, the morphology is strongly negatively correlated with θ_{cr} (7).

From the bottom cobweb of 6.31, we see that in the high-water season (right panel) high values of Y are associated with high discharge values (2), indicating a strong positive correlation between the two. This correlation is not as clear in the dry season. In the dry season (left panel), there is a positive correlation of high values of Y with high values of the roughness coefficients (3). The distributions of the remaining inputs, when conditioning on the top 10 percentile values of Y, are more or less uniform, indicating no correlations.
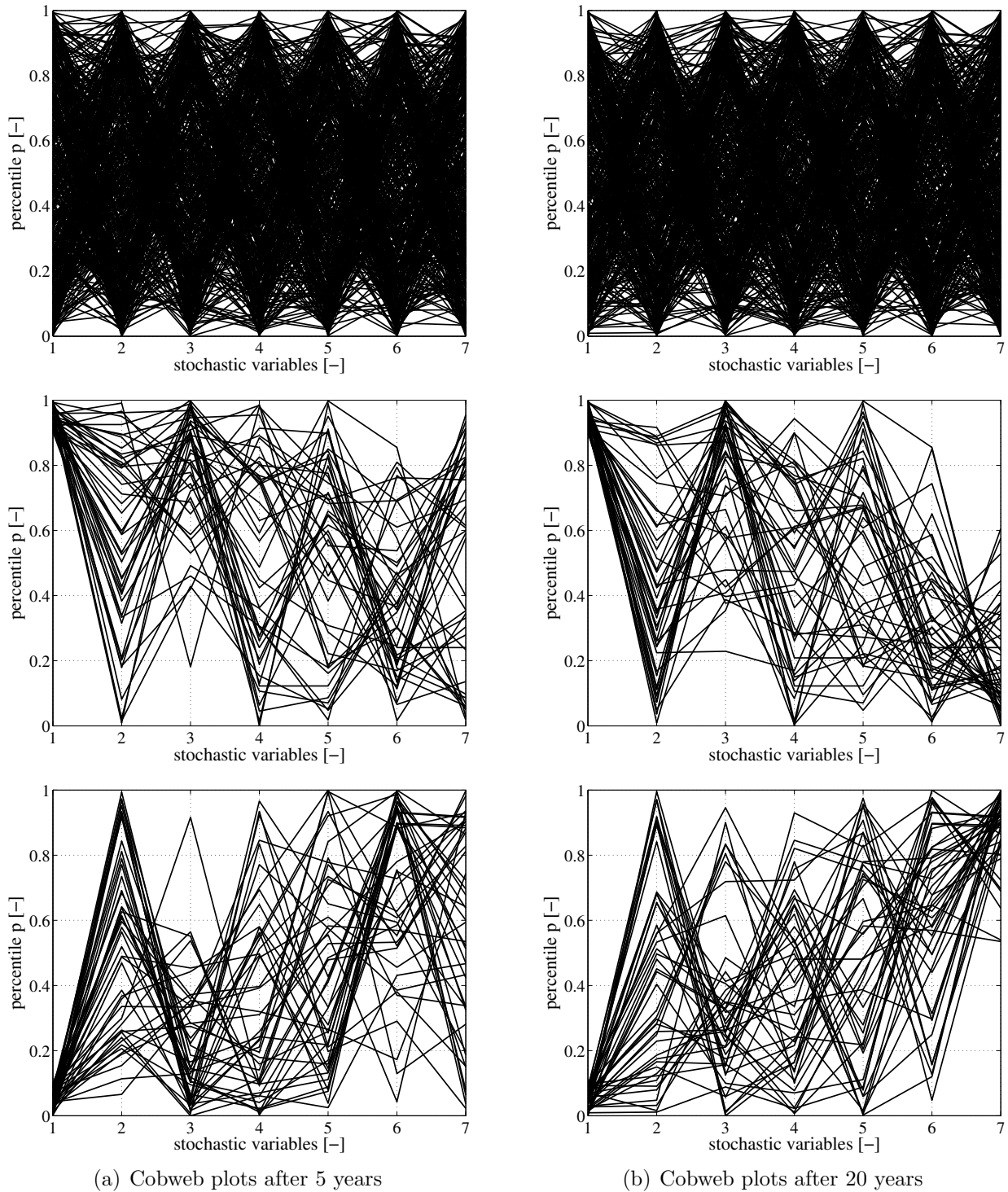
(a) Cobweb plots after 5 years   (b) Cobweb plots after 20 years

From left to right on the horizontal axis: (1) the model output (the cross-sectionally averaged bed level response), and the explanatory inputs (2) river discharge, (3) hydraulic roughness of the main channel, (4) D_{50} grain size characteristic, (5) D_{90} grain size characteristic, (6) exponent of the bed shear stress, (7) critical Shields parameter

Figure 6.30: Cobweb plots of the cross-sectionally averaged bed level response after 5 and 20 years in the high-water season at location km 880.4, for general cobweb (upper panel), and conditional cobweb: top 10 percentiles of the output (middle panel) and bottom 10 percentiles of the output (lower panel)
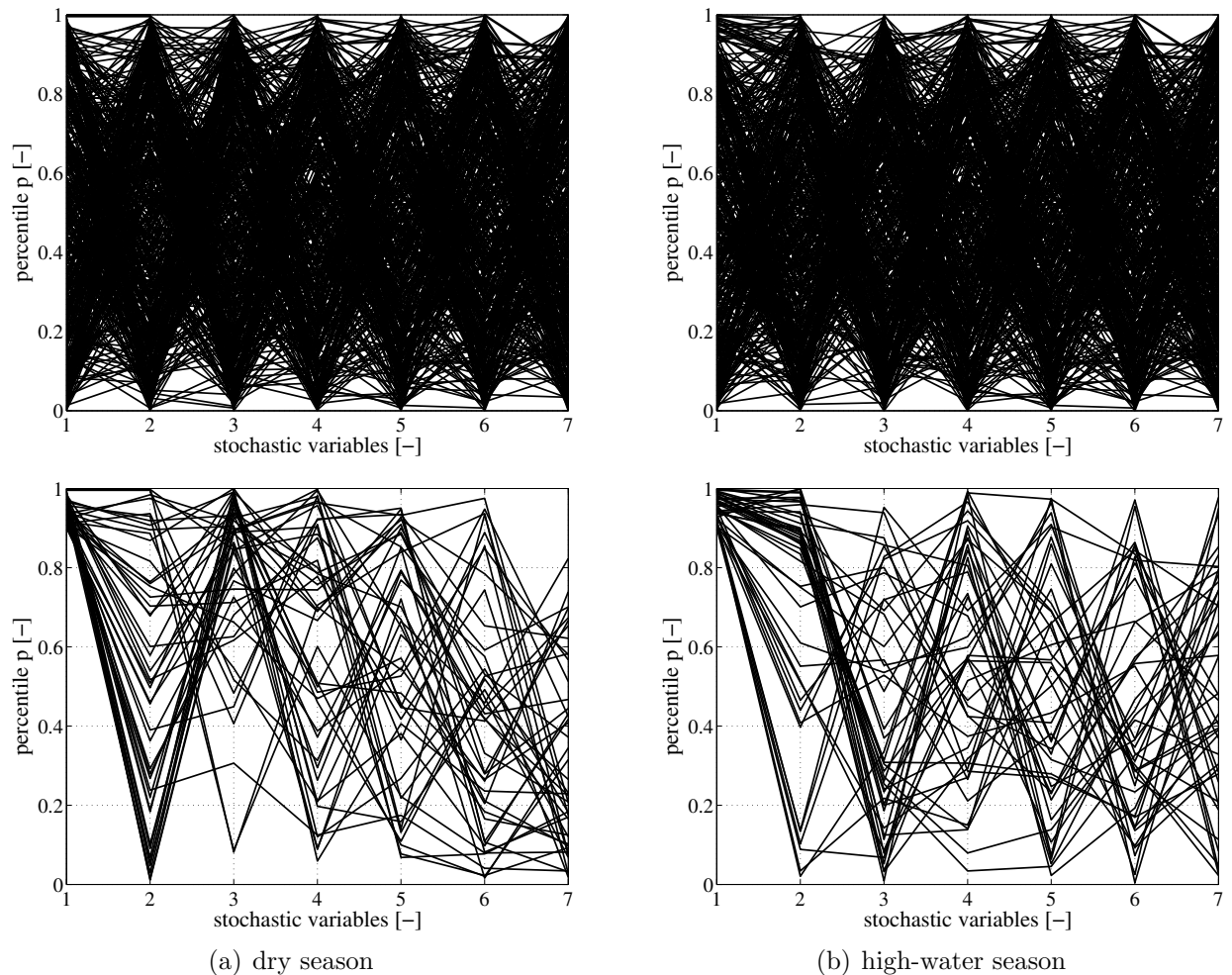
From left to right on the horizontal axis: (1) the model output (the cross-sectionally averaged bed level response), and the explanatory inputs (2) river discharge, (3) hydraulic roughness of the main channel, (4) D_{50} grain size characteristic, (5) D_{90} grain size characteristic, (6) exponent of the bed shear stress, (7) critical Shields parameter

Figure 6.31: Cobweb plots of the cross-sectionally averaged bed level response after 20 years in the high-water and dry season at location km 907.4, for general cobweb (upper panel), and conditional cobwebs: top 10 percentiles of the output (middle panel) and bottom 10 percentiles of the output (lower panel)

In conclusion, estimating the relative contribution appears not to be straightforward, since morphodynamic systems exhibit a non-linear behaviour, combined with a time and space dependent signature, model input that are mutually correlated and a time-lagging effect. As noticed, the size of the confidence interval varies differently for each uncertainty source, as a function of time and space, and the contributions of all sources do not add up linearly to the overall uncertainty. Hence, the relative contribution of each uncertainty source to the overall uncertainty is time and space dependent.

The correlation coefficient, the correlation ratio and the Cobweb-plots give an indication for the relative dependency of each uncertainty source. An explanation for the findings can be

found in Section 6.4-6.6, where the results of the MCS with the uncertainty sources included individually, are discussed. For instance, as a consequence of significant downstream fining of the bed material, the bed level confidence interval resulting from the uncertainty in grain size also decreases in the downstream direction. Uncertainty related to river discharge depends on the uniformness of the river geometry. Apart from river locations close to the bifurcations, uncertainty introduced by the hydraulic roughness is more or less constant along the river. For the river discharge and the hydraulic roughness of the main channel, the temporal evolution over a period of years seems to be insignificant, viz. the morphological response statistics are more or less constant over a period of years. The uncertainty in the bed morphology introduced by the uncertain critical Shields parameter reduces in downstream direction. This can be explained as follow: if the bed shear stress is approximately constant, a smaller (larger) critical Shields parameter enhances (reduces) the sediment transport capacity. As a consequence, a milder (steeper) bottom slope would develop. Therefore, the uncertainty decreases in downstream direction. Over a period of several years, the response statistics in the downstream parts are likely to be affected by those of the locations further upstream, as bottom waves initiated at the upstream locations, propagate downstream and pass at a certain moment the locations downstream, if they have not decayed to almost zero by that time.

Any of these changes in morphological response statistics resulting from an individual uncertainty source, either in space or in time, will affect the relative importance of the others.

Although no sweeping statement can be made, generally speaking, the tuning parameters, turn out to be the most important uncertainty sources for the morphological response. The contribution of the uncertainty in the grain size of the bed material to the uncertain morphological response is negligible. The importance of the discharge to morphology exhibits a seasonal variation, and is more significant at locations with non-uniformities in geometry, whereas at locations in a uniform reach, it is less pronounced.

6.8   Comparison with field observations and measurements

We make use of the bathymetric database of the Dutch Rhine to compare to the bed level variability observed in nature with the estimated stochasticity of the morphodynamics in the previous sections. From 1926 onwards, bed soundings have been performed in the alluvial part of the river at cross-sections with a mutual distance of 100 or 125 m, on a yearly basis in the dry season.

The quality of the data is influenced by factors such as measuring technology, measuring frequency, completeness of registration (gaps in data) and post-processing (see Section 2.3.1). Apart from this, the homogeinity of the database is affected by structural and incidental changes in the system, such as the large-scale regulation works and dredging activities performed in

the 19th and 20th century. Inaccurate and incomplete registration of the latter makes it difficult to homogenise the dataset. Moreover, we have to realise that each bathymetric record reflects a single realisation of the dynamic behaviour of the river system. Conditions, for instance discharge, bed geometry, composition of bed material, etc., made the river evolve into the observed bathymetric state. The historical record can only reveal the ensemble dimension, when we can invoke the principle of ergodicity (see Section 5.5). In that case, the historical records should (1) cover a sufficiently long period, i.e. that gives a proper reflection of the population statistics, and (2) preserve homogeinity, persistency and stationarity. All this has to be taken into consideration when using the bathymetric database for the purpose of comparison.

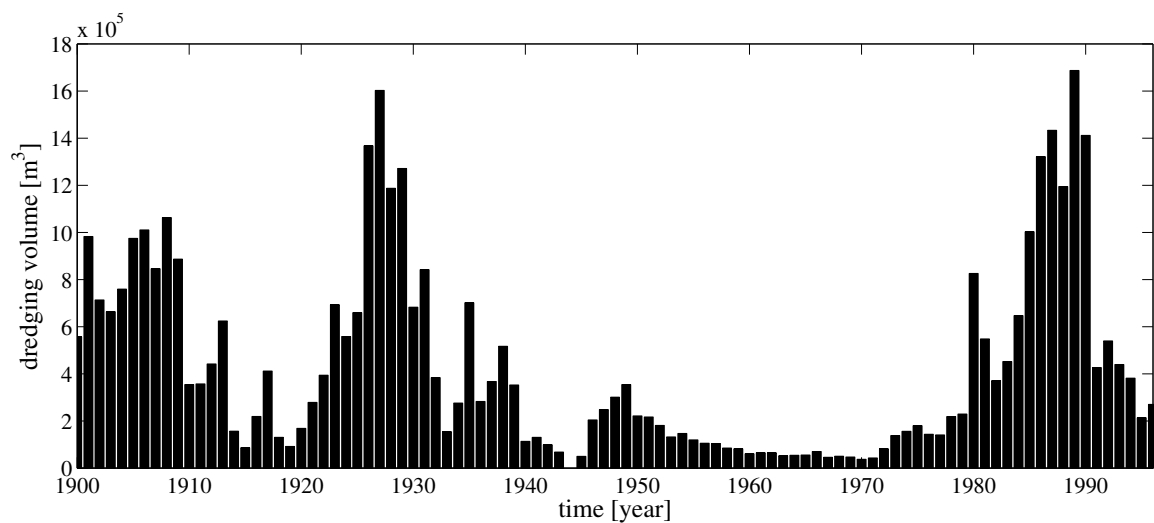|	Structural changes in the Niederrhein and Waal
German Rhine branches	
1890-1970	Large-scale river regulation works, large-scale mining effects and construction of weirs in the German part of the Rhine, leading to a water level reduction and a reduction of sediment load in the Dutch Rhine branches
Niederrhein and Waal	
1850 - 1916	Extensive river improvement schemes began around 1850: main channel systematically fixed and narrowed, navigation channels dredged, islands and sandbanks removed and the river straightened at various points. Non-permeable groynes fixing the main channel, small levees preventing frequent flooding of the floodplains, and high dikes acting as a main flood defence
1872	Construction of the Nieuwe Waterweg, a new outlet to the sea
1885 - 1904	Separation of the Waal and the Meuse at Heerewaarden, Meuse connected with the Amer (till 1904, the Meuse discharged into the Waal at Loevestein)
1908	Deepening of the Nieuwe Waterweg
1927	Construction Meuse-Waal canal
1969	Construction of the Haringvliet dam, regulation of the river outlets by gates
1970	Construction of the Volkerak dam, reducing the downstream storage area and cutting of the tidal influence
1985-1988	Construction of bottom protection in the bend near Nijmegen
1996-1999	Construction of bottom vanes in the bend near Erlecom
1996-1988	Construction of bottom protection in the bend near St. Andries

Table 6.3: Overview of structural changes in the Rhine-system

6.8.1   Non-homogeinity in the bathymetric database

Structural and incidental changes in the Rhine form the major cause of non-homogeinity in the bathymetric database. An overview of structural changes in the Rhine is presented in Table 6.3.
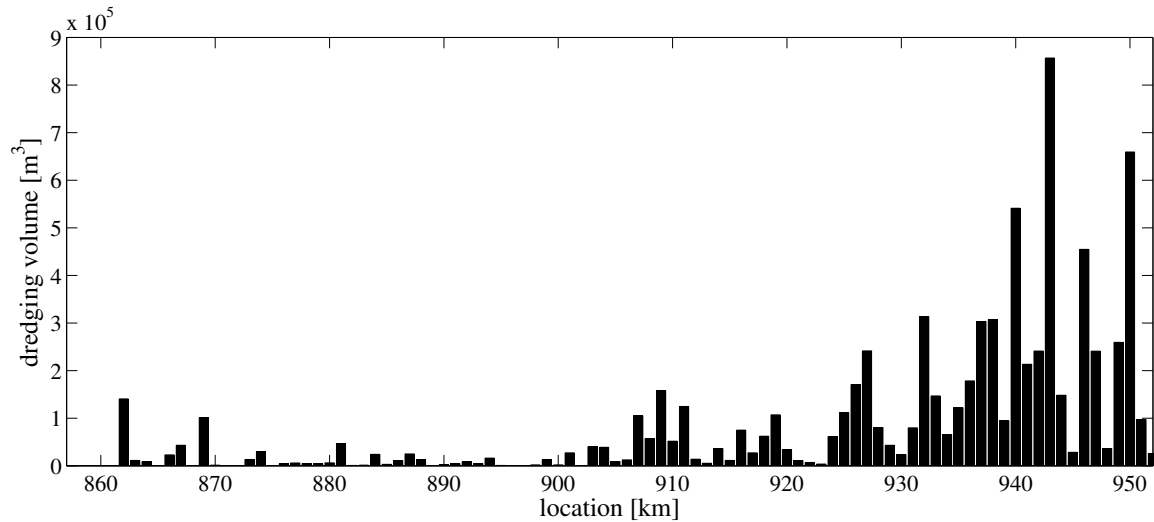
(a) As a function of location, over the 20th century

(b) As a function of time, over all locations

Figure 6.32: Registered dredging activity in the Niederrhein and Waal, in the 20th century

Dredging activities can be considered as incidental changes. Large-scale dredging activities have been undertaken in the 19th and 20th century in the Rhine. Most of this dredging took place 'uncontrolled', without permits or registration. In 1935, a first regulation was introduced, which gave license-holders the permission to dredge a certain volume of sediment. Measures to further reduce the dredging activities were implemented in 1974. In 1991 a new policy was adopted, prescribing that net extraction of sediment is no longer allowed. Dredging for

navigation purposes is permitted, but the dredged volume has to be deposited back into the river. Figure 6.32 shows the registered dredging volume in the Niederrhein and Waal in the 20th century. For most of the registered dredging volume information about the exact dredge location is not available. Adding up the volumes per location (Figure 6.32(a)) results in a total volume that is over a factor 5 smaller than if we add up those per year (Figure 6.32(b)).
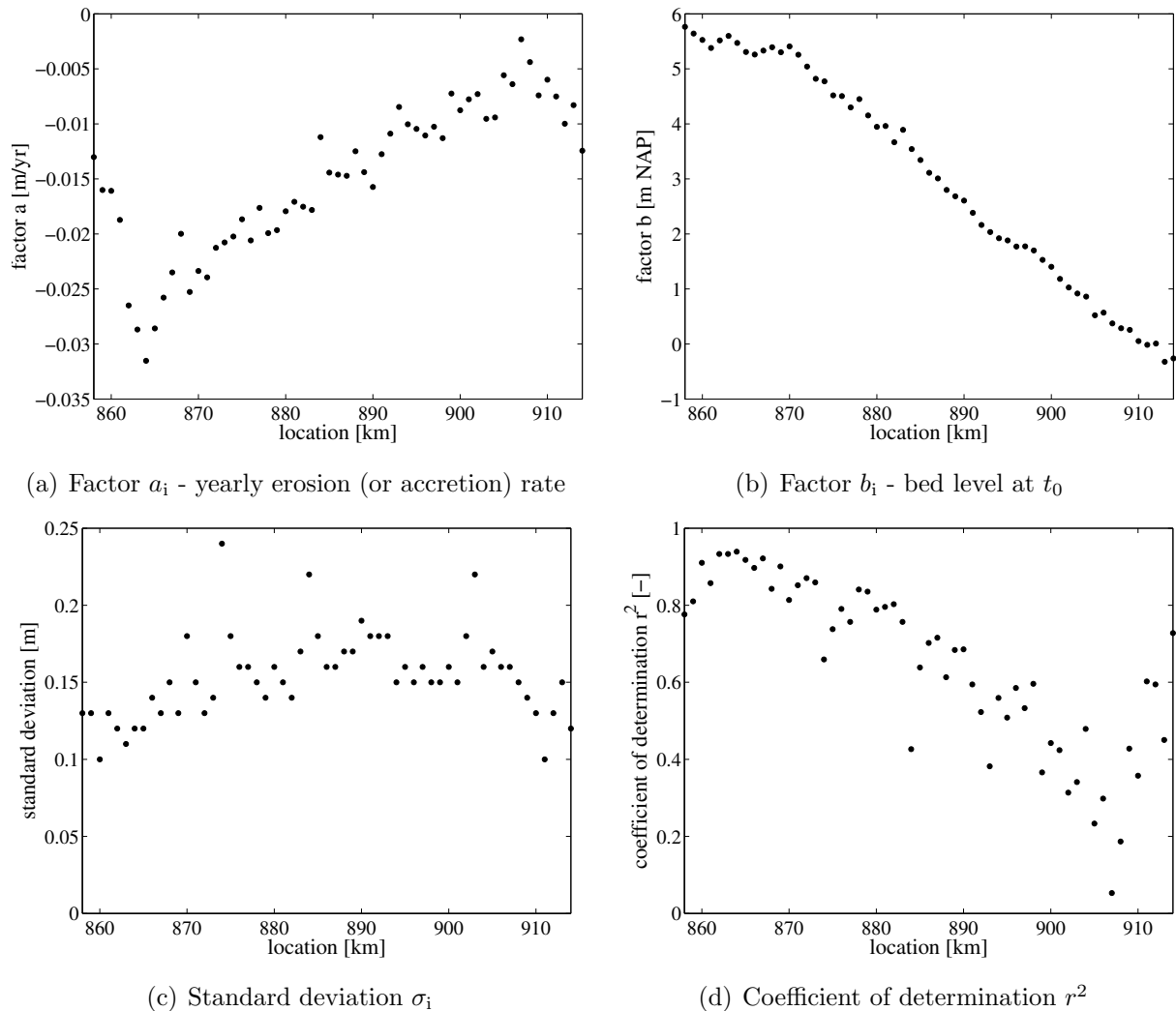

(a) Factor a_i - yearly erosion (or accretion) rate

(b) Factor b_i - bed level at t_0

(c) Standard deviation σ_i

(d) Coefficient of determination r^2

Figure 6.33: Parameters when describing the bathymetry at each location as a linear process

It is by definition wrong to perform a statistical analysis on a dataset that includes non-homogeinity. This becomes more evident, when describing the bathymetry at each location as a linear process:

$$Y_{\text{i}}(t) = a_{\text{i}} \cdot t + b_{\text{i}} + \epsilon_i \tag{6.8}$$

In which a_i represents the yearly erosion (or accretion) rate [m/yr], b_i the bed level at $t_0 = 1926$ [m], and ϵ_i a random offset of Y_i. ϵ_i is normal distributed with μ zero and σ_i. The suffix i stands for the river location. The factors a_{i}, b_{i}, and σ_{i} are presented as a function of location in

Figure 6.33(a)-c. Apparently, the yearly erosion rate consistently decreases in the downstream direction. The primary effect is that the overall slope decreases.

The coefficient of determination, r^2, in Figure 6.33(d), shows to what extent the bed response is linear. A value close to 1 indicates that the bed level process is closely linear. If r^2 approaches 0, the process is far from linear. Downstream of location km 890, r^2 drops below 0.7 and decreases quickly when moving further downstream. Dredging activities becomes more important in this part of the Waal (see Figure 6.32(a)) and may contribute to the perceived non-linearity of the bed response.

6.8.2   Comparison on the basis of a homogeneous subset

Structural and incidental changes in the river system make the bathymetric database less applicable for a proper comparison between the bed level variability observed in nature and the stochasticity of the morphodynamics as estimated in the previous section.

We decide to split the historical record in more or less homogeneous subsets by distinguishing the following periods:

- Period 1953-1970 - period after the large-scale river training;
- Period 1970-1990 - period that is affected by the closure of the Haringvliet and Volkerak;
- Period 1900-2000 - period in which a new dredging policy is adopted that does not allow net extraction of sediment.

In the period 1970-1990, the river system is largely influenced by the closure of the Haringvliet and Volkerak. As a consequence of the closures, the tidal influence in the downstream part of the Waal has been reduced. Hence, the induced reduction of the maximum flow velocity and the sediment transport capacity, led to large-scale accretion of the river bed. Dredging activity were undertaken to keep the river navigable. Both the closures and the dredging was undertaken to counterbalance the induced accretion introduced non-homogeinity in the subset.

For the comparison, the bathymetric data in the period 1990-2000 is used. The Spearman's rank correlation (see Section 3.2.3) is utilised to test the absence of a statistically significant trend in the subset. The yearly bathymetric soundings are mutually independent. The standard deviation of the time-averaged bed level (averaging period 1900-2000) per location is an indication of the bed level variation.

For each MCS, the standard deviation of the time-averaged bed level has been derived for each model simulation from the predicted bed levels in the dry seasons of the first 10 years. For each MCS, the statistical properties of the standard deviation for all model runs - the mean value and the 95%- and 5%-percentile value - are presented in Figure 6.34. The figure shows also the standard deviations derived from the bathymetric data. The difference in percentage terms between the mean values of the standard deviation of the time-averaged bed level for each MCS
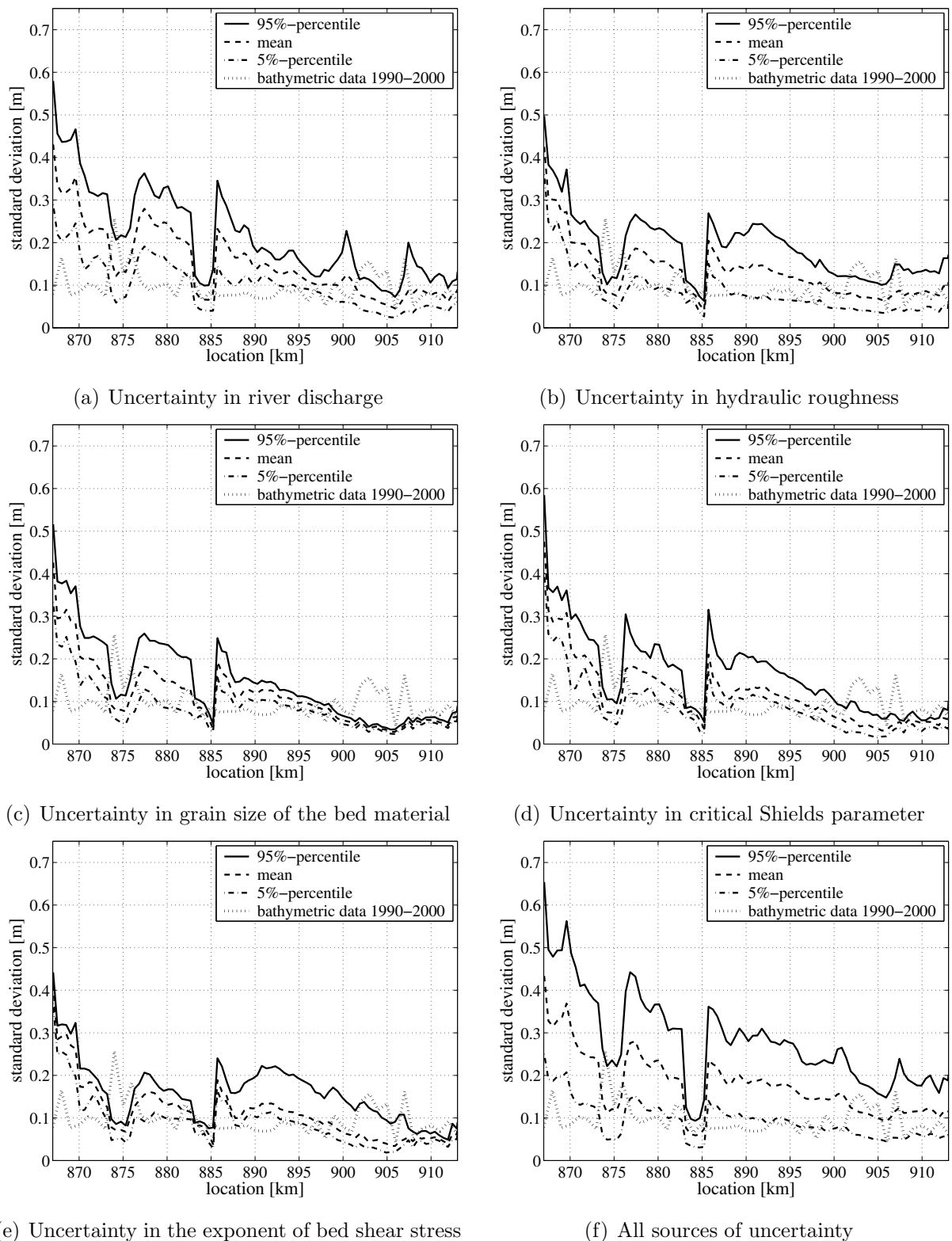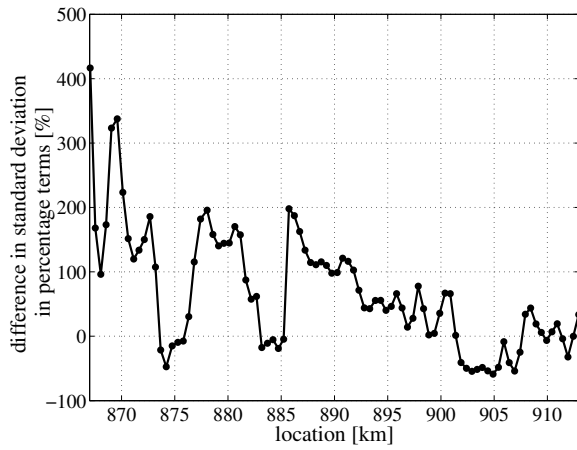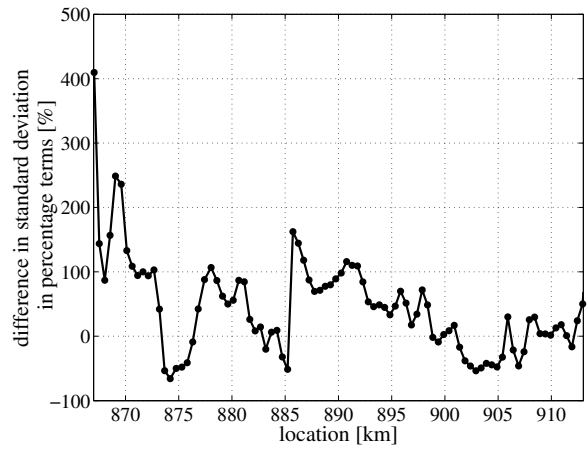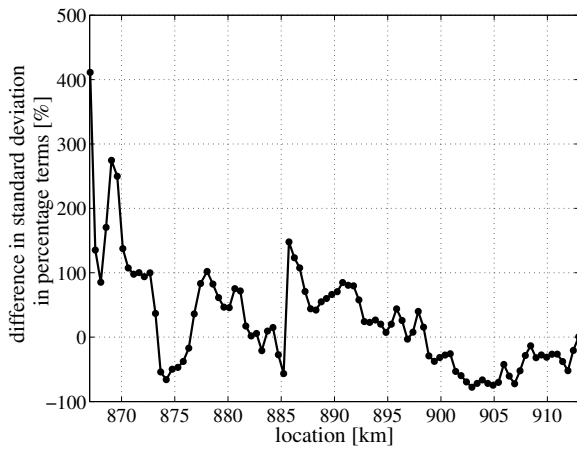
(a) Uncertainty in river discharge

(b) Uncertainty in hydraulic roughness

(c) Uncertainty in grain size of the bed material

(d) Uncertainty in critical Shields parameter

(e) Uncertainty in the exponent of bed shear stress

(f) All sources of uncertainty

Figure 6.34: Statistical properties of the standard deviation of the time-averaged bed level, derived from the predicted bed levels in the dry seasons of 10 years from each MCS and from bathymetric data

(a) Uncertainty in river discharge
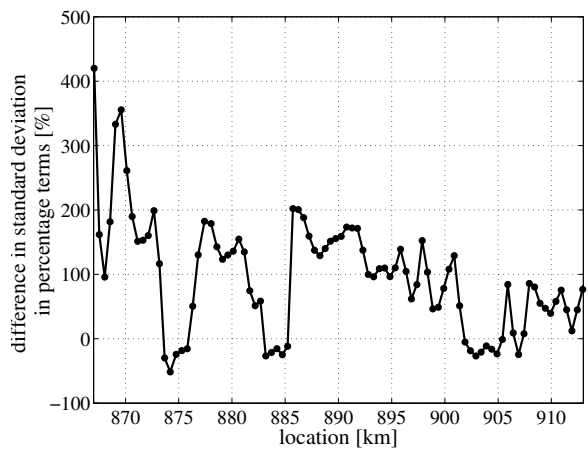
(b) Uncertainty in hydraulic roughness

(c) Uncertainty in grain size of the bed material
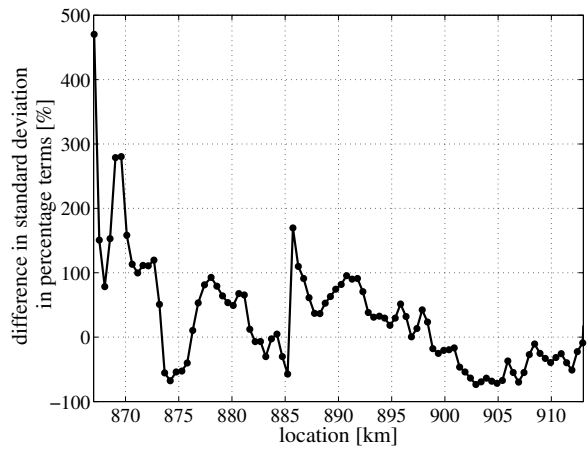
(d) Uncertainty in critical Shields parameter
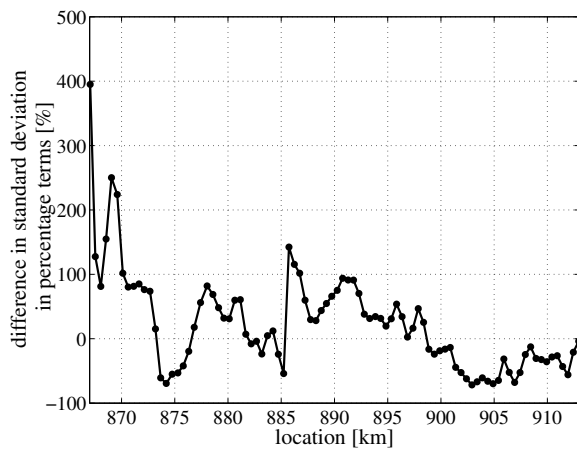
(e) Uncertainty in the exponent of bed shear stress

(f) All sources of uncertainty

Figure 6.35: Difference in percentage terms between the mean values of the standard deviation of the time-averaged bed level for each MCS and the standard deviations of the time-averaged bed level derived from the bathymetric data

and the standard deviations of the time-averaged bed level derived from the bathymetric data is given in Figure 6.35. Apparently, at most locations, the mean standard deviation obtained from each MCS is significantly larger than the standard deviations of the time-averaged bed level of the bathymetric data.

Averaging the mean values of the standard deviation of the time-averaged bed level for each MCS over the length of the river reach results in values that vary in a range of 0.11-0.18 m (see Table 6.4). These values are in the order of 20%-85% larger than the corresponding value derived from the bathymetric data (0.09 m). This discrepancy is not as bad as it may seem, since the bathymetric record is rather short, and therefore does not cover the full range of possible conditions. Moreover, we have to realise that extreme conditions may well have been missed.

The standard deviation of the bathymetric data lies roughly within the 90%-confidence intervals derived from the MCS (Figure 6.34), with exception of the following locations:

- km 867-873: At the Pannerdensche Kop bifurcation, the morphology exhibits large variations. Apparently, these are more pronounced in the model simulations than in the bathymetric data. An empirical nodal-point relation in the model specifies how the sediment transport rates are divided over the outflowing branches of the bifurcation. The distribution of sediment is assumed to be a function of the discharge distribution, but in reality it is rather governed by local two- or three-dimensional flow patterns. We have the impression that the model overestimates the morphological activity, but this requires further investigation.
- km 873-889: Locally, the bed level variation that is derived from the bathymetric data is slightly larger than the computed one. Bottom protection structures at Erlecom (km 873-876) and at Nijmegen (km 882-885) are schematised as fixed layers imposing a lower bound on the bed level in the model. The fixed layers prevent further erosion, resulting in a reduction of the standard deviation. In reality, only the outer bend is protected from scouring, meaning that morphological activity is still present in the inner bend. Hence, the Rhine model underestimates the bed level variation.
  For the same reason, the computed morphological activity immediately downstream of the fixed layers is most probably too large.
- km 900-913: The bed level variation that is derived from the bathymetric data exceeds that of the MCS-computations. Maintenance dredging downstream of location km 900 most likely influences the bathymetry. Maintenance dredging is not incorporated in the Rhine model.

The comparison between the estimated stochastic morphological response and bathymetric data showed that the bed level variability computed with MCS is, in general, much larger (approximately 20%-85%) than the bathymetric data indicate. Because of the inhomogeinity of

the bathymetric data, we had to fall back on a 10-year dataset. The bathymetric record is rather short, and therefore does not cover the full range of possible conditions. Extreme conditions may well have been missed in the 10-year dataset.

	mean σ MCS	mean σ data	difference between MCS and data in percentage terms [%]
Q - river discharge	0.15 m	0.09 m	60%
D - grain size	0.13 m	0.09 m	40%
C - hydraulic roughness	0.11 m	0.09 m	20%
θ_{cr} - critical Shields parameter	0.11 m	0.09 m	20%
α - exponent bed shear stress	0.12 m	0.09 m	25%
all sources	0.18 m	0.09 m	85%

Table 6.4: Averaging the mean values of the standard deviation of the time-averaged bed level for each MCS over the length of the river reach, and the difference in percentage terms between the corresponding value derived from bathymetric data

Still, most of the bed level variability estimated from bathymetric data lies roughly within the 90%-confidence interval derived from the MCS. Large deviations are related either to shortcomings in the model, like the schematisation of bifurcations and bottom protection structures, or to human interventions that are not incorporated in the model, like maintenance dredging.

6.9   Conclusions

We have seen that the hypothetical model in the previous chapter can be used for a quick analysis of the physical system behaviour, but does not reveal various phenomena of interest in real-life situations. Therefore, the hypothetical model is of little use to operation and maintenance practice of real-life rivers. The 1-D Rhine model is run in an MSC-setting, in order to get insight into the uncertainties involved in the morphological predictions of a real-life river. In fact, non-uniformities in the river geometry may lead to the initiation of bottom waves, which migrate downstream, partly decay and interfere with morphological features initiated elsewhere in the river. The result is a complex pattern of morphological behaviour and, correspondingly, a complex propagation of input uncertainties through the system, as we have noticed in this chapter.

The procedure of uncertainty analysis with the 1-D Rhine model, contained the following steps, viz. (1) inventory of the uncertainty sources involved, (2) statistical description of the uncertainty sources and their impact on morphology, (3) interpretation of the MCS results, and (4) comparison with field observations and measurements. The following conclusions can be drawn for each step.

Step 1: Inventory of the uncertainty sources involved

A first ranking of uncertainty sources that are of importance to the 1-D Rhine model was obtained with a global sensitivity analysis. Apparently, the morphological response is most sensitive to the parameters of the sediment transport formula, viz. the exponent of the bed shear stress and the critical Shield parameter. Moreover, sensitivity to the river discharge, the grain size of the bed material and the hydraulic roughness of the main channel, is clearly noticed. The remaining inputs and parameters seem to be of minor importance.

Step 2: Statistical description of the uncertainty sources and their impact on morphology

On the basis of theoretical considerations, data records, expert opinions and literature, either probability distributions of the model inputs were defined, or sets of model inputs were randomly generated by means of resampling techniques.

River discharge - Four different discharge synthesisation methods are evaluated on their capability to reproduce the historical discharge statistics of the Rhine, and to analyse their impact on morphological predictions. Classical probability distribution functions turn out to be less suitable for modelling the natural randomness of discharge time series. It appears difficult to find a multivariate distribution function that properly fits both the maximum, minimum and mean values of the historical record and that also preserves the seasonal dependency of the discharge and the correlation of discharges in successive time intervals. Resampling is a good alternative if one is uncomfortable with the use of theoretical distributions. Resampling departs from classical statistics that is largely based on assumptions regarding the form of a distribution function and its parameters. We recommend the use of resampling techniques to analyse the stochasticity of a morphodynamic river system induced by discharge uncertainty. Either standard Bootstrapping or the more advanced Nearest-Neighbour resampling technique can be utilised.

Grain size of the bed material - The grain size of bed material is statistically described with a bivariate uniform distribution function. The uncertainty in grain size of the Niederrhein appears to have a large affect on the morphological response statistics of the downstream situated Waal. The D_{90} turns out to be of minor importance for the morphological response statistics as compared to the D_{50}.

Model calibration and uncertainty - Tuning parameters in the calibration process of the 1-D Rhine model, viz. the hydraulic roughness of the main channel, and the critical Shields parameter and the exponent of the bed shear stress in the transport formula, are important uncertainty sources for the morphological response.
For the Rhine model, model units have been defined for which roughness coefficients are set such, that the error between water level predictions and observations, at several gauging stations

in the river and under various discharge conditions, is minimised. Just for the Waal branch, this boils down to approximately 368 tuning parameters (16 model units and 23 discharge stages). The resulting optimal roughness parameter set shows a degree of non-uniqueness. Different parameter sets might produce equally acceptable model results. Therefore, the concept that an optimal parameter set exists, loses credibility. The inability to place a reasonable degree of confidence on the estimated calibration parameter values, leaves considerable uncertainty in the model forecasts.

The uncertainty that is involved with the inability to accurately evaluate, in particular, the critical Shields parameter, θ_{cr}, in the Meyer-Peter & Müller (1948)-sediment transport formula seems to be quite important for morphological predictions. The nature of the θ_{cr}-uncertainty does not significantly influence the mean morphological response, but the uncertainty, as such, leads to a large 90%-confidence interval. This interval seems to increase even over the years. Further increase of the θ_{cr}-variance requires more investigation.

Step 3: Interpretation of the MCS results

The interpretation of the MCS results and estimating the relative contribution is not straightforward. The size of the confidence interval varies differently for each uncertainty source, as a function of time and space. It appears that the various contributions to the overall uncertainty do not add up according to the rules of linear error propagation. This may probably be an indication for the degree of non-linearity of morphodynamic river system. However, it may also refer to the presence of correlation structures among the different model inputs. The non-linear behaviour of morphodynamic systems, combined with the time and space dependent signature and the time-lagging effect, presumably results in complex interactions of the various uncertainty sources, ultimately tending to reduce the overall uncertainty.

No sweeping statement on the relative importance of uncertainty sources for the overall uncertainty in the morphological response can be made, because of the demonstrably non-linear behaviour of the river system. It is only through studies such as this one that we can get a better understanding of the interaction of the different sources of uncertainty. Generally speaking, the tuning parameters, turn out to be the most important uncertainty sources for the morphological response. The contribution of the uncertainty in the grain size of the bed material to the uncertain morphological response is negligible. The importance of the discharge to morphology exhibits a seasonal variation, and is more significant at locations with non-uniformities in geometry, whereas at locations in a uniform reach, it is less pronounced.

Out of the various sources of uncertainty involved, we only consider the river discharge in the following chapters. We expect to produce generic knowledge and conclusions on the potential of a stochastic approach in river management practice that also holds in case other uncertainty sources would have been incorporated in the MCS-procedure.

Step 4: Comparison with field observations and measurements

Finally, a comparison between the estimated stochastic morphological response and bathymetric data showed that the bed level variability computed with MCS is, in general, much larger (approximately 20%-85%) than the bathymetric data indicate. By lack of homogeinity of the bathymetric data, we had to fall back on a homogeneous subset. Since this subset covers a period of 10 years only, the bathymetric record does not cover the full range of possible conditions. Extreme conditions may well have been missed in the 10-year dataset.

Most of the bed level variability estimated from bathymetric data lies roughly within the 90%-confidence interval derived from the MCS. Large deviations are related either to shortcomings in the model, like the schematisation of bifurcations and bottom protection structures, or to human interventions that are not incorporated in the model, like maintenance dredging.

Chapter 7

Quasi-3D Waal model

7.1 Introduction

In this thesis, morphodynamic models are run in a stochastic mode to study the stochastic nature of river morphology. Running complex morphodynamic models in an MCS-setting is rather time-consuming. Given that the computational effort per individual simulation differs considerably between 1-D and multi-dimensional models, preference is given to use of a less time-consuming 1-D model approach. The following assumptions are made:

- a 1-D model approach provides general knowledge on the application of stochastic methods in river morphology that can also be of use for multi-dimensional model approaches;

- a 1-D model approach is appropriate to investigate the potential of a stochastic approach in river management practice.

Two different 1-D models are used in this thesis, viz. (1) a hypothetical model having dimensions similar to those of the Waal (Chapter 5), and (2) the more realistic, but also more complex Rhine model (Chapter 6). The 1-D Rhine model is used to investigate the potential of a stochastic approach in management practice of real-life rivers.

The 1-D Rhine model does not discriminate between the left and the right side of the river. The water flow is computed by solving the shallow water equations in one spatial dimension: the model is cross-sectionally averaged. The model produces a width-averaged representation of the morphodynamics of the river bed, meaning that phenomena within the cross-section, such as curvature-induced profile evolution, are not described. This means that two-dimensional features, such as alternate bars, or transverse slopes in bends, are not considered. Neither is the fact that large floodplain areas are located alternately at the left and the right side of the river. Under flood conditions, this may lead to three-dimensional cross-flows over the main channel. In order to investigate to what extent the 1-D model approach is applicable, the step towards a quasi-3D morphodynamic model is made.

A quasi-3D model of the Waal is run in a stochastic mode in this chapter. The model contains locations with large variations in floodplain geometry, bends of moderate curvature and crossings between opposite bends. Hence, the model is appropriate for analysing the importance of multi-dimensional phenomena that are not considered in a 1-D approach, for the stochasticity of the river bed.

The chapter is organized as follows. The step from a deterministic towards a stochastic approach using a Delft3D model is discussed in Section 7.2. In the sections that follow, the next questions are addressed:

1.   What is the importance of phenomena that are not incorporated in a 1-D approach, like the cross-sectional profile evolution imposed by the river alignment, for predicting the stochastic nature of river Waal morphology (Section 7.3)?

2.   What is the physical meaning of the statistics of a width-averaged quantity as compared with those at individual points in the cross-section (Section 7.3)?

3.   How do the statistical characteristics of the width-averaged quantity derived from the quasi-3D Waal model relate to those resulting from the 1-D Rhine model? How can we explain possible differences between the two (Section 7.4)?

The chapter ends with a conclusions on how to interpret the results of the 1-D Rhine model in the light of quasi-3D modelling.

7.2   From a deterministic to a stochastic approach

For the analysis of river bed deformation in the cross-sectional profile, a quasi-3D Waal model, based on the morphodynamic simulation package Delft3D, has been developed by Sloff (2004). The model is described in detail in Section 4.6.3. In Chapter 4, this model is applied in a deterministic way for the purpose of justifying the use a 1-D model approach in this thesis. It has been shown that the 1-D Rhine model provides a first indication of which locations are susceptible to geometrically induced bed level variability and those that are not. Moreover, it is possible to some extent to account for 2D-transverse slope effects by post-processing the numerical 1-D model results. The 1-D model neglects, however, the formation of complex morphodynamic features caused by three-dimensional cross-flows over the main channel, for instance at locations with large floodplain areas that are located alternately at the left and the right side of the river, or at confinements of the floodplains by winter dikes. As outlined in Chapter 4, the bed level variability derived from a deterministic run with the 1-D Rhine model is significantly less than that in the quasi-3D model. Using the quasi-3D Waal model in a stochastic mode must clarify the importance of multi-dimensional phenomena that are not considered in a 1-D approach.

Running the quasi-3D Waal model in an MCS-setting requires an efficient procedure, given the computational effort that is required for a single deterministic simulation (hours or even days). The computational effort is one of the main bottlenecks for applying uncertainty analysis to this kind of model. As outlined in Chapter 4, the morphodynamic model is composed of separate modules, the flow, the sediment transport and the bottom module, of which the flow module requires most of the computational effort. A procedure to reduce the time needed for the laborious flow module is presented in Section 4.6.3. This leads to a significant reduction of the computational effort per individual simulation. The computation time for the entire MCS is furthermore controlled by a carefully chosen sample size. The sample size is fixed at one hundred simulations, which turns out to be sufficient for the convergence of the response statistics.

The morphodynamic quasi-3D Waal model is affected by various uncertainty sources, as outlined in Section 3.3. The cross-sectional profile evolution, like the bed deformation in river bends, is strongly driven by discharge variations. As illustrated in Chapter 5, the river discharge is one of the important sources of uncertainty. For the time-being, the MCS is restricted to the uncertainty in river discharge. Uncertainty sources other than the river discharge are left out of consideration. Bootstrap resampling is applied to construct new discharge time series of 5 years duration, starting from the original 100-year data record, as indicated in Section 6.4. We expect the conclusions drawn in this chapter to also hold for MCS in which other uncertainty sources are considered.

7.3 Stochasticity of the river bed in the cross-sectional profile

7.3.1 Individual points in the cross-sectional profile

The stochastic nature of the river bed in the Waal is analysed on the basis of 100 model runs. We restrict the analysis to the alluvial part of the main channel.

For three longitudinal profiles, namely the river axis and at approximately 125 m left and right of the river axis, the spatial response statistics after 5 years in the high-water season are shown in Figure 7.1. The impact of bends, with a shallow inner and a deep outer bend, is clearly visible in the mean morphological response over 100 model runs (Figure7.1(a)). Bends turn alternately to the left and to the right.
The uncertainty intervals - the standard deviation, the 90%-confidence interval and the absolute maximum bed level difference - in Figure 7.1(b)-(d), give an indication of the variation of the response. The bed level variability appears not to be evenly spread over the cross-section. On average, the intervals for the longitudinal profiles left and right of the river axis are larger than those in the axis. Moreover, the intervals left and right of the axis exhibit stronger fluctuations along the river. This transversal variation in the response statistics is not only induced by

the presence of bends, but can also be attributed to variations in floodplain width, strong confinements of floodplains by winter dikes, and large open water areas and deep ponds in the floodplains, also. Figure 7.4(a) shows that the river alignment of the study area includes all these elements. The open-water areas in floodplains are indicated by gray-coloured spots.
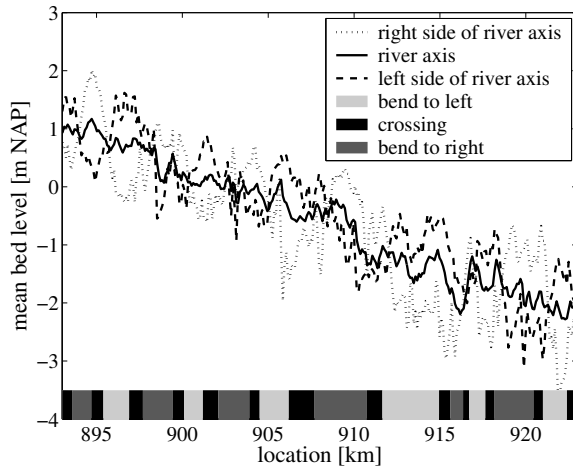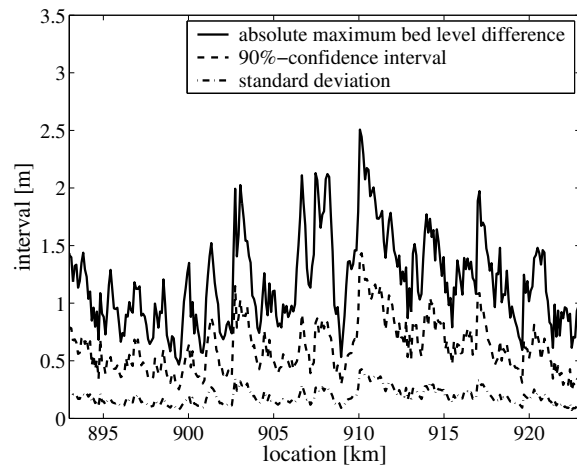

(a) Mean morphological response
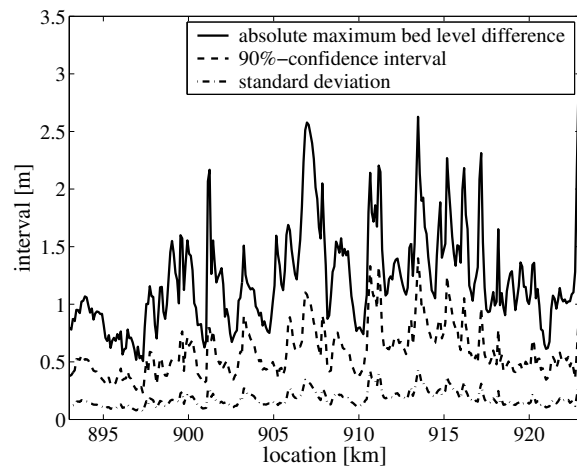
(b) Right side of the river, approximately 125 m of the axis - uncertainty interval
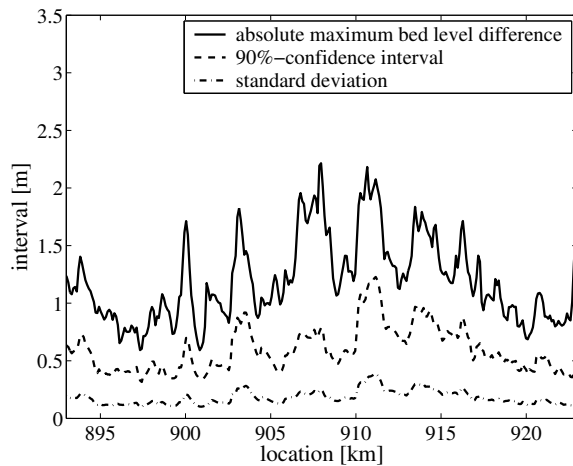
(c) River axis - uncertainty interval

(d) Left side of the river, approximately 125 m of the axis - uncertainty interval

Figure 7.1: Spatial variation of the statistical properties of the bed level response for three different longitudinal profiles in the Waal after 5 years in the high-water season, as computed with the quasi-3D Waal model

Another way of presenting the uncertainty in the morphological response is shown in Figure 7.2. The standard deviation is plotted for the river axis and the profiles left and right of it. This presentation enables coupling the uncertainty to the sinuous and straight sections of the river, along with alternating floodplains and confinements of floodplains by winter dikes.

The variation of the response statistics within the cross-section becomes even more evident if

we consider the temporal response statistics at four different locations, km 896, km 903, km 907 and km 910 (Figure 7.3). First, it can be noticed that locations with strong geometrical non-uniformities (e.g. location km 903, km 907, km 910), have a larger bed level variability than others (e.g. location km 896). The seasonal signature in the confidence interval of the bed level is more pronounced, but it is not evenly distributed over the cross-section. At location km 903 and 910, the 90%-confidence interval at the left side of the river axis strongly oscillates, whereas the seasonal signature is hardly noticed at the right side. In the river axis, the seasonal variation is less pronounced than at the left side. Strong confinements of the floodplains by winter dikes induce cross-flows over the main channel at these locations. Strong cross-flows in the high-water season result in large sediment transport gradients, which enhances the morphological activity. The figure shows the opposite for location km 906, where the bed level variability at right side is larger than that at the left side.
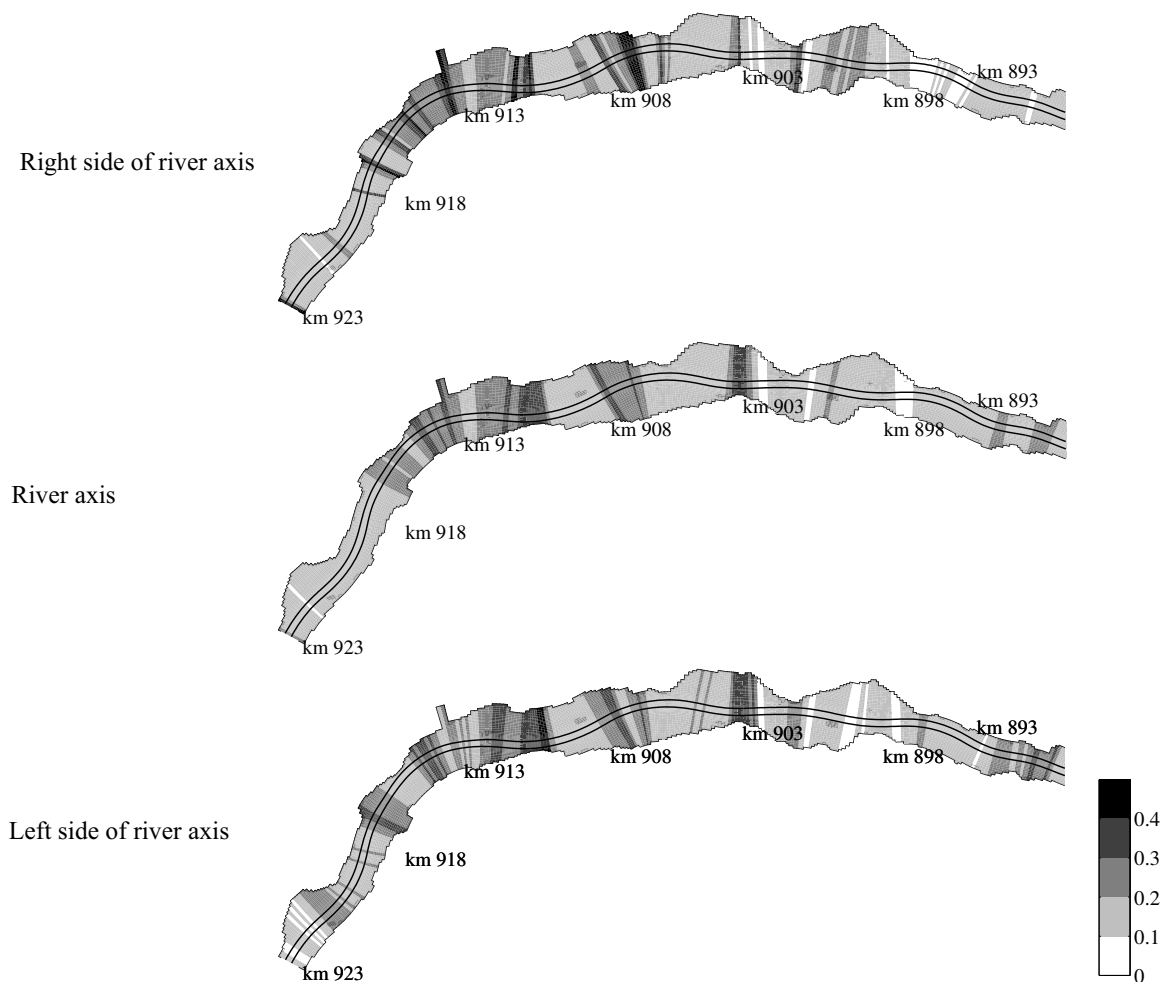

Figure 7.2: Standard deviation of bed level response in the high-water season of the 5th year, along the river at (a) approx. 125 m right of the axis, (b) river axis, (c) approx. 125 m left of the axis, (d) cross-sectionally averaged, as computed with the quasi-3D Waal model
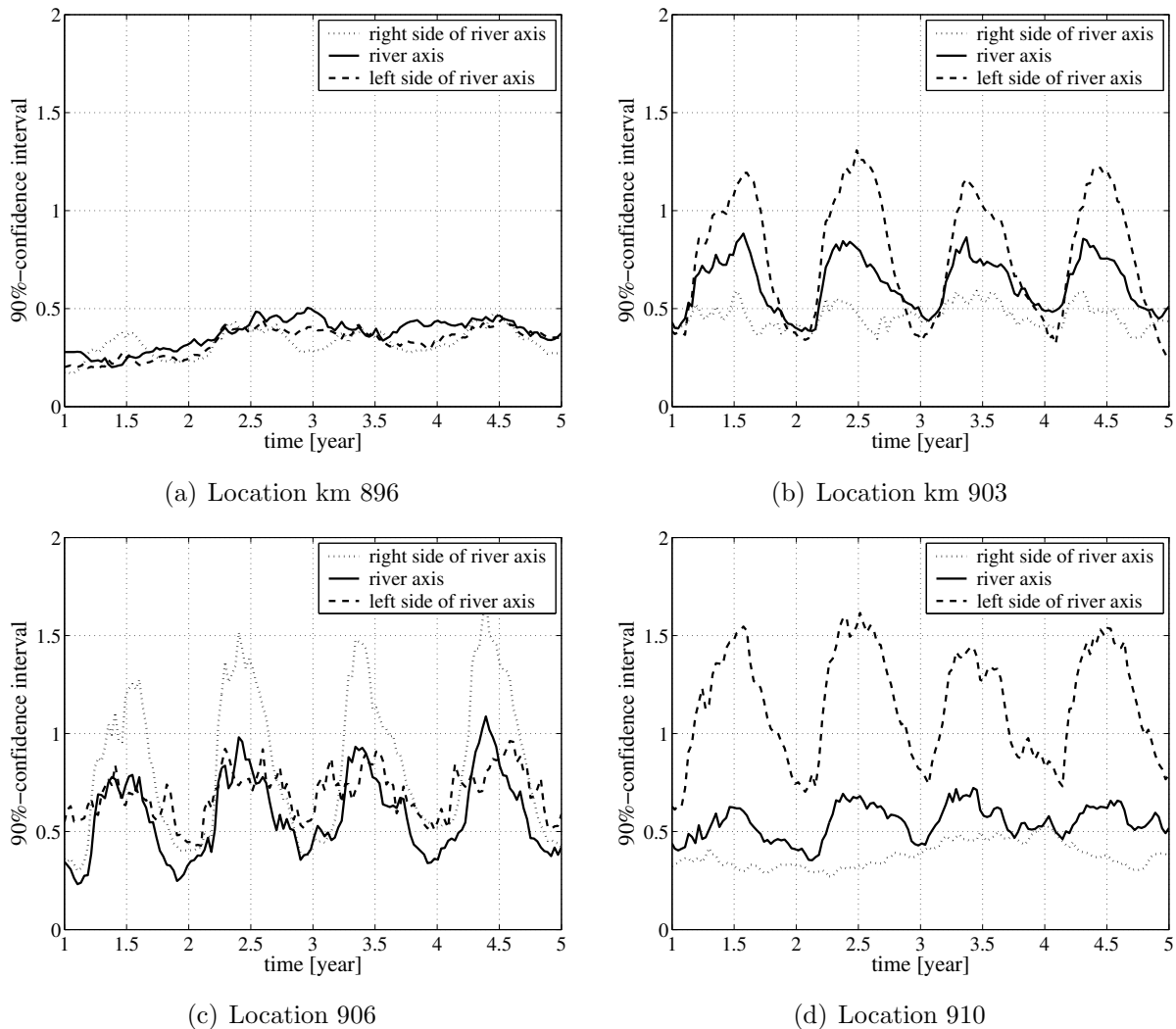
(a) Location km 896

(b) Location km 903

(c) Location 906

(d) Location 910

Figure 7.3: Temporal variation of the statistical properties of the bed level response at four locations in the Waal, as computed with the quasi-3D Waal model, for three different points in the cross-section: at the river axis and approximately 125 m left and right of it

Insight into the morphological response statistics both in time and space is obtained with the time-stack plots in Figure 7.4. As we already noticed, large seasonal variations in the response statistics are found at locations with large non-uniformities in the river alignment. At other locations, this seasonal signature is less (or hardly) noticed. The river alignment in the upper panel makes it easy to link characteristics of the river alignment, like radius of curvature, floodplain width and confinement of the floodplain by winter dikes, to the morphological response statistics. The strong confinements of the floodplains by winter dikes seems to have the strongest effect. Narrow floodplain sections are alternately located left and right of the river. It appears that bends to the right (left) and one-side floodplains located at the right (left) side occur simultaneously. The impact of bends only is hardly noticed in the uncertainty interval. Their impact is, however, dominant in the average response, as can be seen in Figure7.1(a).
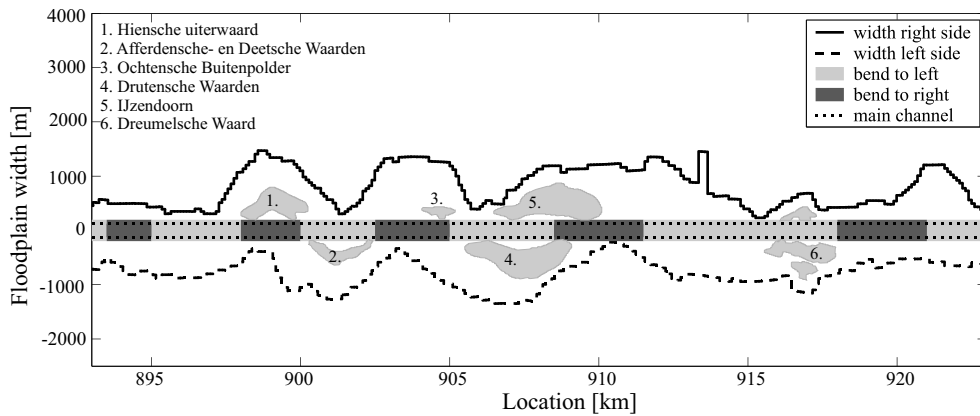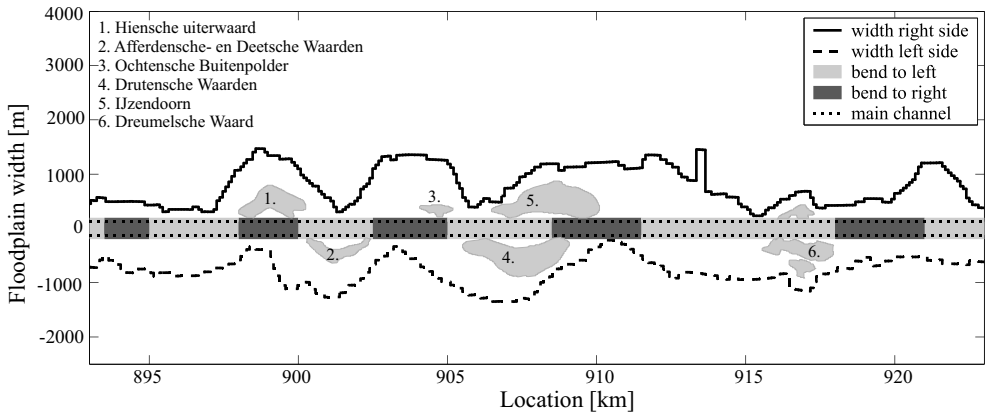
(a) River alignment of the study area
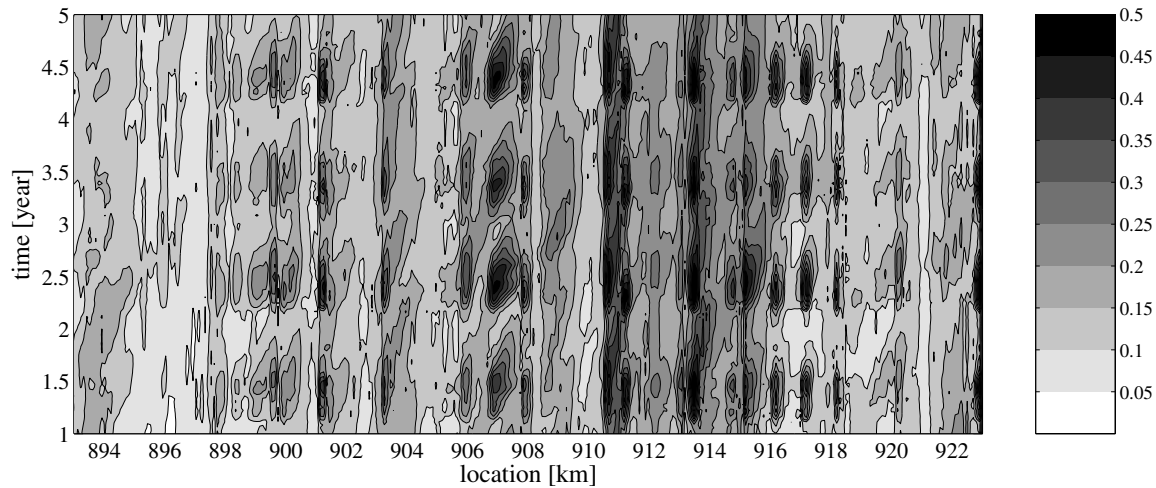
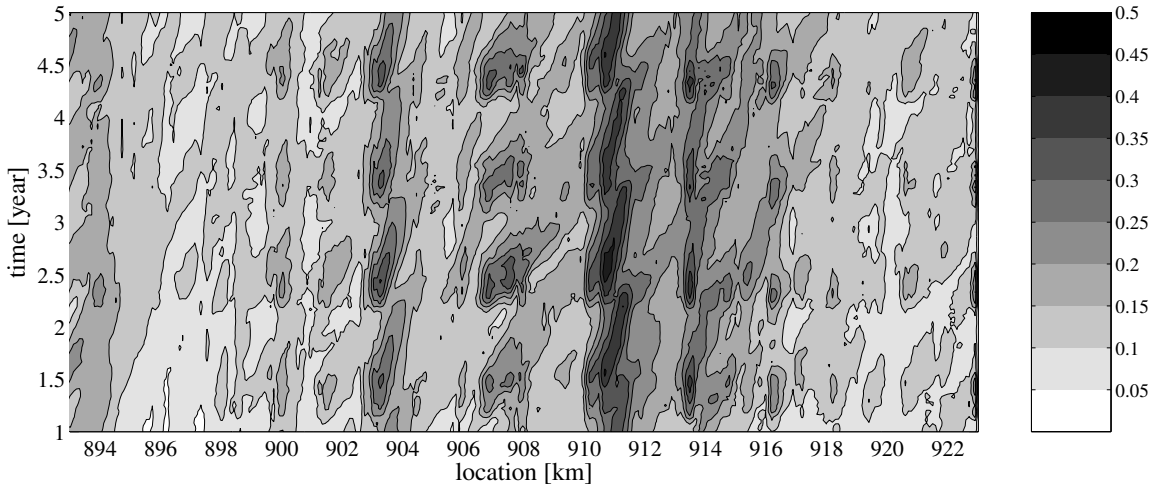(b) Right side of the river, approximately 125 m of the axis
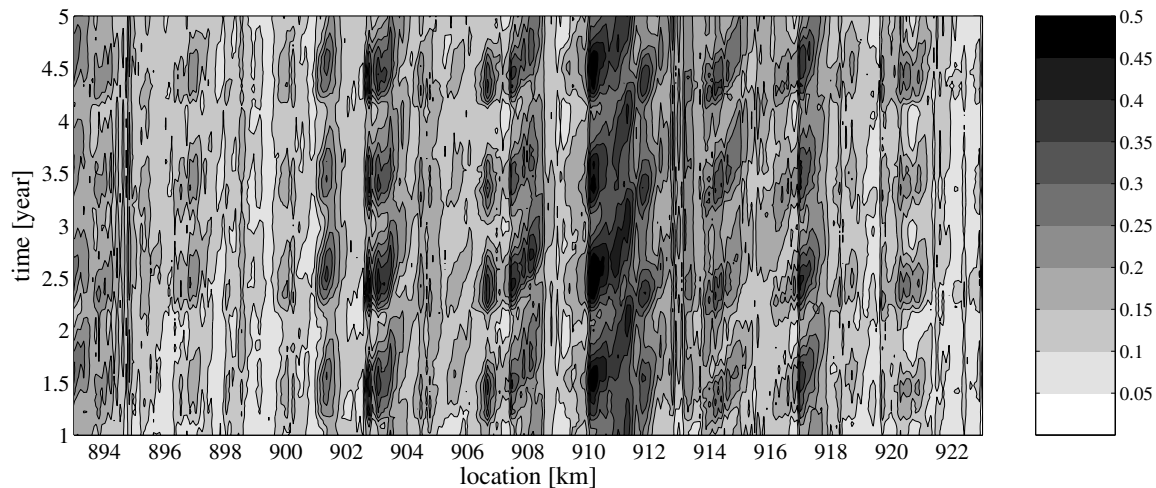
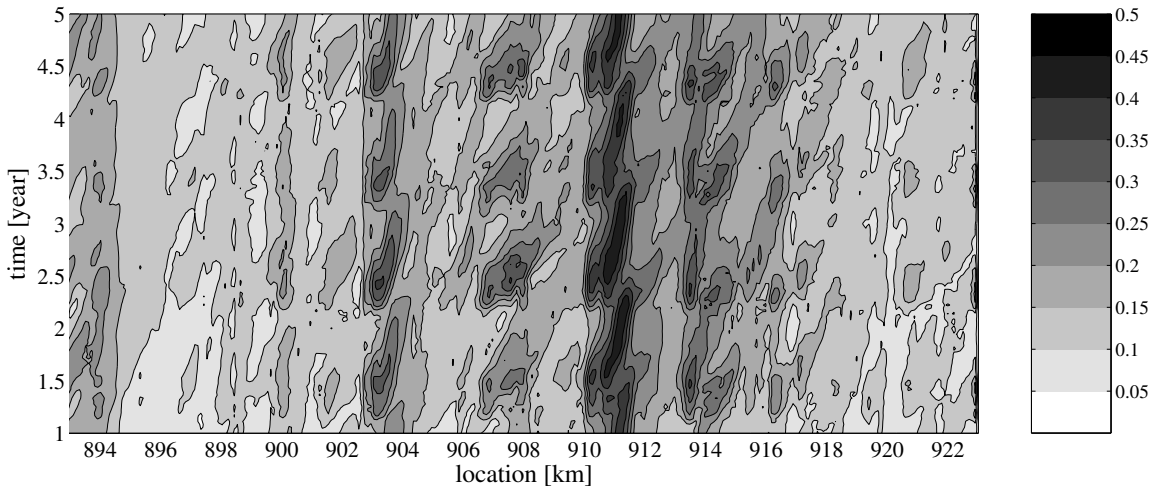(c) Left side of the river, approximately 125 m of the axis

Figure 7.4: Standard deviation of bed level response as a function of time and space, as computed with the quasi-3D Waal model

(a) River alignment of the study area

(b) Cross-sectionally averaged

(c) River axis

Figure 7.5: Standard deviation of bed level response as a function of time and space, as computed with the quasi-3D Waal model

7.3.2 Individual points in the cross-sectional profile vs width-averaged quantity

A 1-D model approach produces a width-averaged representation of the morphological response statistics. In this section, the statistics of the width-averaged quantity per cross-section are derived from the outputs of the quasi-3D Waal model. The statistics are compared with the statistical characteristics at individual points in the cross-sectional profile, in order to assess the physical meaning of the width-averaged quantities.

In the previous section, insight into transversal variation of the morphological response statistics both in time and space (along the river) was obtained from time-stack plots. The standard deviation of the morphological response of the width-averaged response is plotted in a similar way in Figure 7.5. The variations in the standard deviation at either side of the river axis are largely reflected in the statistics of the width-averaged quantity. The standard deviation in the individual points, especially left and right of the axis, however, is much larger than after width-averaging. This is attributed to the averaging-out of relatively large anomalies. The lower panel in Figure 7.5 shows a more or less analogous picture for the standard deviation in the axis. Apparently, the impact of morphological activity at either side of the river axis, extends towards the axis, such that the statistics in the axis are more or less similar to those of the width-averaged quantity.
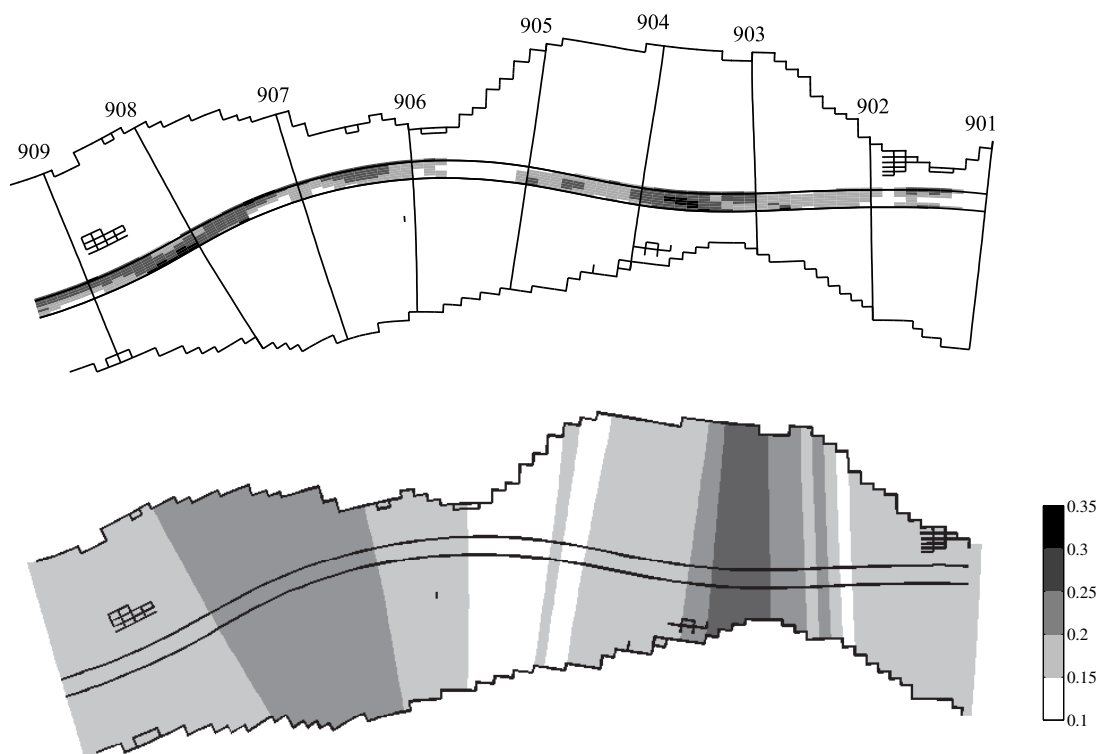

Figure 7.6: Standard deviation of the bed level response over the entire computation period at section km 901-909, within the cross-section (upper panel), and cross-sectionally averaged (lower panel), as computed with quasi-3D Waal model

For two river sections, the variation of the standard deviation over the cross-section is presented in Figure 7.6 and 7.7, along with the standard deviation of the width-averaged quantities. The figures show that the cross-sectional profile evolution imposed by the river alignment is still reflected in the statistical characteristics of the width-averaged quantities. Therefore, we conclude that the width-averaged quantities are practically useful, despite the averaging effect.
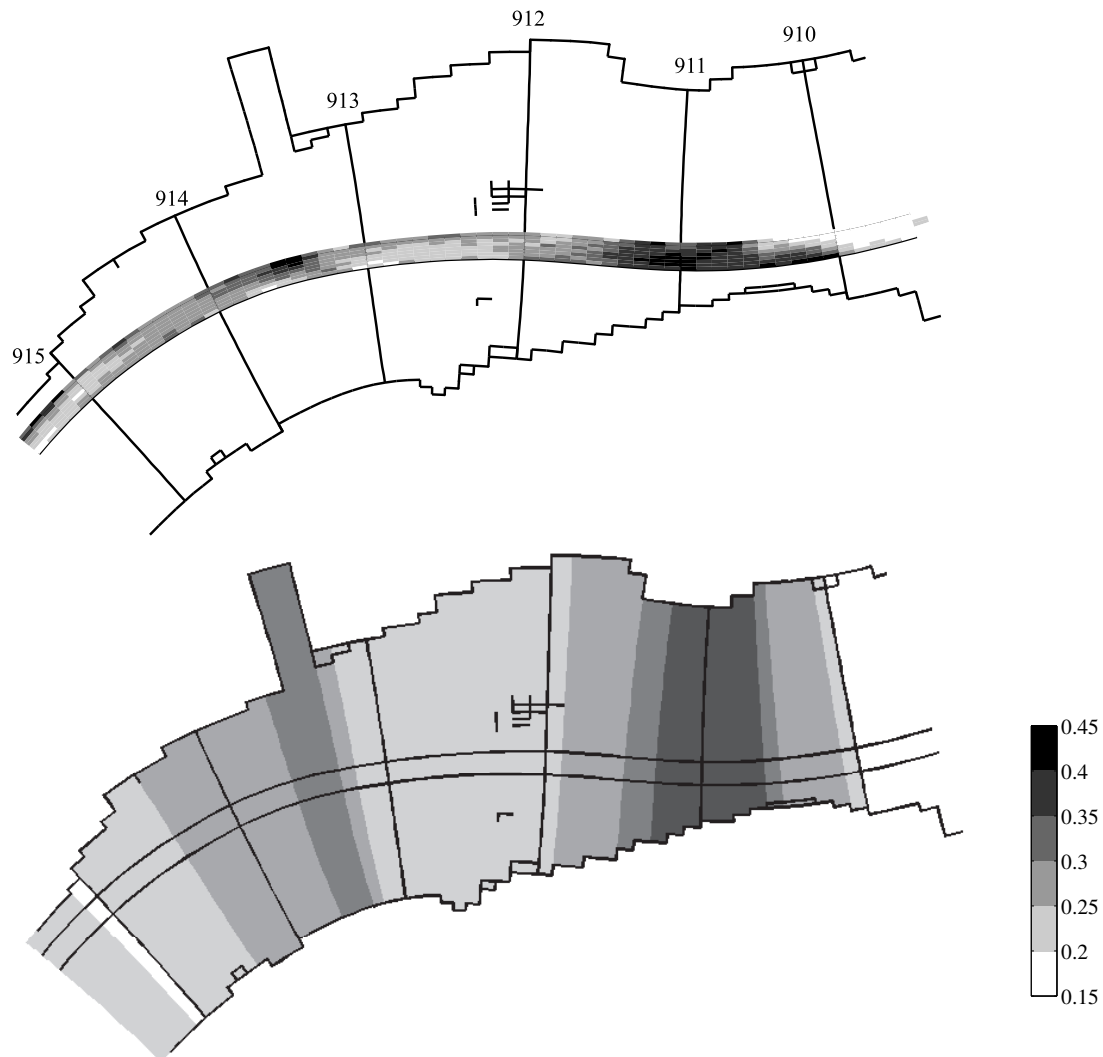
Figure 7.7: Standard deviation of bed level response over the entire computation period at section km 910-915, within the cross-section (upper panel), and cross-sectionally averaged (lower panel), as computed with quasi-3D Waal model

7.4   Quasi-3D Waal model vs 1-D Rhine model

The aim of this chapter is to provide insight into how to interpret the stochastic results obtained with the 1-D model approach, when considering that multi-dimensional morphological phenomena, like cross-sectional profile evolution, are not incorporated. The morphological phenomena

imposed by the river alignment are discernible in the width-averaged response statistics derived from the quasi-3D model, as was shown in the previous section. Yet, this does not guarantee a similar agreement with the 1-D model results. A comparison between the statistics of the width-averaged quantities derived from the quasi-3D Waal model and those of the 1-D Rhine model follows, therefore, in this section.

This comparison is only justifiable if the statistics of the sediment transport volumes along the river in the 1-D Rhine model correspond with those of the quasi-3D model. If the statistics strongly deviate, the morphodynamic processes take place at different speeds, meaning that the morphological response statistics cannot be compared. Figure 7.8 shows a reasonable correspondence between the statistics of the sediment transport volumes of the two models, at least in order of magnitude.

(a) 1-D model - statistical characteristics

(b) 1-D model - uncertainty interval

(c) Quasi-3D model - statistical characteristics

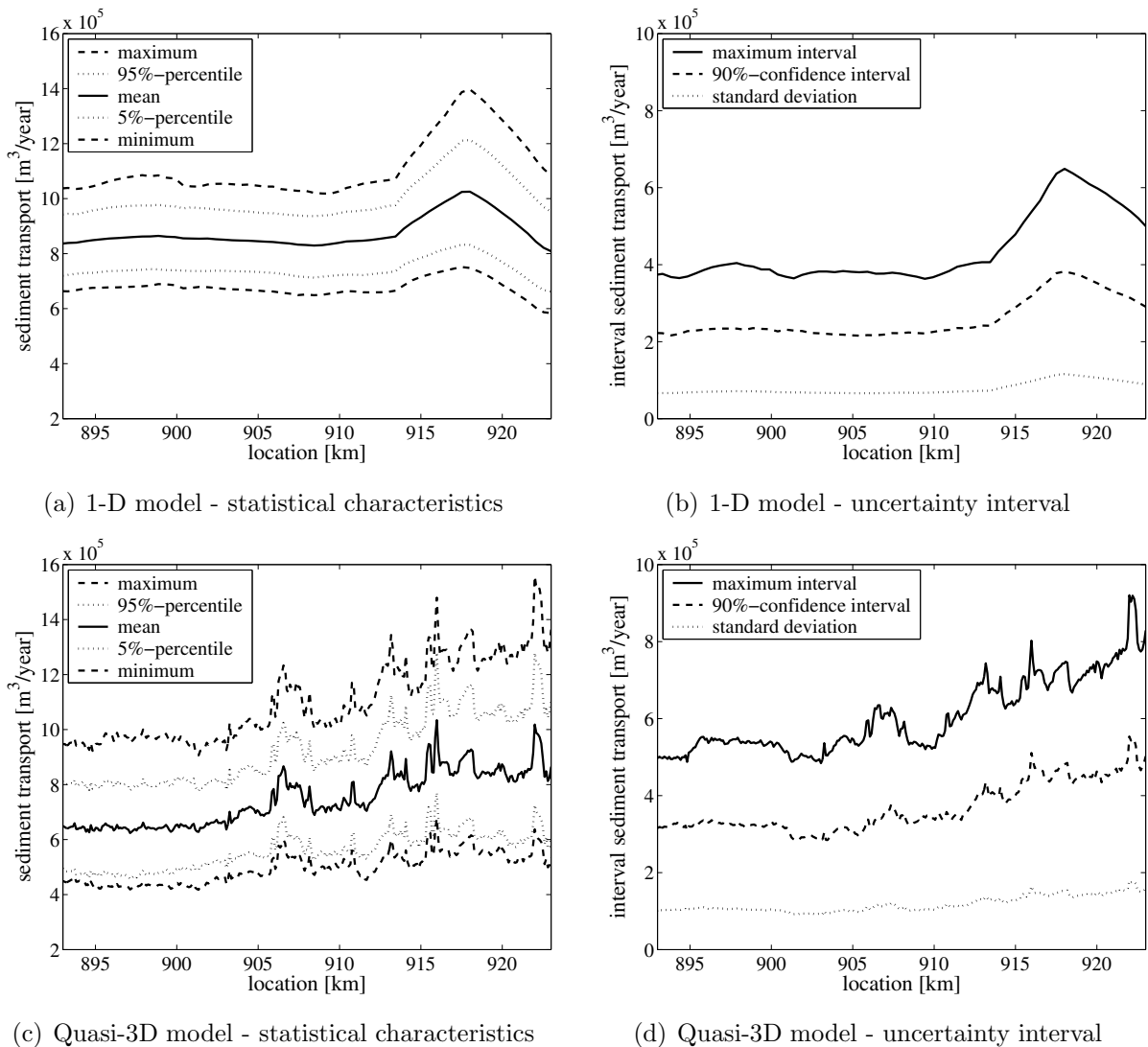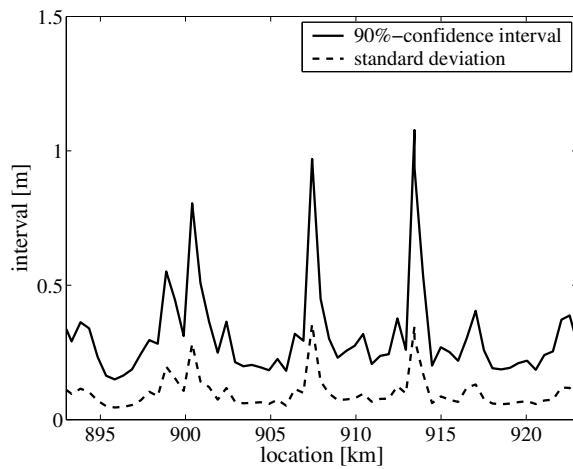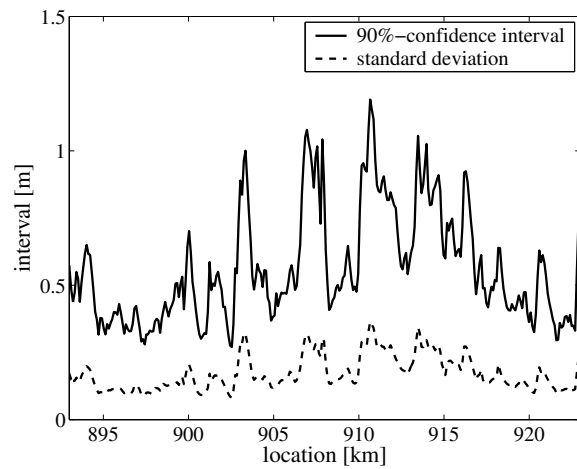(d) Quasi-3D model - uncertainty interval

Figure 7.8: Statistical properties of the sediment transport volume per year along the Waal, as computed with the 1-D Rhine model and quasi-3D Waal model

The statistics of the width-averaged quantities are presented in Figure 7.9. The upper panel gives the uncertainty intervals - 90%-confidence interval and standard deviation - in the cross-sectionally averaged bed level response after a period of 5 years in the high-water season. In the lower panel, the standard deviations of the bed level reponse after 5 years in the dry and high-water season and during the entire 5th year are shown. Apparently, the intervals of the quasi-3D model are significantly larger than those of the 1-D model. This becomes even more pronounced in the time-stack plots of Figure 7.10. Moreover, the variations along the river are more significant in the quasi-3D model.

(a) 1-D model - uncertainty interval after 5 years in the high-water season

(b) Quasi-3D model - uncertainty interval after 5 years in the high-water season
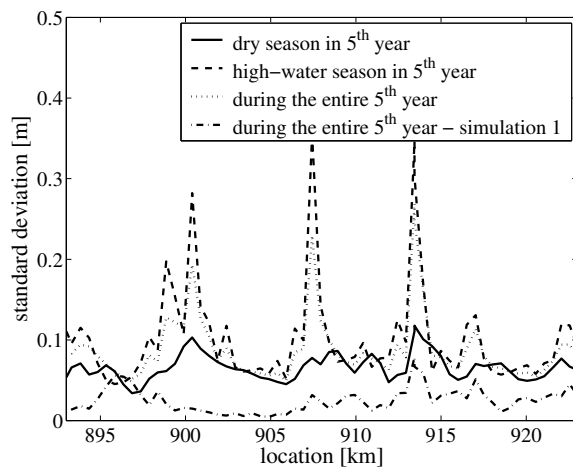
(c) 1-D model - standard deviation
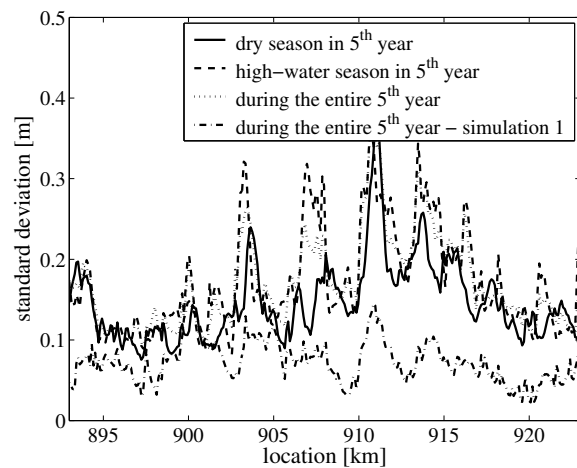
(d) Quasi-3D model - standard deviation

Figure 7.9: Spatial variation of uncertainty intervals for the cross-sectionally averaged bed level response, as computed with the 1-D Rhine model and quasi-3D Waal model
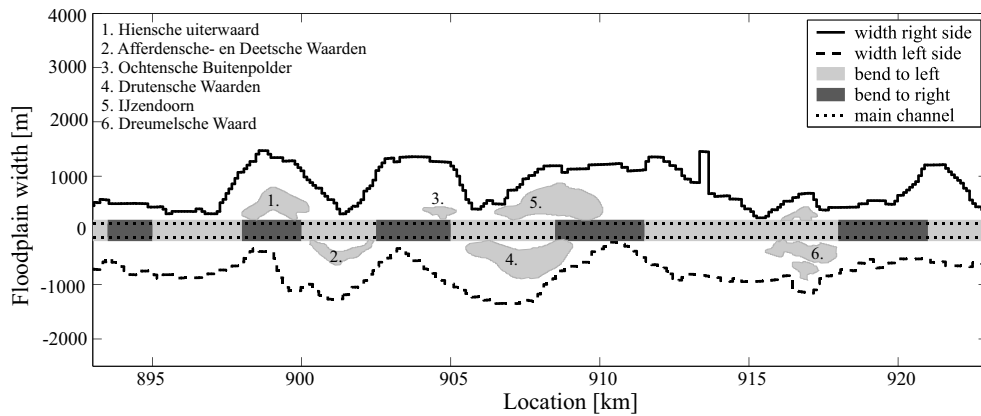
(a) River alignment of the study area
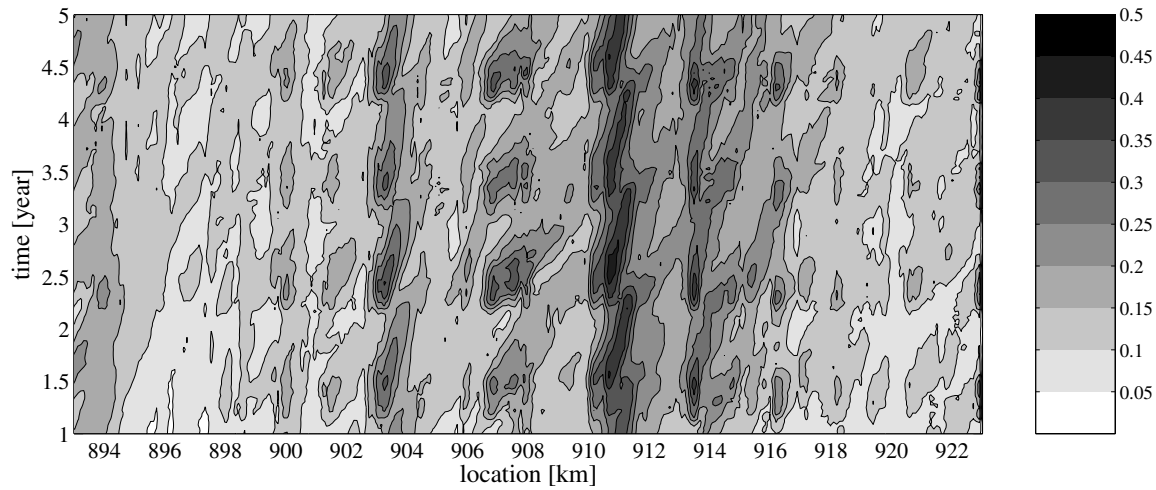
(b) Cross-sectionally averaged response of the quasi-3D Waal model
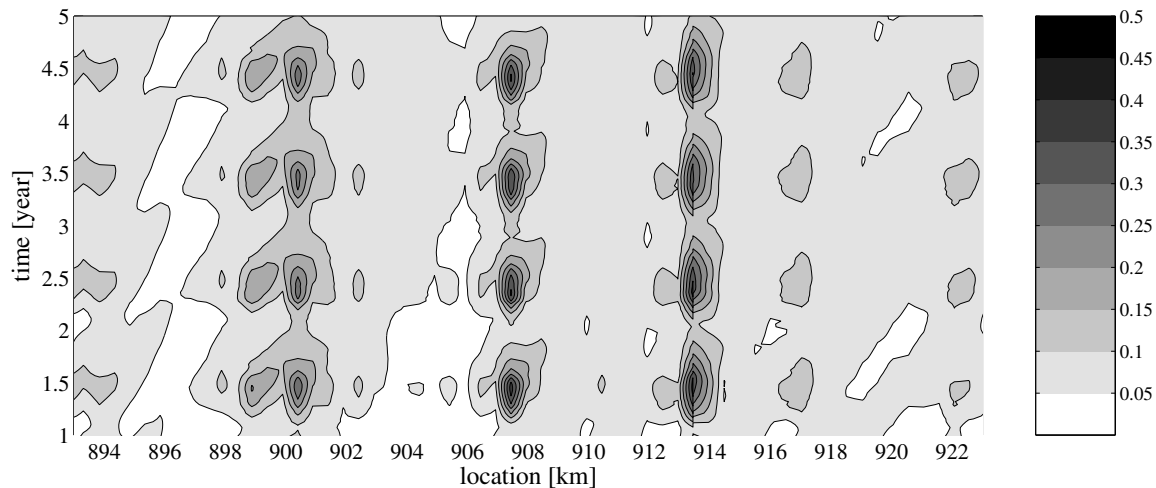
(c) Cross-sectionally averaged response of the 1-D Rhine model

Figure 7.10: Standard deviation of the cross-sectionally averaged bed level response as a function of time and space, as computed with the 1-D Rhine model and quasi-3D Waal model
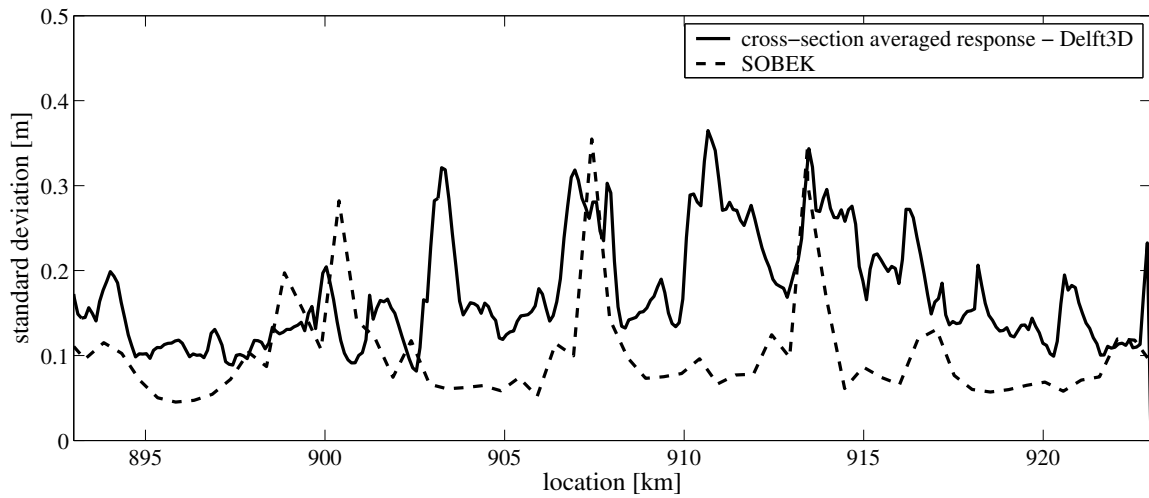
(a) Cross-sectionally averaged response, as computed with the quasi-3D model and 1-D Rhine model
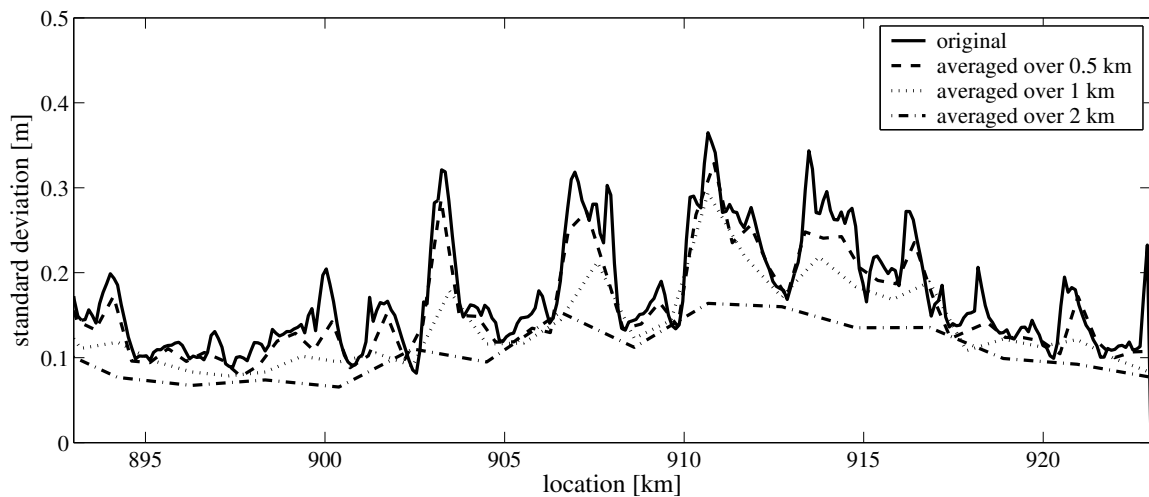
(b) Cross-sectionally averaged response, as computed with the quasi-3D Waal model: original, moving-average response over 0.5 km, moving-average response over 1 km, moving-average response over 2 km

Figure 7.11: Standard deviation of the cross-sectionally averaged bed level response in the high-water season of the 5th year along the river

An explanation for these differences can be found in a combination of the following factors:

1. *Grid resolution*: since the grid resolution of the 1-D model is much less than that of the quasi-3D model, averaging effects must be expected to be stronger in the 1-D model. Morphological phenomena at spatial scales in the order of kilometres can be analysed with the 1-D model ($\Delta x = 500$ m), whereas phenomena at a much smaller scale-level, in the order of hundred of metres, can be observed with the quasi-3D model ($\Delta x = 100$ m).

   The averaging effect is investigated by gradually increasing the grid size along the river axis in the quasi-3D model. The grid size is however not physically enlarged, but

moving-averaged bed positions are derived over a number of grid cells, viz. 5, 10 and 20 cells. Figure 7.11 illustrates that enlarging the grid size leads to a reduction of the uncertainty interval.
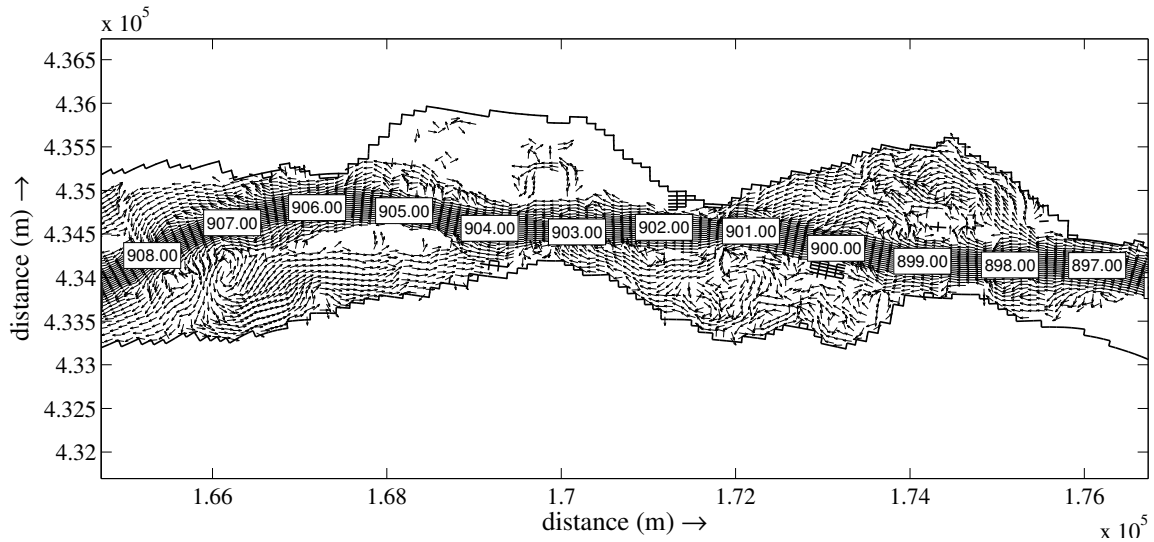
(a) Section km 898-908
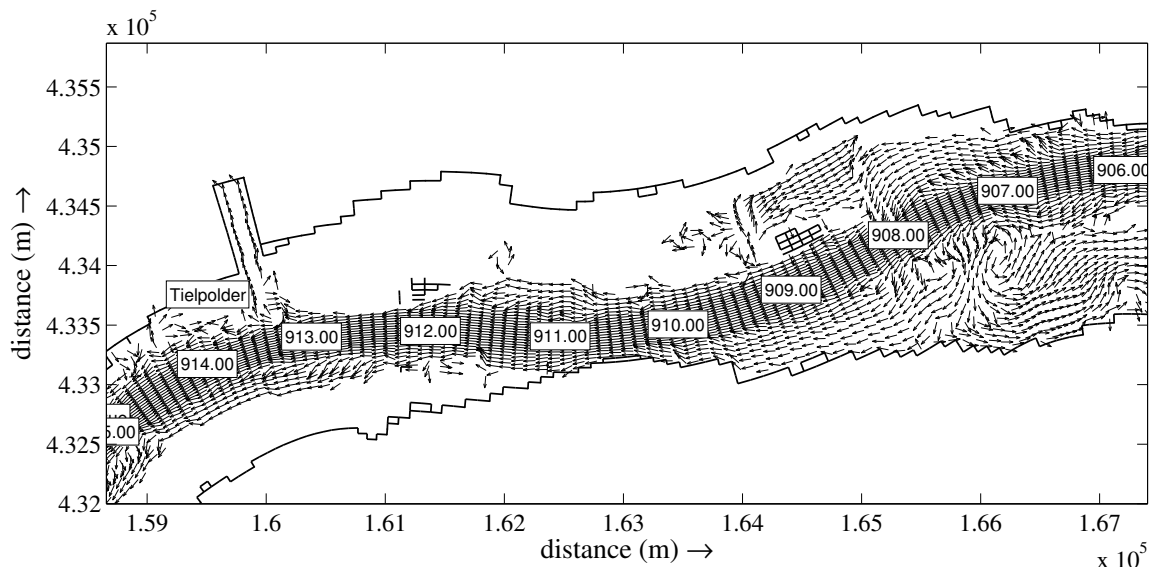
(b) Section km 906-916

Figure 7.12: Flow patterns indicating the depth-averaged flow velocity during a discharge event of 4000 m^3/s, as computed from a single quasi-3D model simulation

2. *1-D versus 2-DH solution of the shallow water equation:* the 1-D model solves the shallow water equations one-dimensionally, cross-sectionally integrated, whereas in the quasi-3D model the equations are solved in two-dimensions. The two-dimensional flow mode (applicable in vertical well-mixed nearly-horizontal flow) is combined with a parametric representation of the curvature-induced secondary flow (quasi-three dimen-

sional). By solving the shallow water equation in a greater detail, flow conditions in regions close to confinements of floodplains, bends and crossing exhibit stronger variations and so enhance the bed level variability. The curvature-induced secondary flow in river bends results in transverse bed slopes and point-bar and pool formation in the inner and outer bend, respectively. As outlined in Section 4.6.4, it is possible to account for this 2D-transverse slope effect to some extent by post-processing the 1-D model results.

3. *Representation of geometrical information*: for the definition of cross-sectional profiles, use is made of topographical maps, digital elevation maps and bathymetric data. The geometrical information left and right of the river axis is averaged in the 1-D model. As a result variations in floodplain width are less pronounced, and strong confinements of floodplains with narrow and wide sections alternately located left and right are not incorporated in the 1-D model. The combination of variation in floodplain width and strong confinements of floodplains, however, induces strong cross-flows over the main channel as indicated by vector plots of flow patterns in Figure 7.12 (derived from quasi 3-D model simulations). The white spots in these vector plots indicate flow patterns that are blocked by either small embankments, areas raised above the high-water level, or other obstacles. The cross-flows results in large gradients in sediment transport that increases the morphological variability. Clearly, these cross-flows are not considered in the 1-D model.

7.5   Conclusions

In principle, river morphology concerns a 3-D problem. However, fully 3-D models are hardly available for river morphology and most problems do not need to be tackled by means of a 'complete' 3-D description. In river engineering practice, 1-D and quasi-3D morphodynamic models, are commonly used. A 1-D model does not discriminate between the left and the right side of a river, and produces a width-averaged representation of the morphodynamic behaviour in a river system. A quasi-3D model incorporates multi-dimensional phenomena, such as time-dependent 2-D river bed deformations, like the curvature-induced profile evolution (pointbar and pool combinations in bends) and the formation of shallow and deep parts alternately at the left and the right side of the river. The major aim of this chapter was to investigate how the results of the 1-D Rhine model could be interpreted in the light of quasi-3D models. Therefore, a quasi-3D model of the Waal is run in an MCS-setting.

It turns out that the response statistics of individual points in the cross-sectional profile along the river do not only exhibit fluctuations along the river, but also a strong transversal variation. This transversal variation in the response statistics is not only induced by the presence of bends,

but must also be attributed to variations in floodplain width, strong confinements of floodplains by embankments and large open water areas and deep ponds in the floodplains. Confinement of floodplains by embankments in the Waal seems to affect statistics the most.

A comparison between the statistics of the width-averaged quantities derived from the quasi-3D Waal model and those of the 1-D Rhine model showed that response statistics of the 1-D Rhine model lag behind. The uncertainty ranges of the quasi-3D model are much larger than those of the 1-D model. Moreover, the variations along the river are significantly larger in the quasi-3D model. The differences can be explained by three factors, viz. (1) grid resolution, (2) detail with which the shallow water equation are solved, and (3) representation of geometrical information. Since the grid resolution of the 1-D model is much less than that of the quasi-3D model, the averaging effect is expected to be stronger in the 1-D model. By solving the shallow water equation in a greater detail in the quasi-3D model, flow conditions at locations with geometrical non-uniformities exhibit stronger variations and thus enhance the bed level variability. Finally, non-uniformities in cross-sectional profiles have been reduced in the 1-D model, by averaging geometrical information left and right of the river axis and defining symmetrical cross-sections.

The applicability of either a 1-D or a quasi-3D model approach depends on the type of problem and the degree of detail that is required, both in terms of resolution and in terms of physical processes. For many relevant questions, a 1-D model approach is practically useful, despite its inherent limitations, to give sufficient insight with considerably lower computation effort. For the strategic planning of an entire river basin, a 1-D model approach is appropriate to provide a first insight into the river system response, for instance, induced by engineering works. In a later stage, a more advanced type of model might be more appropriate to study the impacts of engineering works at locations of special interests. To some extent, problems related to cross-sectional profile evolution, can be studied with a 1-D model approach in combination with analytically based post-processing to account for the 2D-transverse slope effect. A correction for the bed deformation in river bends alone may not be sufficient, since the morphological activity induced by strong cross-flows, at locations where floodplains are confined by winter dikes, seems to be more important for the stochasticity of the river bed. For more detailed types of problems a quasi-3D model is therefore recommended.

As this thesis focuses on a first assessment of stochastic methods in river morphology, the less time-consuming 1-D model approach is mostly taken for practical reasons in the next chapters, be it with incidental comparisons with multi-dimensional models. We expect to produce generic knowledge on the potential of a stochastic model approach in river management practice, obtained with the 1-D approach, that holds also for multi-dimensional model approaches.

Part three: Potential of Monte Carlo Simulation in river management practice

Chapter 8

Morphological impact of river engineering works in the Rhine

8.1 Introduction

The stochastic nature of Rhine river morphology is studied in the previous three chapters, by means of running numerical morphodynamic models in an MCS-setting. This procedure appears to be rather time-consuming, in particular for MCS with multi-dimensional morphodynamic models. The advantages of stochastic methods need to be clearly exposed, in order to contribute to a better insight into the potential of using this 'computational-intensive' approach in river management, including the design of measures, operational forecasting and maintenance of the river system.

In this chapter, we discuss the use of stochastic modelling of river morphology to assess the impact of new engineering works on the morphological evolution of the river system. We will show how a stochastic approach can be useful to assist the river engineer in optimising the design of engineering works. For the purpose of illustration, we consider river improvement measures as proposed in the Room for the River (RfR) scheme, meant to accommodate a higher design discharge in the Rhine.

8.2 Room for the River-scheme

A large part of the Netherlands is located below sea level and below the water levels of the major rivers. Flood defences have been built along coasts and rivers, to make and keep the Netherlands inhabitable. Traditionally, dikes used to be reinforced and heightened to protect the country from ever higher flood levels. Recently, the Netherlands government has adopted the Room for the River (RfR) policy (Silva et al., 2001), which boils down to 'no dike strengthening, unless.....'. It focuses on measures to increase the flood conveyance capacity, such as lowering of groynes and floodplains, implementation of secondary channels and detention basins, removing

obstacles and setting back river dikes (Figure 8.1). As compared with dike reinforcement, these measures may have a stronger impact on flow and sediment transport fields, thus stronger morphological effects.
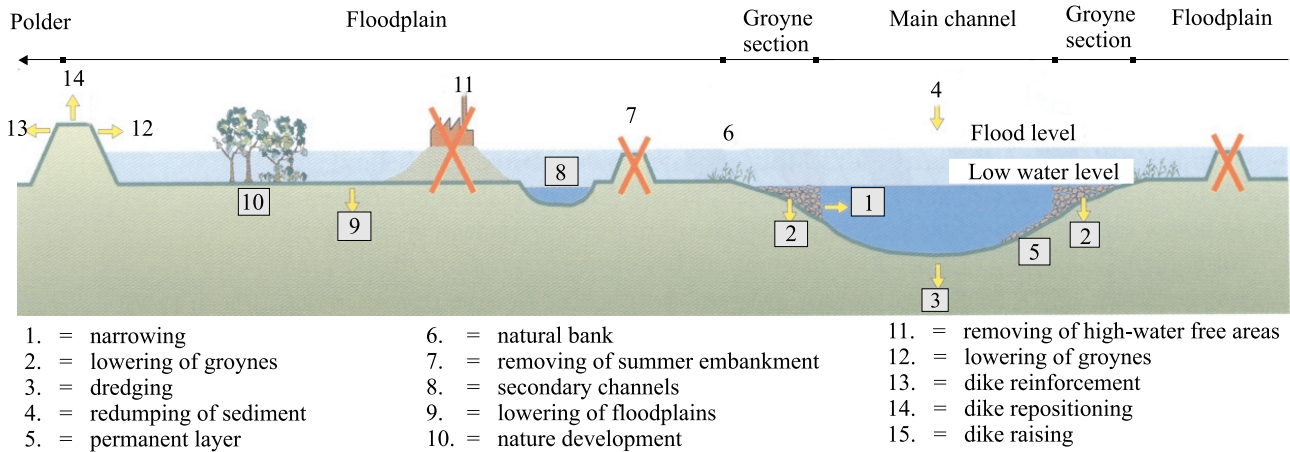

1.	=	narrowing	6.	=	natural bank	11.	=	removing of high-water free areas
2.	=	lowering of groynes	7.	=	removing of summer embankment	12.	=	lowering of groynes
3.	=	dredging	8.	=	secondary channels	13.	=	dike reinforcement
4.	=	redumping of sediment	9.	=	lowering of floodplains	14.	=	dike repositioning
5.	=	permanent layer	10.	=	nature development	15.	=	dike raising

Figure 8.1: Measures proposed in the Room for the River study in the Netherlands (Silva *et al.*, 2001)

The RfR-scheme is not purely a flood protection scheme, it has two main objectives, viz. (1) increasing the river's flood conveyance capacity, and (2) improving the spatial quality by means of nature development.

In this chapter, two case studies are considered:

- Lowering floodplains along the Waal (Section 8.4);
- Combination of RfR-measures in the Rhine (Section 8.5).

The extent to which these river improvement measures affect the morphology and enhance the bed level variability, relative to a reference situation with traditional dike reinforcement, will be investigated for different design alternatives.

8.3   Method

Although we consider a multi-dimensional morphodynamic problem, we use the 1-D Rhine model to analyse the hydraulic and morphological changes in the river system. By doing so, we neglect the 2-D phenomena such as the asymmetry of river cross-sections and the cross-sectional profile evolution. Moreover, the lateral sediment exchange between the main channel and the floodplains is neglected. All sediment transport is assumed to take place through the main channel. The reason for using the 1-D Rhine model, is that the major aim is not to exactly predict the stochastic morphodynamic response to engineering works, but rather to have a quick insight into the potential of a stochastic approach in the design stage of engineering works.

From the various sources of uncertainty involved in the 1-D Rhine model, we only consider the uncertainty in the river discharge. MCS is utilised to quantify the uncertainty in the morphological response to the river improvement measures in the case studies. For each model run, a new discharge time series is constructed by means of Bootstrap resampling, as indicated in Section 6.4. The seasonal dependency of the discharge (dry season with low discharges in summer, high-water season with floods in winter) and the correlation of discharges in successive periods are taken into account. On the basis of the outputs of all model runs, the morphological response statistics (e.g. the expected value and 90%-confidence band of the bed level change) are analysed. A sample size of 500 turns out to be large enough to have sufficiently converged output statistics.

8.4 Lowering floodplains along the Waal river

8.4.1 Cases

This case study focuses on the impact of large-scale floodplain lowering along the Waal river (see Van Vuren & Van Breen (2003)). Three cases are considered (see Figure 8.2):

1. reference situation showing the further evolution of the system without any additional human intervention;
2. case with floodplain lowering. Over a distance of 45 km (river section km 885-930), the floodplains are lowered by 1.5 m;
3. case similar to case 2, but with the summer levees removed.

In addition to the hydraulic effect of lowering the water level in the main channel, floodplain lowering induces a morphological response. The long-term and large-scale morphological response in the main channel of the Waal as a result of floodplain lowering with and without the removal of summer levees is analysed. 'Long-term' refers to periods of several decades up to a century. 'Large-scale' refers to spatial development of the order of ten to hundreds of kilometres.

The morphological response to large-scale floodplain lowering depends on the following factors:

- Lowering the floodplains: Depending on the flow stage, lowering the floodplains will influence the discharge distribution between the floodplains and the main channel: a greater part of the discharge will be conveyed through the floodplains. This inevitably has morphological consequences. It seems logical to assume that the morphological response will increase in magnitude as the floodplains are lowered more.
- Rate of accretion in the floodplains: The rate of accretion in the floodplains may increase, due to the increased lateral sediment transport into the floodplains caused by changes in the discharge distribution, and due to the increased trapping efficiency of the lowered floodplains. Therefore, floodplain lowering is not a self-sustaining measure.

Without any countermeasures, the situation of the past is likely to be restored in the long run.

- Nature development and (re-)landscaping in the floodplains: Nature development is another important function of the floodplains. Nature development is incorporated in the (re-)landscaping programs, which tend to replace the traditional agricultural land in the floodplains by various types of more natural vegetation. This entails an enhanced hydraulic roughness, which usually increases as the vegetation grows, thus counteracting the effect of floodplain lowering on the discharge distribution between the main channel and the floodplains.
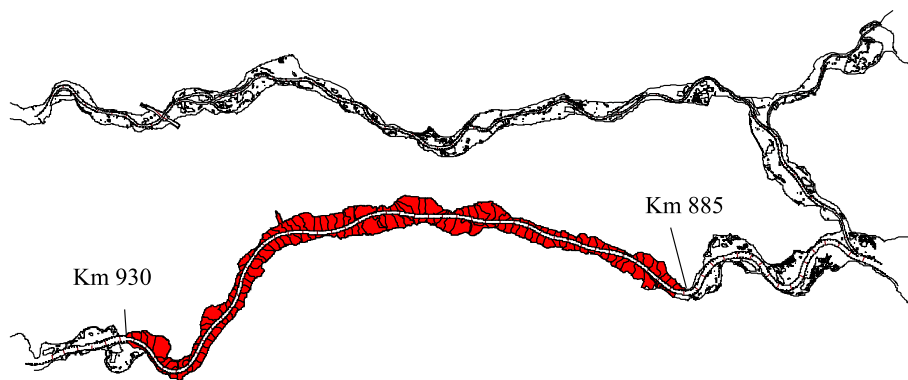
(a) River section in which the floodplains are lowered by 1.5 m
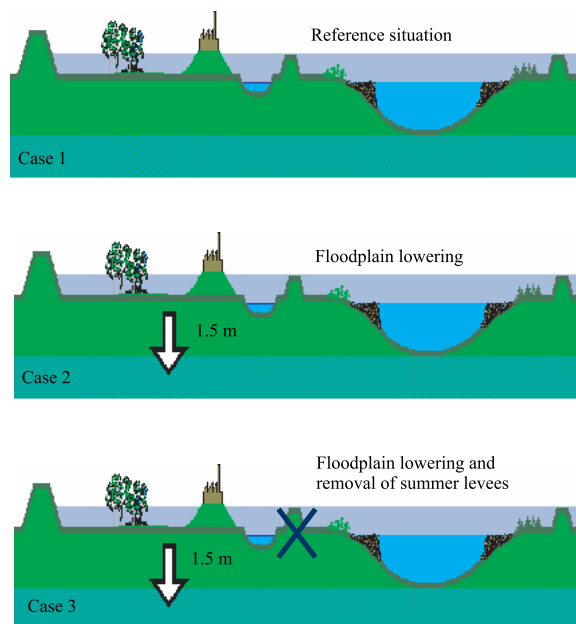
(b) Cases

Figure 8.2: Case study - Impact of large-scale floodplain lowering along the Waal

In this case study, it is assumed that the floodplains are lowered instantaneously, after which their level is maintained. In this way, the extra sediment transport into the floodplains is neglected. Nature development and (re-)landscaping of floodplains is not incorporated in the analysis. The type of vegetation in the floodplains is assumed to be the same before and after lowering.

8.4.2 Impact on morphological response statistics

Figure 8.3 shows the morphological response statistics in the main channel for the three cases after 100 years in December. The figure presents the mean bed level changes and the (size of the) 90% confidence interval of the bed level changes in the Waal section between the Pannerdende Kop (km 886) and Tiel (km 915). The 90% confidence interval means that with a probability of 90% the bed level changes are within this range. Note that the lines of the confidence interval represent the envelopes of all realisations. As can be seen from Figure 8.3(a), the bed level of the main channel gradually decreases over the simulation period. The size of the confidence band is an indication for the variation of the response.

In Chapter 6, we have shown that the bed level in the existing situation already exhibits a strong spatial and temporal variation. Uncertainty due to the inherent variability of many model inputs in time and space, along with the lack of complete understanding of the processes involved, leads to an uncertain morphological response. The stochastic approach does not only show that many morphological states are possible. It also shows that in some reaches this uncertainty is more pronounced than in others, mainly due to strong spatial changes in geometry, such as bifurcation points, width variation in floodplains and the presence of hydraulic and man-made structures.

Lowering floodplains and maintaining summer levees results in a similar response as in the reference situation (dashed line in Figure 8.3(a)-b). The summer levees keep the flooding frequency of the floodplains from increasing. Occasionally, when the water level exceeds the crest level of the levees, flooding occurs and the degree floodplain lowering will have an effect on the morphological response. Due to the low frequency of occurrence of this situation , it has little effect on the total morphological response.

Lowering the floodplains combined with removal of the summer levees has a much stronger effect on the morphological response (dashed-dotted line in Figure 8.3(a)-b). It leads to more frequent and more extensive flooding of the floodplains, whence the impact is more pronounced. With respect to the reference situation, sedimentation takes place in the main channel of the lowered reach. Not only does the mean bed level increases at the location of the floodplain lowering, also the size of the confidence interval increases.
The latter is also noticed in Figure 8.4 that shows the cumulative distribution and density distribution of the bed level response at location km 907.4, for the reference situation and the

situation with floodplain lowering and removal of summer levees. A shift to the right of the probability distribution (in the left panel), indicates sedimentation in the main channel of the lowered reach with respect to the reference situation. A reduction in steepness of the distribution curve shows an increase in uncertainty involved in the morphological evolution. This can also be noticed in the wider density function shown in right panel of the figure. Furthermore, the uncertainty about the morphological effect in situation with floodplain lowering and summer levees removal, where the bed level is more effected by flooding of the floodplains, is more skewed than in the reference situation.

(a) Morphological response statistics

(b) 90%-confidence interval

(c) Difference in mean morphological response with respect to reference situation

(d) Difference in 90%-confidence interval with respect to reference situation
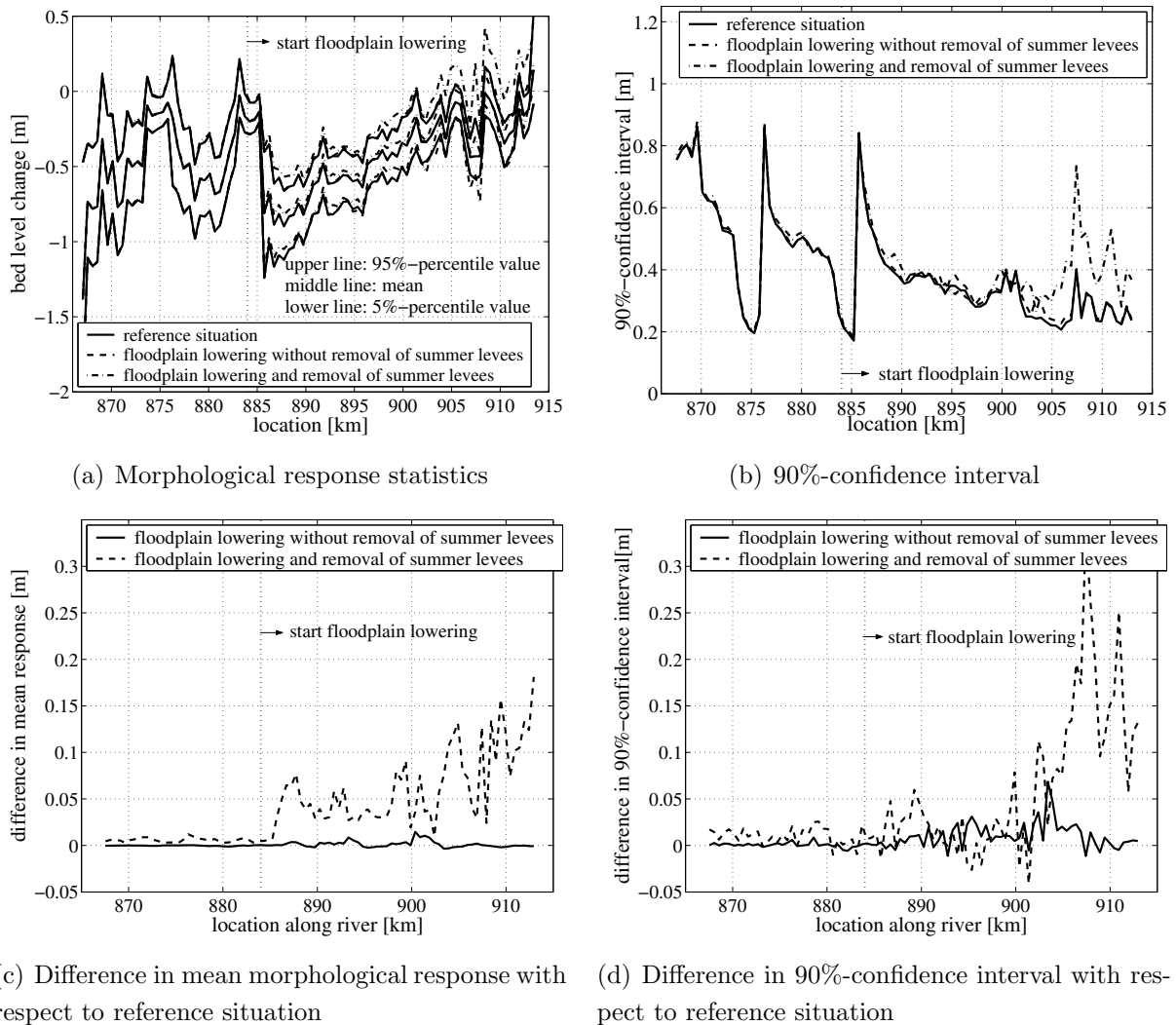
Figure 8.3: Spatial variation of the statistical properties of the cross-sectionally averaged bed level response in the Waal in December of the 100th year, as computed with the 1-D Rhine model

Figure 8.5 shows the impact of floodplain lowering combined with summer levee removal on the temporal variation of the response statistics. The seasonal fluctuation of the confidence interval becomes more pronounced, especially at locations with large geometrical non-uniformities, such as km 907.4. Apparently, the temporal response statistics at more or less uniform river sections,

like km 895.3, are less influenced by the intervention.

(a) Cumulative probability distribution function

(b) Probability density function
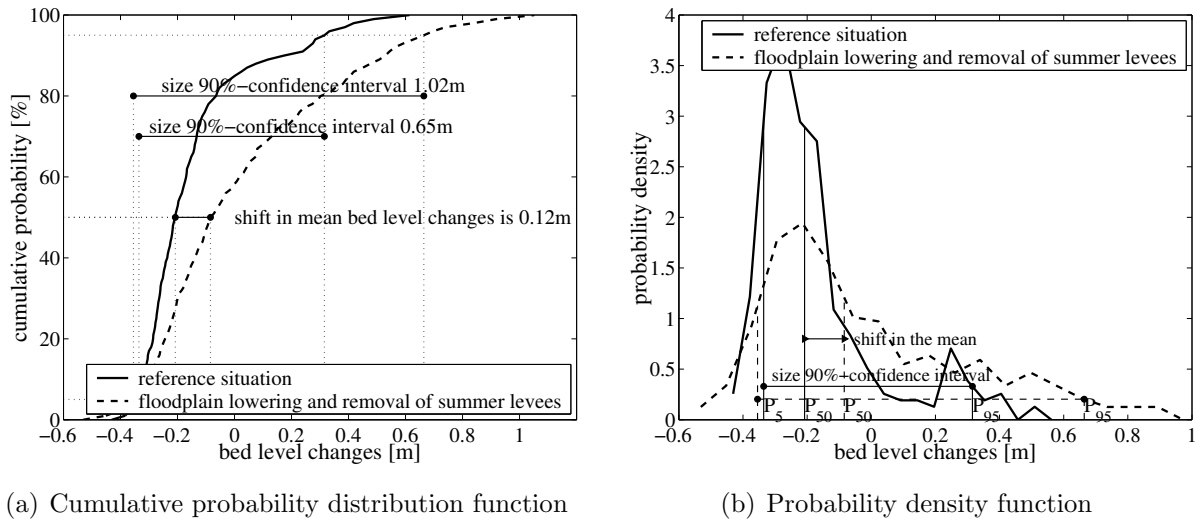
Figure 8.4: Cumulative probability distribution and density function of the cross-sectionally averaged bed level response at location km 907.4 after 100 years for the reference situation and the situation with floodplain lowering and removal of summer levees, as computed with the 1-D Rhine model

(a) Location km 907.4

(b) Location km 895.3
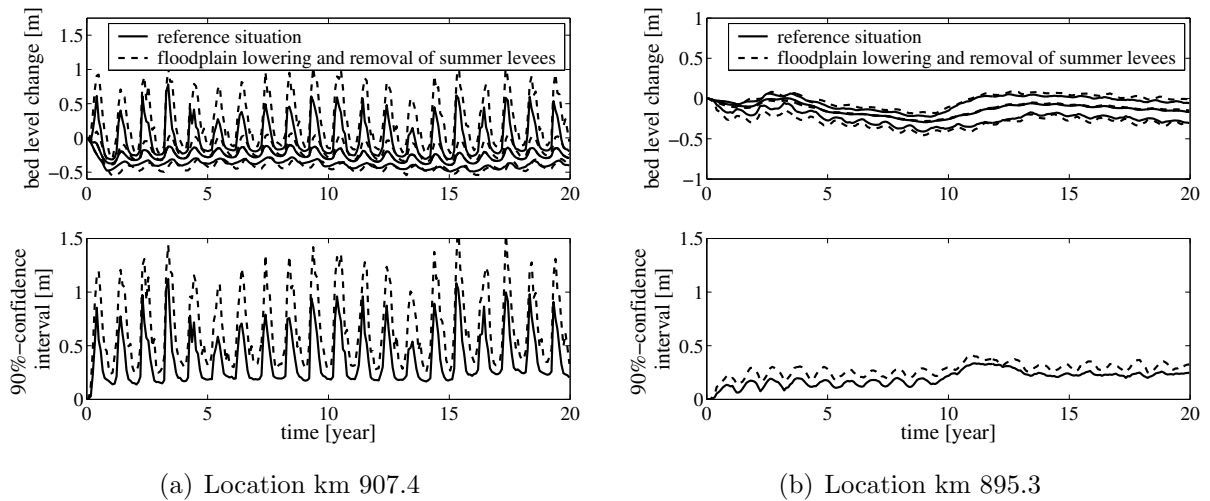
Figure 8.5: Temporal variation of of the statistical properties of the cross-sectionally averaged bed level response at two locations in the Waal, as computed with the 1-D Rhine model

8.4.3 Conclusions concerning the morphological effects of floodplain lowering

The stochastic approach offers a different perspective on the morphological response to floodplain lowering and summer levee removal at different locations along the Waal. It shows that many morphological states are possible. Furthermore, it shows that at some locations the impact of identical engineering measures is more pronounced than at others (in terms of mean response, bed level variability, and possibly seasonal variation).

If floodplains are lowered and the summer levees are maintained, the response is similar to the reference situation, because of the frequency of flooding of these floodplains does not increase. If floodplains are lowered and the summer levees removed, the morphological response is much stronger, due to the more frequent flooding. Not only does the mean bed level increase at the location of the floodplain lowering, also the size of the confidence band increases and has more pronounced peaks. The latter occurs especially in the river sections with large geometrical non-uniformities. In order to avoid a strong morphological response with a large variability and uncertainty, the summer levees would better be maintained. However, there might be a subset of the summer levees that could be removed without having a large adverse effect.

8.5   Combination of RfR-measures in the Rhine

8.5.1   Cases

Using only one type of measure for the entire river, e.g. floodplain lowering over a distance of 45 km, as considered in the previous section, will not be the optimal solution for each of the individual river sections. As mentioned above, at some locations the impact of a certain measure is more pronounced than at others. Moreover, some of the measures in Figure 8.1 appear to be only of use in upstream parts of the river (lowering of groynes, floodplain lowering; also see (Silva et al., 2001)), whereas others are more feasible downstream, like dredging of the main channel. At urban bottlenecks, where urbanisation at either side of the river leaves no room for floodplains, the local flood conveyance capacity is low and floods create high water levels. Such bottlenecks can either be removed, e.g. by dike set-back, or by-passed via so-called green rivers inland of the main dikes.

From a cost-effectiveness point of view, dike strengthening turns out to be the most attractive measure. However, the RfR-policy boils down to 'no dike strengthening, unless....'. Large-scale dike set-back, the construction of green rivers, and groyne lowering are attractive alternatives (Silva et al., 2001). They yield the largest water level reduction per million Euros invested. The costs of hydraulic bottleneck removal and main channel dredging are slightly higher. Conversely, floodplain lowering appears to be the most expensive and thus economically least desirable measure. Nonetheless, this measure may be attractive, since it can often be combined with nature development and sand and clay mining. Nature development offers an other opportunity for local government. Sand and clay mining yields an economic benefit that may compensate the extra costs.

Therefore, different sets of river improvement measures are proposed for each river section in the RfR-study. In principle, a large number of possible alternatives for the re-design of the Rhine could be defined by combining RfR-measures. Eventually, two basic design alternatives

have been compiled, each enabling a safe discharge of 16.000 m^3/s through the Rhine system. An overview of the characteristics of the river improvement measures and maps showing the locations of the measures per design alternative are given in Figures 8.6 and 8.7.

Design alternative 1 is also known as the budget variant. In order to stay within the available budget of 1.9 billion Euro, a selection is made of mostly technical measures (dike strengthening), and some cost-effective RfR-measures, like lowering groynes and deepening the main channel by means of dredging. Costly measures, such as large-scale floodplain lowering in combination with nature development, are mostly avoided.

Design alternative 2 emphasizes the RfR-philosophy. Technical measures, such as dike strengthening, are avoided as long as spatial measures are applicable. Nature development and landscaping of floodplains play an important role in this alternative. The estimated costs of this alternative exceed the available budget.

8.5.2   Impact on morphological response statistics

First, we focus on the stochasticity of the river bed in the Waal and the IJssel in the reference situation. The 90%-confidence interval after a period of 15 years is shown in Figure 8.8, for the high-water and the dry season, respectively.

Apparently, the uncertainty in the morphological evolution of the Waal is much larger than that of the IJssel. Moreover, the seasonal variation seems to be more prominent in the Waal. This difference can be explained by the difference in morphological time-scale between the two branches. As indicated in Section 4.2.2, these time-scales differ, in particular as a consequence of differences in sediment transport rate. The mean yearly transport of bed material in the Waal is roughly 500,000 m^3. For the IJssel, the mean sediment load is approximately 37,000 m^3/year. Hence, the morphological time-scale of the IJssel is much larger than that of the Waal. This means that the morphology in the IJssel responds slower to changes in the discharge than that in the Waal. This results in much less variability of the IJssel morphology.

The morphological response statistics in the main channel of the Waal and the IJssel are presented for the two design alternatives in the upper panels of Figures 8.9 and 8.10, along with results for the reference situation. The lower panels show the deviation of the stochastic morphodynamic response from the reference situation.

Design alternative 1

The emphasis of this alternative is on technical measures, such as dike strengthening, combined with large-scale lowering of groynes and dredging of the main channel, as illustrated in Figure 8.6.

Type of measures in design alternative 1 'Budget'	Waal	IJssel
- floodplain (re-)landscaping incorporating floodplain lowering and nature development	1x	10x
- removal of hydraulic obstacles	0x	3x
- setting back river dikes	2x	2x
- deepening the main channel by means of dredging	0 km	26 km
- dike strengthening	0 km	50 km
- lowering groynes	66 km	0 km

Figure 8.6: Locations of the river improvement measures proposed in Design alternative 1

Type of measures in design alternative 2 'RfR-philosophy'	Waal	IJssel
- floodplain (re-)landscaping incorporating floodplain lowering and nature development	9x	20x
- removal of hydraulic obstacles	1x	3x
- setting back river dikes	2x	3x
- deepening the main channel by means of dredging	0 km	26 km
- dike strengthening	0 km	6 km
- lowering groynes	0 km	64 km

Figure 8.7: Locations of the river improvement measures proposed in Design alternative 2

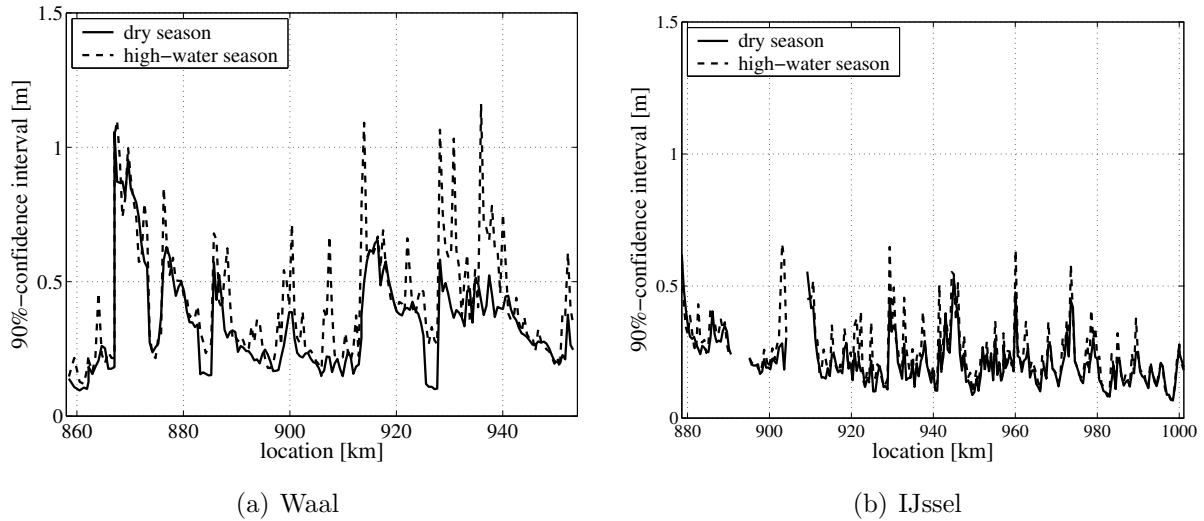(a) Waal   (b) IJssel

Figure 8.8: 90%-confidence interval of the cross-sectionally averaged bed level response in the reference situation after 15 years, in the dry season and the high-water season, as computed with the 1-D Rhine model

The impact of the proposed measures on the Waal morphology turns out to be limited: there is no significant change in the response statistics.

At a few IJssel locations (viz. km 912-920, km 950-960, km 970-980, km 980-1000) floodplain (re-)landscaping plans have been proposed, which induce a pattern of accretion and sedimentation along the IJssel. The confidence interval only slightly increases. Downstream km 980, the main channel of the IJssel is dredged. The deepened main channel induces a re-distribution of the river discharge between the main channel and the floodplain. During flood events, a smaller part of the discharge will be conveyed through the floodplains, resulting in a reduction of the sediment transport gradients, hence a lower morphological activity in the main channel.
The relatively small confidence interval throughout the IJssel is probably due to the relatively large morphological time-scale, implying that the river bed of the IJssel slowly adapts to discharge fluctuations. Consequently, the bed level variability is hardly affected by the RfR-measures.

Design alternative 2

(Re-)landscaping of floodplains, including floodplain excavation and nature development, is an important type of measure in this alternative, as shown in Figure 8.7.

In the Waal near Nijmegen (km 884-890), dike set-back is combined with floodplain lowering, the construction of a secondary channel in the floodplains and nature development. This scheme induces accretion of the river bed and an increase of the confidence interval of the morphological response. In the river section km 924-958 various floodplain (re-)landscaping plans are proposed.
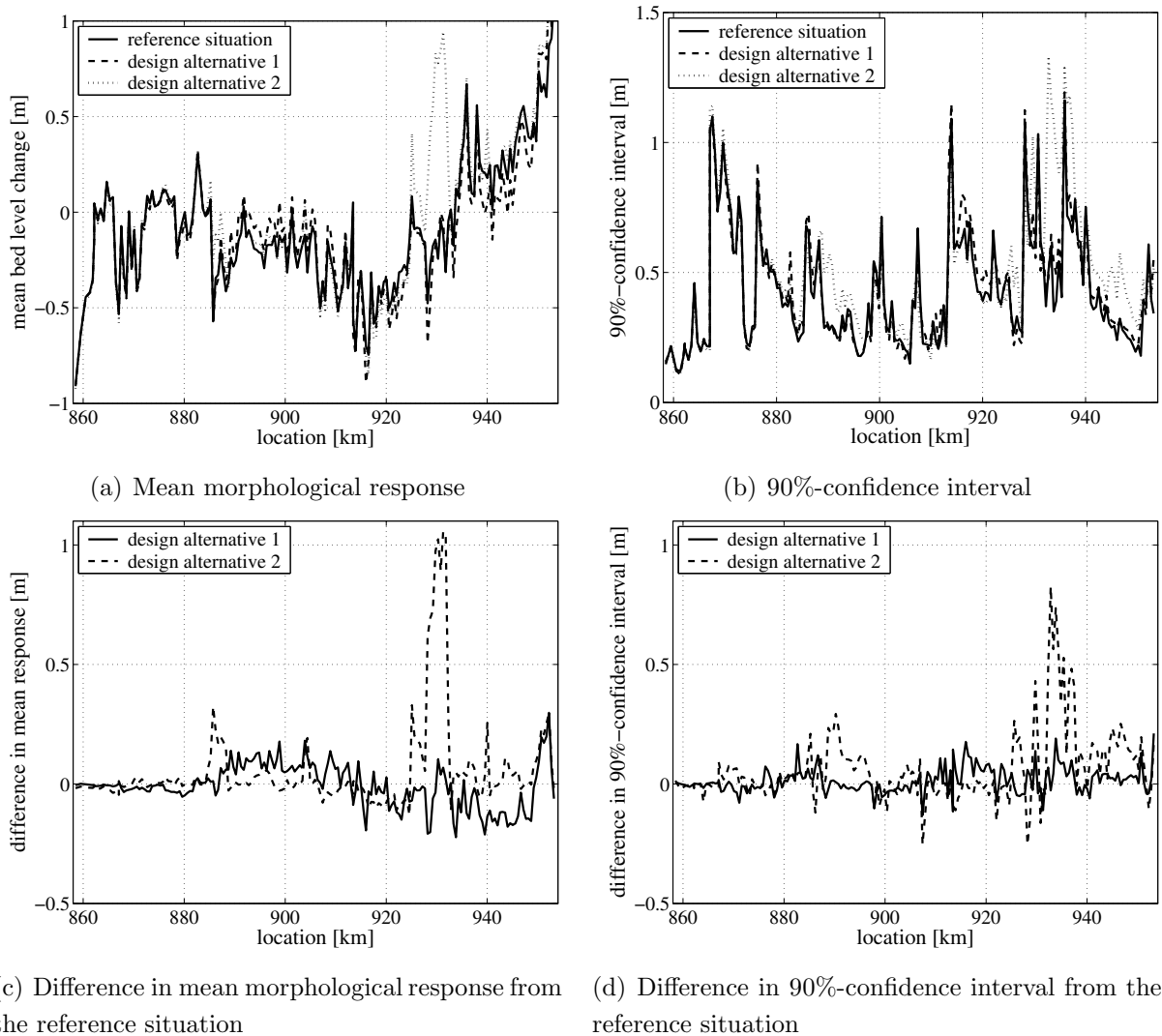
(a) Mean morphological response

(b) 90%-confidence interval

(c) Difference in mean morphological response from the reference situation

(d) Difference in 90%-confidence interval from the reference situation

Figure 8.9: Spatial variation of the statistical properties of the cross-sectionally averaged bed level response in the Waal after 15 years in the high-water season, as computed with the 1-D Rhine model

The morphological response induced by these measures is much stronger, due to more frequent flooding. Not only does the mean bed level increase, also the size of the confidence interval increases and has more pronounced peaks. All in all, the morphological response here is much more pronounced than in the section near Nijmegen.

The morphological impact of this alternative on the IJssel is more or less similar to that of the budget alternative. Despite the greater number of floodplain (re-)landscaping measures, morphological activity in the main channel hardly increases for the reason mentioned before.

8.5.3 Conclusions concerning the morphological effects of RfR-alternatives

The stochastic approach provides insight into the morphological response to different sets of RfR-measures and the uncertainty involved. It shows that some locations are more susceptible

to the proposed schemes than others. At some locations, the RfR-measures locally enhance the bed level variability, and so lead to a significant increase of the uncertainty range in the predicted morphological response. Apart from this, the mean morphological state may locally respond to the RfR-measures by the formation of accretion and erosion patterns.
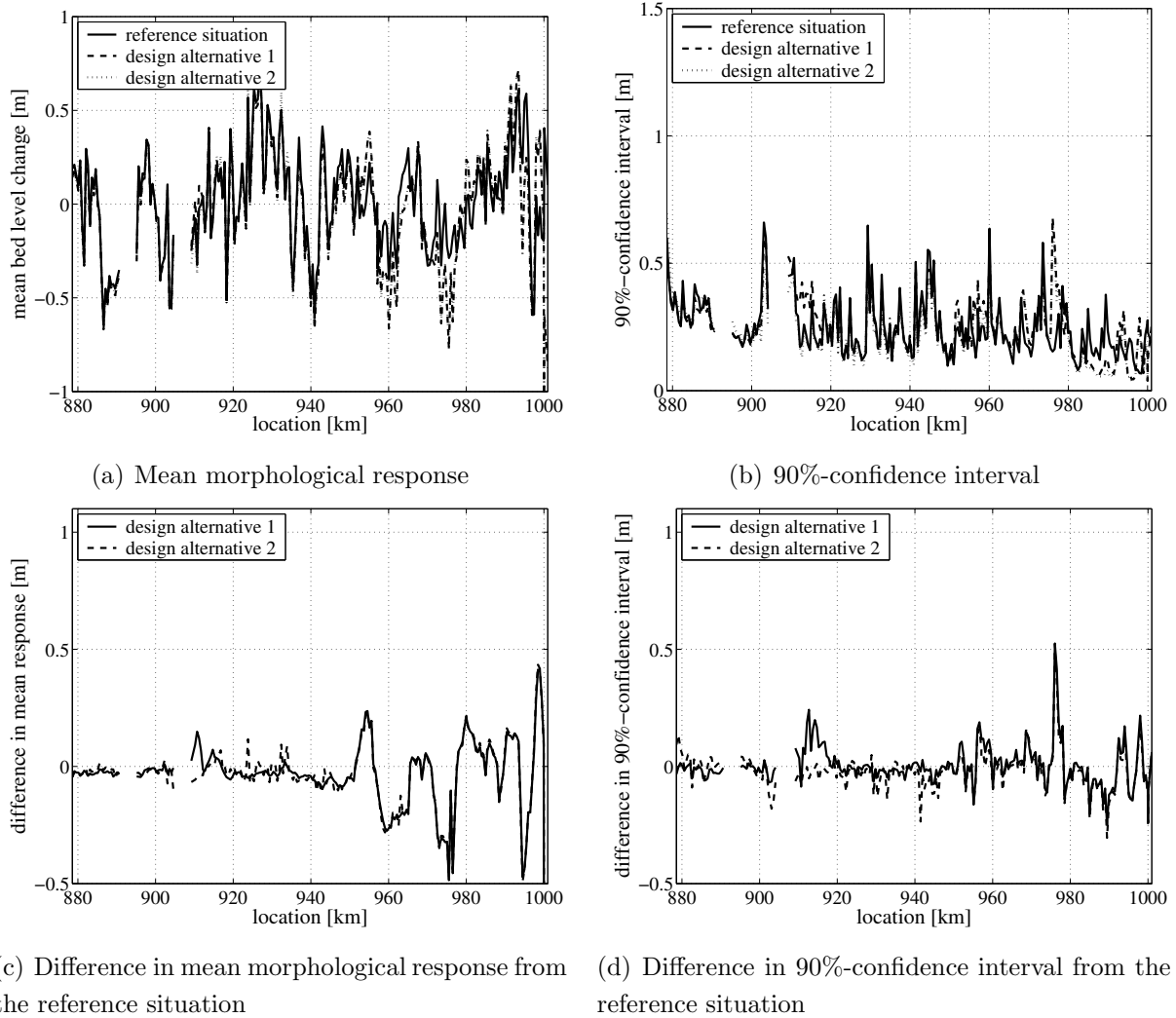

(a) Mean morphological response

(b) 90%-confidence interval

(c) Difference in mean morphological response from the reference situation

(d) Difference in 90%-confidence interval from the reference situation

Figure 8.10: Spatial variation of the statistical properties of the cross-sectionally averaged bed level response in the IJssel after 15 years in the high-water season, as computed with the 1-D Rhine model

Design alternative 2, which mostly consists of floodplain (re-)landscaping plans including floodplain excavation and nature development, has a more pronounced impact on the morphology of the Waal than Design alternative 1. This can be explained from the type of RfR-measures in Design alternative 2 that have a stronger impact on the frequency and the extent of floodplain inundation.

For the IJssel, this difference in morphological impact between the two alternatives is not found, despite the greater number of floodplain (re-)landscaping plans in Design alternative 2. The relatively large morphological time-scale of the IJssel makes the river bed respond much slower

to changes. Flood events of relatively short duration, for instance, have a lesser effect on the morphology than in the Waal.

8.6   Conclusions

This chapter shows that a stochastic approach can be useful to assess the impacts of engineering works. It provides insight into the range of possible morphological responses to different design alternatives, and their probability of occurrence. Not only does the stochastic approach show that a range of morphological states can occur, it also shows that the uncertainty in the predicted morphological response in the Waal is much larger than in the IJssel, due to the smaller morphological time-scale in the Waal. Consequently, the Waal morphology responds faster to discharge fluctuations and human interventions. Moreover, it appears that at some locations the impact of identical engineering measures is more pronounced than at others. This goes for the mean response, as well as for the variability, and also for the seasonal variation.

Knowledge on the spatial and temporal variation of morphological response statistics is of importance to the design of river improvement schemes. Some locations have the potential to develop into nautical bottlenecks, involving high maintenance costs. At other locations, the uncertain morphological response may affect the flood level. During a flood, the riverbed is very active, meaning a large uncertainty range in the bed level, which may affect the predicted height of the flood wave.

The next two chapters consider the impact of uncertainty in morphology on the extreme flood level predictions (Chapter 9) and the prediction of navigability and maintenance dredging (Chapter 10) in further depth.

Chapter 9

Protection against flooding

9.1 Introduction

River flooding is a worldwide problem. In recent years, many countries suffered from major river floods, like the Meghna complex in Bangladesh, the Yangtze in China, the Oder and the Vistula in Poland, the Moldau in the Czech Republic and the Elbe in Germany. A large part of the Netherlands lies below sea and river flood levels. Without flood defences, much of the country would be flooded regularly. In the Netherlands, the 1995 flood event in the Rhine caused 250.000 people to be evacuated. Although no major flooding occurred at the time, economical and societal damage were considerable. It may be expected that in the future, due to the changing climate, higher discharge levels will occur, leading to higher and more frequent river floods, which increase the flood risk level, unless adequate measures are taken to prevent this.

Worldwide, this leads to an increasing demand of reliable flood risk predictions to support decision-making and design processes for flood risk management schemes. To that end, fixed-bed hydrodynamic models are often used, in which the geometrical schematisation is a representation of the 'actual' state of the river. The adequacy of the geometrical schematisation turns out to be critical. An 'a priori' judgement of safety against flooding on the basis of fixed-bed forecasting in morphologically dynamic river systems may even be misleading (De Vriend, 2002). In such cases, the use of a mobile-bed approach is more appropriate. This problem is addressed in this chapter, taking flood protection in the Netherlands as example. This chapter is largely based on Van Vuren et al. (2005).

In the Netherlands, flood protection is laid down in law and summarised in the Flood Defence Act (1996). According to this law, the Netherlands are divided into 53 so-called dike rings, each with its own level of protection, depending on the location. The dike rings along the Rhine branches are claimed to have a protection level of 1/1250 per year. This means that the flood defences are designed for water levels with a probability of exceedance of 1/1250 per year. These water levels are known as design water levels (DWLs). The DWLs are computed with

a fixed-bed hydrodynamic model based on the 'actual' (latest-measured) cross-sections of the river. The model is driven by the design discharge hydrograph. The peak of this hydrograph is claimed to have a probability of exceedance of 1/1250 per year, on the basis of a statistical analysis of all flood events on record. The shape of the discharge hydrograph is derived from averaging the wave shapes of historical flood events that are linearly scaled up to the 1/1250 peak level. So, actually, only one stochastic variable is involved in the establishment of the design water levels: the peak discharge.

Traditionally, the safety against flooding is obtained by building and strengthening dikes. Recently, the Room for the River (RfR) scheme has been adopted by the parliament. The underlying policy, called 'Dike strengthening? No, ..., unless ...', focuses on river improvement measures to increase the flood conveyance capacity (see Section 8.2). Unlike dike reinforcement, the RfR-measures reduce the DWLs and may have an extra impact on the flow and sediment transport fields in the river. This may result in extra morphological effects. As a consequence of the latter, the river's flood conveyance capacity may decrease over time. Hence, the determination of DWLs using a fixed-bed hydrodynamic model (instead of a morphodynamic model) may suggest an unrealistic safety level.

In this chapter, we investigate the impact of three phenomena of the uncertain morphology on design flood level predictions, viz.

1.   the impact of the spatial morphological variation over years at intermediate scale (years);
2.   the impact of the seasonal morphological variation;
3.   the impact of the morphological variability around bifurcation points.

To that end, two different methods of analysis are proposed in Section 9.3. We investigate to what extent morphology effects flood levels, and to what extent it is still justified to use a fixed-bed hydrodynamic model for design water level computations (Section 9.4). Furthermore, the effect of morphological phenomena on the exceedance probability of water levels is investigated as this may subsequently lead to second-order changes in DWLs and changes in the exceedance frequency of the current DWLs.

9.2   Potential effect of river morphology on flood conveyance

In Chapter 6, we have shown that the bed level in the Waal exhibits a strong spatial and temporal variation. Various sources of uncertainty, like the uncertain discharge, hydraulic roughness and grain size of the bed material, together with large geometrical non-uniformities, lead to an uncertain morphological response. The stochastic approach does not only show that many morphological states are possible, it also shows that in some reaches the spatial and temporal

bed level variations are more pronounced than in others.

Large-scale floodplain lowering in combination with removal of summer levees strongly enhances the morphological response, for instance, as compared to the reference situation with dike reinforcement (Section 8.4). On average, the uncertainty in the morphological response increases with some 20%.

Consequently, the river's flood conveyance capacity will vary over time. Hence, the determination of DWLs using a fixed-bed hydrodynamic model, instead of a morphodynamic model, may underestimate the DWLs. In the next section, we will investigate to what extent the bed level variability affects the design water level (DWL) and to what extent it is justified to compute this DWL with a fixed-bed hydrodynamic model. To that end, we will use two different methods of analysis (see Section 9.3).

Special attention will be paid to the Pannerdensche Kop bifurcation, because the present management policy is to maintain the discharge distribution at the bifurcation point under all discharge conditions. Yet, the discharge distribution is bound to vary slightly in time, as a result of time-dependent morphological changes around the bifurcation point. The question is to what extent this may lead to substantial differences in the DWL.

9.3   Methods of analysis

9.3.1   Method based on current design flood level prediction method

Most present-day flood level predictions are derived from a fixed-bed hydraulic model, driven by the design discharge hydrograph. The 'fixed-bed' is the latest-measured state of the river. Since bed level surveys are made through the year, this probably does not represent a 'snapshot' of the actual state of the river at any point in time. The design discharge is based upon a statistical analysis of the yearly peak discharges from 100 years of daily discharge measurements at Lobith. A combination of 3 probability distributions - a Gumbel distribution, a Pearson III distribution and a lognormal distribution - is used to extrapolate the data to the design probability of exceedance (Parmet et al., 2002). These probability distribution types fit the best to the discharge measurements. The relation between the yearly exceedance frequency f and the river discharge Q, as shown in Figure 9.1(a), is given by:

$$
\begin{aligned}
Q &= 1520 \cdot \ln\left(1/f\right) + 5965 \qquad 1/2 \leq f \leq 1/25 \\
Q &= 1315 \cdot \ln\left(1/f\right) + 6615 \qquad 1/25 \leq f \leq 1/10000
\end{aligned}
\tag{9.1}
$$

The design discharge is revised every five years. As a consequence of the 1993 and 1995 flood events, the probability curve has changed and the discharge has gone up from 15,000 m^3/s to 16,000 m^3/s. The wave shape of the design discharge hydrograph is found by linear upscaling

of the discharge hydrograph of historical flood events. Each discharge hydrograph is therefore multiplied with the ratio of the design discharge to the peak discharge of this hydrograph. The mean of all upscaled hydrographs is used as a wave shape of the design discharge hydrograph (Figure 9.1(b)).
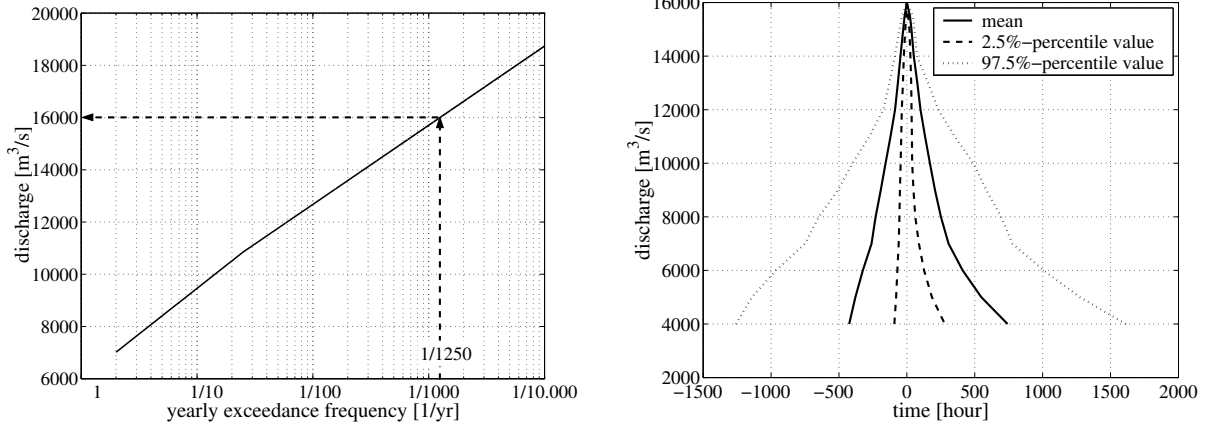
(a) Relation between the yearly exceedance frequency f and the river discharge Q

(b) Mean value and 95% and 5% percentile values of the design flood wave with peak 16,000 m^3/s

Figure 9.1: Design discharge wave in the Rhine, after Parmet et al. (2002)

First, the DWL reduction of the floodplain measure is determined in a deterministic way using the fixed-bed hydraulic model, meaning that the impact of morphology on this reduction is neglected. In order to determine to what extent morphological changes affect the design water levels, MCS is applied subsequently using the same model in a morphodynamic mode. This 1-D morphodynamic Rhine model, which was described in Section 4.5.4, is run in an MCS-setting with sample size 300, in order to estimate the uncertainty in the morphological response. The bed topography resulting from each run at a certain point in time is fixed and a standard design flood computation is made for that particular bed topography. The morphological evolution during this flood event is not taken into consideration. The computations yield 300 design water levels at each location and at each time-point in the flood computation. This gives insight into how morphological changes may affect the design flood conditions.

In the MCS procedure, only one uncertainty source is considered, namely the river discharge. Model runs were made with statistically equivalent discharge time series, randomly synthesised by means of Bootstrap resampling in combination with a flood event predictor (see Section 6.4).

9.3.2   New method for design flood level predictions

The current method of DWL computation is extended with a second random variable, river morphology, in order to determine the effects of uncertainties in the river's morphological state

on the exceedance probability of water levels. The extended method involves the following steps:

1. Again, 300 morphological states at a certain point in time T are computed with the morphodynamic Rhine model run in MSC-mode. The resulting morphological states are statistically equivalent, each with a probability of occurrence $P(M_j)$ of 1/300;

2. This time, the flood model is run on each of the 300 bed topographies, using a range of 15 constant discharges varying from 13,000 to 20,000 m^3/s, in discrete steps of 500 m^3/s. Again, the morphological evolution during these high discharges is not considered. The probability P of the discharge level Q_i is derived from Eq. 9.1:

$$P(Q \le Q) = f(Q) = e^{-((Q-6615)/1315)}$$
$$P(Q_i) = P(Q \le Q_i + 250) - P(Q \le Q_i - 250)$$

(9.2)

This results in 15 water level distributions per simulated morphological state.

3. The probabilities of the morphological state $P(M_j)$ and the discharge level $P(Q_i)$ are multiplied to determine the probability of the computed water levels $P(WL_{ij})$.

4. On the basis of the set of outputs (4500 water levels, each with its corresponding probability), a cumulative probability distribution curve of the water level at each location is determined by numerical integration. The probability of exceedance indicated by this curve includes the potential effect of morphological changes. The water level with a probability of exceedance of 1/1250 per year (DWL$_{new}$) can now be compared with the value computed with the traditional method (DWL$_0$). Moreover, the curve can be used to determine an 'updated' exceedance probability of the DWL$_0$, now including morphological effects.

This extended method generally results in higher DWLs than the current method. The reason is that the tail of the probability distribution of the water levels becomes bigger, and therefore the water level with exceedance probability of 1/1250 will be higher. On the other hand, we also observe a continued tilting of the river about the hinge point near Tiel. Hence, in some parts of the river lower design water levels are found, and in other parts there will be higher design water levels.

9.4 River morphology effects on design flood levels

9.4.1 Effect of spatial morphological variation over a period of years

At a time-scale of decades to a century, the large-scale tilting of the Waal is expected to continue. Hence, long-term erosion is to be expected in the part of the Waal between km 867 and km 915. This leads to an ongoing reduction of the DWLs (Figure 9.2). Near Tiel (km 913) there is a hinge point, downstream of which long-term sedimentation takes place. Clearly, this comes with an ongoing increase of the water level in the reach downstream of Tiel.
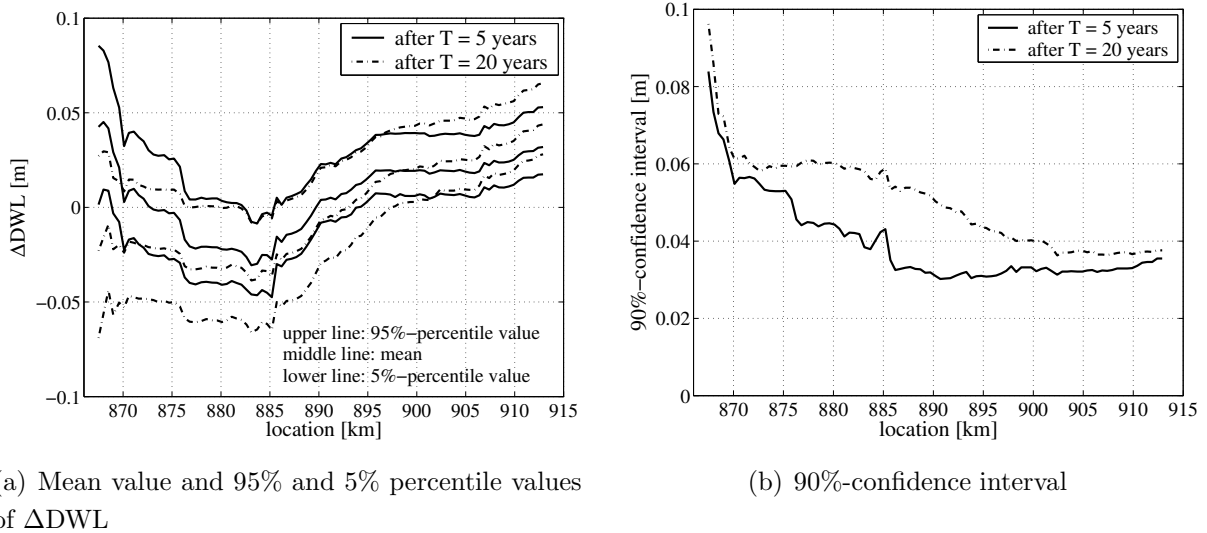
(a) Mean value and 95% and 5% percentile values of ΔDWL

(b) 90%-confidence interval

Figure 9.2: Spatial variation of the statistical properties of ΔDWL ($= DWL_T$ - DWL_{T0}) along the Waal after a period T of 5 and 20 years, respectively, in the reference situation (no interventions)

The uncertainty in this long-term morphological response is reflected in the DWLs, as becomes apparent from Figure 9.2. This figure shows the spatial distribution of the statistical properties of ΔDWL ($= DWL_T$ - DWL_{T0}), after a period of 5 and 20 years, respectively in the high-water season for the reference situation (no interventions), as computed with the current method. The 90%-confidence interval gives an indication of the variation in ΔDWL resulting from differences in morphological state. The confidence interval increases as a function of time. Since the water levels close to Tiel are determined to an increasing extent by the downstream water level, the confidence interval decreases in downstream direction. The DWLs vary with a probability of 90% within a range of 5 - 10 cm, which is not much as compared to the expected uncertainty originating from other sources (e.g. in bed roughness predictor).

The application of the new method results in a set of 4500 water level computations and their corresponding probability. These are used to derive the cumulative probability distribution of the water levels per river location. Figure 9.3 shows this curve at km 884.7, after a period of 20 years of morphological evolution. In the same figure, the curve derived with the hydrodynamic model with a fixed-bed level at time T_0 is shown.

The figure shows a decrease in DWL of 0.06 m in 20 years when taking the uncertain morphological changes into account. According to the new curve, the exceedance probability of DWL_{T0} comes down from 1/1250 to 1/1460 per year. Given the other sources of uncertainty playing a role at this extreme end of the probability distribution, these differences are minor.

Doing this for all locations along the Waal leads to the spatial distributions of ΔDWL shown in Figure 9.4. The conformity with the large-scale rotation around the hinge point near km 900 is striking. Apparently, this rotation is the prime cause of the long-term changes in DWL.
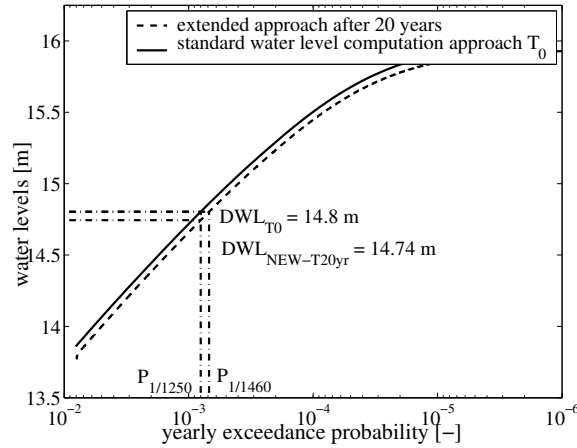
Figure 9.3: Exceedance probability of water levels at location km 884.7 at T_0 and after 20 years, in the reference situation (no interventions)
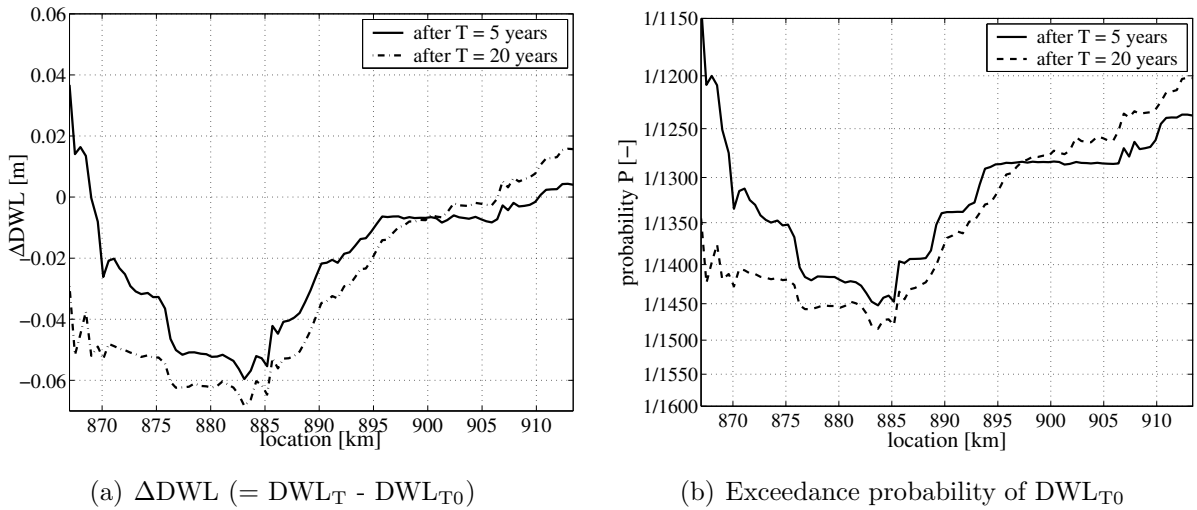

(a) ΔDWL ($=$ DWL$_T$ - DWL$_{T0}$)

(b) Exceedance probability of DWL$_{T0}$

Figure 9.4: Spatial distribution of ΔDWL ($=$ DWL$_T$ - DWL$_{T0}$) and exceedance probability of DWL$_{T0}$ along the Waal after a period T of 5 and 20 years, respectively, in the reference situation (no interventions)

9.4.2 Effect of seasonal morphological variation

At some river locations, we noticed a large seasonal variation of the statistical properties of the morphological response (see Figure 8.5). The largest uncertainties in the morphological response are found in the high-water season. Computations have shown that seasonal variations in the river morphology hardly affect the DWLs (see Figure 9.5).
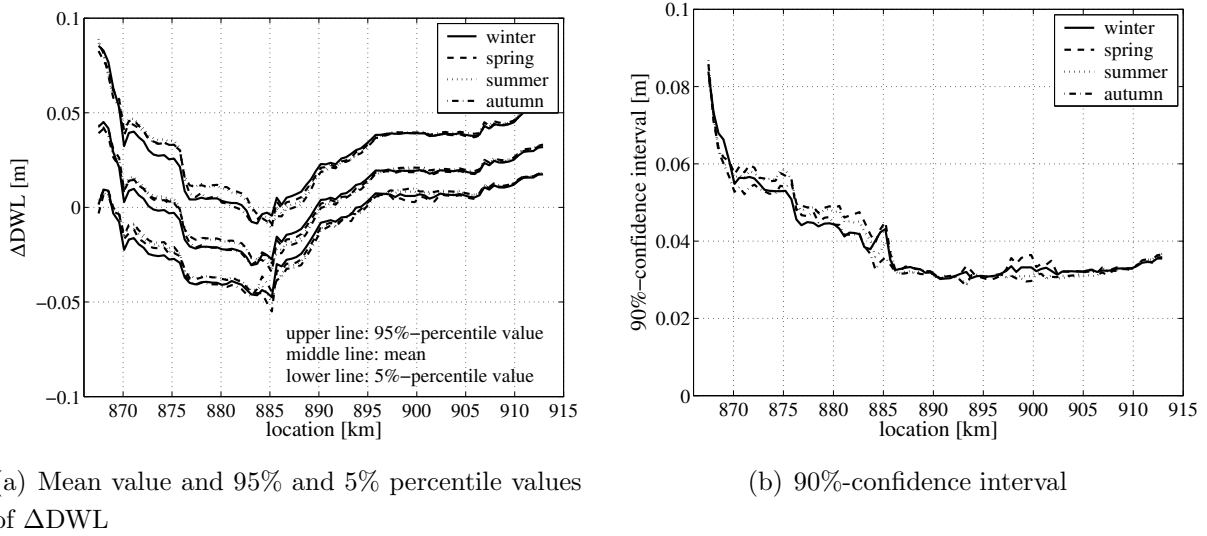
(a) Mean value and 95% and 5% percentile values
of ΔDWL

(b) 90%-confidence interval

Figure 9.5: Spatial variation of the statistical properties of ΔDWL (= DWL_T - DWL_{T0}) along the Waal in four different seasons, in the reference situation (no interventions)

9.4.3   Effect of morphological variability around bifurcation point

Local morphological changes around the bifurcation point Pannerdensche Kop may lead to variations in the discharge distribution. Discharge measurements show variations between tens and hundreds of cubic metres per second (see Figure 6.1). In the computations so far, we have kept the discharge distribution at the bifurcation point fixed. We will now adopt a statistical description of the discharge distribution, based upon daily discharge records at the Pannerdensche Kop in the period 1961-2000. For each fixed-bed hydrodynamic model run, covering a period of 20 years, a new discharge distribution is drawn from this statistical description.

The effect of this uncertain discharge distribution on the DWL predictions is shown in Figure 9.6. This figure shows the spatial distributions of the statistical properties of the DWL after 20 years, for the fixed and the uncertain discharge distributions, respectively. On average, the DWL for the uncertain discharge distribution is slightly larger than that for the fixed distribution. The variation in the DWL, however, is significantly enhanced by the uncertainty in the discharge distribution.

9.5   Conclusions

The bed level in the existing situation already exhibits a strong spatial and temporal variation. The stochastic approach reveals not only that many morphological states are possible, it also shows that in some reaches the uncertainty in the bed response is more pronounced than in others, mainly due to strong spatial changes in geometry, such as bifurcation points, width variation in floodplains and the presence of hydraulic and man-made structures.
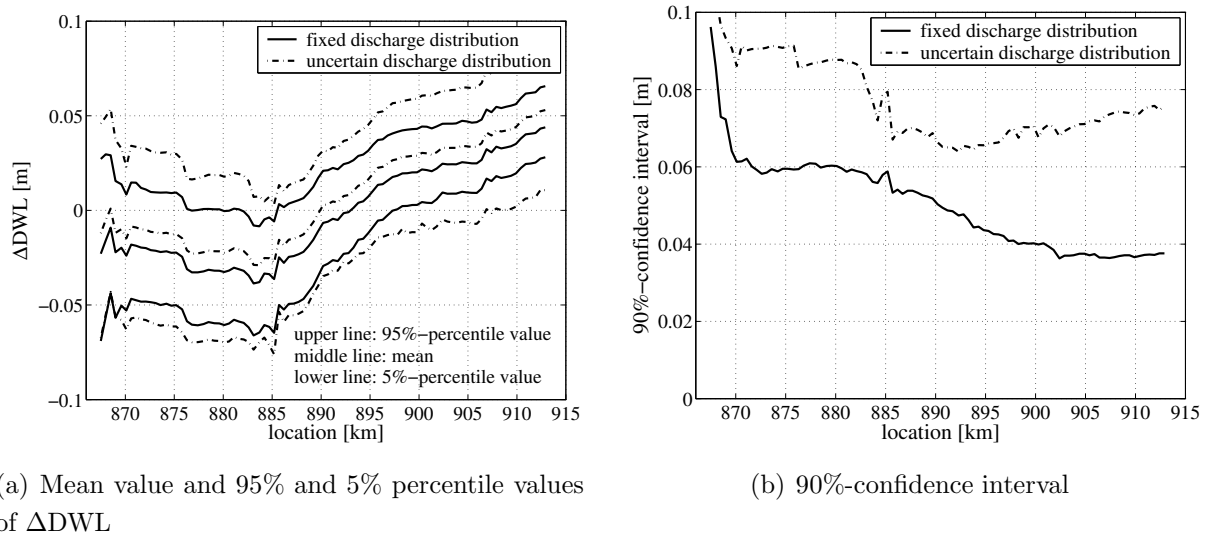
(a) Mean value and 95% and 5% percentile values of ΔDWL

(b) 90%-confidence interval

Figure 9.6: Spatial variation of the statistical properties of ΔDWL ($= \mathrm{DWL_T} - \mathrm{DWL_{T0}}$) along the Waal after a period T of 20 years, in the reference situation (no interventions) with the fixed and the uncertain discharge distribution, respectively

Given this uncertainty in the predictions of the morphological evolution, the question arises to what extent the computation of design water levels with a fixed-bed hydrodynamic model based on the present state of the river is appropriate. Three phenomena of morphological uncertainty are considered. The effects of seasonal morphological variations turn out to be negligible. The other two phenomena (long-term spatial variation over years and the morphological variability near the bifurcation point) appear to have a larger effect on the computed design water levels (order of magnitude 0.05 - 0.1 m). Absolutely speaking, this is still rather small, given the other uncertainties in the model and those in the determination of the design discharge. It is recommended to investigate the impact of other sources of uncertainty that contribute to uncertainties in DWLs. Amongst others, the uncertainty involved with the hydraulic roughness predictor is expected to have a significant effect, since it affects both the hydraulic and the morphodynamic computations.

The uncertainty ranges found here are not small in comparison with the centimetre-accuracy claimed for the design water levels for the assessment of the flood defences in the Netherlands, or in the light of plans to spend millions of Euros to river improvement measures that reduce the design water level by a few centimetres. An 'a priori' judgement of safety against flooding on the basis of fixed-bed forecasting in morphologically dynamic river systems seems to be quite misleading, taking the role of morphological changes in flood forecasting into consideration.

Chapter 10

Navigation and maintenance dredging

10.1 Introduction

Over the last two hundred years the river Rhine in the Netherlands has faced a series of changes. Due to rapid population growth and economic development in its riparian zones, flood control and navigability became most important issues in the management of the Rhine branches in the Netherlands.

The Rhine is the main shipping connection between the port of Rotterdam and Germany, and became one of the most important inland waterways in Europe. Around half of the cargo transport from and to Germany goes via this waterway connection. Safe, efficient and profitable inland shipping requires a deep and wide navigation channel, now and in the future. The river manager uses dredging as a means of maintaining or improving the navigation conditions. In this chapter, we focus on the navigation function of the Niederrhein and Waal, and the IJssel, investigating amount of maintenance dredging required to keep these rivers navigable.

Inland navigation in the Netherlands is embedded in the National Traffic and Transportation Plan. According to this plan, the river manager has to guarantee a certain navigable channel profile for river discharges above a certain threshold value. In fact, the navigability of the river depends on the least available water depth along the entire shipping route. Whenever the navigation depth is less than required, navigation is congested and/or ships may carry less cargo. As a consequence, maintenance dredging might be required.

The predictability of navigation conditions is complicated, since water depths are inherent uncertain and exhibit spatial and temporal variations, due to changes in the morphodynamic river system. In this chapter, the 1-D Rhine model (see Section 4.5.4) is utilised for water depth predictions. The Rhine model is run in an MCS-mode to account for uncertainty introduced via the uncertain river discharge. Other sources of uncertainty, such as the hydraulic roughness coefficient or the modelling process, are left out of consideration. The water depth predictions resulting from all model runs are used to statistically assess the river's navigability for ships with various draughts, and to locate nautical bottlenecks. Furthermore, the amount of maintenance

dredging to keep the river navigable can be derived. In line with the Dutch dredging policy, the dredged material should be deposited elsewhere in the river, since no net sediment extraction is allowed. We examine three different dredging strategies, viz. (1) removal of the dredged material, (2) removal of the dredged material, and further deposition upstream, and (3) removal of the dredged material, and further deposition downstream.

The chapter starts with the economic importance of inland navigation to the Netherlands and the associated river management policy (Section 10.2). We further elaborate the method to predict navigability and maintenance dredging in Section 10.3. The actual statistical assessment of the navigability of Niederrhein, Waal and IJssel follows in Section 10.4, along with the required maintenance dredging in Section 10.5. The impact of maintenance dredging on the navigation conditions is shown next. Finally, the extent to which a 1-D model approach is applicable for the assessment of navigability and the estimation of maintenance dredging is discussed. Section 10.7 summarises the conclusions.

10.2   Inland navigation in the Netherlands

International shipping transport is economically important to the Netherlands. About 55% of all international and 25% of all national transport is carried by ship. Due to its advantageous location in the Rhine Delta, the inland waterways in the Netherlands form a natural access to the continent of Europe. The Rhine is the most heavily navigated inland waterway in Western Europe. The Niederrhein and Waal, along with the Lower-Rhine and Lek, form important East-West transport routes.

Traditionally, inland navigation is the safest and cheapest transport mode. The integration of inland navigation into the transport chain, including an effective linking with rail and road transport is most important for further development. To that end, inland navigation has to be capable of 'just in time' delivery with a high reliability (Filarski & Brolsma, 1989). This requires an inland waterway with a high capacity that is always navigable, without any physical obstruction. This means that a deep and wide navigation channel is essential to safe, efficient and profitable inland shipping transport.

In 1954, the European Conference of Ministers of Transport defined design vessels and their dimensions. The Western European waterways were divided into six categories. The Niederrhein and Waal are classified in category VIc. Thus pushing units with a length up to 269.m m and a width up to 34.5 m should be able to navigate safely. The IJssel dimensions are much smaller, hence the IJssel is classified in a lower category, viz. category Va. This means the IJssel should be navigable for pushing units with a length up to 110 m and a width up to 12.5 m.

The National Traffic and Transportation Plan (2001) gives guidelines with respect to the navigation channel requirements for each branch of the Dutch Rhine system. According to this plan, during discharges above a threshold value of 1020 m^3/s at Lobith, the navigation channel in the Niederrhein and the Waal must have a guaranteed width of 170 m and a depth of 2.8 m, and the IJssel should have a width of 40-80 m[1] and a depth of 2.5 m. The discharge with the threshold value 1020 m^3/s is also known as the agreed low-water discharge and is exceeded during 95% of the time.

In order to improve the navigability of the Niederrhein and Waal, the channel depth has recently been increased from 2.5 m to 2.8 m. An increase of the channel width from 150 m up to 170 m is planned according to the National Traffic and Transportation Plan (NTTP), but not yet realised. Therefore in this study, the navigability requirements are fixed at 2.8 m depth and 150 m width at a discharge of 1020 m ^{3}/s at Lobith.

Dredging is utilised to maintain the prescribed navigation conditions in the Rhine. According to the dredging specifications, every year after the high-water season (assumed to end in May) navigability is checked as the discharge at Lobith drops below 3000 m^3/s. A discharge of 1020 m^3/s is projected on the actual state of the river, whence the actual dimensions of the navigation channel can be derived. If the requirements are not met, dredging takes place. Subsequently, if the discharge drops below 2000 m^3/s at any time during the dry season, another check follows. In 1991, a new policy concerning dredging activities was adopted, prescribing that net extraction of sediment is no longer allowed, so as to prevent further large-scale tilting of the river. In conformity with this policy, the dredged volume has to be deposited elsewhere in the river.

10.3 Method to predict navigability and maintenance dredging

10.3.1 Navigability

In dynamic rivers, the water depth exhibits spatial and temporal variations. The worst navigation conditions are to be expected in the dry season, between August and October. The cargo ships in the Rhine have a draught of approximately 2.5 up to 4.5 m. The NTTP gives guidelines with respect to the minimum navigation channel requirements. The navigability assessment is twofold (Van Vuren & De Vriend, 2004):

1. the navigability is assessed for ships with various draughts ranging from 1.5 to 5 m;
2. the probability of satisfying the navigation channel requirements imposed by the NPPT is estimated.

An important criterion is the percentage of navigable days per year. The analyses make it possible to identify nautical bottlenecks in the river.

---

1. In the IJssel, the required width of the navigation channel depends on the radius of curvature. In sharp bends, the required width to safely manoeuvre through the system is larger than in straight sections.

Stochastic approach

The 1-D Rhine model is utilised to simulate water depths as a function of space and time. We make morphodynamic simulations covering a period of 15 years, with a time step of 10 days and a grid size of 500 m. Since, the model is subject to various uncertainty sources, which are either related to uncertainty inherent to the river system behaviour, or introduced via the modelling process, the Rhine model is run in a Monte Carlo-setting. Out of the various sources uncertainty involved in the 1-D Rhine model, we only consider the uncertainty in the river discharge. For each model run, a new discharge time series is constructed by means of Bootstrap resampling in combination with a flood event predictor, as indicated in Section 6.4. The sample size is fixed at 500 simulations.

Water depth correction for transverse bed slopes in bends

The Rhine model is purely one-dimensional, meaning that the model yields width-averaged bed levels and water depths. The effect of multi-dimensional phenomena, such as transverse bed slopes in bends, is therefore not considered in the model. Yet, shallow inner bends may become critical to navigation under low flow conditions. It is possible to some extent to account for 2D-transverse slope effects by post-processing the numerical results. The axi-symmetrical approximation for lateral bed slopes given by Struiksma et al. (1985) can be used to that end:

$$\tan i_{\mathrm{b}} = -A f_{\mathrm{s}}(\theta) \frac{d}{R_{\mathrm{b}}} \tag{10.1}$$

in which A is the secondary flow direction coefficient [-], $f_{\mathrm{s}}(\theta)$ is a function of the Shields parameter θ [-], d is the water depth [m] and R_{b} is the radius of curvature [m]. The secondary flow direction coefficient is defined as (De Vriend, 1977):

$$A = \frac{2\epsilon}{\kappa^2} \left(1 - \frac{\sqrt{g}}{\kappa C}\right) \tag{10.2}$$

in which ϵ is a tuning coefficient [-], κ is the Von Karmann coefficient (≈ 0.4) [-], C is the Chézy coefficient [m$^{1/2}$/s] and g is the acceleration due to gravity [m/s^2].
The function $f_{\mathrm{s}}(\theta)$ can be approximated as (Talmon et al., 1995):

$$f_{\mathrm{s}}(\theta) = 9 \left(\frac{D_{50}}{h}\right)^{0.3} \sqrt{\theta} \tag{10.3}$$

in which D_{50} is the median grain size of the bed material [m].

The width-averaged water depth predictions $\overline{d}(x,t)$ of the 1-D Rhine model are corrected as follows (Figure 10.1):

$$d_{\min}(x,t) = \overline{d}(x,t) - d_{\mathrm{a}}(x) = \overline{d}(x,t) + \left(\frac{B(x)}{2} - B_{\mathrm{S}}(x) - B_{\mathrm{N}}(x)\right) i_{\mathrm{b}}(x) \tag{10.4}$$

in which $d_{\min}$ is the critical depth in the cross-section of the navigation channel [m], d_{a} the transversal slope correction [m], B the main channel width [m], B_{S} the safety distance from the river bank [m], B_{N} the navigation channel width [m], and i_{b} the transversal slope [-]. Time and space are represented by t and x, respectively.
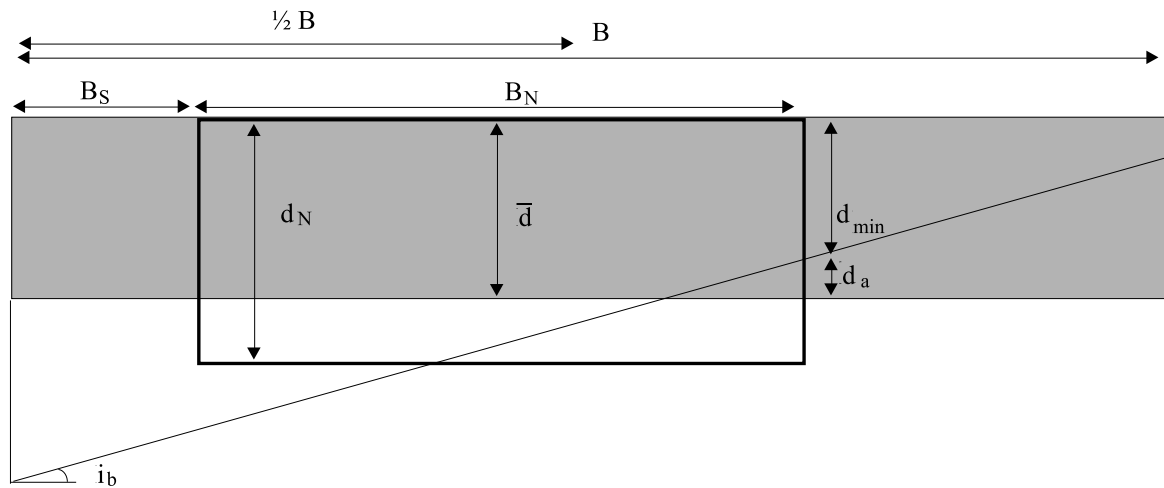

Figure 10.1: Graphical representation of navigation channel requirements and transverse slope correction

In practice, the axi-symmetrical solution for transverse slopes will hardly be reached, since river bends are limited in length and do not have a constant radius of curvature. Moreover, transverse slopes tend to lag behind discharge fluctuations. Nevertheless, we calculate constant transverse slope corrections for each river location using a characteristic Rhine discharge. The water depth corrections for transverse slopes along with the radius of curvature are shown in Figure 10.2. Outer bend structures for navigation purposes have been built in the sharp Waal bends at Erlecom (bottom groynes over km 873-876), Nijmegen (outer-bend fill-up over km 883-885) and St. Andries (outer-bend fill-up over km 924-928). For this reason, the correction for the transverse slope is set to zero at these locations. The radii of curvature in the IJssel are much smaller than in the Niederrhein and the waal, implying shaper bends and larger water depth correction.

10.3.2 Maintenance dredging

In line with the dredging strategy in the Netherlands, maintenance dredging is undertaken correctively. This is also implemented in the model simulations. During each simulation of 15 years, the navigation channel conditions are checked every year after the high-water season, when the discharge at Lobith drops below 3000 m³/s. The low-water discharge of 1020 m³/s is projected on the computed river state, after which the channel conditions are checked. Maintenance dredging is undertaken, when the channel requirements of NTTP are not met. Dredging

is simulated by an extraction of sediment. The extra check, when the discharge drops below
2000 m^3/s at any time in the dry season, is left out of consideration.

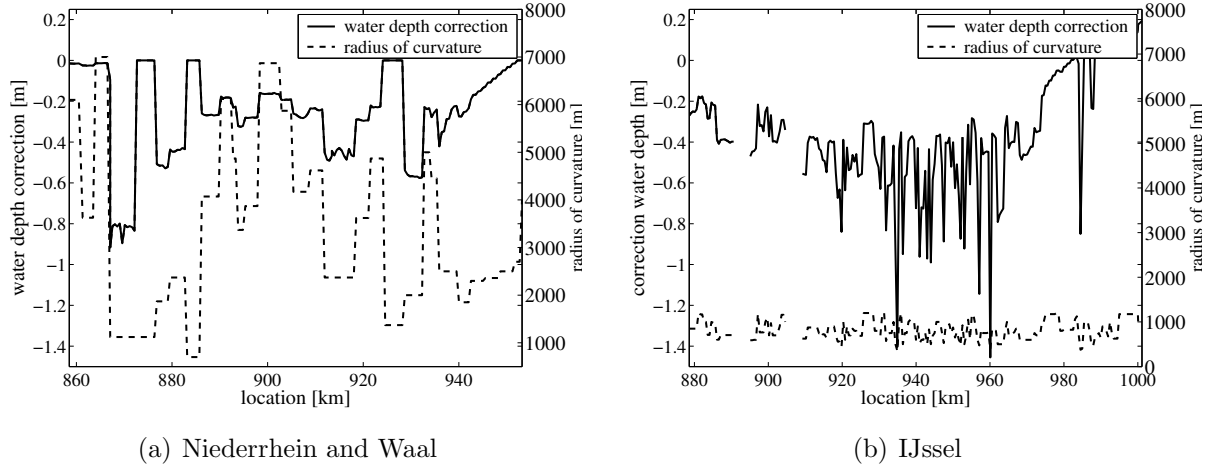(a) Niederrhein and Waal

(b) IJssel

Figure 10.2: Radius of curvature and water depth correction for transverse slope along the Rhine

Amount of dredging

Figure 10.3 illustrates the amount of dredging (grey-shaded surface) that is required when
the navigation channel conditions are not fulfilled. The dredging volume is described with (De
Rooij, 2005):

$$V_{\mathrm{D}}\left(x\right) = \frac{1/2 \cdot \left(d_1\left(x,t\right)\right)^2}{\tan\left(i_{\mathrm{b}}\left(x\right)\right) + \tan\left(\alpha - i_{\mathrm{b}}\left(x\right)\right)} \cdot L\left(x\right) \tag{10.5}$$

in which d_1 equals $d_0 \cdot \cos\left(i_{\mathrm{b}}\right)$ [m], i_{b} the transversal slope [-], α the angle of internal friction of
the bed material after dredging [∘], and L the length of the river section [m].

Distance d_0 is defined as:

$$d_0\left(x,t\right) = d_{\mathrm{N}}\left(x\right) - d_{\min}\left(x,t\right) + d_{\mathrm{e}} \tag{10.6}$$

in which d_{N} is the navigation channel depth [m] and d_{e} an extra depth of 0.5 m on top of the
required dredging depth.

Strategies for deposition of dredged material

According to the current dredging policy, the dredged volume has to be deposited elsewhere in
the river. We examine the following dredging strategies:

1.   removal of the dredged material without deposition elsewhere in the river;

2.   removal of the dredged material, and the dredged volume is deposited further upstream
        in the river;

3.   removal of the dredged material, and the dredged volume is deposited further down-
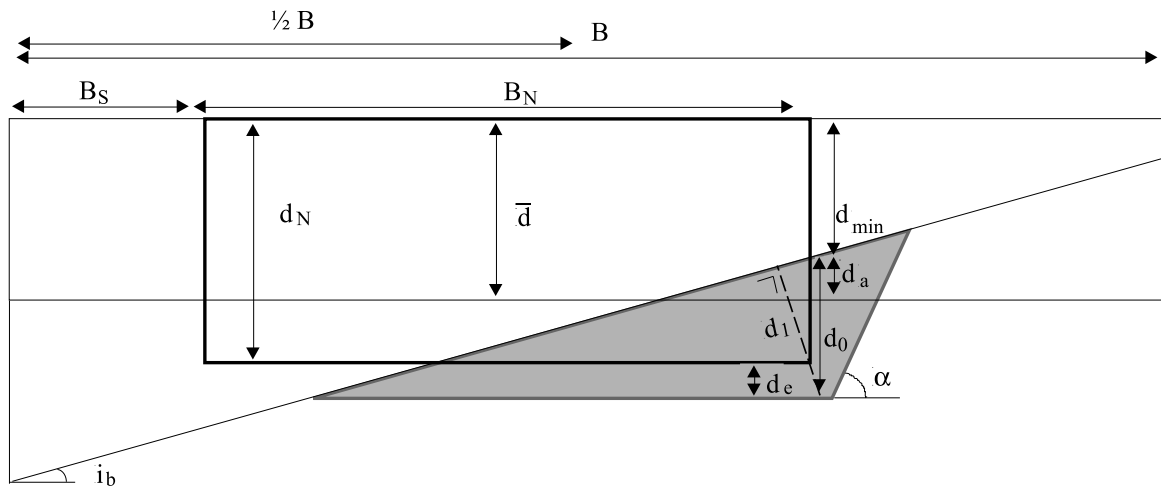   stream in the river.

Figure 10.3: Dredging volumes in the navigation channel

Obviously, the dredged volume is deposited at locations that have sufficient over-depth. We avoid deposition just upstream of locations that form (nearly) nautical bottlenecks. In that case, the sediment is deposited further up- or downstream.

Analytical equation for bed recovery after dredging

The major aim of dredging activity is to maintain or improve the navigation conditions. After dredging is undertaken, the river bed will however slowly return to the situation before dredging. Dredging is not a self-sustaining measure, it should be repeated every now and then. The process of bed recovery after dredging, illustrated in Figure 10.4, is defined as (De Rooij, 2005):

$$d\left(x,t\right) = d_{\min}\left(x,t\right) + d_0\left(x,t_0\right) \cdot e^{-t/T} \tag{10.7}$$

in which $d\left(x,t\right)$ is the critical water depth [m] at time t, $d_{\min}$ the critical depth in the cross-section of the navigation channel before dredging [m], d_0 the instantaneous deepening of the navigation channel by dredging [m] at time t_0.

The speed at which the bed position is restored is characterised by the time scale T, which is approximated as:

$$T = \frac{\lambda_{\mathrm{s}}\left(x,t_0\right) \cdot \overline{d}\left(x,t_0\right)}{s\left(x,t_0\right)} \tag{10.8}$$

in which λ_{s} is the adaptation length of bed topography development, $\overline{d}$ is the width-averaged water depth [m], and s the sediment transport rate per unit width [m^3/m/s].

The adaptation length of bed topography development is defined as (Struiksma et al., 1985):

$$\lambda_{\mathrm{s}} = \pi^{-2} \cdot \left(B/\overline{d}\right)^2 \cdot f\left(\theta\right) \cdot \overline{d} \tag{10.9}$$

in which B is the width of the disturbance in the river section [m], and $f_s(\theta)$ a function of the Shields parameter θ (Eq. 10.3). Time scale T is subsequently described with:

$$T = \frac{\lambda_s(x, t_0) \cdot \overline{d}(x, t_0)}{s(x, t_0)} = \frac{1}{\pi^2} \cdot \frac{B^2 \cdot f_s(\theta)}{s} \tag{10.10}$$
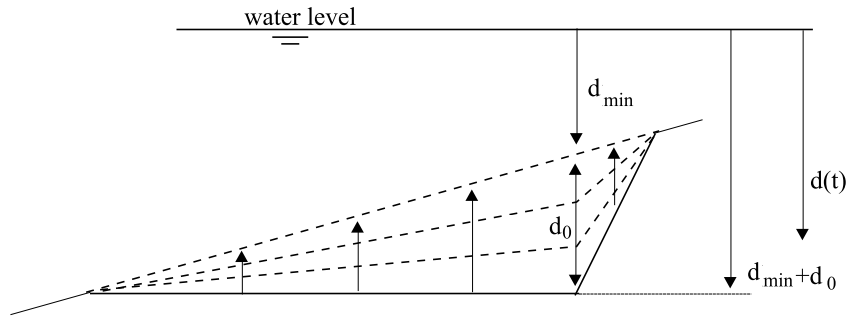
Figure 10.4: River bed recovery after maintenance dredging

The expression for the analytical recovery of the river bed is utilised in the impact assessment of dredging on navigability in Section 10.5.2.

10.4 Navigability of the Rhine

The MCS-results are utilised to quantify the uncertainty in the water depths along Niederrhein, Waal and IJssel. The width-averaged water depth predictions, $\overline{d}(x, t)$, are corrected for the transverse slope effect. For each location at each time step, the critical depth in the cross-section of the navigation channel $d_{min}(x, t)$ can be derived with the help of Eq. 10.4. In this section, navigability is statistically assessed without incorporating any dredging activity. In the analysis only the last 10 years of the 15 year simulation period are incorporated.

10.4.1 Navigability at various draughts

The navigability of the Rhine branches Niederrhein, Waal and IJssel for ships with a draught between 1.5 and 5 m is statistically assessed on the basis of 500 model runs. Each model run, driven by one out of 500 synthesised discharge time series, results in one possible future hydraulic and morphological evolution. For each model run, at successive time steps of 10 days, the most critical water depths are estimated along the entire length of the Rhine branches considered. The statistical properties of the navigability at various draughts can subsequently be determined.

Figure 10.5(a) shows the navigable percentage for the Niederrhein and the Waal at various draughts in the 10-year period between 2002 and 2012, for three different model runs. The differences between these model runs give a first impression of the uncertainty involved. Apparently, each model run is driven by a different discharge time series, and thus represents only one possible state of the navigability of the river.
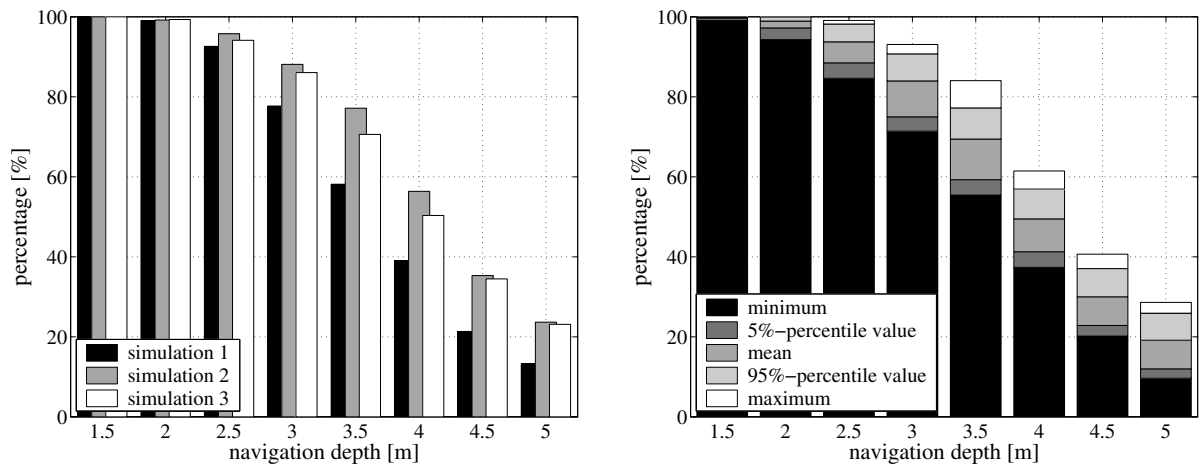
(a) Percentage for three individual model runs

(b) Statistical characteristics of the percentage for all model runs

Figure 10.5: Percentage of navigable time as a function of ship draught for the Niederrhein and the Waal in the period between 2002 and 2012

Using the results of all model simulations, the statistical characteristics of the navigable percentage are presented in Figure 10.5(b). The 10-year averaged percentage of navigable time for ships with a draught of 3 m, for instance, is 84% at the Niederrhein and the Waal. The figure also shows that for this draught there is a 90% probability that the percentage of navigable time lies between 75% and 91%. The size of the 90% confidence interval can easily be computed as the difference between the 95th percentile and 5th percentile. For a draught of 3 m, the 90%-confidence interval is approximately 16%. The maximum difference in percentage of navigable time for a draught of 3 m over all model simulations, is 93%-71%=22%.

A more or less similar picture is found for the IJssel (Figure 10.6). The navigability at various draughts differs for each model run, but it is generally much worse than in the Niederrhein and Waal. The navigability decreases suddenly for draughts larger than 2.5 m. The navigation channel dimensions of the IJssel are relatively small and the IJssel contains many sharp bends (see Figure 10.2(b)). The sharp bends result in a large correction to the water depth. Both aspects restrict the navigability at larger draughts.
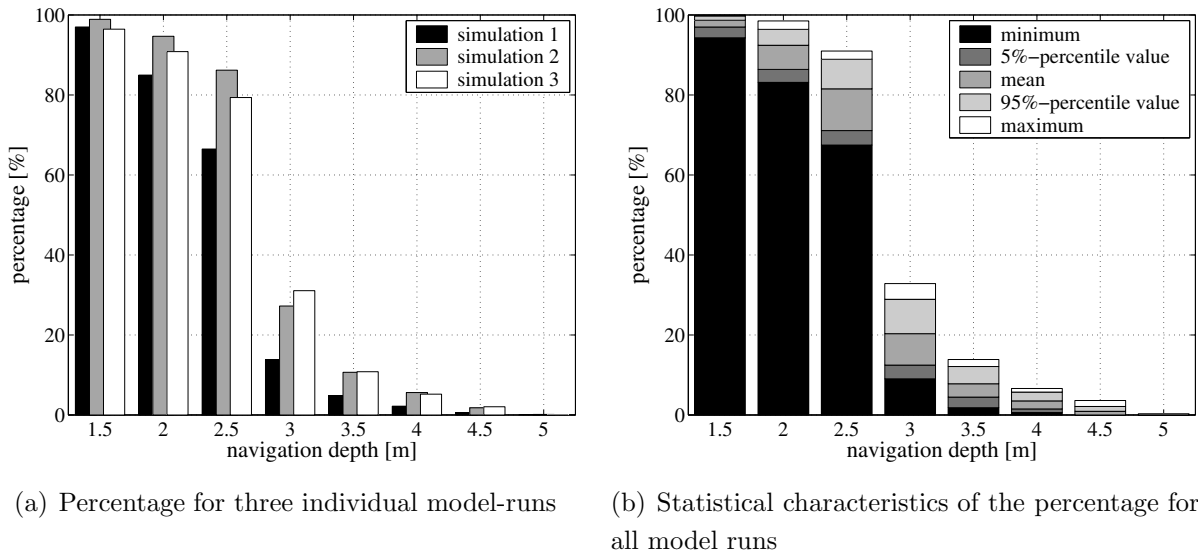
(a) Percentage for three individual model-runs

(b) Statistical characteristics of the percentage for all model runs

Figure 10.6: Percentage of navigable time as a function of ship draught for the IJssel in the period between 2002 and 2012

10.4.2 Probability of fulfilling navigation channel requirements

The probability of not fulfilling the navigation channel requirements of the National Traffic and Transportation Plan for ships of 2.8 m draught (for the Niederrhein and Waal) and 2.5 m (for the IJssel), at discharges beyond the threshold value of 1020 m^3/s at Lobith is of interest to both the river manager and the users of the inland waterway. It indicates to what extent the river manager manage to maintain the required navigation condition. Figure 10.7(a) shows the cumulative distribution function of the minimal navigation depth over a period of 10 years, for all simulations individually and the aggregate line of all simulations together.
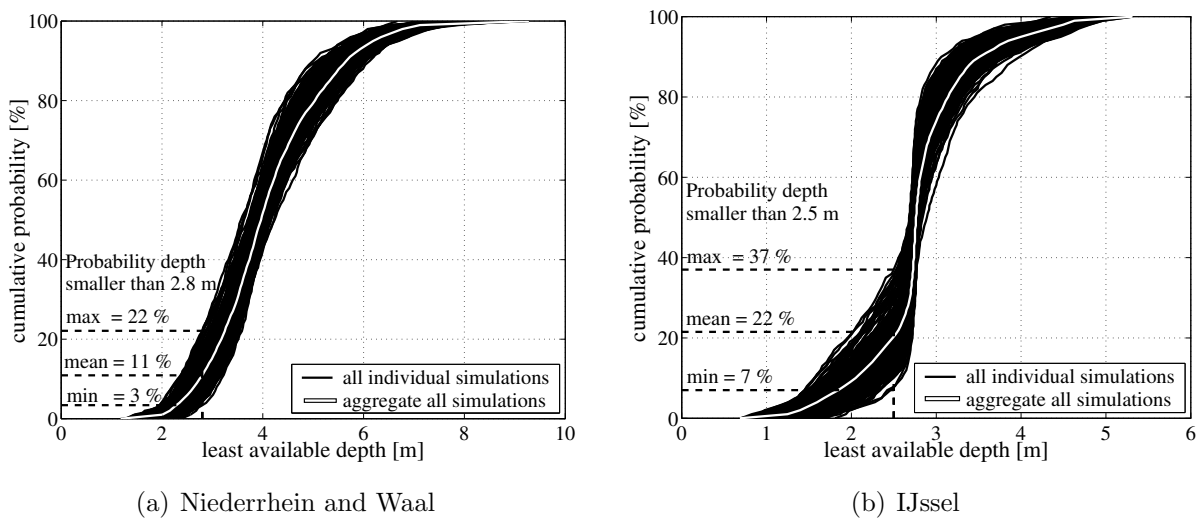

(a) Niederrhein and Waal

(b) IJssel

Figure 10.7: Cumulative probability distribution of the least navigable depth for all simulations individually (black lines) and the aggregate line (white line) together

The figure indicates that the probability of meeting the requirements, i.e. ships can navigate at draught of at least 2.8 m, is 89% (100% minus 11%). The minimum and maximum probability to meet the navigation criterion is 78% and 97%, respectively. This wide range shows the importance of MSC as compared to single deterministic simulations.

For the IJssel, the probability of fulfilling the navigation channel requirements is much smaller, namely 78% (100% minus 22%), see Figure 10.7(b). The probability of not meeting the conditions differs considerable for each simulation, as indicated by the width of the black band. This probability varies between 63% and 93% for all individual simulations.
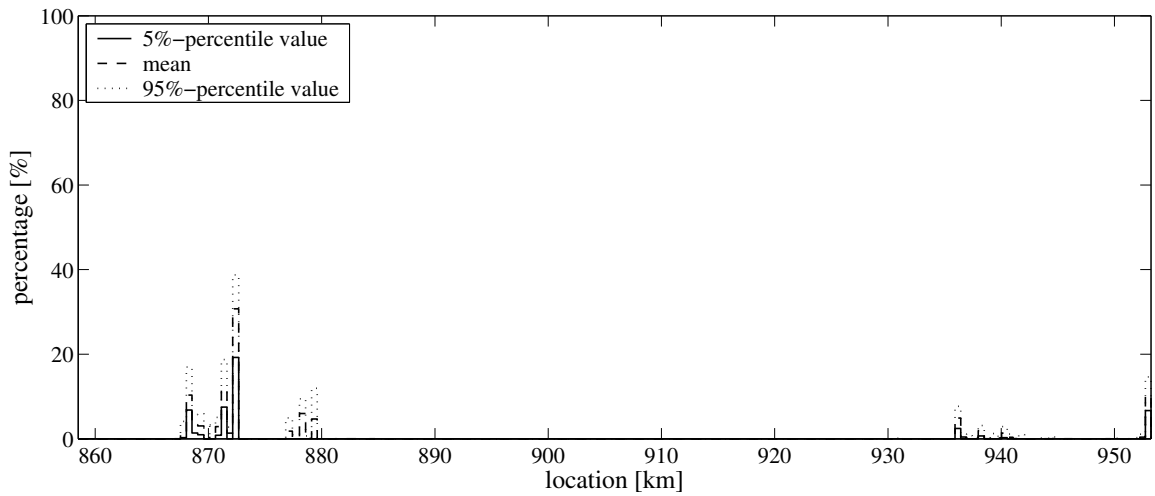
10.4.3 Nautical bottlenecks

The location that is the most restrictive to navigability at a certain point in time, meaning the location that has the lowest water depth of the complete stretch, is an important parameter for the river manager. This location is called the 'nautical bottleneck'. The curves in Figure 10.7 are composed of the critical depths at these bottleneck locations. The percentage of time that a location forms a nautical bottleneck is shown in Figure 10.8.

Clearly, locations with sharp bends have a high probability of forming a nautical bottleneck. At the Niederrhein and Waal, high percentages are found in the sharp bend section just downstream of the Pannerdensche Kop bifurcation (km 867-884). Moreover, nautical bottlenecks are formed in the downstream region km 935-940. The sharply curved IJssel bends at km 884, km 935, km 944 and km 985 have a high probability of containing the lowest depth of the complete stretch.

Figure 10.8 indicates, however, only the few locations that are critical to the entire stretch. It gives no valuable information on the navigability at any arbitrary location that does not contain the critical depth. Figure 10.9 illustrates the percentage of navigable time as a function of the river location for a different draughts in the Niederrhein and Waal, and the IJssel. This provides insight into which locations are also restricting the river's navigability.
It appears that locations with sharp bends (see Figure 10.9(e)-(f)), along with locations containing geometrical non-uniformities, such as the bifurcation Pannerdensche Kop (km 867), and the outer bend fill-up near Nijmegen (km 882 - 885), may evolve into navigation bottlenecks. Moreover, there seems to be a correlation between the variation in floodplain width and the percentage of time that a location forms a bottleneck, with a lag of approximately 0.5 to 1.0 km. Clearly, this is associated with the bed wave forming at these locations (see Section 6.4.2). Most of these bottlenecks become manifest in the dry season.
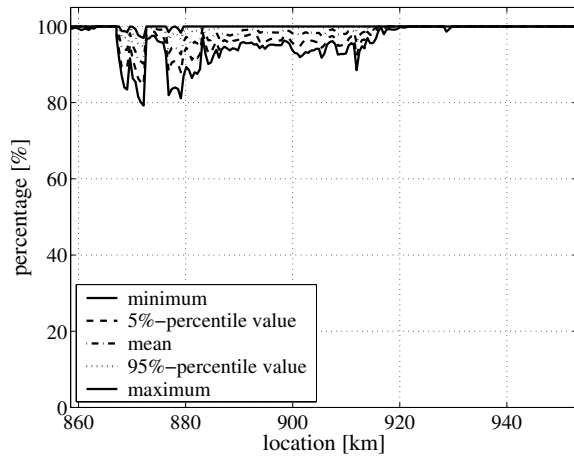
(a) Niederrhein and Waal
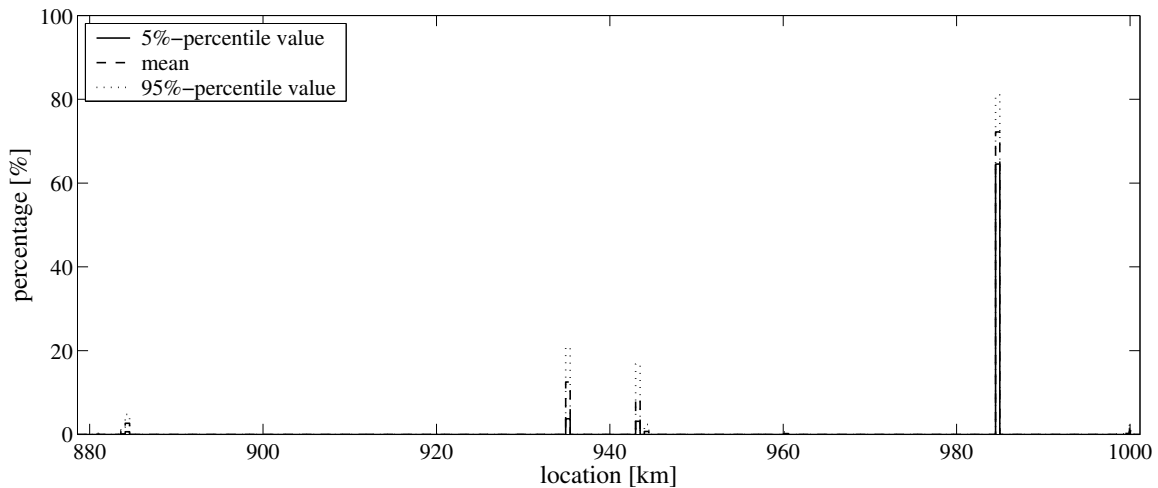
(b) IJssel

Figure 10.8: Percentage of time that a location forms a nautical bottleneck

10.4.4 Verification with field observations and measurements

Least Measured Depths in the Niederrhein and Waal, available over the period 1993-2003, give an impression of the river's navigability, and of bottlenecks in the navigation channel.

The users of the inland waterway are informed every day about the limitations of the navigation channel. When the water level at Nijmegen (km 884) drops below 9m + NAP, the Least Measured Depth (LMD) is announced, being the critical depth along the complete Niederrhein and Waal stretch. This enables the navigation traffic to adjust its cargo, hence its draught, to this depth. Beyond the water level of 9m + NAP, the navigation channel is supposed to be fully open and the cargo capacity of ships is not restricted.
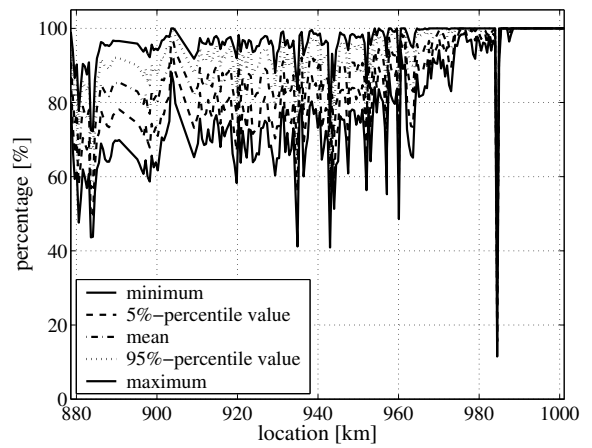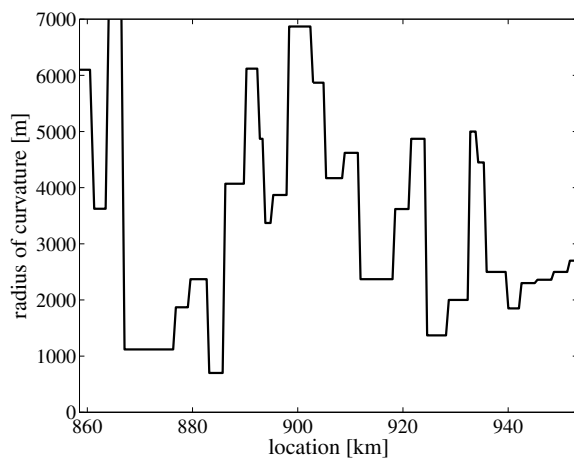
(a) Niederrhein and Waal - navigation depth 2.8 m
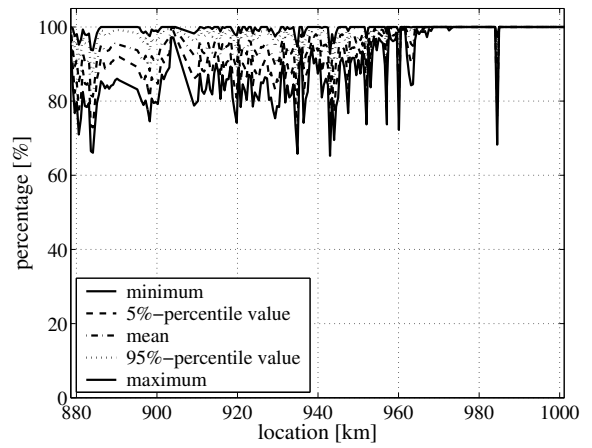
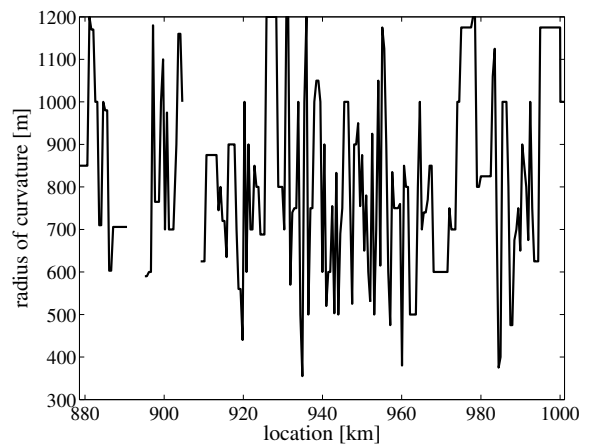(b) IJssel navigation depth 2.5 m
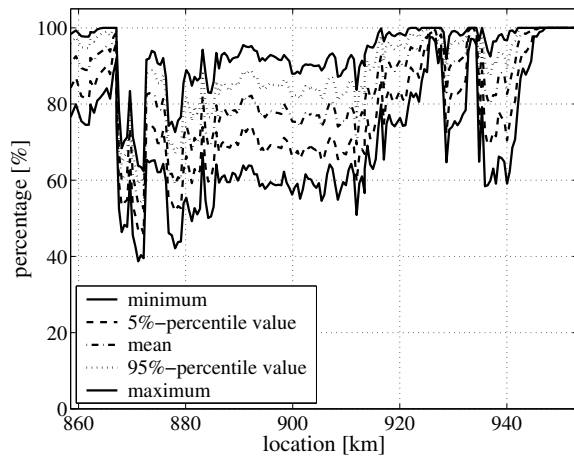
(c) Niederrhein and Waal - navigation depth 4 m

(d) IJssel - navigation depth 3 m

(e) Niederrhein and Waal - radius of curvature

(f) IJssel - radius of curvature

Figure 10.9: Percentage of navigable time over a period of 10 years as a function of the river location for ships of two different draughts

Only one bottleneck location along with its LMD is defined in the LMD-database at a certain point in time, viz. the location with the critical depth. In fact, the bottleneck may occur at more than one location at a time, but only one of them is included in the database. The LMD-database is used in this section for validation purposes. A comparison between the observations and the model results is made on the basis of two aspects:

1.   the probability of fulfilment of the navigation channel requirements;

2.   the percentage of time that every location forms a bottleneck.

Since LMD-data is not available for the IJssel, we restrict this verification to the Niederrhein and Waal.

Figure 10.10 shows the LMD in the Niederrhein and Waal, in the period 1993-2003, and the water level at Nijmegen as a function of the discharge at Lobith. In practice, the LMD is determined when the water level at Nijmegen drops below 9m + NAP. As becomes apparent from the figure, the maximum discharge at which an LMD is established is 4090 m^3/s, whereas the minimum discharge without LMD is 2200 m^3/s. So there is not a unique relationship between the discharge at Lobith and the water level at Nijmegen (see Figure 10.10(b)). The largest observed LMD equals 5.2 m. The LMD is meant to inform the navigation traffic. Since, the largest cargo ships in the Rhine have a maximum draught of 4.5 m, it is not necessary to announce LMDs larger than approximately 5 m.

(a) Least Measured Depth as a function of the discharge at Lobith

(b) Water level at Nijmegen as a function of the discharge at Lobith
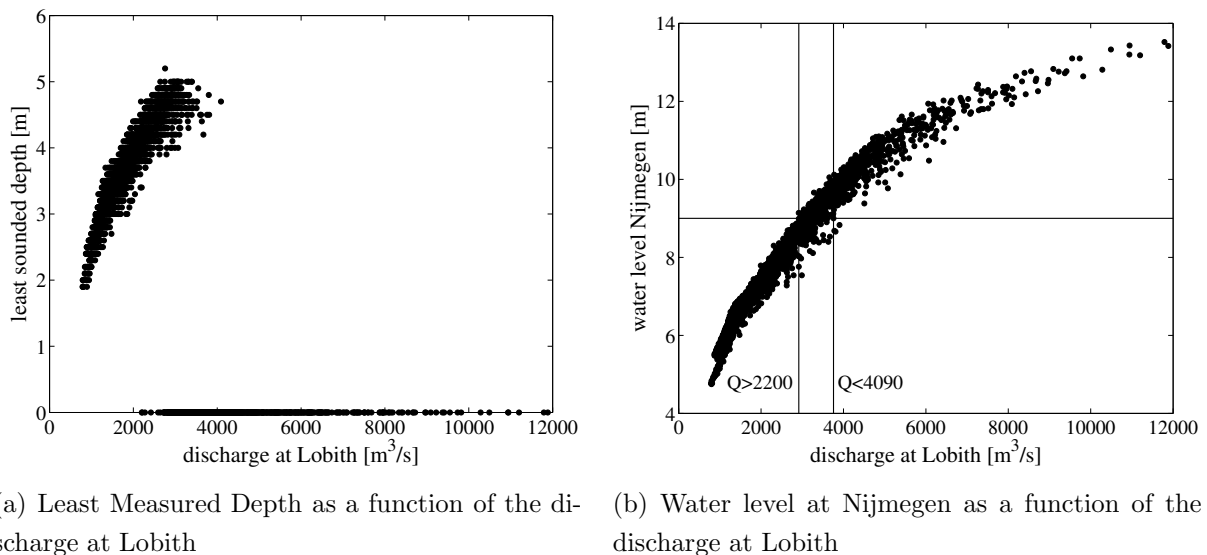
Figure 10.10: Least Measured Depth in the Niederrhein and Waal and water level at Nijmegen as a function of the discharge at Lobith

Probability of fulfilment of the navigation channel requirements

In order to make the Rhine model results comparable to the LMD-data, we consider only the least computed depths less than 5.2 m. Figure 10.11 shows the cumulative probability

distribution of the LMD-data and the 1-D Rhine model simulations for depths less than 5.2 m. The grey area indicates the statistical uncertainty around the probability distribution curve of the Rhine model computations. The Rhine model computations match reasonably well with the LMD data, as the curve of LMD-data mostly lies within this grey area for LMDs less than 4 m. Yet, there is a systematic discrepancy (measured data have less variance).
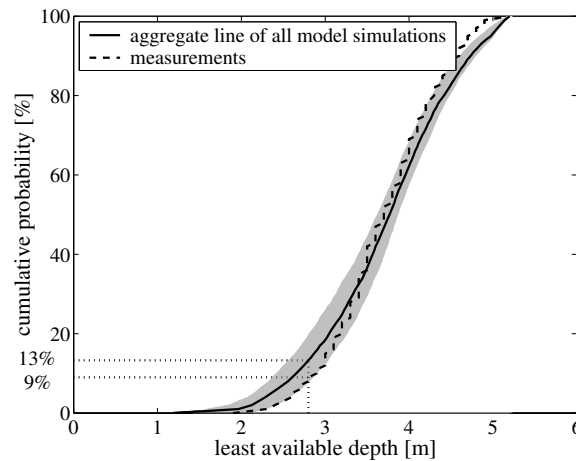

Figure 10.11: Cumulative probability distribution of the least measured depth and the least available depth derived from all 1-D Rhine model simulations for the Niederrhein and Waal

The probability of a water depth below 2.8 m appears to exceed the limit set by the NTTP of 5% for both cases, viz. 9% and 13% for the LMD-data and the model computations, respectively. The required channel depth has been increased from 2.5 m to 2.8 m only recently. Considering the 'old' depth requirement, the probability of having a draught less than 2.5 m reduces to 3% and 7% for the LMD-data and the model computations, respectively.

Percentage of time that a location forms a bottleneck

The percentage of time (with the water level at Nijmegen below 9m + NAP) that a location forms a nautical bottleneck is shown in Figure 10.12, for the LMD-data and the mean percentage values of the model results. There is a strong discrepancy between the LMD-data and the model predictions. Considering the model hindcasts, downstream of Pannerdensche Kop bifurcation up to km 884, the probability of bottleneck formation is high, whereas in practice an LMD seldom occurs in this section. Contrarily, the percentage that a location in the section between km 898 and 920 forms a nautical bottleneck is rather large, whereas the model predicts very low percentage values.

This discrepancy can, first of all, be explained from practice of buoy placement. Especially in sharp bends, buoys are frequently replaced in order to have a narrower but deeper navigation channel. In the section between the Pannerdensche Kop and Nijmegen (km 867-885), and the

Waal section between Winssen (km 895) and Ophemert (km 919), the navigation channel width
is regularly reduced by buoys to enhance the channel depth. This suggests that the LMDs cannot
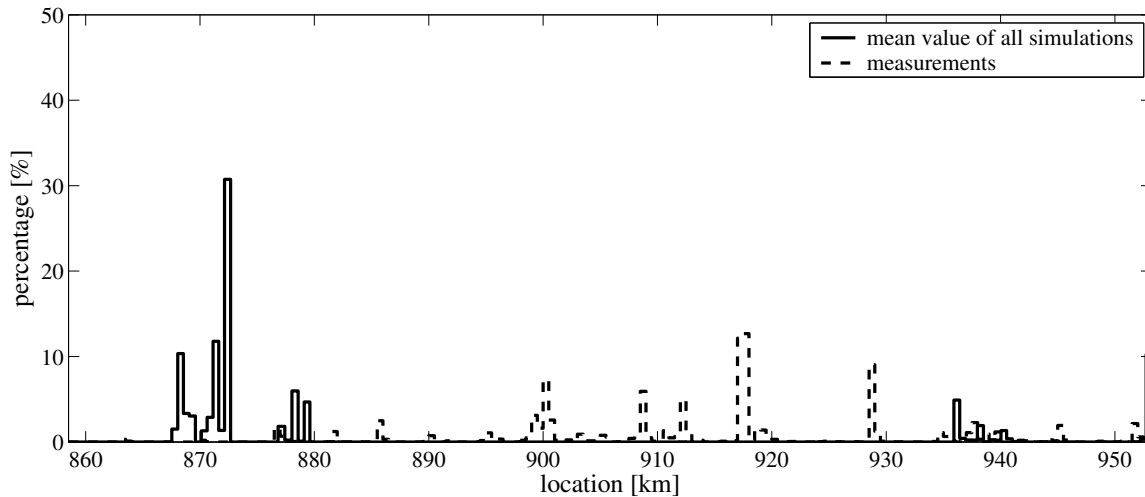be interpreted properly without taking the buoy placement into account.

Figure 10.12: Percentage of time that a location forms a nautical bottleneck for the Niederrhein and
Waal

Subsequently, as outlined in Chapter 6, the model seems to overestimate the morphological
activity between Pannerdensche Kop bifurcation and km 873. The bed level variability is more
pronounced in the model simulations than in bathymetric data. The overestimation of the
morphological activity in the model may induce nautical bottlenecks.

Although we account for the 2D-effect induced by sharp bends, the 1-D model neglects certain
morphological processes, such as the formation of complex morphodynamic features caused by
three-dimensional cross-flows over the main channel at locations with large floodplain areas
that are located alternately at the right and the left side of the river, or at confinements of
the floodplains by winter dikes. Shoals may be formed in the middle of the river at crossings
between two opposite bends. Groyne flames may extend some tens of metres into the main
channel. These complex morphodynamic features may become critical to navigability under
low-flow conditions. The model does not account for these multi-dimensional features, whereas
in the LMD-data these effects are incorporated.

It was also found that navigation-induced currents affect the bathymetry of the river in flat-
tening the tops of the dunes (Wilbers, 2004). Finally, the river is subject to continuous dredging
for enhancing its navigability. This, of course, has a large influence on the LMD-data.

10.5   Maintenance dredging in the Rhine

10.5.1 Dredging strategies

In line with the Dutch policy, the dredged volume has to be deposited elsewhere in the river. Three different dredging strategies are evaluated, viz. (1) removal of the dredged material, (2) removal of the dredged material, and further deposition upstream, and (3) removal of the dredged material, and further deposition downstream. For the Waal, maintenance dredging is mainly concentrated in one part of the river, viz. the section between the Pannerdensche Kop and Nijmegen (km 867- 884), whereas in the IJssel dredging takes place throughout the river. There is no need for maintenance dredging in the Niederrhein.

Figure 10.13 shows the distance between dredge and dump location for the strategy of upstream and downstream depositioning. Figure 10.14 shows the statistics of the yearly amount of dredging in Waal and IJssel. The dashed lines in Figure 10.14 represent the dredging volumes obtained from historical data.
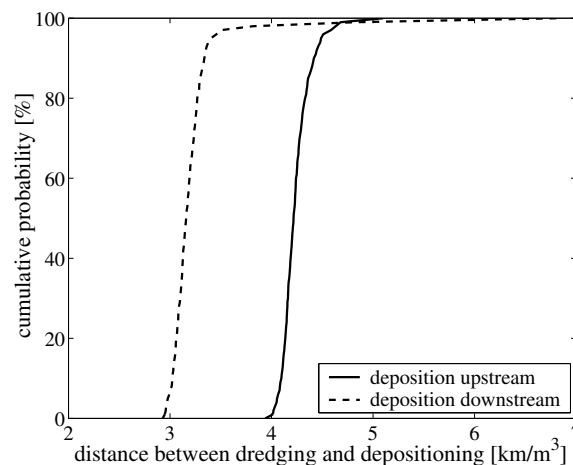
Figure 10.13: Cumulative probability distribution of distance between dredge and dump location for the strategy of upstream and downstream depositioning

Apparently, there is a large uncertainty involved in the prediction of dredging volumes. The historical dredging data turns out to stay within the 90% bandwidth derived for each of the three dredging strategies, though mostly at the lower end.

For the entire Niederrhein, Waal and IJssel (Figure 10.14(a)), dredging without depositing the dredged material elsewhere in the river results in the lowest dredging volumes, whereas deposition of dredged material in upstream direction yields the largest dredging effort. Deposition downstream leads to lower dredging volumes than deposition upstream. A first explanation may be found from the analytical equilibrium model, presented in Section 5.2.1.
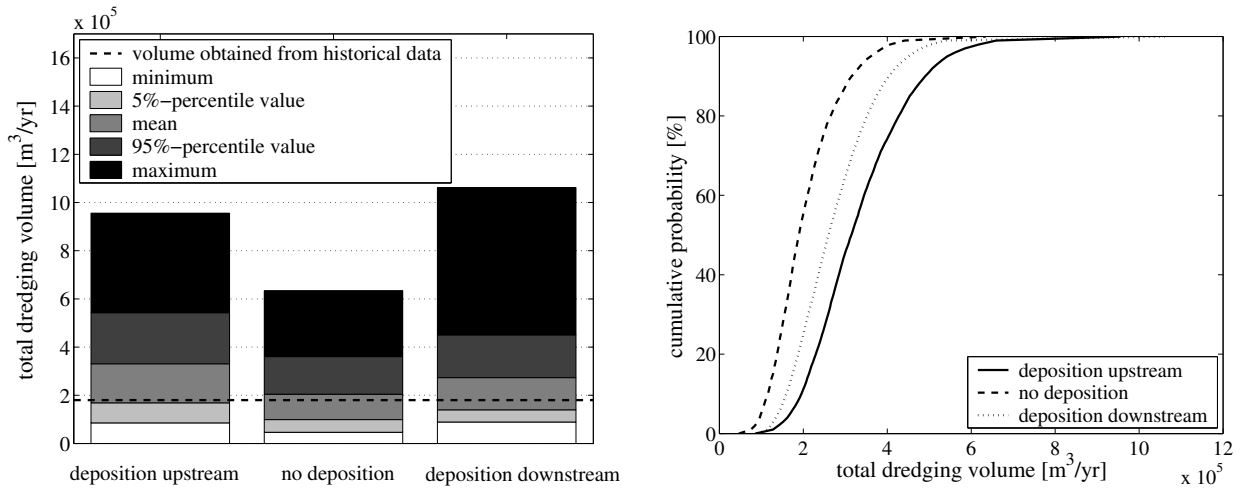
(a) Total amount of dredging in Waal and IJssel
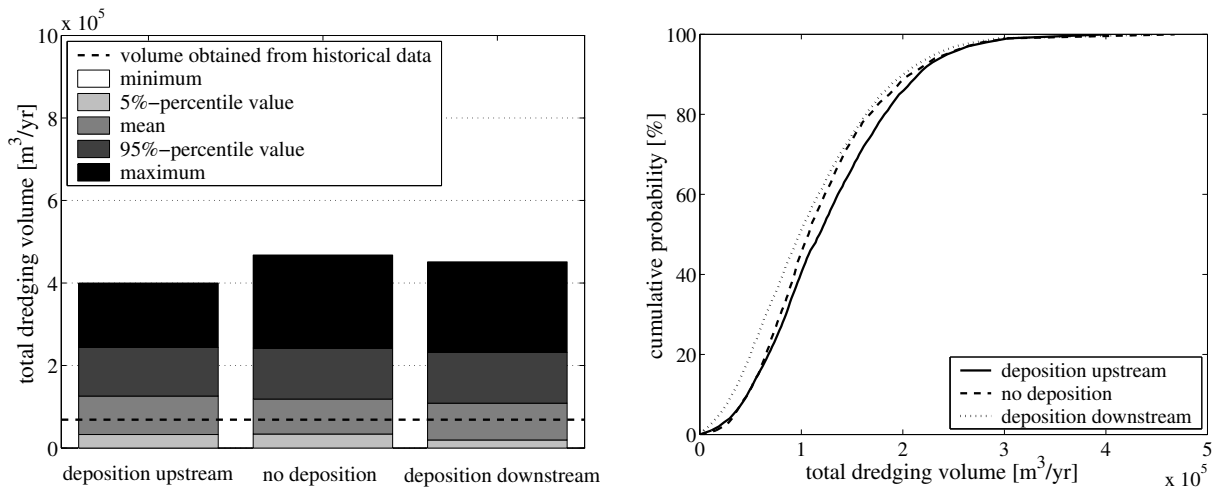
(b) Waal
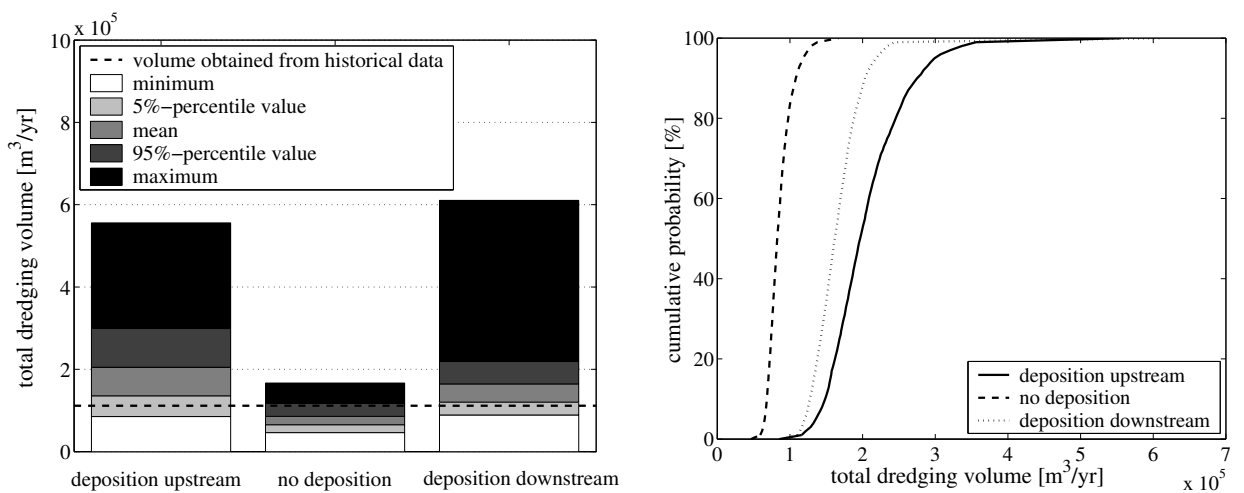
(c) IJssel

Figure 10.14: Statistical properties of dredging volumes in the Rhine branches per dredging strategy

Although a static equilibrium will never be reached, it gives a first indication of the long-term longitudinal profile changes caused by either deposition strategy. The equilibrium state is described by the following formulae for the bed slope $i_{\text{eq-0}}$ and the water depth $h_{\text{eq-0}}$:

$$i_{\text{eq-0}} = \left(\frac{S}{mB_{\text{s}}}\right)^{3/n} \frac{B_{\text{s}}}{C^2 Q} \tag{10.11}$$

$$h_{\text{eq-0}} = \left(\frac{S}{mB_{\text{s}}}\right)^{-1/n} \frac{Q}{B_{\text{s}}} \tag{10.12}$$

in which S is the total amount of sediment transported per unit time through the river cross-section, Q the discharge, B_{s} the sediment transporting width, m and n parameters in the (power-law) sediment transport formula, and C the Chézy coefficient.

If sediment is withdrawn from the river and always deposited further downstream, the amount of sediment to be transported per unit of time by the river is reduced from S_0 to $S_0 - \Delta S$. Downstream deposition therefore leads to a reduction of the longitudinal bed slope:

$$i_{\text{eq}} = \left(\frac{S_0 - \Delta S}{mB_{\text{s}}}\right)^{3/n} \frac{B_{\text{s}}}{C^2 Q} = \left(1 - \frac{\Delta S}{S_0}\right)^{3/n} \cdot i_{\text{eq-0}} \tag{10.13}$$

and water depth will be increased:

$$h_{\text{eq}} = \left(\frac{S_0 - \Delta S}{mB_{\text{s}}}\right)^{-1/n} \frac{Q}{B_{\text{s}}} = \left(1 - \frac{\Delta S}{S_0}\right)^{-1/n} \cdot h_{\text{eq-0}} \tag{10.14}$$

The enhancement of the water depth results in a smaller dredging demand.

Contrarily, deposition upstream leads to a steeper bed and a reduction of the water depth. Accordingly, the required amount of dredging is enhanced.

Upstream deposition also entails a larger distance between dredge and dump location, as illustrated in Figure 10.13, so the strategy of downstream deposition of dredged material is preferable from an economical point of view.

If we consider the Rhine branches separately, a similar picture can be observed for the IJssel. Dredging occurs in the entire branch, therefore extracted sediment is deposited along the entire branch, as well. Both upstream and downstream deposition of the dredged material leads to the formation of new bottlenecks, through which extra maintenance dredging is required. Consequently, both strategies lead to much larger volumes than when deposition is not compulsory.

In contrast, in the Niederrhein and Waal downstream deposition of the dredged volume results in slightly lower volumes than in the situation without deposition of the dredged material elsewhere in the river. This is clearly illustrated in the right panel of Figure 10.14(a), as the cumulative probability curve of the former strategy is positioned left from that of the latter. This can be explained by the fact that extraction of sediment is restricted to a few locations in the section between Pannerdensche Kop and Nijmegen. The dredged material is deposited

further downstream and does not entail new bottlenecks. So, the strategy does not induce extra maintenance dredging elsewhere, as we found in the IJssel. Furthermore, slightly more water is drawn into the Waal for the dredging strategy with downstream deposition, (Figure 10.15). This yields larger water depths and therefore in a lower dredging effort.
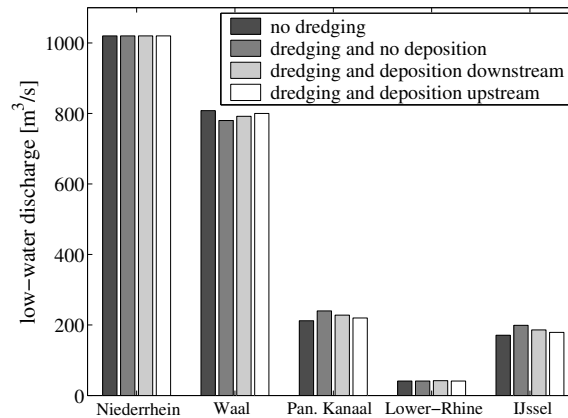

Figure 10.15: Discharge distribution over the Rhine for low-water conditions (1020 m^3/s at Lobith)
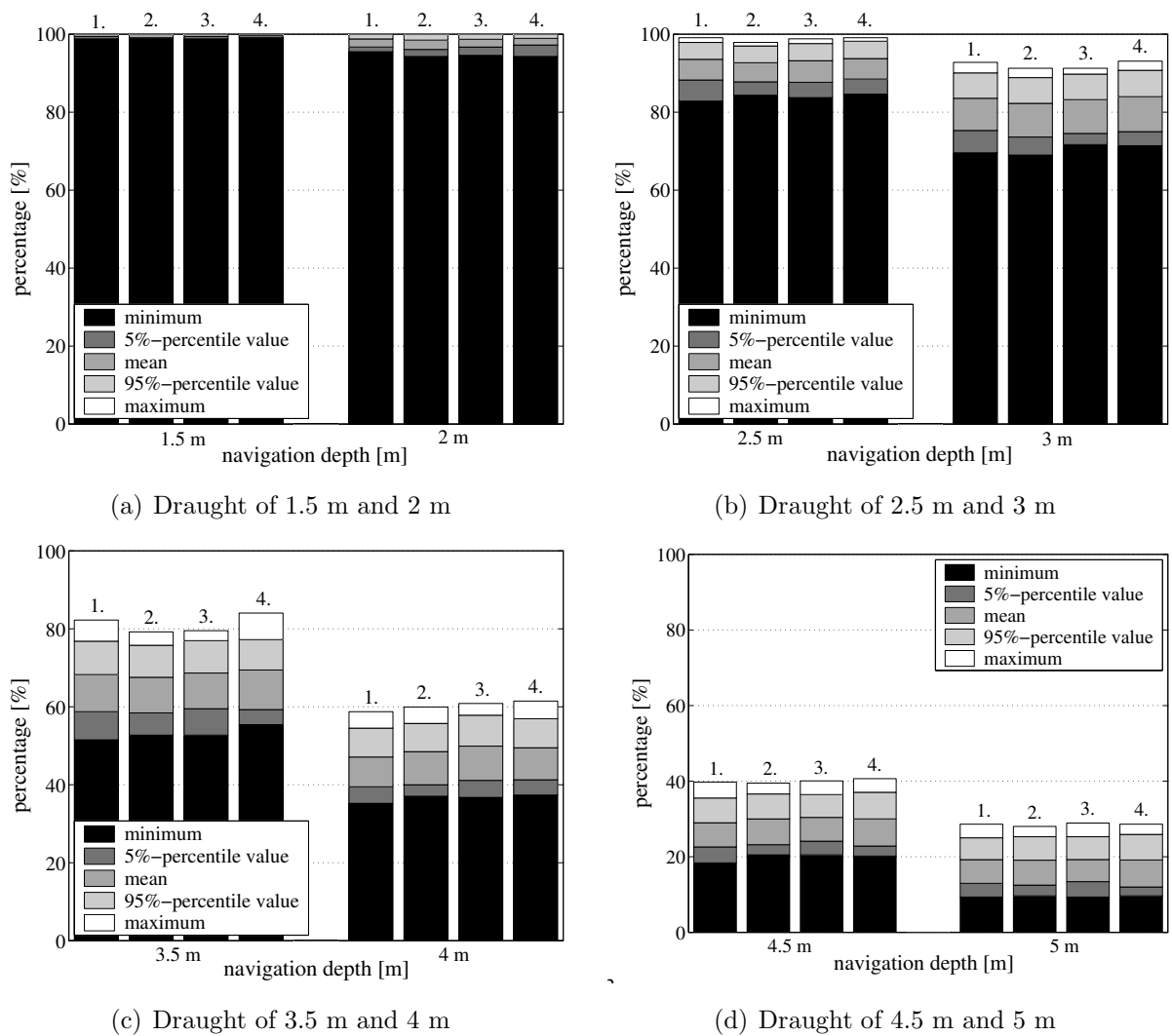
10.5.2 Impact of maintenance dredging on navigability

The principal aim of dredging is to maintain the navigability. The impact of the different dredging strategies on navigability is assessed in this section.

Bar plots in Figure 10.16 show the percentage of navigable time in the Niederrhein and Waal as a function of ship draught for the different dredging strategies, along with the reference situation in which no dredging takes place.

Apparently, dredging in the Niederrhein and Waal does not have a large influence on navigability. It seems that the difference between the different strategies and the situation without dredging is only marginal. This, can amongst, others be explained by the fact that the dredging strategies inducing a change in discharge distribution at the Pannerdensche Kop bifurcation. As indicated in Figure 10.15 slightly more water flows into the Pannerdensche Kanaal than in the no-dredging case, at the expense of the discharge into the Waal. It seems that the discharge reduction counteracts the enlargement of water depths realised by means of dredging.

If one remove nautical obstacles and deposit the material elsewhere, it will take a time for a new bottleneck to form. Until then, navigability is improved. So, dredging must not be expected to provide for a definitive solution, one has to keep on doing it. The bed recovery in the Waal after dredging takes place rather fast. In approximately 150-200 days the bed adapts towards the situation before dredging. As the dry season ends in November and dredging takes place in May, nautical bottlenecks can be formed again at the end of the dry season.

(a) Draught of 1.5 m and 2 m

(b) Draught of 2.5 m and 3 m

(c) Draught of 3.5 m and 4 m

(d) Draught of 4.5 m and 5 m

(1) no dredging, (2) dredging and upstream deposition, (3) dredging without deposition, (4) dredging and downstream deposition

Figure 10.16: Percentage of navigable time as a function of ship draught for the Niederrhein and Waal in the period between 2002 and 2012 for four situations

Although the conclusion that navigability is hardly affected by means of dredging, the model findings are in line with the first experiences with dredging in the Waal. Evaluation of this new policy in practice indicates that maintenance dredging in combination with upstream deposition hardly effect the navigation conditions (personal communication with river manager).

For the IJssel the opposite can be noticed in Figure 10.17. Navigability turns out to be improved by means of maintenance dredging. Dredging without deposition of the dredged material elsewhere in the river yields the best navigability. Due to either upstream or downstream deposition of the extracted sediment, new nautical bottlenecks forming elsewhere restrict navigability. The strategy of downstream deposition yields a better navigability than upstream deposition. This can be explained partly by the fact that slightly more water is drawn into the IJssel in the former case (see Figure 10.15). Conversely, consistent downstream deposition of dredged

material, leads to a reduction of the bed slope and an increase of the water depth. The opposite
is expected for the strategy with upstream deposition, viz. a steeper bed and a reduction of the
water depth. In conclusion, navigability benefits more from downstream than from upstream
deposition.

(a) Draught of 1.5 m and 2 m

(b) Draught of 2.5 m and 3 m

(c) Draught of 3.5 m and 4 m
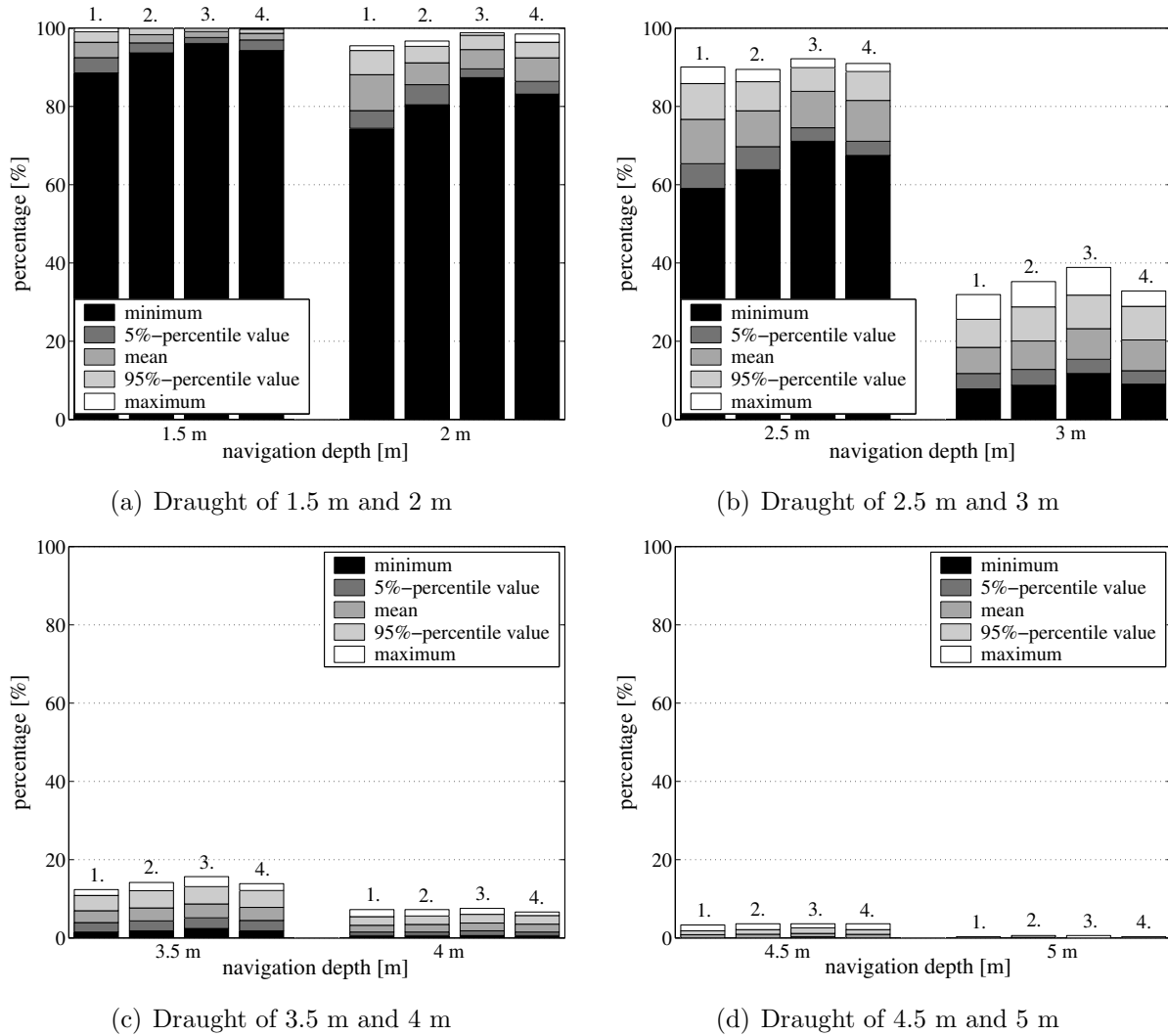
(d) Draught of 4.5 m and 5 m

(1) no dredging, (2) dredging and upstream deposition, (3) dredging without deposition, (4) dredging and downstream deposition

Figure 10.17: Percentage of navigable time as a function of ship draught for the IJssel in the period
between 2002 and 2012 for four situations

10.6 Adequacy of a 1-D model approach in navigability assessment

The problem of excluding multi-dimensional phenomena in the 1-D model was briefly addressed
in Section 10.4.4. The major aim of this section is to further investigate to what extent the
1-D model approach in combination with analytically based post-processing to account for the

2D-transverse slope effect is sufficient to assess navigability, or whether a multi-dimensional model is more appropriate. To that end, the quasi-3D model as discussed in Chapter 7 is used. For a good comparison between the two models, we restrict the research area in both models to a 30 km Waal reach, from km 893 to km 923. The model computations of both models cover a period of 5 years and the sample size of the MCS has been reduced to 100 simulations to limit the computational effort. A 1 year spin-up is considered sufficient to dissipate errors induced by the initial bathymetry and model settings.
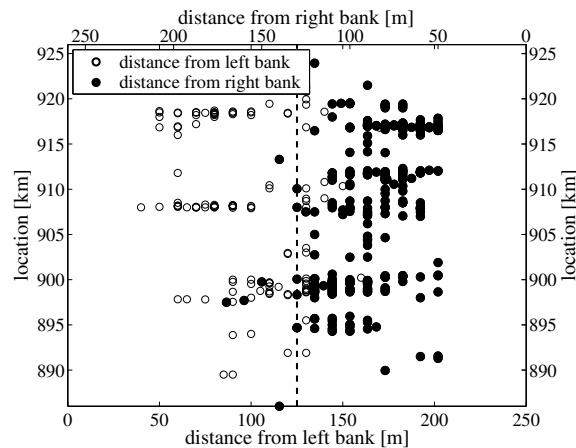

Figure 10.18: Distance of LMD from the river bank in the Middle-Waal, as derived from LMD-data

Shortening the computation period from 10 to 5 years, will entail a somewhat larger uncertainty range, as the effect of random behaviour, for instance in discharges, becomes more pronounced with a shorter simulation period (Hetzer, 2005). With a longer period, navigability is affected by a larger number of extreme conditions, both low-water and flood conditions, hence the statistics are less influenced by random behaviour. The uncertainty smooths out, but does not necessarily go to zero in the very long run. The sample size of 100 simulations appears to be sufficient to let the statistics of the percentage of navigable time at various draughts converge.

The 1-D model yields only cross-sectionally averaged water depths, whereas the quasi-3D model provides additional information on the depth distribution over the cross-section. Due to transverse slope development, and the formation of shoals in the middle of the river, for instance, the depth is not uniformly distributed, but shallow parts can be found anywhere in the cross-section. This is clearly indicated in Figure 10.18 that shows the position of the nautical bottlenecks in the cross-section, derived from LMD-data measured at a certain distance from the left or right bank. The quasi-3D model incorporates multi-dimensional phenomena that could play an important role for navigability. Beyond that, multi-dimensional models also allow for examining the navigable width in combination with the water depth and thus may give a better view on navigability in reality.

For the quasi-3D model, first a navigation channel of 150 m width has been defined at a

security distance of 25 m from the outer bend, where the largest depths are found. Subsequently, the critical depths $d_c(x,t)$ within this channel profile are derived for all model outputs. The navigability is then assessed for ships with draughts varying from 1.5 to 5 m (Hetzer, 2005). The left panel of Figure 10.19 shows the navigable percentage at various draughts for three arbitrarily chosen simulations, whereas the statistics of all simulations are plotted in the right panel.
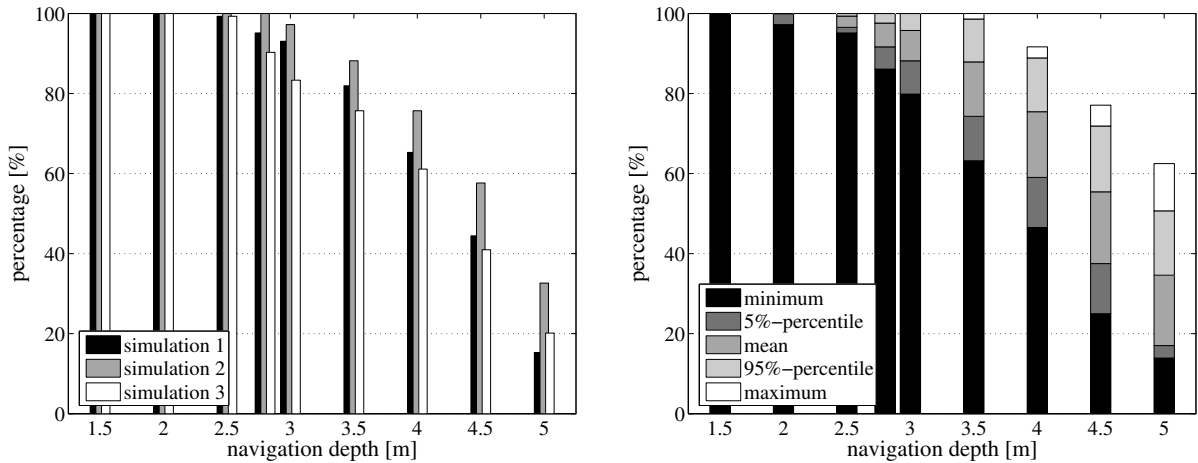
(a) Percentage for three individual model runs   (b) Statistical characteristics of the percentage for all model runs

Figure 10.19: Percentage of navigable time as a function of ship draught for the Waal reach in the period between 2004-2009, as derived from the quasi-3D model
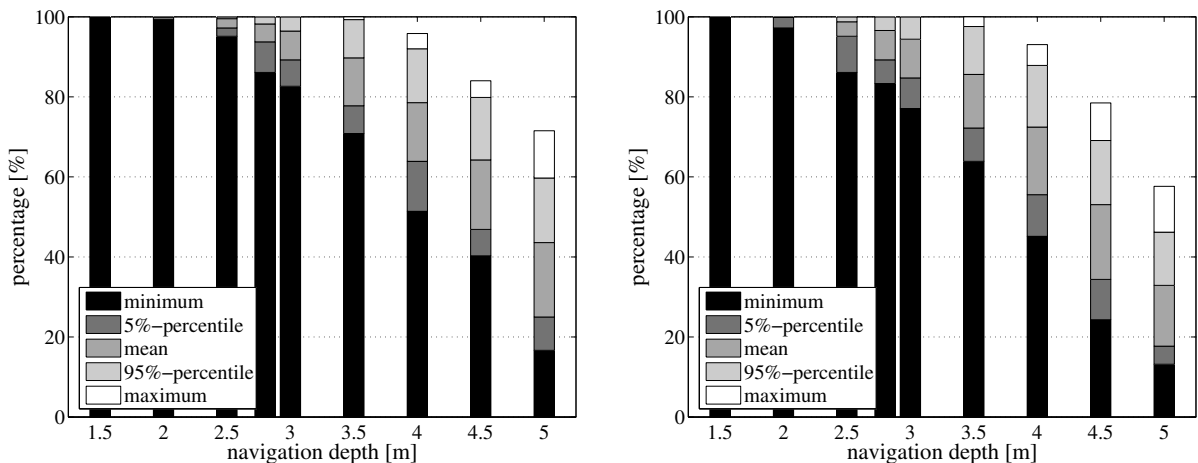
(a) Without transverse slope correction   (b) With transverse slope correction

Figure 10.20: Percentage of navigable time as a function of ship draught for the Waal reach in the period between 2004-2009, as derived from the 1-D Rhine model

In Figure 10.20, the statistics of the navigable percentage are shown for the 1-D model with and without transverse slope correction. It seems that the difference between the 1-D model with

transverse slope correction and the quasi-3D model is only marginal. For instance, for a draught of 2.8 m, the mean navigable percentage is for both models 97%. The size of the 90% confidence interval is 26% (100%-84%) for the 1-D model versus 24% (100%-86%) for the quasi-3D model. The 1-D model in combination with a correction for transverse slope appears to perform quite well. If we do not account for 2D-transverse slope effect, the predicted navigability increases, but deviates stronger from the results of the quasi-3D model.

The cumulative probability distribution curve of the least available depth for the quasi-3D model, along with those for the 1-D model with and without transverse slope correction is shown in Figure 10.21. If we do not account for the transverse slope effect, the curve is positioned right from the other ones, meaning that the navigability is much better and the probability of not fulfilling the NTTP criterion of 2.8 m is lower. The plots show a good fitting between the quasi-3D model, the 1-D model with transverse slope correction and the LMD-data.
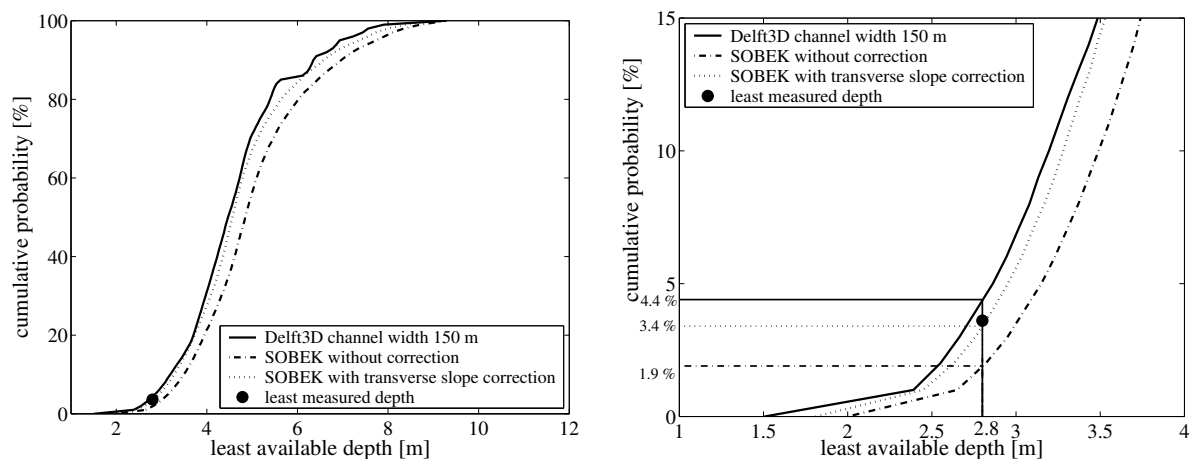
Figure 10.21: Cumulative probability distribution of the least available depth, as derived from both models. The right panel is a blow-up of the lower part of the left panel.

The quasi-3D approach enables assessing the navigability in two dimensions, meaning that the probability of fulfilling the navigation channel requirements of a certain width and a certain depth can be derived. Stack plots in Figure 10.22 show these probabilities as a function of time and space for channel dimensions of 150 m width by 2.8 m and 3.5 m depth, respectively. Obviously, the probability of having a 150 m wide navigation channel of 3.5 m depth is much lower than for one with a depth of 2.8 m. The dark shaded areas indicate where and when navigation is restricted, the white spots show the opposite. Darker horizontal bands indicate time periods with a lower navigability, whereas darker vertical bands indicate locations where nautical bottlenecks frequently occurs. The pictures show a strong seasonality (yearly horizontal bands).
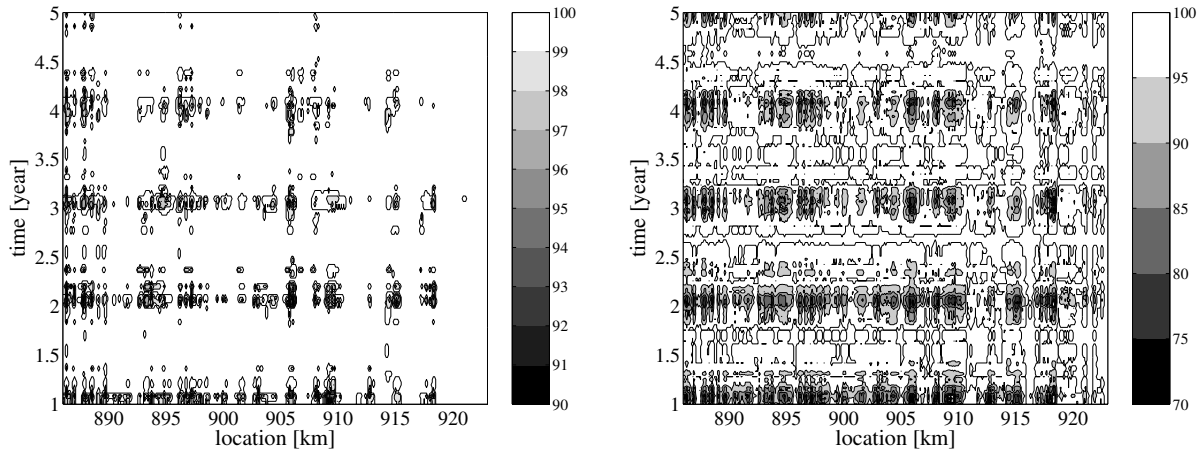
(a) For a shipping width of 150 m and a draught of 2.8 m

(b) For a shipping width of 150 m and a draught of 3.5 m

Figure 10.22: Probability of fulfilling navigation conditions as a function of time and space for the navigation channel requirements of 150 m width and 2.8 m and 3.5 m draught, respectively, as derived from the quasi-3D model

From an economical point of view, the river manager prefers to keep a channel depth of 3.5 m as long as possible. Accordingly, when the depth drops below 3.5 m, he will attempt placing buoys in order to delineate a narrower, but deeper navigation channel. The channel width might be even reduced to a width smaller than the NTTP-width requirement of 150 m. This is done until a channel width of 100 m is reached, from then on the channel width is no longer reduced, but the LMD is announced. Data of the placement of buoys is available for the period 1999 to 2003. Figure 10.23 shows the locations where buoys are positioned on a regular basis, along with the percentage of time that the channel width is smaller than 200 m and 150 m, respectively.
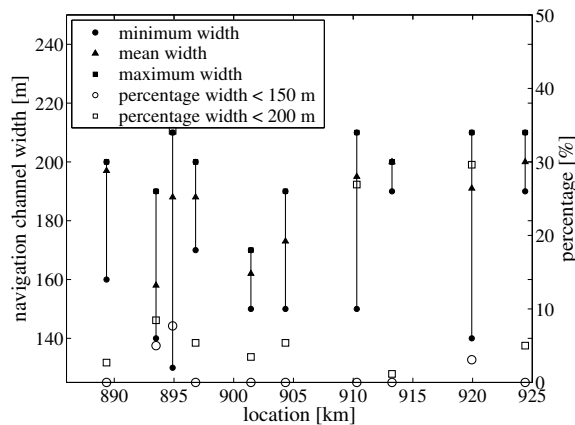
Figure 10.23: Navigation channel restriction along the Waal and percentage of a width smaller than 200 m and 150 m on the basis of data of the placement of buoys

The navigable width for a draught of 3.5 m is derived from the quasi-3D model simulation. Figure 10.24 shows the statistics of this width in the dry and the high-water season. The seasonal variation in navigable width is significant, as it reduces significantly during the dry season. The largest channel dimensions are found in the high-water season. Time-stack plots in Figure 10.25 give the minimum, mean value and standard deviation of the navigable width for a draught of 3.5 m as a function of time along the river. It can be seen that locations with frequent buoy placement also show a high standard deviation of this width. Locations with a high variability in navigable width also form bottleneck locations in reality, as at these locations the channel is delineated by buoys on a regular basis.

(a) Dry season

(b) High-water season
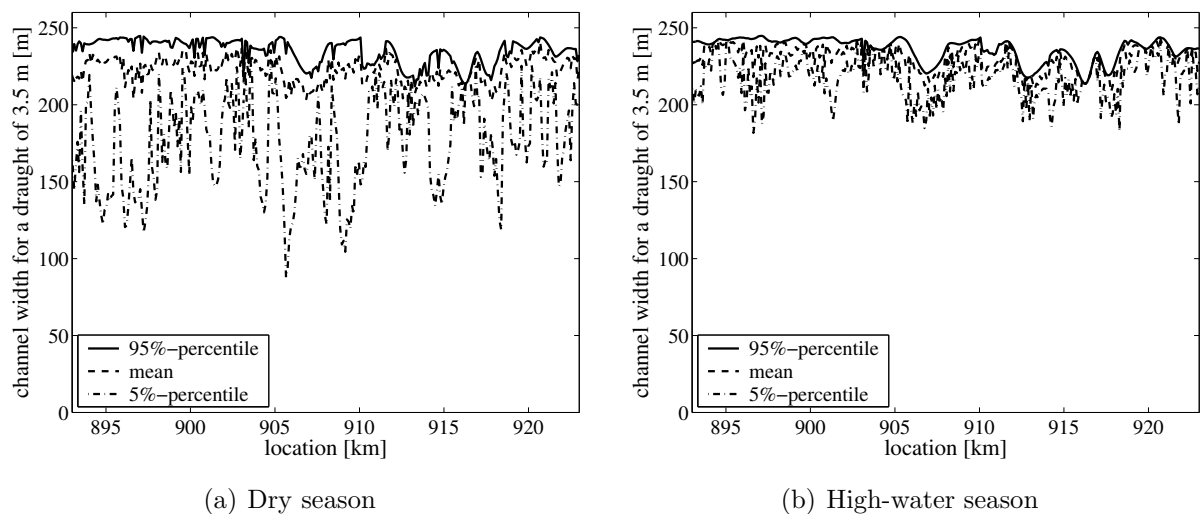
Figure 10.24: Statistics of the navigation channel width for a draught of 3.5 m, as derived from the quasi-3D model

10.7 Conclusions

In the foregoing we have shown that the navigability is strongly influenced by the stochastic nature of the river behaviour. The method discussed in this chapter can be used to assess the impact of various human intervention measures (widening, river engineering) on the river's navigability and maintenance costs (dredging). The following conclusions can be drawn.

Navigability of the Rhine

The percentage of navigable time for ships at various draughts depends much on the discharge time series involved. The percentage of navigable time for a draught of 3 m in the Niederrhein and Waal, for instance, can vary some 20% for different discharge time series. The navigability of
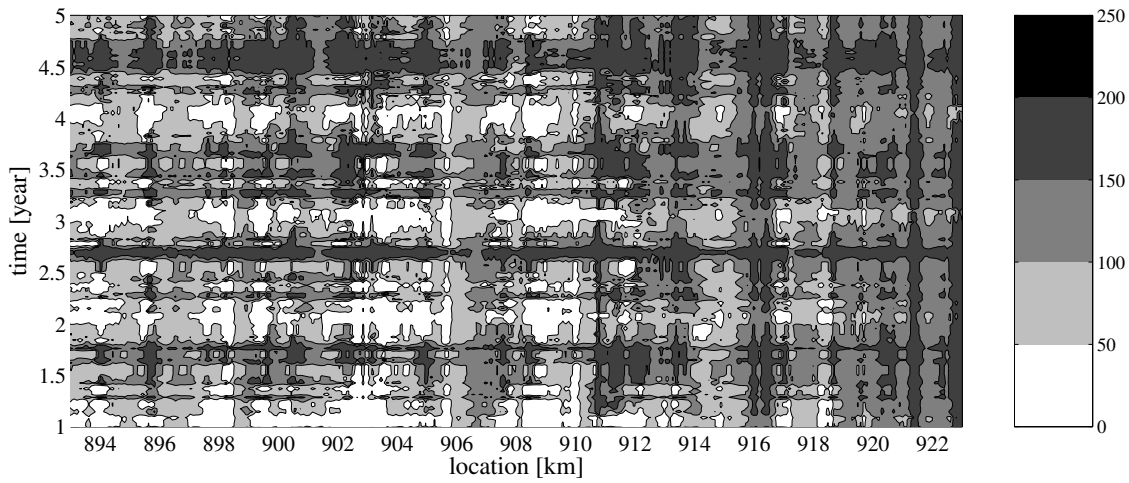
(a) Navigation channel width - minimum
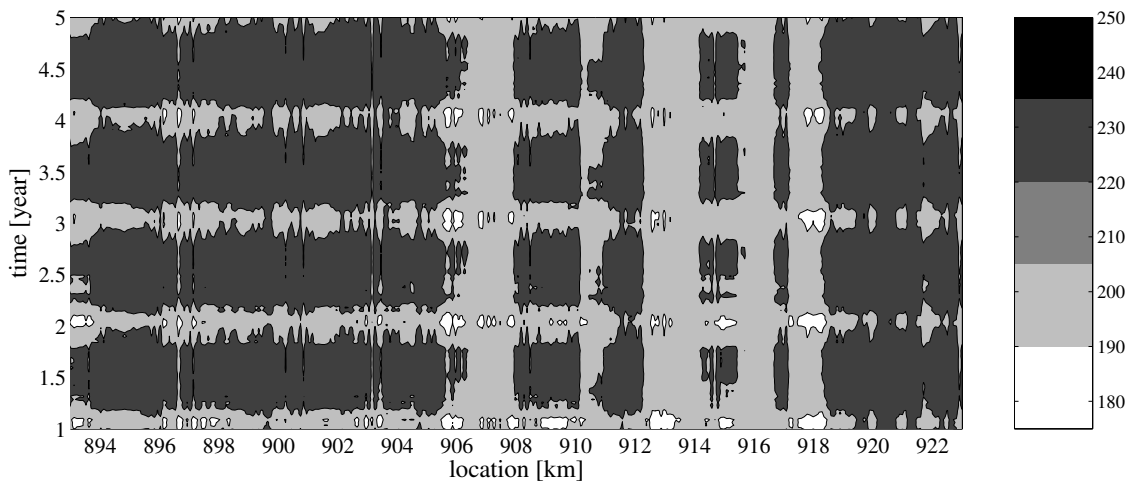
(b) Navigation channel width - mean
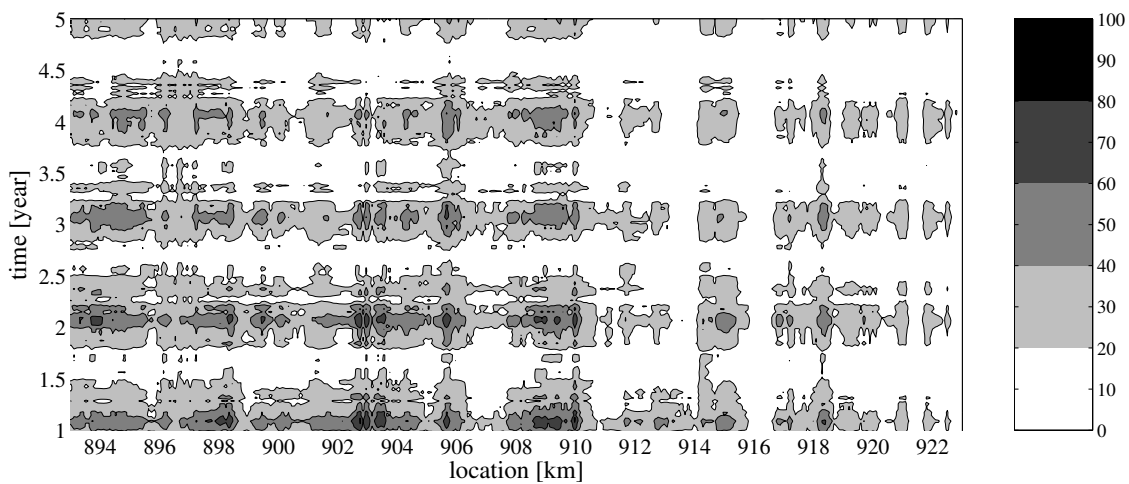
(c) Navigation channel width - standard deviation

Figure 10.25: Statistics of the navigation channel width for a draught of 3.5 m

the IJssel differs also considerably for different model runs. Due to the small channel dimensions of the IJssel, combined with the large number of sharp bends, the navigability is much worse than in the Niederrhein and Waal.

At least 95% of the time the Niederrhein and Waal should be navigable for ships at a draught of 2.8 m and a corresponding channel width of 150 m. The same goes for the IJssel for a draught of 2.5 m and a width of 150 m. It appears that the probability of meeting these conditions differs considerably for each simulation. A comparison between data and model computations indicates that the cumulative probability distribution of the least available depth of the ensemble of all model simulations agrees rather well with the curve derived from Least Measured Depth (LMD) data.

In some river sections, uncertainty in spatial and temporal variability of the water depths is more pronounced than in others. Some locations could develop into nautical bottlenecks, the removal of which may involve high costs. There is a strong discrepancy between nautical bottlenecks predicted with the 1-D model and observed in reality. On the one hand, the model seems to overestimate the morphological activity in some reaches and does not reproduce all kind of multi-dimensional morphodynamic features. On the other hand, the placement of buoys, continuous dredging operations and the flattening effect of navigation traffic on the tops of river dunes have a large influence on the LMD data.

So, the 1-D model approach appears to be applicable for assessing several aspects of navigability. Apparently, the 1-D model gives a good estimate for the probability of fulfilling navigation channel requirements, as long as a correction for transverse slope effects is applied. The 1-D model does well for the assessment of navigability at various draughts. The difference in the statistics of the navigable percentage at various draughts between the 1-D model with transverse slope correction and the quasi-3D model is only marginal. The predictive capability concerning the exact locations where nautical bottlenecks occur, is however limited.

The quasi-3D model provides the possibility to assess the navigability in two dimensions, in terms of navigable width and depth. The probability of fulfilling the navigation channel requirements to width and depth can be assessed. Statistical information on the navigable width for various draughts can also be derived from the quasi-3D model simulation.

Maintenance dredging in the Rhine

In line with the Dutch policy, the dredged material has to be deposited elsewhere in the river. Three different dredging strategies are evaluated, viz. (1) removal of the dredged material, (2) removal of the dredged material, and further deposition upstream, and (3) removal of the dredged material, and further deposition downstream. The historical dredging data turns out to fall within the 90% bandwidth derived for each of the three dredging strategies, but mostly

at the lower end.

In general, dredging without depositing the dredged material elsewhere in the river results in the lowest dredging volumes, whereas deposition of dredged material further upstream yields the largest dredging effort. Deposition further downstream leads to lower dredging volumes than upstream deposition. Since upstream deposition also entails a larger distance between dredge and dump location, the strategy of downstream deposition of dredged material is preferable from a economical point of view.

The model predicts most of the dredging activity in the Waal to take place close to the Pannerdensche Kop bifurcation. Subsequently, the discharge distribution at the bifurcation is influenced, viz. slightly less water is drawn into the Waal for all dredging strategies. This seems to have a negative effect on the navigability of the Waal. Combined with the fast bed recovery after dredging, it makes dredging hardly improve the river's navigability. The impact of dredging on discharge and sediment distribution at the Pannerdensche Kop bifurcation, the process of bed recovery and their impact on navigability require further investigation.

The model findings are in line with the first experiences with dredging in the Waal. Evaluation of the new policy in practice indicates that maintenance dredging in combination with upstream deposition hardly effect the navigation conditions. One of the principal objectives of upstream deposition, however, was to prevent further large-scale tilting of the river. It looks as if this objective is met by means of upstream deposition. Further investigation on this part is needed, however.

The IJssel benefits from the discharge reduction in the Waal. Its navigability turns out to be improved by maintenance dredging. Dredging without deposition of the dredged material elsewhere leads to the best navigability. Due to either upstream or downstream deposition of the extracted sediment, new nautical bottlenecks are formed elsewhere in the river. The strategy of downstream deposition yields a better navigability than upstream deposition.

Chapter 11

Conclusions and recommendations

The objectives of this thesis are (1) to study the stochastic nature of non-tidal lowland river morphology and to identify the uncertainty sources that contribute most to the stochastic morphodynamic river behaviour, (2) to produce general knowledge on the application of stochastic methods in river morphology, and (3) to investigate the potential of a stochastic approach in river management practice. This chapter summarises the answers to the research questions that we formulated in Section 1.4 in order to meet these objective. We end this thesis with recommendations for further research.

11.1 Conclusions

Methods of stochastic modelling in river morphodynamics

A number of stochastic methods exists to cope with uncertainties in system behaviour, such as First Order Reliability Method (FORM), Monte Carlo Simulation (MCS), Stochastic Differential Equations, Numerical Integration, etc. The applicability of these stochastic methods to study the stochastic nature of river morphology depends on how well these methods deal with the strong non-linearity and complexity of river morphodynamics. Since existing deterministic morphodynamic models are important and widely-used tools in present-day engineering practice, stochastic methods that make use of such models are recommendable.

On the basis of these criteria many stochastic methods can be eliminated from the list of potentially suitable methods for river morphology. Monte Carlo Simulation (MCS) with crude sampling appears to be a robust and suitable method to quantify uncertainties involved in morphodynamic predictions. MCS gives accurate results, as long as the sample size is large enough and the description of the input uncertainty adequate. The appropriate sample size depends on the desired degree of accuracy. A careful consideration on the desired precision is therefore important.

Use of numerical morphodynamic models in a stochastic setting

Application of MCS to three different morphodynamic models

In this thesis, three different morphodynamic models are applied in an MCS-mode, viz. (1) a simple hypothetical 1-D model having dimensions similar to those of the Waal (one of the Rhine branches in the Netherlands), (2) a more realistic, but also more complex multi-branches 1-D Rhine model, and (3) a quasi-3D model of the Waal. The 1-D Rhine model has been set-up, calibrated and validated by Jesse & Kroekenstoel (2001). The quasi-3D Waal model has been developed by Sloff (2004).

1.   Hypothetical 1-D model having dimensions similar to those of the Waal

The hypothetical 1-D model concerns a highly idealised situation in which the river is schematised as a prismatic channel with an initially plane sloping bed. The hypothetical model is appropriate to make a first investigation of the morphological response, for instance induced by isolated geometrical variations or human interventions. It provides rapid insight into the physical system behaviour and the uncertainties involved. The stochastic approach provides insight into the possible states that may occur and in particular the likelihood of predictions. It gives the opportunity to estimate the probability of occurrence of undesired morphological effects. A drawback of the hypothetical model, however, is that the model concerns a highly idealised situation. Therefore, it is of little use to operation and maintenance practice of real-life rivers.

The reason for still using the hypothetical model, is that the potential of a stochastic approach can best be investigated by first examining simple cases in which the morphological processes are fully transparent. This model is used, for instance, to test whether a computationally intensive MCS-procedure is required, or whether a long deterministic model run will yield most of the output statistics of interest. To that end, output samples are gathered over time, instead of over many short simulations, like in MCS. Apparently, part of the output statistics could be reproduced by time series analysis (TSA). It provides similar information on the location of potential bottlenecks (e.g. nautical bottlenecks or locations with an enhanced danger of destabilisation of hydraulic structures). Yet, it is not straightforward to produce information about when and how frequently the river does not meet the required conditions.
TSA is not suitable for river systems in transition periods, for instance, when a river adapts to new river works or undergoes systematic long-term changes. The usability of TSA in maintenance practice of real-life rivers is therefore limited. This underpins the importance of stochastic methods in more complex real-life situations.

2.   1-D Rhine model

The more complex Rhine model incorporates much more of the real-life complexity of the river. Non-uniformities in the river geometry turn out to yield bottom waves, which migrate down-

stream, partly decay and interfere with morphological features initiated elsewhere in the river. The result is a complex pattern of morphological behaviour and, correspondingly, a complex propagation of input uncertainties through the system.

Uncertainty due to the inherent variability of many model inputs in time and space, along with the lack of complete understanding of the processes involved, leads to an uncertain morphological response. The stochastic approach does not only show that many morphological states are possible, it also shows that in some reaches this uncertainty is more pronounced than in others, mainly due to strong spatial changes in geometry, such as bifurcation points, width variation in floodplains and the presence of hydraulic and man-made structures.

The 1-D model is valuable to gain insight into the stochastics of morphological processes at macro-scale level, thus the longitudinal profile evolution. Furthermore, the 1-D model gives a reasonable indication of the statistical properties of the width-averaged profiles and provides a first indication of locations that are susceptible to geometrically induced bed level variability and those that are not.

3. Quasi-3D Waal model

In the quasi-3D Waal model, morphodynamic phenomena at meso and macro-scale level are considered, meaning that time-dependent 2-D river bed deformations are included, like the transverse bed slope formation (pointbar and pool combinations in bends) and the formation of shallow and deep parts alternately at the left and the right side of the river. From the results of an MCS with the quasi-3D model we can conclude that the response statistics of individual points in the cross-sectional profile along the river do not only exhibit fluctuations along the river, but also a strong transversal variation. This means that the response statistics are not evenly spread over the cross-sectional profile. On average, the uncertainty intervals for the longitudinal profiles left and right of the axis, is larger than those in the axis. Moreover, the intervals at the left and the right side exhibit stronger fluctuations along the river. This transversal variation in the response statistics is not only induced by the presence of bends, but must also be attributed to variations in floodplain width, strong confinements of floodplains by embankments, and large open water areas and deep ponds in the floodplains. Confinement of floodplains by embankments seems to affect statistics the most.

On the use of a 1-D approach vs a quasi-3D approach

Comparing the 1-D Rhine model with a quasi-3D model of the Waal clarified the importance of multi-dimensional phenomena that are not considered in the 1-D approach. A comparison between the statistics of the width-averaged quantities derived from the quasi-3D Waal model and those of the 1-D Rhine model showed that response statistics of the 1-D Rhine model lag behind. The cross-sectional profile evolution imposed by the river alignment is reflected to a larger extent in the statistical characteristics of the width-averaged quantities derived from

the quasi-3D model than in those of the 1-D model. The uncertainty ranges of the quasi-3D model are much larger than those of the 1-D model. Moreover, the variations along the river are significantly larger in the quasi-3D model. The differences can be explained by three factors, viz. (1) grid resolution, (2) detail with which the shallow water equation are solved, and (3) representation of geometrical information. Since the grid resolution of the 1-D model is much less than that of the quasi-3D model, the averaging effect is stronger in the 1-D model. By solving the shallow water equation in a greater detail in the quasi-3D model, flow conditions at locations with geometrical non-uniformities exhibit stronger variations and thus enhance the bed level variability. Finally, non-uniformities in cross-sectional profiles have been reduced in the 1-D model, by averaging geometrical information left and right of the river axis and assuming symmetrical cross-sections.

In principle, river morphology concerns a 3-D problem. However, fully 3-D models are hardly available for river morphology and most problems do not need to be tackled by means of a 'complete' 3-D description. A degree of schematisation is possible in many cases. Based on the problem definition, decisions have to be made about the number of dimensions in the model. In river engineering practice, 1-D and quasi-3D morphodynamic models, like the models mentioned above, are commonly used. The applicability of either a 1-D or a quasi-3D model approach depends on the type of problem and the degree of detail that is required, both in terms of resolution and in terms of physical processes. For many relevant questions, a 1-D model approach is practically useful, despite its inherent limitations, to give sufficient insight with considerably lower computation effort. For the strategic planning of an entire river basin, a 1-D model approach is appropriate to provide a first insight into the river system response, for instance, induced by engineering works. In a later stage, a more advanced type of model might be more appropriate to study the impacts of engineering works at locations of special interests. To some extent, problems related to cross-sectional profile evolution, can be studied with a 1-D model approach in combination with analytically based post-processing to account for the 2D-transverse slope effect. A correction for the bed deformation in river bends alone may not be sufficient, since the morphological activity induced by strong cross-flows, at locations where floodplains are confined by winter dikes, seems to be more important for the stochasticity of the river bed. For more detailed types of problems a quasi-3D model is therefore recommended.

The computation effort per individual simulation differs considerably between 1-D and multi-dimensional models. This difference in computation effort will increase substantially when running these models in an MCS-setting. As this thesis focuses on a first assessment of stochastic methods in river morphology, the less time-consuming 1-D model approach is mostly taken for practical reasons, be it with incidental comparisons with multi-dimensional models. Knowledge on (1) the application of stochastic methods in river morphology and (2) the potential of a stochastic model approach in river management practice, obtained with the 1-D approach, holds also for multi-dimensional model approaches.

Types of uncertainty important to river morphological modelling

Morphodynamic models are affected by different types of uncertainties. The 1-D Rhine model is used to illustrate how the various sources of uncertainty influence the morphological predictions. In this assessment, uncertainties introduced by the model schematisation, numerical solution technique and the specification of future scenarios are left out of consideration.

A first ranking of uncertainty sources that are of importance to morphology was obtained with a global sensitivity analysis. Apparently, the morphological response is most sensitive to the parameters of the sediment transport formula, viz. the exponent of the bed shear stress and the critical Shields parameter. Moreover, sensitivity to the river discharge, the grain size of the bed material and the hydraulic roughness of the main channel, is clearly noticed. The impact of these sources is further investigated through MCS. The remaining inputs and parameters seem to be of relatively minor importance.

On the basis of theoretical considerations, data records, expert opinions and literature, either probability distributions of the model inputs are defined, or sets of model inputs for the MCS are randomly generated by resampling. A key source of uncertainty is the choice of the statistical model to come up with a good definition for the uncertainties considered. It becomes clear that resampling techniques are robust, adequate and efficient for modelling the natural randomness of discharge time series. The other uncertainty sources are described best with a classical probability distribution function. The lognormal distribution appears to be a good representation for many physical quantities, such as the hydraulic roughness.

Interpreting the MCS results and estimating the relative contribution is not straightforward. The size of the confidence interval varies differently for each uncertainty source, as a function of time and space, and the contributions of all sources do not add up linearly to the overall uncertainty. The non-linear behaviour of morphodynamic systems, combined with the time and space dependent signature and the time-lagging effect, presumably results in complex interactions of the various uncertainty sources, ultimately tending to reduce the overall uncertainty.

No sweeping statement on the relative importance of uncertainty sources for the overall uncertainty in the morphological response can be made, because of the demonstrably non-linear behaviour of the river system. It is only through studies such as this one that we can get a better understanding of the interaction of the different sources of uncertainty. Generally speaking, the tuning parameters, viz. the hydraulic roughness of the main channel, and the critical Shields parameter and the exponent of the bed shear stress in the transport formula, turn out to be the most important uncertainty sources for the morphological response. The contribution of the uncertainty in the grain size of the bed material to the uncertain morphological response is negligible. The importance of the discharge to morphology exhibits a seasonal variation, and is more significant at locations with non-uniformities in geometry, whereas at locations in a uniform reach, it is less pronounced.

Potential of a stochastic approach in river management practice

The MCS-procedure can be rather time-consuming, in particular for MCS with multi-dimensional morphodynamic models. The potential of a stochastic approach is exposed by means of three applications, in order to clarify how this 'computationally-intensive' approach can contribute to river management practice. For this purpose, mostly use is made of the 1-D Rhine model.

The stochastic approach can be useful to assist the engineer in optimising the design of engineering works. For the purpose of illustration, various river improvement measures in the Rhine are evaluated. The stochastic approach provides insight into the range of possible morphological responses to different design alternatives, and their probability of occurrence. It appears that at some locations, the impact of identical engineering measures is more pronounced than at others. This holds for the mean response, as well as for the variability, and also for the seasonal variation.

Furthermore, the uncertainty in the morphological evolution of the Waal is much larger than in the IJssel. The seasonal variation seems to be more prominent in the Waal also. This difference is explained by the difference in morphological time-scale between the two branches, mainly as a consequence of differences in sediment transport rate. Hence, the morphological time-scale of the IJssel is much larger than that of the Waal. This means that the morphology in the IJssel responds slower to changes in the river regime than that in the Waal. This results in much less variability of the IJssel morphology. Consequently, the Waal morphology responds faster to changes in the river regime, like RfR-measures.

Knowledge on the spatial and temporal variation of morphological response statistics can be of importance to the decision on where to implement which river improvement measures.

In morphologically dynamic river systems, morphology may affect flood levels. Most present-day flood level predictions are, however, done with a fixed-bed hydraulic model, in which the geometrical schematisation is a representation of the 'actual' state of the river. The adequacy of the geometrical schematisation turns out to be critical. An 'a priori' judgement of safety against flooding on the basis of fixed-bed forecasting in morphologically dynamic river systems may even be misleading. We have therefore investigated to what extent morphology affects flood levels and to what extent it is justified to compute flood levels with a fixed-bed model.

The effects of seasonal morphological variations turn out to be negligible. Other morphological phenomena, viz. long-term spatial variations and morphological variability near the bifurcation point, appear to have a larger effect on the flood levels (order of magnitude 0.1 m). Absolutely speaking, this is still rather small, but it is not small as compared with the centimetre-accuracy claimed for the design water levels for the assessment of the flood defences in the Netherlands, or in the light of plans to spend millions of Euros to river improvement measures that reduce the design water level by a few centimetres.

The Rhine is one of the most important inland waterways in Europe. Some locations have the

potential to develop into nautical bottlenecks, involving high maintenance costs. In fact, the navigability of a river depends on the least available water depth along the entire shipping route. Whenever the navigation depth is less than required, navigation is congested or ships may carry less cargo.

The impact of the stochastic nature of the river behaviour on navigability is addressed by means of MCS applied to the 1-D Rhine model and the quasi-3D Waal model. Apparently, the 1-D model approach is applicable for assessing several aspects of navigability, as long as a correction for transverse slope effects is applied. The difference in the statistics of the navigable percentage at various draughts between the 1-D model with transverse slope correction and the quasi-3D model is only marginal. The quasi-3D model offers more the possibility to assess the navigability in two dimensions, both in width and depth. Statistical information on shipping widths for various draughts can, for instance, be derived.

Dredging is utilised to maintain the prescribed navigation conditions in the Rhine. Three different dredging strategies are evaluated, viz. (1) removal of the dredged material, (2) removal of the dredged material, and further deposition upstream, and (3) removal of the dredged material, and further deposition downstream. In general, dredging without depositing the dredged material elsewhere in the river results in the lowest dredging volumes, whereas deposition of dredged material further upstream yields the largest dredging effort. Deposition further downstream leads to lower dredging volumes than upstream deposition. Since upstream deposition also entails a larger distance between dredge and dump location, the strategy of downstream deposition of dredged material is preferable from a economical point of view. A drawback of the strategy of downstream deposition is that it may further enhance the large-scale tilting of the river.

The stochastic method could be used to assess the impact of various human intervention measures on the river's navigability and maintenance costs. Insight into the statistics of maintenance dredging requirements can help the river manager in drawing up performance-contracts with dredging companies.

11.2 Recommendations

Further research following up this thesis should preferably address the following issues:

- Using a quasi-3D model in a Monte Carlo-setting, in order to fill up the caveats left by the 1-D models, is considered promising. Running a more complex morphodynamic model in an MCS-setting requires, however, extra computational effort. Further research on the development of a more efficient approach to quantify uncertainty in computationally intensive numerical models is recommended. This could be either the development of a more efficient way of doing MCS, or the development and application of a stochastic method other than MCS.

- The influence of the lack of understanding of the physical processes, and the inability to represent complex physical processes or phenomena which ensues from the use of a particular model concept, are left out of consideration in this thesis. Regarding the latter, one may even argue whether the physical processes and phenomena of a natural river system can be described, at all, by models using a set of deterministic differential equations, empirical sediment transport formulae and a number of adjustable model parameters. Further research on the topic of 'model' uncertainty should be given a high priority.

- The definition of input uncertainty is a point of concern in stochastic analysis. MCS gives accurate results, as long as the description of the input uncertainty is adequate. Theoretical considerations, data records, expert opinions and literature can be used to come up with proper definitions. Limited availability and complex interlinking of data, for instance if model inputs are stochastically dependent, or include a correlation structure in space or in time, can make this definition rather difficult. The imposed correlation structure may require sample characteristics different from those of the historical record. Moreover, it may occur that none of the classical probability distribution functions properly fits the values of the historical record. We recommend further investigation into how to deal with the description of the statistics of input uncertainty taking these aspects into account.

- Uncertainty resulting from tuning parameters in morphodynamic models plays an important role in the uncertainty involved in morphodynamic river behaviour. In highly non-linear models, however, there may be many different parameter sets that produce equally acceptable model results. Therefore, the 'optimal' calibration parameter set shows a degree of non-uniqueness. The inability to place a reasonable degree of confidence on the estimated calibration parameter values leaves considerable uncertainty in the model forecasts. The topic of uncertainty and model calibration should be addressed further. Most probably, we have to leave the concept of an optimal parameter set.

- In the present thesis, the importance of an adequate description of the distribution of water and sediment at river bifurcations has become evident. It is recommended to further investigate the processes at bifurcations in multi-branched rivers, like the Rhine in the Netherlands, and the incorporation of the physical mechanisms governing these processes in morphodyanmic models.

- In this thesis we have attempted verifying the stochastic results with available data records. Historical data records do not cover the full range of possible conditions, but reflect only a single realisation of the dynamic behaviour of the river system. Extreme conditions may well have been missed, whereas MCS enables the generation of conditions beyond the historical record. Therefore, the use of historical records for stochastic

model verification has its limitations. We advise to further investigate ways to verify and validate the results of stochastic model approaches.

References

Aronica, G., Hankin, B., & Beven, K. (1998). Uncertainty and equifinality in calibrating distributed roughness coefficients in a flood propagation model with limited data. *Advances in Water Resources, 22*(4), 349-365.

Baptist, M. J. (2005). *Modelling floodplain biogeomorphology.* Ph.D. thesis, ISBN 90-407-2582-9, Delft University of Technology, the Netherlands.

Beersma, J. J., & Buishand, T. A. (2004). The joint probability of precipitation and discharge deficits in the Netherlands. *Water Resources Research, 40*(12), W12508 10.1029/2004WR003265.

Benjamin, J. R., & Cornell, C. A. (1970). *Probability, statistics and decision for civil engineers.* ISBN 07-004549-6, McGraw-Hill, Inc. book compagny, USA, 684 pp.

Beven, K. (1993). Prophecy, reality and uncertainty in distributed hydrological modelling. *Advances in Water Resources, 16*, 41-51.

Blom, A. (2003). *A vertical sorting model for rivers with non-uniform sediment and dunes.* Ph.D. thesis, ISBN 90-9016663-7 , University of Twente, the Netherlands.

Box, G. E. P., Jenkins, G. M., & Reinsel, G. C. (1994). *Time series analysis; forecasting and control* (3rd ed.). ISBN 0 13 060774 6, Englewood Cliffs: Prentice Hall, 598 pp.

Box, G. E. P., & Tiao, G. C. (1973). *Bayesian inference in statistical analysis.* New York: Addisson-Wesley, USA, 588 pp.

Buishand, T., & Brandsma, T. (2001). Multisite simulation of daily precipitation and temperature in the Rhine basin by nearest-neighbor resampling. *Water Resources Research, 37*(11), 2761-2776.

Bulle, H. (1926). *Untersuchungen über die Geschiebeableitung bei der Spaltung von Wasserläufen (Investigations on the sediment diversion at a channel bifurcation).* Berlin: VDI Verlag (in german).

Burcharth, H. F., & Lui, Z. (1994). On the extreme wave height analysis. In *International conference on hydro-technical engineering for port and harbour construction.* Yokosuka, Japan.

Cesare, M. A. (1991). First-Order Analysis of open-channel flow. *Journal of Hydraulic Engineering, 117*(2), 242-247.

Chang, C.-H., Tung, Y.-K., & Yang, J.-C. (1994). Monte Carlo simulation for correlated variables with marginal distributions. *Journal of Hydraulic Engineering, 120*(3), 313-331.

Chang, C.-H., Yang, J.-C., & Tung, Y.-K. (1993). Sensitivity and uncertainty analysis of a sediment transport model: a global approach. *Stochastic Hydrology and Hydraulics, 7*, 299-314.

Coles, S., Heffernan, J., & Tawn, J. (1999). Dependence measure for extreme value analysis. *Extremes, 2*(4), 339-365.

Coles, S. G., & Tawn, J. A. (1991). Modelling extreme multivariate events. *Journal of Royal Statistical Society, 53*(2), 377-392.

Cooke, R. M. (1991). *Experts in uncertainty, opinion and subjective probability in science. Environmental ethics and science policy.* ISBN 0-19-506465-8, New York Oxford University Press, 321 pp.

Cooke, R. M., & Van Noortwijk, J. M. (1999). Local probabilistic sensitivity measures for comparing FORM and Monte Carlo calculations illustrated with dike ring reliability calculations. *Computer Physics Communications, 117*, 86-98.

CUR. (1997). *Kansen in de civiele techniek. Deel 1: Probabilistisch ontwerpen in theorie.* (Tech. Rep. No. 190. ISBN 9037601022.). CUR. Ministerie van Verkeer en Waterstaat. Directoraat-Generaal Rijkswaterstaat. (in dutch).

Dahmen, E. R., & Hall, M. J. (1989). *Screening of Hydrological data. Tests for Stationary and Relative Consistency.* ISBN 9070754 231, ILRI - International Institute for Land Reclamation and Improvement Publication, (Vol. 49), Wageningen, the Netherlands.

De Rooij, D. (2005). *Baggeren op de Nederlandse Rijntakken. Een onderzoek naar modellering en invloed van baggerstrategie op bevaarbaarheid.* M.Sc. thesis, Delft University of Technology, the Netherlands. (in dutch).

De Vriend, H. J. (1977). A mathematical model of steady flow in curved shallow channels. *Journal of Hydraulic Research, 15*(1), 37-54.

De Vriend, H. J. (1999). Long-term morphodynamics of alluvial rivers and coasts. In G. Bianchi (Ed.), *Environmental applications of mechanics and computer science* (p. 1-19). CISM Courses and Lectures. No. 409. Springer Wien New York.

De Vriend, H. J. (2002). Model-based morphological prediction: from art to science. In D. Bousmar & Y. Zech (Eds.), *Proceedings of River Flow 2002* (Vol. 2, p. 3-12). Louvain-la-Neuve, Belgium: Balkema Publishers, a member of Swets & Zeitlinger, Lisse, the Netherlands.

De Vries, M. (1965). Considerations about non-steady bed-load transport in open channels. In *Proceedings 11th IAHR-congress.* Leningrad.

De Vries, M. (1973). Riverbed variations. aggradation and degradation. In *IAHR seminar.* New Delhi.

De Vries, M. (1975). A morphological time-scale for rivers. In *Proceedings 16th IAHR-congress* (Vol. 2, pp. paper B3, 17-23). São Paulo.

De Vries, M. (1993). *Use of models for river problems* (Tech. Rep. No. 51). UNESCO Publishing.

Ditlevsen, O. (1979). Narrow bounds for structural systems. *Journal of Structural Mechanics*, *1*(4), 453-472.

Duits, M. T. (1997). *Baggeroptimalisatie in rivierbochten*. M.Sc. thesis, Delft University of Technology, the Netherlands. (in dutch).

Duits, M. T., Havinga, H., & Van Noortwijk, J. M. (2000). Nauwkeurigheidsanalyse ruimte voor riviertakken. Onzekerheden in waterstanden en kosten onderzocht. *Land + Water*, *9*, 55-61 (in dutch).

Eerkens, J. W. (1996). *Longitudinal profiles of rivers with a composite cross-section*. M.Sc. thesis, Delft University of Technology, the Netherlands.

Efron, B. (1982). *The Jackknife, the Bootstrap, and other resampling plans*. ISBN 0-89871-179-7, Philadelphia publisher, 92 pp.

Engelund, F., & Hansen, E. (1967). *A monograph on sediment transport in alluvial streams*. Copenhagen.

Fan, X., & Wang, L. (1996). Comparibility of jackknife and bootstrap result: an investigation for a case of canonical correlation analysis. *Journal of Experimental Education*, *64*, 173-189.

Filarski, R., & Brolsma, J. U. (1989). New opportunities for European inland navigation. *Bulletin of the Permanent International Association of Navigation Congress*, *63*(66), 110-122.

Gardner, R. H., & O'Neill, R. V. (1983). Parameter uncertainty and model predictions: a review of Monte Carlo results. In M. B. Beck & G. Van Straten (Eds.), *Uncertainty and forecasting of water quality*. Berlin: Springer-Verlag.

Gates, T. K., & Al-Zahrani, M. A. (1996a). Spatiotemporal stochastic open-channel flow. I: model and its parameter data. *Journal of Hydraulic Engineering*, *122*(11), 641-651.

Gates, T. K., & Al-Zahrani, M. A. (1996b). Spatiotemporal stochastic open-channel flow. II: simulation experiments. *Journal of Hydraulic Engineering*, *122*(11), 652-661.

Goda, Y., & Kobune, K. (1990). Distribution function fitting for storm wave data. In *International Conference on Coastal Engineering*. Delft, the Netherlands.

Grimmett, G. R., & Stirzaker, D. R. (1992). *Probability and random processes* (2nd ed.). ISBN 0 19 853665 8, Oxford Science Publications, 541 pp.

Hammersley, J. M., & Handscomb, D. C. (1964). *Monte Carlo Methods*. Londen: Methuen & Co Ltd., 178 pp.

Hersbach, H., Mureau, R., Opsteegh, J. D., & Barkmeijer, J. (1998). An EPS for the short and early medium range. In *ECMWF seminar on predictability*.

Hetzer, S. (2005). *Navigability of the river Waal. A stochastic approach*. M.Sc. thesis, Delft University of Technology, the Netherlands.

Hirano, M. (1971). River bed degradation with armouring. *Transactions Japanese Society of*

Civil Engineering, *3*, 194-195.

Iman, R. L., & Helton, J. C. (1988). An investigation of uncertainty and sensitivity analysis techniques for computer models. *Risk Analysis*, *8*(1), 71-90.

Jansen, P. P., Bendegom, J., Van den Berg, J., De Vries, M., & Zanen, A. (1979). *Principles of river engineering, the non-tidal alluvial river*. Delft: Delftse Uitgevers Maatschappij.

Janssen, P. H. M., Slob, W., & Rotmans, J. (1990). *Gevoeligheidsanalyse en Onzekerheidsanalyse: een Inventarisatie van Ideeën, Methoden en Technieken* (Tech. Rep. No. 958805001). RIVM, Research for man and Environment, Bilthoven (in dutch).

Jazwinsy, A. H. (1970). *Stochastic processes and filtering theory*. New York: Academic Press.

Jesse, P., & Kroekenstoel, D. F. (2001). *1-D Morfologisch Sobek Rijntakken model* (Tech. Rep. Nos. ISBN 9036953952, RIZA report 2001.040). RIZA, Ministerie van Verkeer en Waterstaat. Directoraat-Generaal Rijkswaterstaat. (in dutch).

Johnson, P. A. (1996a). Uncertainty in estimations of excess shear stress. In Tickle, Goulter, Xu, Wasimi, & Bouchart (Eds.), *Stochastic Hydraulics'96* (Vol. 2, p. 521-525). Balkema Publishers.

Johnson, P. A. (1996b). Uncertainty of hydraulic parameters. *Journal of Hydraulic Engineering*, *112*(2), 112-114.

Johnson, P. A., & Ayyub, B. M. (1992). Assessing time-variant bridge reliability due to pier scour. *Journal of Hydraulic Engineering*, *118*(6), 887-903.

Johnson, P. A., & Ayyub, B. M. (1996). Modelling uncertainty in prediction of pier scour. *Journal of Hydraulic Engineering*, *122*(2), 66-72.

Julien, P. Y., Klaassen, G. J., Ten Heggeler, M., & Wilbers, A. W. E. (2002). Case Study: bed Resistance of Rhine river during 1998 Flood. *Journal of Hydraulic Engineering*, *128*(12), 1042-1050.

Kleinhans, M. G. (2002). *Sorting out sand and gravel: sediment transport and deposition in sand-gravel rivers*. Ph.D. thesis, Utrecht University, the Netherlands.

Kloeden, P. E., Platen, E., & Schurz, H. (1994). *Numerical solutions of stochastic differential equations through computer experiments*. Berlin: ISBN 3-540-57074-8, Berlin, Spinger, pp 292.

Klopstra, D., Barneveld, H. J., Van Noortwijk, J. M., & Van Velzen, E. H. (1997). Analytical model for hydraulic roughness of submerged vegetation. In *27th Congress of the International Association for Hydraulic Research* (Vol. A, p. 775-780). San Francisco.

Knight, D. W. (2001). Flow and sediment transport in two-stage channels. In *Proceedings of IAHR symposium on River, Coastal and Estuarine Morphodynamics* (p. 1-20). Obihiro, Japan.

Kuczera, G. (1988). On the validity of first-order prediction limits for conceptual hydrologic models. *Journal of Hydrology*, *103*, 209-247.

Lall, U., & Sharma, A. (1996). A nearest neighbor bootstrap for resampling hydrologic time

series. *Water Resources Research*, *32*(3), 679-693.

Lambeek, J. J. P., Jagers, H. R. A., & Van der Klis, H. (2004). Monte Carlo method applied to a two-dimensional morphodynamic model. In M. Greco, A. Carravetta, & R. Della Morte (Eds.), *Proceedings of River Flow 2004* (Vol. 1, p. 191-196). Napoli, Italy: Balkema Publishers.

Leander, R., Buiteveld, H., De Wit, M. J. M., & Buishand, T. A. (2004). Application of a weather-generator to simulate extreme river discharges in the Rhine and Meuse basins. In *NCR-days 2004*. Wageningen, the Netherlands.

Maurer, M., Kelamener, Y., & Bechteler, W. (1997). The effects of inaccurate input parameters on deposition of suspended sediment. *International Journal of Sediment Research*, *12*(3), 191-198.

McKay, M. D. (1997). Nonparametric variance-based methods of assessing uncertainty importance. *Reliability Engineering and System Safety*, *57*, 267-279.

Meyer-Peter, E., & Müller, R. (1948). Formulas for bed load transport. In *Proceedings of the 2nd Congres IAHR* (Vol. 2, p. 39-64). Stockholm.

Morgan, M. G., & Henrion, M. (1990). *Uncertainty; a guide to dealing with uncertainty in quantitative risk and policy analysis.* Cambridge University Press.

Mosselman, E., Sieben, A., Sloff, C. J., & Wolters, A. (1999). Effect of spatial grain size variations on two-dimensional river bed morphology. In *Proceedings of IAHR symposium on River, Coastal and Estuarine Morphodynamics* (Vol. I, p. 499-507). Genova.

Parmet, B. W. A. H., Van de Langemheen, W., Chbab, E. H., Kwadijk, J. C. J., Diermanse, F. L. M., & Klopstra, D. (2002). *Analyse van de maatgevende afvoer van de Rijn te Lobith* (Tech. Rep. No. RIZA-report 2002.012). RIZA, Ministerie van Verkeer en Waterstaat. Directoraat-Generaal Rijkswaterstaat. (in dutch).

Pearson, E. S., & Kendall, M. G. (1970). *Studies in the history of statistics and probability.* London, Griffin, 481 pp.

Rajagopalan, B., & Lall, U. (1999). A k-nearest-heighbor simulator for daily precipitation and other weather variables. *Water Resources Research*, *35*(10), 3089-3101.

Reeve, D., Chadwick, A., & Fleming, C. (2004). *Processes, Theory & Design Practice.* ISBN 0-415-26840-0, London Spon.

Seminara, G., & Tubino, M. (1989). Alternate bars and meandering: free, forced and mixed interactions. In G. Parker & S. Ikeda (Eds.), *River meandering. agu Water Resources Monograph* (Vol. 12, p. 267-320).

Shapiro, M. D., & Wilcox, D. W. (1996). Generating non-standard multivariate distributions with an application to mismeasurement in the CPI. *NBER Technical Working Paper*, *196*, 17.

Shiono, K., & Muto, Y. (1998). Complex flow mechanisms in compound meandering channels with overbank flow. *Journal of Fluid Mechanics*, *376*, 2221-261.

Silva, W., Klijn, F., & Dijkman, J. (2001). *Room for the Rhine branches in the Netherlands; What the research has taught us* (Tech. Rep. No. R3294 & RIZA-report 2001.031). RIZA, Ministerie van Verkeer en Waterstaat, Directoraat-Generaal Rijkswaterstaat & WL| Delft Hydraulics, 160 pp (in dutch).

Slijkhuis, K. A. H., Van Gelder, P. H. A. J. M., Vrijling, J. K., & Vrouwenvelder, A. C. W. M. (1999). On the lack of information in hydraulic engineering models. *Safety and Reliability*, *1*, 713-718.

Sloff, C. J. (2004). *Tweedimensionale bodemveranderingen in de vaarweg van de Waal* (Tech. Rep. No. Q3811.00). WL|Delft Hydraulics (in dutch).

Sloff, C. J., Bernabè, M., & Baur, T. (2003). On the stability of the Pannerdense Kop river bifurcation. In A. Sanchez-Arcilla & A. Bateman (Eds.), *Proceedings of IAHR symposium on River, Coastal and Estuarine Morphodynamics* (p. 1001-1011). Barcelona.

Sloff, C. J., & Jagers, H. R. A. (2004). *2D morfologische berekeningen Lent* (Tech. Rep. No. Q3560.00). WL|Delft Hydraulics (in dutch).

Smith, P. J., & Kojiri, T. (2003). Short-term rainfall-runoff prediction with weather radar and Monte Carlo Simulation. In G. Korfiatis & G. Christodoulou (Eds.), *XXX IAHR Congress* (Vol. Theme D Hydroinformatics and advanced data technology in engineering practice, p. 183-190). Thessaloniki, Greece.

Sorooshian, S., Duan, Q., & Gupta, V. K. (1993). Calibration of rainfall-runoff models: Application of global optimization to the Sacramento soil moisture accounting model. *Water Resources Research*, *29*(4), 1185-1194.

Southgate, H. N. (1999). Guideline for error assessment in models of long-term coastal morphology. In *IAHR Symposium on River, Coastal and Estuarine Morphodynamics* (Vol. 2, p. 299-308). University of Genova.

Southgate, H. N., & Capobianco, M. (1997). The role of chronology in long-term morphodynamics: theory, practice and evidence. In E. Thornton (Ed.), *Coastal Dynamics '97- ASCE* (p. 943-952). New York.

Struiksma, N., Olesen, K. W., Flokstra, C., & De Vriend, H. J. (1985). Bed deformation in curved alluvial channels. *Journal of Hydraulic Research*, *23*(1), 57-79.

Talmon, A. M., Van Mierlo, M. C. K. M., & Struiksma, N. (1995). Laboratory measurements of the direction of sediment transport on transverse alluvial-bed slopes. *Journal of Hydraulic Research*, *33*(4), 495-517.

Ten Brinke, W. B. M., Bolwidt, L. J., Snippen, E., & Van Hal, L. W. J. (2001). *Sedimentbalans Rijntakken 2000* (Tech. Rep. Nos. ISBN 9036953995, RIZA report 2001.043). RIZA, Ministerie van Verkeer en Waterstaat, Directoraat-Generaal Rijkswaterstaat (in dutch).

Ten Brinke, W. B. M., Schoor, M. M., Sorber, A. M., & Berendsen, H. J. A. (1998). Overbank sand deposition in relation to transport volumes during large-magnitude flood in the Dutch sand-bed Rhine river system. *Earth Surface Processes and Landforms*, *23*, 809-

824.

Ten Heggeler, M., Uijlenhoet, R., Berne, A., Delobbe, L., Dierickx, P., De Wit, M., et al. (2004). Hydrological application of weather radar in the Ourthe basin; a preliminary investigation. In *NCR-days 2004.* Wageningen, the Netherlands.

Thoft-Christensen, P., & Baker, M. J. (1982). *Structural reliability theory and its applications.* ISBN 3-540-11731-8, Berlin Springer, 267 pp.

Van Bendegom, L. (1947). Enige beschouwingen over riviermorfologie en rivierverbetering. *De Ingenieur, 59*(4), b1-b11, (in dutch) English translation: Some considerations on river morphology and river improvement, Nat. Res. Council of Canada, Tech. Transl. 1054, 1963.

Van der Klis, H. (2003). *Uncertainty analysis applied to numerical models of river bed morphology.* Ph.D. thesis, ISBN 90-407-2440-7, Delft University of Technology, the Netherlands.

Van Gelder, P. H. A. J. M. (2000). *Statistical methods for risk-based design of civil structures.* Ph.D. thesis, Delft University of Technology, the Netherlands.

Van Gelder, P. H. A. J. M., & Vrijling, J. K. (1997). A comparative study for different parameter estimation methods for statistical distribution functions in civil engineering applications. *Structural Safety and Reliability, 1*, 665-668.

Van Rijn, L. C. (1984). Sediment transport: Part 3: bedforms and alluvial roughness. *Journal of Hydraulic Engineering, 110*, 1733-1754.

Van Rijn, L. C. (1993). *Principles of sediment transport in rivers, estuaries and coastal seas.* ISBN 90-800356-2-9, Amsterdam Aqua Publications.

Van Vuren, S., & De Vriend, H. J. (2004). River hydraulic and morphological response to navigation: A case study of the River Rhine in the Netherlands. In *Symposium on river sedimentation* (Vol. III, p. 1645-1653). Yichang, China.

Van Vuren, S., De Vriend, H. J., Ouwerkerk, S., & Kok, M. (2005). Stochastic modelling of the impact of flood protection measures along the river Waal in the Netherlands. *Journal of Natural Hazards, 36*(1-2), Special issue on Flooding in Europe: Risks and Challenges, 81-101.

Van Vuren, S., & Van Breen, L. E. (2003). Morphological impact of floodplain lowering along a low-land river: a probabilistic approach. In G. Korfiatis & G. Christodoulou (Eds.), *Proceedings of XXX IAHR Congress* (Vol. D, p. 191-200). Thessaloniki, Greece.

Van Vuren, S., Van der Klis, H., & De Vriend, H. (2002). Large-scale floodplain lowering along the river waal: a stochastic prediction of morphological impacts. In D. Bousmar & Y. Zech (Eds.), *Proceedings of River Flow 2002* (Vol. 2, p. 903-912). Louvain-la-Neuve, Belgium: Balkema Publishers, a member of Swets & Zeitlinger, Lisse, the Netherlands.

Vanoni, V. A., & Hwang, L. S. (1967). Relation between bed forms and friction in streams. *Journal of the Hydraulic Divisions, 93*(3), 121-144.

Verlaan, M. (1989). *Efficient Kalman Filtering Algorithms for Hydrodynamic Models.* Ph.D.

thesis, Delft University of Technology, the Netherlands.

Visser, P. J., Havinga, H., & Ten Brinke, W. B. M. (1999). Hoe houden we de rivier bevaarbaar? Daling zomerbed Rijntakken vraagt aandacht. *Land + Water*, *9*(9), 24-27 (in dutch).

Vreugdenhil, C. B. (2002). Accuracy and reliability of numerical river models. *Journal of the American Water Resources Association*, *38*(4), 1083-1095.

Wang, S. S. Y., & Weiming, W. (2004). River sedimentation and morphological modelling - the state of the art and future development. In *Ninth International symposium on River Sedimentation* (Vol. I, p. 71-94). Yichang, China.

Werner, M. (2004). *Spatial flood extent modelling. A performance-based comparison.* Ph.D. thesis, ISBN 90-407-2558-6, Delft University of Technology, the Netherlands.

Wiberg, P. L., & Smith, J. D. (1989). Model for calculating bed load transport of sediment. *Journal of Hydraulic Engineering*, *115*(1), 101-123.

Wilbers, A. W. E. (2004). *The development and hydraulic roughness of subaqueous dunes.* Ph.D. thesis, Utrecht University, the Netherlands.

Yamaguchi, M. (1996). Intercomparison of parameter estimation methods in external wave analysis. In *International conference on coastal engineering.* Orlando, Florida.

Yang, C. T. (1996). *Sediment transport; theory and practice.* ISBN 0-07-912265-5, McGraw-Hill series in water resources and environmental engineering, New York, McGraw-Hill, 396 pp.

Yeh, K.-C., & Deng, S.-T. (1993). Uncertainty and sensivity analyses of sediment transport formulas. *International Journal of Sediment Research*, *13*(1), 20-33.

Yeh, K.-C., & Tung, Y.-K. (1993). Uncertainty and sensitivity analyses of pit-migration model. *Journal of Hydraulic Engineering*, *119*(2), 262-283.

Yossef, M. F. M. (2005). *Morphodynamic of rivers with groynes.* Ph.D. thesis, Delft University of Technology, the Netherlands.

Yossef, M. F. M., & Klaassen, G. J. (2002). Reproduction of groyne-induced river bed morphology using LES in a 2-D morphological model. In D. Bousmar & Y. Zech (Eds.), *Proceedings of River Flow 2002* (Vol. 2, p. 1099-1108). Louvain-la-Neuve, Belgium: Balkema Publishers, a member of Swets & Zeitlinger, Lisse, the Netherlands.

Met dank aan

Op de dag af een jaar geleden zat ik in de tuin nog redelijk ontspannen na te denken over de opbouw van mijn proefschrift. Het was de 'kick-off' van het echte schrijfwerk. Een jaar na dato zit ik weer in die tuin. Nu toch meer ontspannen, mijn boek is af.

Vandaag kijk ik terug op de afgelopen periode. Het was niet de promotie, maar het onderwerp dat me bewoog mijn promotie-onderzoek te starten. Ik heb nu ruim vier jaar met veel plezier aan mijn promotie-onderzoek gewerkt. Het was veelzijdig, diepgaand, interessant en leerzaam. Allesomvattend, het was een fantastische periode. Ik heb genoten van de vrijheid om zelfstandig onderzoek te doen en mijn eigen lijnen uit te stippelen.

In het bijzonder dank hiervoor aan Huib de Vriend. Onder zijn hoede, heb ik me kunnen ontwikkelen tot ingenieur en onderzoeker. Huib, bedankt voor je enthousiasme, je correcties en je altijd constructieve kritiek en aanmoediging. Ik heb veel van je mogen leren en kijk terug op een goede samenwerking en hoop dat deze nog lang mag duren.

De kritische noot van Han Vrijling tijdens mijn promotie-onderzoek is ook belangrijk geweest voor het uiteindelijke resultaat. De discussies over tekortkomingen van modellen en de toepasbaarheid van de modelresultaten bleken uiterst nuttig. Han, je was in je opmerkingen vaak zeer direct, maar ik heb je enorm leren te waarderen. Ik denk met veel plezier terug aan onze samenwerking.

De vertaalslag van modelresultaten naar bruikbare informatie voor de rivierbeheerder was de grootste uitdaging binnen mijn onderzoek en resulteerde in een door Rijkswaterstaat gefinancieerd onderzoeksproject. Hendrik Havinga, bedankt voor de mogelijkheid om mijn onderzoek toe te passen in de beheerspraktijk.

Ook wil ik mijn dank uitspreken richting Stichting Technische Wetenschappen (STW) voor het financieren van mijn onderzoek en RIZA en WL | Delft Hydraulics voor het beschikbaarstellen van de morfodynamische modellen. Tijdens mijn onderzoek heb ik veel tijd doorgebracht bij HKV$_{\text{LIJN IN WATER}}$ en WL | Delft Hydraulics. Het beschikbaarstellen van een werkplek, de begeleiding en stimulerende discussies heb ik zeer gewaardeerd.

Een dankwoord als deze wordt gemakkelijk een erg onpersoonlijke opsomming, met het gevaar dat ik personen vergeet te bedanken die - al dan niet inhoudelijk - hebben bijgedragen aan het

uiteindelijke resultaat. Daarom wil ik graag besluiten met het bedanken van mijn promotiecommissie, de leden van de STW-gebruikersgroep, mijn kamergenoten en collega's van de vakgroep Waterbouwkunde, HKV_{LIJN IN WATER} en WL | Delft Hydraulics, en al mijn afstudeerders.

Uiteraard is er nog een andere groep zeer belangrijk voor me geweest. De laatste twee jaren waren soms niet makkelijk. Met name de periode na de plotselinge dood van mijn goede vriendin Nicole op 29 november 2003 was erg verdrietig. Toen ben ik sceptisch geworden over de noodzaak van het afronden van mijn onderzoek en het was moeilijk mij op mijn werk te concentreren. Door de steun en liefde van mijn familie en vrienden ben ik het gelukkig weer anders gaan zien.

Mijn proefschrift ligt voor u, ik woon samen met Marcel in de binnenstad van Delft, ik heb een mooie baan bij WL | Delft Hydraulics en in juni ben ik tante geworden van Ruben... de zon schijnt volop...

Curriculum Vitae

Saskia van Vuren was born on September 7th 1977 in s'-Hertogenbosch. She attended high school at CSG Oude Hoven in Gorinchem and received her VWO diploma in 1995.

She continued her academic education at Twente University. As part of her study Civil Engineering and Management, she worked as a trainee for Royal Haskoning at the Punggur Utara Irrigation Project in Sumatra, Indonesia. With her MSc-project, entitled 'The development of a stochastic model to optimise maintenance costs along the Dutch coast', commissioned by Road and Hydraulic Engineering division of the Ministry of Transport, Public Works and Water Management, she completed her masters degree.

In December 2000 Saskia started her PhD-research on stochastic modelling of river morphology at Delft University of Technology, Faculty of Civil Engineering and Geosciences, Section of Hydraulic Engineering. This resulted in the present dissertation. The research has been partly fulfilled at HKV$_{\text{LIJN IN WATER}}$ and WL | Delft Hydraulics and is supervised by prof. dr. ir. H.J. de Vriend, prof. drs. ir. J.K. Vrijling and dr. ir. M. Kok. The work was founded by the Foundation for Technical Sciences (STW), applied science division of NWO and the technology programme of the Ministry of Economic Affairs, under contract number DCB 5302. In 2004, she worked for a period of six month on a research project, entitled 'Impact assessment of Room for River Rhine-measures on navigation and maintenance dredging', commissioned by Directorate for Public Works and Water Management

In October 2005, she joined the River Engineering Department of WL | Delft Hydraulics.